
Deformations of Toric Quiver Gauge Theories

José A. CERQUEIRA SÁ

*A thesis submitted in fulfilment of the requirements
for the degree of Doctor of Philosophy*

at



Department of Mathematical Sciences
DURHAM UNIVERSITY

November 2024

Deformations of Toric Quiver Gauge Theories

José A. CERQUEIRA SÁ

*Submitted for the degree of
Doctor of Philosophy*

Abstract

We explore various aspects of toric quiver gauge theories, with a particular focus on their deformations and the associated geometric and algebraic structures. We review fundamental concepts in algebraic geometry, toric geometry, and quiver representation theory, delving into the construction of toric varieties and quiver representations, examining their roles in the moduli of toric quiver gauge theories, particularly through Geometric Invariant Theory (GIT) and symplectic reduction. We study 4d $\mathcal{N} = 1$ supersymmetric quiver gauge theories, emphasizing their representation via quiver diagrams and brane tilings, and analyzing dualities that link different quiver theories. Central to this thesis is the study of one-parameter families of $U(1)^2$ -preserving deformations, defined by zig-zag paths in the brane tiling. These deformations, which correspond to Hanany-Witten moves in the dual (p, q) -web, are explored in the context of their impact on moduli spaces and RG flows between SCFTs on D3-branes probing local toric (pseudo) del Pezzo surfaces. Finally, we extend our analysis to non-reflexive polytopes, applying algorithms to uncover flows between toric phases of quiver gauge theories, with particular attention to those described by toric diagrams with 2 internal points.

Declaration

The work in this thesis is based on research carried out in the Department of Mathematical and Computer Sciences at Durham University under the supervision of Prof. Stefano Cremonesi. The author was supported by Fundação para a Ciência e a Tecnologia I.P. through grant SFRH/BD/136280/2018.

The first part of the thesis aims to introduce the reader to mathematical and physical approaches to brane tilings in the context of 4d $\mathcal{N} = 1$ quiver gauge field theory, as well as set the conventions used throughout the text. The second part is based on results obtained in the publication:

- S. Cremonesi and J. Sá, *Zig-zag deformations of toric quiver gauge theories. Part I. Reflexive polytopes*, *JHEP* **05** (2024) 114 [[2312.13909](#)]

The third part is based on the continuation of the previous work and yet to be published. An extensive amount of code was also developed during this research:

- J. Sá, “QuiverGaugeTheory: a Mathematica package for 4d $\mathcal{N} = 1$ quiver gauge theories.” Available at github.com/jose-a-sa/QuiverGaugeTheory, 2023
- J. Sá, “InterfaceM2: a Macaulay2 interface for Mathematica.” Available at github.com/jose-a-sa/InterfaceM2, 2023
- J. Sá, “LieACh: a LieART extension for 1-dim Lie algebra representations.” Available at github.com/jose-a-sa/LieACh, 2023

The associated data can be found in github.com/jose-a-sa/zig-zag-deformation-data.

No part of this thesis has been submitted elsewhere for any degree or qualification.

Copyright © 2024 José A. Cerqueira Sá.

“The copyright of this thesis rests with the author. No quotation from it should be published without the author’s prior written consent and information derived from it should be acknowledged.”

Acknowledgements

First, I would like to thank my supervisor, Stefano Cremonesi. I feel extremely privileged to have worked with someone with such an awe-inspiring range of knowledge in theoretical physics and mathematics. The opportunity to learn from his way of thinking has not only made me a better researcher, but his humility has also profoundly influenced me personally. His patience, encouragement, and willingness to provide assistance (or jump on a Zoom call) whenever I needed it have been invaluable during these years. His unwavering guidance and support throughout the many ups and downs of my PhD journey have been crucial. For all of this, I am truly grateful.

I would like to thank Federico Carta, Michele Del Zotto and Cyril Closset for their collaboration, perspective, and the many afternoon discussions that made the lockdowns much more bearable. From these, I learned much about the nature of quivers and gained insights that helped shape this work. To my fellow office and department mates, Sophie, Gabriel A., Connor, Viktor, Dario, Gabriele D., I thank the many discussions and laughs shared during lunch. I want to give a nod to Dan for the many philosophical debates we had. I also appreciate the opportunity to participate in seminars and meetings with the members of the CPT group at Durham's maths department. Special thanks to Prof Simon Ross and the maths office staff for supporting my yearly letters to my funding body.

I would like to thank my parents for all the love, support and sacrifices have made during my many years of study allowed to me to journey far beyond my wildest dreams. Also, my brother, for his comic-relief and joyfulness, which always manages me to lighten me up in any situation. To my borrowed family, Carlos, Carmo, Sara and Inês, I want to thank for treating me like a son/brother and always being present for me and my parents. To my friends, Rifath, Artur, Emanuelle, Filipe and Alexandra, for all the support.

This thesis was supported by Fundação para a Ciência e a Tecnologia I.P. through grant SFRH/BD/136280/2018. Co-financed by:



Dedicated to

*My parents, Domingo and Rosa,
and brother, Cristiano*

Contents

Abstract	iii
Acknowledgements	vii
Contents	xi
List of Figures	xv
List of Tables	xix
1 Introduction	1
1.1 Motivation	1
1.1.1 Strings and branes	1
1.1.2 Quivers from D-brane stacks	7
1.1.3 Toric singularities and brane tilings	10
1.2 Thesis outline	13
1.3 Code developed	15
I Review of concepts	19
2 Mathematical preliminaries	21
2.1 Toric geometry	21
2.1.1 Rings, ideals and varieties	21
2.1.2 Toric varieties, cones and fans	25
2.1.3 Homogeneous coordinate ring of a toric variety	30
2.1.4 Calabi-Yau affine cones, toric diagrams and crepant resolutions	35
2.2 Quiver representation theory	40
2.2.1 Quiver representations and path algebras	40
2.2.2 Moduli of quiver representations	43
2.2.2.1 Proj GIT quotient	44
2.2.2.2 Symplectic reduction	45

2.2.2.3	Kempf-Ness theorem	47
2.2.3	θ -stability of quiver representations	48
3	Quiver gauge theories and Brane Tilings	51
3.1	4d $\mathcal{N} = 1$ supersymmetric gauge theory	51
3.2	Brane tilings	56
3.2.1	Perfect matchings	58
3.2.2	Zig-zag paths	59
3.3	Master space and other moduli	61
3.3.1	Geometric and baryonic branches	61
3.3.2	$\mathcal{N} = 2$ Coulomb branches	62
3.4	A-maximization and conformal invariance	63
3.5	Fast-forward algorithm	65
3.6	Dualities of brane tilings	67
3.6.1	Toric-Seiberg duality	67
3.6.2	Specular duality	68
II	Study of del Pezzo geometries	71
4	Zig-zag deformation of toric (pseudo) del Pezzo theories	73
4.1	Zig-zag operator	74
4.2	Mesonic moduli from chiral rings	76
4.3	RG flows between toric del Pezzos	77
4.3.1	PdP _{3c} to PdP _{3b}	79
4.3.2	Higher order non-isolated singularities	85
4.4	RG flow to a nontoric geometry: $L^{1,3,1}/\mathbb{Z}_2$ to marginal deformation of PdP ₅	88
4.5	Zig-zag deformation under Mirror Symmetry	90
5	Zig-zag deformation and resolutions	95
5.1	Minimal GLSM	95
5.2	Kähler chambers from θ -stability	98
5.3	(p, q) -webs, 2-cycles and zig-zags	100
5.4	Zig-zag deformation as a Hanany-Witten move	106
III	Beyond reflexive polytopes	111
6	Zig-zag deformations of geometries from non-reflexive polytopes	113
6.1	Zig-zag operator generalized	113
6.1.1	Revisiting the conifold	114
6.1.2	Hanany-Witten move of a 7-brane “bound” state	117

6.2	Polytopes with 2 internal points	121
6.2.1	Algorithmic approach	122
6.2.1.1	Generating toric phases	123
6.2.1.2	Finding zig-zag deformations	127
6.2.2	Non-orbifold example: zig-zag deformations of $L^{5,4,1}$	132
6.2.3	Summary of zig-zag deformations for 2 internal points	135
7	Discussion	141
	Appendices	143
A	Details of deformations for reflexive polytopes	145
A.1	Deformations to toric models	145
A.1.1	$\text{PdP}_1, \mathbb{C}^3 / \mathbb{Z}_4 (1, 1, 2)$ to $\mathbb{F}_0, \mathcal{C} / \mathbb{Z}_2 (1, 1, 1, 1)$	146
A.1.2	PdP_2 to dP_2	146
A.1.3	$\text{PdP}_{3a}, \mathbb{C}^3 / \mathbb{Z}_6 (1, 2, 3)$ to $\text{PdP}_{3c}, \text{SPP} / \mathbb{Z}_2 (0, 1, 1, 1)$	146
A.1.4	$\text{PdP}_{3c}, \text{SPP} / \mathbb{Z}_2 (0, 1, 1, 1)$ to PdP_{3b}	147
A.1.5	PdP_{3b} to dP_3	148
A.1.6	PdP_{4b} to PdP_{4a}	149
A.1.7	$\mathbb{C}^3 / (\mathbb{Z}_4 \times \mathbb{Z}_2) (1, 0, 3)(0, 1, 1)$ to $L^{1,3,1} / \mathbb{Z}_2 (0, 1, 1, 1)$	150
A.1.8	$\mathbb{C}^3 / (\mathbb{Z}_4 \times \mathbb{Z}_2) (1, 0, 3)(0, 1, 1)$ to $\text{PdP}_5, \mathcal{C} / \mathbb{Z}_2 \times \mathbb{Z}_2 (1, 0, 0, 1)(0, 1, 1, 0)$	152
A.2	Deformations to marginal deformations of toric models	154
A.2.1	$L^{1,3,1} / \mathbb{Z}_2 (0, 1, 1, 1)$ to $\text{PdP}_5, \mathcal{C} / \mathbb{Z}_2 \times \mathbb{Z}_2 (1, 0, 0, 1)(0, 1, 1, 0)$	154
B	Details of deformations for polytopes with 2 internal points	157
B.1	Deformations between toric phases with $g = 7$	157
B.1.1	$L^{4,3,2}$ to $K^{2,4,1,1}$	157
B.2	Deformations between toric phases with $g = 8$	158
B.2.1	$\mathbb{C}^3 / \mathbb{Z}_8 (1, 3, 4)$ to $L^{1,3,1} / \mathbb{Z}_2 (1, 0, 0, 1)$	158
B.2.2	$\mathbb{C}^3 / \mathbb{Z}_8 (1, 3, 4)$ to $\mathcal{C} / \mathbb{Z}_4 (0, 1, 2, 1)$	158
B.2.3	$\text{dP}_1 / \mathbb{Z}_2 (1, 0, 0, 1)$ to $K^{2,5,1,1}$	158
B.2.4	$L^{3,5,2}$ to $K^{2,4,1,2}$	158
B.2.5	$\text{PdP}_{4c} (2)$ to $\text{PdP}_{4e} (3)$	159
B.2.6	$\text{PdP}_{4d} (2)$ to $\text{PdP}_{4f} (2)$	159
B.3	Deformations between toric phases with $g = 9$	159
B.3.1	$L^{5,4,1}$ to $K^{2,4,1,3}$	159
B.3.2	$L^{5,4,1}$ to $K^{4,3,2,2}$	159
B.3.3	$\text{SPP} / \mathbb{Z}_3 (1, 0, 0, 2)$ to $K^{2,5,1,2}$	160
B.3.4	$\text{PdP}_{5b} (2)$ to $\text{PdP}_{5c} (3)$	161
B.4	Deformations between toric phases with $g = 10$	161

B.4.1	$\mathbb{C}^3/(\mathbb{Z}_2 \times \mathbb{Z}_5) (1, 0, 1)(0, 1, 4)$ to $L^{1,4,1}/\mathbb{Z}_2 (1, 0, 0, 1)$	161
B.4.2	$\mathbb{C}^3/(\mathbb{Z}_2 \times \mathbb{Z}_5) (1, 0, 1)(0, 1, 4)$ to $L^{2,3,2}/\mathbb{Z}_2 (1, 0, 0, 1)$	162
B.4.3	$\text{PdP}_2/\mathbb{Z}_2 (1, 1, 1, 1)$ to $K^{2,5,1,3}$	162
B.4.4	$\text{PdP}_2/\mathbb{Z}_2 (1, 1, 1, 1)$ to $K^{4,4,2,2}$	163
B.4.5	$\text{PdP}_{6a} (2)$ to $\text{PdP}_{6b} (3)$	163
B.4.6	$\text{PdP}_{6a} (2)$ to $\text{PdP}_{6c} (3)$	164
B.5	Deformations between toric phases with $g = 11$	164
B.5.1	$L^{5,6,1}$ to $K^{2,5,1,4}$	164
B.5.2	$L^{5,6,1}$ to $K^{4,4,2,3}$	164
B.6	Deformations between toric phases with $g = 12$	165
B.6.1	$\mathbb{C}^3/(\mathbb{Z}_2 \times \mathbb{Z}_6) (1, 0, 1)(1, 0, 5)$ to $L^{1,5,1}/\mathbb{Z}_2 (1, 0, 0, 1)$	165
B.6.2	$\mathbb{C}^3/(\mathbb{Z}_2 \times \mathbb{Z}_6) (1, 0, 1)(1, 0, 5)$ to $\text{SPP}/(\mathbb{Z}_2 \times \mathbb{Z}_2) (1, 0, 0, 1)(0, 1, 1, 0)$	165
B.6.3	$\mathbb{C}^3/(\mathbb{Z}_2 \times \mathbb{Z}_6) (1, 0, 1)(1, 0, 5)$ to $\mathcal{C}/(\mathbb{Z}_3 \times \mathbb{Z}_2) (1, 0, 0, 2)(0, 1, 1, 0)$	166
C	Kähler chamber mapping of PdP_{3a} to PdP_{3c} phase A	167
	Bibliography	175

List of Figures

1.1	D-brane depiction as endpoints of open strings.	3
1.2	Affine Dynkin diagram for the A_{n-1} family (a) leading to the quiver for the $\mathbb{C}^2/\mathbb{Z}_n \times \mathbb{C}$ quiver gauge theory.	8
1.3	Toric diagram (a), coamoeba (b) and amoeba (c) projections of the Σ curve for orbifold geometry $\mathbb{C}^3/\mathbb{Z}_3$. Normals of the toric diagram (a) map to NS5 cycle intersection that wrap \mathbb{T}^2 , as well as defining the (p, q) -legs in (c). Brane tiling in (b) is obtained by mapping $(N, \pm 1)$ regions (blue/orange) to white/black nodes.	12
1.4	Toric-to-toric 4d $\mathcal{N} = 1$ RG flows, connecting geometries with reflexive toric diagrams via zig-zag deformations. Rows and columns are organized by the number of nodes G in the quiver and the number of extremal points n_e in the polytope, following [55]. Links in the arrows point to details in appendix A.	14
2.1	Fan of \mathbb{P}^2	29
2.2	Fan of $\mathbb{P}^2/\mathbb{Z}_3(0, 1, 2)$, with lattice $N = \mathbb{Z}^2$	34
2.3	Fan of $\mathbb{P}^2/\mathbb{Z}_3(0, 1, 2)$, with lattice $N' = \{(a/3, b/3) \mid a + b \equiv 0 \pmod{3}\}$	34
2.4	Reflexive toric diagrams. Black dots are vertices, red is for the origin (internal). Yellow dots are non-vertex points in facets revealing the presence of an A_n -type singularities.	37
2.5	A full resolution $\sigma_\Delta \rightarrow \tilde{\Sigma}$ of the cone $\sigma_\Delta = \text{Cone}(\Delta \times \{1\})$ describing the singular Calabi-Yau 3-fold $\mathbb{C}^3/(\mathbb{Z}_3 \times \mathbb{Z}_3)(1, 0, 2)(0, 1, 2)$ to a smooth fan $\tilde{\Sigma}$	39
3.1	Model PdP _{3c} Phase B [55]: (a) brane tiling decorated with zig-zag paths; (b) toric diagram with normal vectors (p, q) associated to zig-zags; (c) quiver diagram.	60
3.2	Toric (Seiberg) duality as an operation on the brane tiling. Colored arrows represent chiral superfield products. Often, one must integrate out massive fields by shrinking pairs of edges which share a bivalent vertex.	67

3.3	Untwisting map, followed by the identification of punctures with gauge groups.	68
4.1	Tiling of PdP _{3c} phase B, focusing on the two parallel zig-zag paths and $\mathcal{N} = 2$ fractional branes strips associated to the most relevant (lowest R_{sc}) zigzag deformation. The red edge, X_{53}^2 , indicates the F-term equation that relates the two non-zero winding mesons of the strip in the chiral ring, i.e. $X_{31}X_{15}X_{53}^1 \simeq X_{34}X_{45}X_{53}^1$.	74
4.2	Lattice of the $U(1)^2$ mesonic flavor charges of the generators of PdP _{3c} phase B (see table 4.1).	80
4.3	(a) Lattice of $U(1)^2$ mesonic flavor charges of the generators and (b) toric diagram of PdP _{3b} .	82
4.4	Tiling of PdP _{3c} phase B with integrated-in node along the deformation zig-zag (yellow), highlighting the two possible (purple/blue) zig-zag moves that realize the deformation.	84
4.5	Tilings and toric diagrams of PdP _{3b} phase B, obtained by applying to the tiling of figure 4.4 the zig-zag move depicted by the purple arrows (a) and blue arrows (b), keeping the original fundamental domain fixed.	85
4.6	Tiling of $\mathbb{C}^3/(\mathbb{Z}_4 \times \mathbb{Z}_2)$ $(1, 0, 3)(0, 1, 1)$, with emphasis on the zig-zag paths associated to the non-isolated A_3 singularity.	86
4.7	Brane tiling of PdP ₅ phase A, showcasing the zig-zag paths of the parent model in fig. 4.6 and the reversed zig-zag paths after the deformation.	87
4.8	Zig-zag move to obtain PdP ₅ Phase B (b) from the integrated-in edges $\mathbb{C}^3/(\mathbb{Z}_4 \times \mathbb{Z}_2)$ model (a).	88
4.9	Brane tilings of phase A (a) and phase B (b) of $L^{1,3,1}/\mathbb{Z}_2$ $(0, 1, 1, 0)$. The two tilings are Seiberg dual by mutating node 4.	89
4.10	Diagram representing the connection between length 4 zig-zag deformations and Seiberg duality on the specular dual models.	91
4.11	(a) Graph with toric-Seiberg dualities (solid black edges) and specular dualities (dashed red edges) of $g = 8$ reflexive models. (b) Brane tiling of PdP ₅ phase D, specular dual to the model $\mathbb{C}^3/(\mathbb{Z}_4 \times \mathbb{Z}_2)$ $(1, 0, 3)(0, 1, 1)$.	92
5.1	Region plot of open string Kähler chambers for PdP ₁ , using stereographic projection of (ξ_1, ξ_2, ξ_3) . Swatch legend shows the resolution parameters (ζ_1, ζ_2) as piecewise linear functions of the FI parameters for each of the choices of $(p_{(-1,0)}, p_{(0,0)})$.	98

5.2	Subquivers of PdP_1 obtained by deleting edges from the perfect matching of the chamber $(f_{(-1,0)}, s_{(0,0)}) = (f_1, s_1)$	100
5.3	(a) Brane tiling of dP_1 , with each edge labelled with perfect matching it belongs to. (b) Toric diagram of dP_1	102
5.4	(p, q) -webs associated to the two resolutions of the complex cone over dP_1 , related by a flop transition (at $\zeta'_2 = -\zeta_2 = 0$). For the choice of $p_{(0,0)} = s_3$, we have $\zeta_1 = \xi_1 - \xi_2$ and $\zeta_2 = -\zeta'_2 = \xi_2 + \xi_3$	103
5.5	Brane tiling and toric diagram for $\mathbb{C}^3/\mathbb{Z}_6(1, 2, 3)$, highlighting the three parallel zig-zag paths associated to the A_2 singularity.	104
5.6	Regions formed by the stability of reps. of $Q_{g_i}, Q_{f_j}, Q_{g_i, f_j}$ in the PdP_{3a} quiver.	106
5.7	Hanany-Witten move mapping resolution T_Δ of PdP_{3a} to $T_\Delta^{(2)}$ of PdP_{3c} . 5-branes are in black, 7-branes are in blue, and monodromy cuts in dashed red. Volumes of holomorphic cycles ζ_a are superimposed.	108
5.8	Hanany-Witten move mapping resolution T_Δ of PdP_{3a} to $T_\Delta^{(1)}$ of PdP_{3c} . Volumes of holomorphic cycles ζ_a are superimposed.	108
6.1	Quiver of the $\mathbb{C}^2/\mathbb{Z}_2 \times \mathbb{C}$ theory.	115
6.2	Brane tiling of the $\mathbb{C}^2/\mathbb{Z}_2 \times \mathbb{C}$ theory.	116
6.3	Hanany-Witten move of a single 7-brane ($r = 1$). As we rotate the monodromy cut (dashed red), with direction (x, y) , we observe a conical gap open due to the identification of directions $(x, y) \sim M_{-1,0}^{-1}(x, y) = (x - y, y)$ of the two semi-infinite lines. The 5-branes crossing the gap/cut are also identified (dotted line).	119
6.4	Hanany-Witten move of a bound state of two 7-brane ($r = 2$). The conical gap represents the identification $(x, y) \sim (M_{-1,0}^{-1})^2(x, y) = (x - 2y, y)$ associated to the monodromy cut (dashed red).	119
6.5	Lattice width w_η with respect to toric diagram facet normal η	120
6.6	Original Seiberg duality of a $\mathcal{N} = 1$ SQCD $\text{SU}(N_c)$ gauge field theory.	124
6.7	Seiberg duality of a $\mathcal{N} = 1$ quiver gauge theory, with $G = \prod_{i=1}^g \text{SU}(N_i)$. The mutated node has $\tilde{N}_k = \sum_{i \neq k} N_i a_{ik} - N_k = \sum_{j \neq k} a_{kj} N_j - N_k$	124
6.8	Steps in the BFS exploring the graph toric phases of $K^{4,3,2,2}$. Undirected edges correspond to a pair of directed edges in both directions. Highlighted nodes/phases in red have been found in a previous step but not yet <i>visited</i>	128

6.9	Brane tiling of generalized conifold $L^{3,5,2}$	129
6.10	Brane tiling of model $K^{2,4,1,2}$	131
6.11	Brane tiling (a) and toric diagram (b) of the single toric phase of $L^{5,4,1}$. . .	132
6.12	Lattice of generators of $L^{5,4,1}$, at height 1 in (a) and height 2 in (b). Some points in (b) represent relations in the mesonic ideal. The labelled triplets represent the points in the 3d lattice, as well as the $U(1)^3$ consistent charges of the mesonic global symmetry.	133
6.13	Toric phases of $K^{2,4,1,3}$ obtained from deforming $L^{5,4,1}$ by a single operator \mathcal{O}_{η_i} , as summarized in fig. 6.19. Dimer (III) is isomorphic to dimer (I) by mutating node 7.	134
6.14	Toric phases of $K^{4,3,2,2}$ obtained from deforming $L^{5,4,1}$ by an operator $\mathcal{O}_{\eta_i} + \mathcal{O}_{\eta_j}$, as summarized in B.3.2. Dimers (III) and (V) are isomorphic by mutating node 5 or 7.	135
6.15	Graph of zig-zag deformations starting from $L^{5,4,1}$, as well as the graph of toric-Seiberg dualities of the involved models, showcasing flows between different toric phases depending on zig-zag paths triggering the deformation.	135
6.16	Zig-zag deformation between polytopes with $g = 6$	136
6.17	Zig-zag deformation between polytopes with $g = 7$	136
6.18	Zig-zag deformation between polytopes with $g = 8$	137
6.19	Zig-zag deformation between polytopes with $g = 9$	137
6.20	Zig-zag deformation between polytopes with $g = 10$	138
6.21	Zig-zag deformation between polytopes with $g = 11$	138
6.22	Zig-zag deformation between polytopes with $g = 12$	139

List of Tables

1.1	Massless states in type-IIA string theory	4
1.2	Massless states in type-IIB string theory	5
1.3	Brane configuration in 9+1 dimensions in IIB string theory. D3-branes are transverse to and are represented by a point in the CY 3-fold.	7
1.4	5-brane configuration in 9+1 dimensions in IIB string theory, equivalent to D3-branes probing a toric Calabi-Yau singularity after T-dualizing the 2 circles on the 57-directions. NS5-brane wraps a Riemann surface Σ	12
3.1	Specular duality mapping	69
4.1	Table of generators of the mesonic moduli space for PdP _{3c} phase B, where $f = \prod_{i=1}^2 f_i$, $g = \prod_{i=1}^2 g_i$ and $s = \prod_{i=1}^7 s_i$ (perfect matchings on fig. 3.1). The superconformal R-charge $U(1)_R$ can be obtained via a-maximization [99–101].	79
4.2	Partial table of generators of the mesonic moduli space for the integrated in PdP _{3c} phase B model.	84
5.1	Description of the D-terms for the GLSM associated to a toric model.	96
5.2	Minimal GLSM, with one p.m. variable per lattice point in Δ . The resolution parameter $\zeta_a(\xi)$ control the Kähler volumes of a basis of holomorphic 2-cycles, which depend linearly on the FI parameters in each open string Kähler chamber.	96
5.3	Table encoding D-term equations of the GLSM and toric diagram of PdP ₁	97
5.4	Minimal GLSM for PdP ₁ , with $\zeta_a(\xi)$ given in fig. 5.1.	98
6.1	Number of toric phases connected by toric-Seiberg dualities, for all the toric geometries from polytope with 2 internal points.	127

Chapter 1

Introduction

1.1 Motivation

The research presented in this thesis delves into various aspects of supersymmetric gauge theories in relation to string theory and geometry. The focus is on understanding the landscape of 4-dimensional gauge field theories with minimal supersymmetry, and also understanding their low-energy dynamics. In particular, we research a particular class of 4d $\mathcal{N} = 1$ theories whose gauge group and matter content is described by a quiver diagram (a directed graph), resulting from D3-branes probing toric Calabi-Yau 3-folds (CY₃) and deformations thereof. These topics have attracted significant interest both in the high-energy physics and pure mathematics communities. For many years, physicists have worked on geometric engineering of 4-dimensional quantum field theories, with lower amounts of supersymmetry ($\mathcal{N} = 2$ and $\mathcal{N} = 1$), with the hopes of reconciling compactified supersymmetric high-energy theories with low-energy gauge dynamics. This is particularly important in the ongoing efforts of constructing a model for beyond-Standard-Model physics. On the other hand, geometric engineering is not just about building physical theories, as it utilizes advanced mathematical concepts. In particular, the framework of quiver gauge theories presents itself as an alternative playground to explore complex theoretical topics in quiver representations and algebraic geometry. This intersection has led to fruitful exchanges between mathematics and theoretical physics, providing insights and tools for both fields.

1.1.1 Strings and branes

String theory [5–10] has been an elegant framework in theoretical physics, offering a proposal for physics beyond the Standard Model. It tackles the problem of unifying gauge and gravitational interactions in a quantum mechanically well-defined theory. As such, it proves to be a quantum gravity theory, successfully recovering the Einstein’s theory of gravity as a

low-energy effective theory applicable at energy levels below a characteristic threshold known as the string length scale

$$\ell_s = \sqrt{\alpha'} . \quad (1.1)$$

A string is introduced as a generalization of a relativistic point particle. The simplest generalization is to extend a point traveling in spacetime (worldline) to a $1d$ segment or loop (open or closed string) tracing a 2-dimensional worldsheet Σ embedded in a target space N . We denote this map by $X : \Sigma \rightarrow N$. A natural action to consider is the Nambu-Goto action, which is proportional to the area of the traced path:

$$S_{\text{NG}}[X] = -\frac{1}{2\pi\alpha'} \int_{\Sigma} d^2\sigma \sqrt{-\gamma} , \quad (1.2)$$

where $\gamma_{ab} = (X^*\eta)_{ab} = \eta_{\mu\nu} \partial_a X^\mu \partial_b X^\nu$ is the induced metric on the worldsheet by the target space flat metric η , and the dimensionful overall constant is the string tension $T = 1/(2\pi\alpha')$. As the string moves in time, we have options of having closed strings (Σ homeomorphic to $\mathbb{R} \times S^1$) or open strings ($\mathbb{R} \times D^1$). The bosonic closed string theory is successful in recovering the Einstein theory as an effective theory at length scales larger than the string length ℓ_s , while completing the theory in the ultraviolet (UV). In the string frame, the effective action is

$$S[\Phi, B, G] = \frac{1}{2\kappa_0^2} \int_N d^d x \sqrt{-G} e^{-2\Phi} R - \frac{1}{2\kappa_0^2} \int_N e^{-2\Phi} \left(4 d\Phi \wedge \star d\Phi - \frac{1}{2} dB_2 \wedge \star dB_2 \right) \quad (1.3)$$

When quantized, the bosonic string introduces a graviton multiplet (Φ, B_2, G) consisting of a dilaton, a Kalb-Ramond field and a metric field, which arise respectively as the trace, antisymmetric and traceless symmetric components of the massless (level 1) states. The Newton constant is determined dynamically by the vacuum expectation of the dilaton Φ , $8\pi G_N = k_0^2 e^{2\langle\Phi\rangle} \sim (\ell_s)^{d-2} g_s^2$, while also setting the value for the string coupling $g_s = e^{\langle\Phi\rangle}$. So the only free parameter in the theory is the string tension. In bosonic string theory, we must set the critical dimension $d = 26$ in order to cancel the Weyl conformal anomaly. The mode expansions of the theory require the regularized zero point energy $-a = -(d-2)/24$, as each massless bosonic state contributes with a $-1/12$ factor.

Open strings present the same classical action as in (1.2). However, we will have additional contributions to the sigma-model on the worldsheet boundary $\partial\Sigma$, which is coupled to a gauge connection A_μ . The dynamics depend on which boundary conditions we decide to apply at the endpoints of the string length, parametrized by $\sigma \in [0, \pi]$. If the open string is moving freely in spacetime (only Neumann boundary conditions), we obtain a U(1) Maxwell theory as the tree-level effective action

$$S[A] = -\frac{1}{4g_{\text{YM},0}^2} \int_N e^{-\Phi} F \wedge \star F , \quad (1.4)$$

where $F = dA$. Note that we cannot have open string states without also closed strings, as open strings can interact and join to form closed strings, adding contributions to the sigma-model weighted by $(g_s)^{\delta\chi}$, $\delta\chi = -1$ for open strings and $\delta\chi = -2$ for open strings.

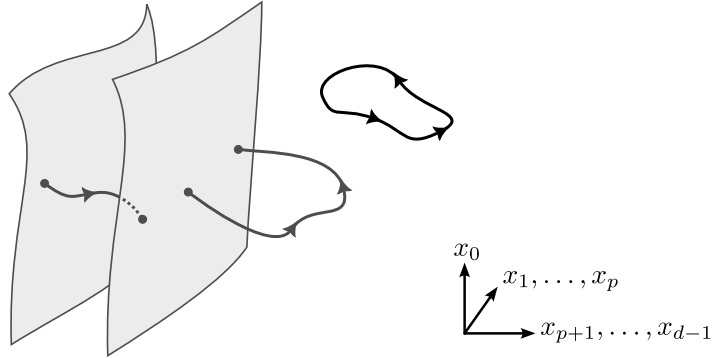


FIGURE 1.1: D-brane depiction as endpoints of open strings.

On the other hand, we can fix some coordinates under Dirichlet boundary conditions and while others obey Neumann or ‘free’ boundary conditions. Specifically, at both ends of the string, the conditions are as follows:

$$\begin{aligned} \partial_\sigma X^a|_{\sigma=0,\pi} &= 0 & \text{for } a = 0, \dots, p & & \text{(Neumann)} \\ X^I|_{\sigma=0,\pi} &= c_{0,\pi}^I & \text{for } I = p+1, \dots, d-1 & & \text{(Dirichlet)} \end{aligned} \quad (1.5)$$

where $c_{0,\pi}^I$ are constants. These conditions anchor the string’s endpoints within a $(p+1)$ -dimensional hypersurface known as a *Dp-brane* (where “D” stands for Dirichlet), breaking the spacetime $\text{SO}(1, d-1)$ Lorentz group symmetry to $\text{SO}(1, p) \times \text{SO}(d-p-1)$ in the process. The $\text{U}(1)$ gauge field A_a , $a \in \{0, \dots, p\}$, represents a spin 1 photon with oscillations longitudinal to the *Dp*-brane and transforming under the $\text{SO}(1, p)$ Lorentz group. The remaining $d-p-1$ string modes constitute a set of scalar perturbations ϕ^I , which can be seen as transverse fluctuations of the brane. From the space-time perspective they are interpreted as Goldstone bosons for the translation invariance spontaneously broken by the D-brane.

These transverse fluctuations led people to realize that string theory is fundamentally about branes, not just strings. D-branes should be regarded as dynamic objects in their own right, extending beyond the concept of strings. For *e.g.*, a D0-brane is equivalent to a point particle, a D1-brane corresponds to a string, and *Dp*-branes could be understood as higher dimensional generalizations of strings. Thus, we can formulate an action that describes the classical dynamics of a D-brane, analogous to the Nambu-Goto action for strings, where we now pullback spacetime quantities by an embedding $X : \mathcal{W} \rightarrow N$, where \mathcal{W} represents the worldvolume spanned by the brane. This leads to the famous Dirac-Born-Infeld action, a generalization of the Born-Infeld action [11],

$$S_{\text{DBI}} = -\tau_p \int_{\mathcal{W}} d\xi^{p+1} e^{-\Phi} \sqrt{-\det(G + B_2 + 2\pi\alpha' F)} \quad , \quad (1.6)$$

where the brane tension is given by $\tau_p = 1/(2\pi)^p \ell_s^{p+1} g_s$. For a flat infinite brane, we can make use of the reparameterization invariance to work in static gauge $X^a(\xi) = \xi^a$, $a \in \{0, \dots, p\}$, we can obtain the free U(1) Maxwell theory coupled to the scalars ϕ^I , obtained by rescaling the transverse coordinates $X^I(\xi) = 2\pi\alpha' \phi^I(\xi)$, demonstrating that D-branes are indeed dynamical. The pullback of the B -field is necessary, as only the combination $B_2 + 2\pi\alpha' F$ is invariant under a gauge transformation.

While the initial bosonic description was successful in describing gravity, the theory failed to describe fermionic matter states. Another inconsistency is the presence of tachyon states as the ground state (level 0). Furthermore, the high number of dimensions $d = 26$ required seems to be not very convincing. Given these inherent limitations, theoretical physicists were compelled to explore supersymmetric extensions that could incorporate fermions onto the worldsheet theory.

Type II strings adds both left and right moving fermionic partners $\psi^\mu(t, \sigma)$ to the bosonic counterparts $X^\mu(t, \sigma)$ in the worldsheet theory. The spacetime is now required to be a $d = 10$ dimensional spacetime due to the same zero-point energy argument as in the bosonic case. In the Ramond-Neveu-Schwarz (RNS) quantization of superstring we have two choices of boundary conditions on fermions: periodic and anti-periodic. This leads to the separation of modes into the Neveu-Schwarz (NS) and Ramond (R) sectors, respectively. Requiring the removal of the tachyonic instabilities combines the states of the two sectors into two distinct ways, which generate two superstring theories: type IIA and type IIB. In both cases

Sector	Fields	SO(8)
(NS ₊ , NS ₊)	dilaton Φ Kalb-Ramond 2-form B_2 graviton G	$\mathbf{8}_v \otimes \mathbf{8}_v = \mathbf{1} \oplus \mathbf{28} \oplus \mathbf{35}_v$
(NS ₊ , R ₋)	Majorana gravitino ψ_L^μ Majorana dilatino λ_L	$\mathbf{8}_v \otimes \mathbf{8}_s = \mathbf{8}_c \oplus \mathbf{56}_c$
(R ₊ , NS ₊)	Majorana gravitino ψ_R^μ Majorana dilatino λ_R	$\mathbf{8}_c \otimes \mathbf{8}_v = \mathbf{8}_s \oplus \mathbf{56}_s$
(R ₊ , R ₋)	1-form gauge field C_1 3-form gauge field C_3	$\mathbf{8}_c \otimes \mathbf{8}_s = \mathbf{8}_v \oplus \mathbf{56}_v$

TABLE 1.1: Massless states in type-IIA string theory

the bosonic fields (Φ, B_2, G) are present, matching the states of the NS-NS sector, being a vector representation $\mathbf{8}_v \otimes \mathbf{8}_v$ of the Lorentz group SO(8), with the same dynamics as in eq. (1.3). These are not the only massless bosonic excitations allowed, as we have additional Ramond-Ramond (RR) fields arising from bispinor representations which decompose into multiple antisymmetric p -forms C_p , with enhanced field strength

$$F_{p+1} = dC_p + C_{p-3} \wedge H_3 \quad (1.7)$$

Sector	Fields	SO(8)
(NS ₊ , NS ₊)	dilaton Φ Kalb-Ramond 2-form B_2 graviton G	$\mathbf{8}_v \otimes \mathbf{8}_v = \mathbf{1} \oplus \mathbf{28} \oplus \mathbf{35}_v$
(NS ₊ , R ₊)	Majorana-Weyl gravitino ψ_L^μ Majorana-Weyl dilatino λ_L	$\mathbf{8}_v \otimes \mathbf{8}_c = \mathbf{8}_s \oplus \mathbf{56}_s$
(R ₊ , NS ₊)	Majorana-Weyl gravitino ψ_R^μ Majorana-Weyl dilatino λ_R	$\mathbf{8}_c \otimes \mathbf{8}_v = \mathbf{8}_s \oplus \mathbf{56}_s$
(R ₊ , R ₊)	scalar field C_0 2-form gauge field C_2 4-form gauge field C_4 (self-dual)	$\mathbf{8}_c \otimes \mathbf{8}_c = \mathbf{1} \oplus \mathbf{28} \oplus \mathbf{35}_c$

TABLE 1.2: Massless states in type-IIB string theory

where $H_3 = dB_2$. In type IIA, we have a 1-form C_1 and 3-form C_3 gauge fields, whereas in type IIB, we have a scalar C_0 , a 2-form C_2 and a 4-form C_4 . However, the C_4 field strength $\tilde{F}_5 = dC_4 - \frac{1}{2}C_2 \wedge H_3 + \frac{1}{2}B_2 \wedge F_3$ is restricted to be self-dual, $\tilde{F}_5 = \star \tilde{F}_5$. See tables 1.1 and 1.2. In both Type IIA and Type IIB string theories, not all D-brane configurations are stable. Stable Dp -branes in the type II string theories are charged under the Ramond-Ramond fields C_{p+1} , with the usual minimal coupling

$$\tau_p \int_{\mathcal{W}} C_{p+1} . \quad (1.8)$$

If a Dp -brane couples electrically to the RR-potential C_{p+1} , there exists also a magnetic dual $(7-p)$ -form \tilde{C}_{7-p} , such that $\tilde{F}_{9-p} = \star F_{p+1}$. From the available RR fields we can see that type IIA contains only p -even D-branes: a D0-brane (point particle), a D2-brane and their magnetic duals, a D6-brane and D8-brane.¹ Similarly, type IIB has only p -odd D-branes: a D1-string with magnetic dual D5-brane, a self-dual D3-brane, and there is an D(-1) instanton with a D7-brane magnetic dual.

$$\begin{aligned} \text{IIA} & : \text{D0, D2, D4, D6, D8, F1, NS5} \\ \text{IIB} & : \text{D(-1), D1, D3, D5, D7, D9, F1, NS5} \end{aligned} \quad (1.9)$$

The fundamental string (F-string) is a shared object in both string theories, with a tension $\tau_{\text{F1}} = 1/(2\pi\alpha')$, distinct from the D1-string from type IIB. Furthermore, instead of interacting with a RR potential, it couples electrically with the gauge-invariant NS-NS 2-form potential $B_2 + 2\pi\alpha'F$,

$$\tau_{\text{F1}} \int_{\Sigma} B_2 + \int_{\partial\Sigma} A_1 . \quad (1.10)$$

¹The D9-brane and the D8-brane are exceptions. D9-brane is non-dynamical and D8-brane is equivalent to a domain-wall solution that magnetically generates a locally constant F_0 .

(The second term, required by gauge invariance, implies that endpoints in $\partial\Sigma = W_1 \sqcup (-W'_1)$ form worldlines of point particles charged $+1/-1$.) By spacetime Hodge duality, we can find a NS-NS B_6 form ($dB_6 = \star dB_2$) which naturally couples to a world-volume of a 5-brane. This NS-NS object is the NS5-brane, which the magnetic dual of the fundamental string.

Type IIA and type IIB string theories transform into each other under *T-duality* [6–8, 10]. Specifically, a type IIA string theory compactified on a circle of radius R is equivalent to type IIB on a circle of radius α'/R . Considering a closed string moving in a spacetime $X^9 \times S^1$ with one dimension compactified on a circle S^1 of radius R , the string will have momentum modes with quanta $p_n = n/R$ and winding modes $w_m = mR/\alpha'$, where $n, m \in \mathbb{Z}$. The mass spectrum and level matching condition of the string are given by

$$\begin{aligned} M^2 &= \frac{n^2}{R^2} + \frac{m^2 R^2}{\alpha'^2} + \frac{2}{\alpha'}(N + \tilde{N} - 2) \\ 0 &= N - \tilde{N} + nm \end{aligned} \tag{1.11}$$

which are invariant under the exchange

$$n \leftrightarrow m \quad , \quad R \leftrightarrow \frac{\alpha'}{R} . \tag{1.12}$$

When applying T-duality to open strings, it can be shown that a Neumann boundary condition, which allows the string endpoint to move freely along S^1 , transforms into a Dirichlet boundary condition in the dual theory. Conversely, it also changes Dirichlet boundary conditions into Neumann. In terms of D-branes, it implies that a Dp -brane maps into a $D(p-1)$ -brane in the dual theory if the dualized circle lies in the original worldvolume. On the other hand, Dp -brane turns into a $D(p+1)$ -brane under a transverse T-duality. Additionally, RR gauge potentials change from C_{p+1} to p -forms and $p+2$ forms in a manner consistent with the D-brane mapping under T-duality. This transformation is consistent with the stable p -even/ p -odd configurations of Dp -branes in type IIA/B.

T-duality also acts in the NS-NS sector, mixing the B_2 -field and the metric $G_{\mu\nu}$, while rescaling the string coupling

$$g_s \leftrightarrow \frac{\ell_s}{R} g_s . \tag{1.13}$$

This mixing has consequences on how T-duality impacts NS5-branes. Starting from a spacetime with no NS5-branes, *i.e.*, $B_2 = 0$, if we dualize along a circle that shrinks in the spacetime geometry, we can go from a purely geometric configuration to one with NS5-branes where the original circle shrinks. The converse also holds. Dualizing along the worldvolume of the NS5-brane, T-duality simply maps a type IIA NS5-brane to a IIB NS5-brane and vice versa.

1.1.2 Quivers from D-brane stacks

Engineering gauge theories using D-branes has become a cornerstone in modern theoretical physics [12–14]. By arranging multiple D-branes in specific configurations, researchers have been able to generate diverse gauge field theories and interactions, with the objective of getting insights into low-energy physics and the fundamental structure of spacetime. By placing N parallel D-branes of the same type, open strings have now N^2 options on which brane the endpoints should attach to, giving rise to a $U(N)$ gauge connection. This is an enhancement from the $U(1)$ case in the bosonic action (1.4), where the diagonal elements are $U(1)$ gauge bosons and the W-bosons-like off-diagonal elements carry $(+1, -1)$ or $(-1, +1)$ charge under $U(1)_n \times U(1)_m$ (see eq. (1.10)).

A common method to engineer gauge theories is by placing a parallel stack of D3-branes with worldvolume spanning 4-dimensional $\mathbb{R}^{1,3}$, and transverse to a 3-complex-dimensional Calabi-Yau (CY₃) manifold \mathcal{Y} . From this perspective, the D3-brane can be thought as a point particle probing the geometry of the CY₃. If the point being probed is locally smooth, the worldvolume gauge theory is four-dimensional maximally supersymmetric Yang-Mills [15]. In $\mathcal{N} = 1$ supersymmetry notation, the $\mathcal{N} = 4$ multiplet splits into a $\mathcal{N} = 1$ vector multiplet and three chiral multiplets $\{\Phi_i\}_{i=1,2,3}$ interacting via a superpotential

$$W = \text{Tr } \Phi_1 [\Phi_2, \Phi_3] \quad (1.14)$$

where a trace on gauge indices is taken. From the $\mathcal{N} = 1$ point-of-view, we can think of this gauge theory as the simplest quiver gauge theory, where the quiver diagram is a node for the gauge group $U(N)$ and 3 incoming/outgoing arrows from the single node representing the 3 adjoint fields.

	0	1	2	3	4	5	6	7	8	9
D3	○	○	○	○						
CY ₃					○	○	○	○	○	○

TABLE 1.3: Brane configuration in 9+1 dimensions in IIB string theory. D3-branes are transverse to and are represented by a point in the CY 3-fold.

However, historically, the original motivation for studying quiver gauge theories comes from D3-branes configurations probing singular Calabi-Yau 3-folds. The simplest example stems from groundbreaking work by Douglas and Moore [16, 17] on ALE (Asymptotically Locally Euclidean) spaces, resulting in the emergence of 4-dimensional $\mathcal{N} = 2$ superconformal gauge theories as the low-energy effective field theory on the D3-branes worldvolume. The ALE spaces locally resemble the orbifold \mathbb{C}^2/Γ , where Γ is a discrete subgroup of $SU(2)$, which is labelled using the ADE classification (named after the A_n , D_n , and E_n families), as they line perfectly with the classification of semisimple simply-laced Lie algebras.

Toric Calabi-Yau 3-fold singularities accept crepant resolutions by blowing-up a combination of 2-cycles and/or 4-cycles [18, 19]. In the ALE case, resolving the singularity introduces 2-cycles intersecting according to the Dynkin diagram of the associated A/D/E algebra. Wrapping D5-branes on each such 2-cycle leads to a $\mathcal{N} = 2$ vector multiplet ($\mathcal{N} = 1$ vector plus $\mathcal{N} = 1$ adjoint chiral), arising from open strings extending between two D5-branes in a given stack. Open strings extending between D5-branes wrapping two distinct but intersecting stacks of D5-branes leads to a $\mathcal{N} = 2$ hypermultiplet (two conjugate $\mathcal{N} = 1$ chiral multiplets) in the bifundamental representation of the two gauge groups. The structure of vector and hyper multiplets is encoded in the simply laced Dynkin diagram of the associated A/D/E Lie algebra. One can also wrap an anti-D5-brane on the sum of the above 2-cycles, with -1 unit of worldvolume gauge flux: this extends the finite A/D/E Dynkin diagram to the corresponding affine A/D/E Dynkin diagram, which has one extra node. Nodes of the affine Dynkin diagram encode the gauge groups ($\mathcal{N} = 2$ vector multiplets), edges encode the matter content ($\mathcal{N} = 2$ hypermultiplets in the bifundamental representation). If we have N wrapped

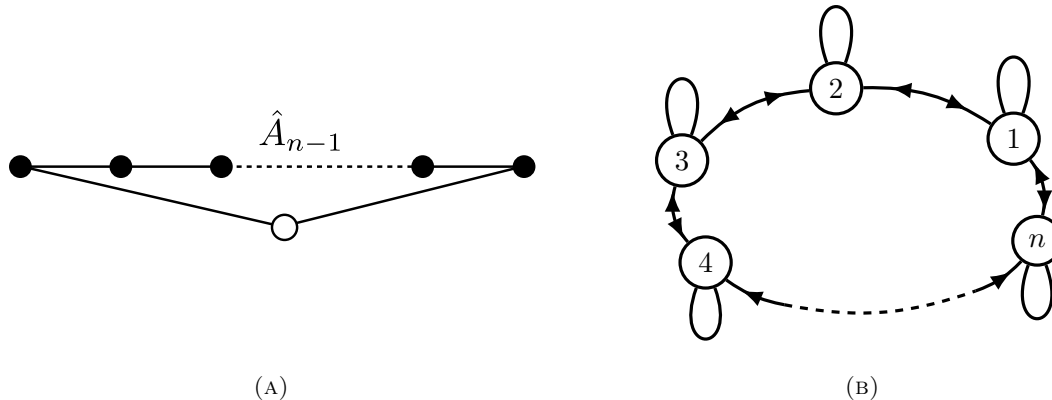


FIGURE 1.2: Affine Dynkin diagram for the A_{n-1} family (a) leading to the quiver for the $\mathbb{C}^2/\mathbb{Z}_n \times \mathbb{C}$ quiver gauge theory.

D-branes of each type, then the quiver diagram will have a $U(N)$ gauge factor for each node in the affine Dynkin diagram. Switching to $\mathcal{N} = 1$ notation where circles denote $\mathcal{N} = 1$ vector multiplets and arrows denote $\mathcal{N} = 1$ chiral multiplets in a bifundamental representation, each circle in the affine Dynkin diagram is replaced by a circle with an arrow forming a loop, and each edge is replaced by a pair of oppositely oriented arrows. This is the quiver diagram encoding the gauge group and matter content of the theory, exemplified in fig. 1.2.

The same conclusion is reached by directly quantizing open strings in the singular orbifold, with no need to resolve the geometry. In the orbifold limit, the 2-cycles shrink and the above wrapped D5-branes are mapped to so-called *fractional D3-branes* [18, 20]. The world-volume theory probing a \mathbb{C}^3/Γ orbifold, with $\Gamma \subset SU(3)$, is determined by the action of the regular representation of Γ acting on the D-brane stack, and by specifying the action of the finite

subgroup on \mathbb{C}^3 as

$$\rho(g) : \mathbb{C}^3 \rightarrow \mathbb{C}^3 \quad z^i \mapsto \rho(g)^i_j z^j . \quad (1.15)$$

Furthermore, the regular representation of Γ , $\gamma(g)$, acts on the bosonic adjoint fields with the transformation law

$$\gamma(g) A_\mu \gamma(g)^{-1} = A'_\mu \quad \gamma(g) Z^i \gamma(g)^{-1} = \rho(g)^i_j Z'^j \quad (1.16)$$

where the sums over the Chan-Paton indices are implicit. Note that the complex fields Z^i transform in the same way as \mathbb{C}^3 coordinates, since the diagonal of Z^i represent transverse perturbations of each of the D-branes along z^i . The regular representation of the finite group is reducible, with decomposition $\gamma = \bigoplus_{a=1}^{|\Gamma|} \dim(\gamma_a) \gamma_a$, such that $|\Gamma| = \sum_{a=1}^{|\Gamma|} \dim(\gamma_a)^2$. Invariance under the action (1.16) requires the gauge field A_μ to be in a block diagonal form. As such, we can interpret the gauge theory resulting from N D3-branes probing an orbifold singularity as a $4d \mathcal{N} = 4$ U($|\Gamma|N$) on \mathbb{C}^3 , the $|\Gamma|$ -cover of \mathbb{C}^3/Γ , where we project the gauge symmetry down to

$$\prod_{a=1}^{|\Gamma|} \text{U}(k_a N) , \quad k_a = \dim(\gamma_a) . \quad (1.17)$$

The quiver arises from the decomposition $\gamma \otimes \gamma_i = \bigoplus_{a=1}^{|\Gamma|} a_{ij} \gamma_j$ where γ_i maps to the quiver node i and Dynkin diagram, and a_{ij} is adjacency between nodes. For the orbifold \mathbb{C}^2/Γ , with $\Gamma \subset \text{SU}(2)$, this is the McKay quiver, and the McKay correspondence [21] is the extended (affine) Dynkin diagram of the associated simple Lie algebra.

For example, the abelian orbifold with the \hat{A}_{n-1} quiver in fig. 1.2b is a particular case where the finite subgroup $\Gamma = \mathbb{Z}_n$ acts solely on the coordinates (z_1, z_2) . In order for the orbifold to be Calabi-Yau, we require the complex and Kähler structures to be preserved under the action of \mathbb{Z}_n , fixing the action of \mathbb{C}^3 to $\rho(g)(z_1, z_2, z_3) = (gz_1, g^{-1}z_2, z_3)$. The regular representation $\gamma(g)$ permutes the D3-branes cyclically with the action,

$$\gamma(g) = \begin{pmatrix} 0 & 0 & \cdots & 0 & 1 \\ 1 & 0 & \cdots & 0 & 0 \\ 0 & 1 & \cdots & 0 & 0 \\ \vdots & \vdots & \ddots & \vdots & \vdots \\ 0 & 0 & \cdots & 1 & 0 \end{pmatrix} \quad \gamma(g^k) = \gamma(g)^k \quad (1.18)$$

which decomposes into 1-dimensional (character) representations $\gamma_a(g) = g^a$. Fractional D3-branes of a -type are states localized at the singularity that transform into an irreducible representation γ_a of \mathbb{Z}_n . The invariance on the bosonic fields Z^i under \mathbb{Z}_n requires most of its

components to vanish and the fields to take the form,

$$Z^1 = \begin{pmatrix} 0 & 0 & \cdots & 0 & \phi_{n,1} \\ \phi_{21} & 0 & \cdots & 0 & 0 \\ 0 & \phi_{32} & \cdots & 0 & 0 \\ \vdots & \vdots & \ddots & \vdots & \vdots \\ 0 & 0 & \cdots & \phi_{n,n-1} & 0 \end{pmatrix} \quad Z^2 = \begin{pmatrix} 0 & \phi_{12} & 0 & \cdots & 0 \\ 0 & 0 & \phi_{23} & \cdots & 0 \\ \vdots & \vdots & \vdots & \ddots & \vdots \\ 0 & 0 & 0 & \cdots & \phi_{n-1,n} \\ \phi_{1,n} & 0 & 0 & \cdots & 0 \end{pmatrix} \quad (1.19)$$

while the last field must be diagonal, $Z^3 = \text{diag}(\phi_1, \phi_2, \dots, \phi_n)$. We can obtain the non-trivial superpotential by expanding the 4d $\mathcal{N} = 4$ superpotential in eq. (1.14) and restoring the $\mathcal{N} = 1$ supersymmetry to the fields. The superpotential for the \hat{A}_{n-1} quiver can be written as

$$W = \text{Tr} \sum_{a=1}^n \Phi_a (X_{a,a-1} X_{a-1,a} - X_{a,a+1} X_{a+1,a}) \quad (1.20)$$

Note that ϕ_{ab} are the complex scalars in a $\mathcal{N} = 1$ chiral multiplet X_{ab} , which transform under the bifundamental representation of $U(k_a N) \times U(k_b N)$. On the other hand, ϕ_a are the scalar components of $\mathcal{N} = 1$ $U(k_a N)$ adjoint superfields Φ_a .

1.1.3 Toric singularities and brane tilings

Quiver gauge theories describing the low-energy dynamics on D-branes probing singularities have been extensively studied for more than 25 years [12–17, 22–27], particularly in the context of the AdS/CFT correspondence [28, 29] and for model building in string theory [30, 31]. Engineering strongly coupled field theories in this way allows for the geometrization of many of their properties, which are otherwise difficult to access directly in field theory. Conversely, understanding the field theories from first principles can shed light on aspects of the associated geometry.

One class of singularities that have been central to these studies are toric Calabi-Yau 3-folds.² These are irreducible varieties containing a torus \mathbb{T}^3 as a dense open subset and a torus automorphism action which extends naturally to the entire space. The worldvolume theory of a stack of D3-branes probing a toric CY cone is a 4d $\mathcal{N} = 1$ quiver gauge theory. In the context of AdS/CFT, backreaction of $N \gg 1$ D3-branes leads to near-horizon $AdS_5 \times X_5$ geometry [24, 32–36], where X_5 is a Sasaki-Einstein manifold X_5 that is the base of the original CY 3-fold cone. The geometries contain a $U(1)^3$ isometry dual to a rank 3 global (mesonic) symmetry in the gauge theory, with a $\mathcal{N} = 1$ $U(1)$ R-symmetry as a subgroup, generated by the Reeb vector of the Sasaki-Einstein manifold. From the toric geometry perspective, we can see the CY_3 a “complex” cone over a 2-dimensional toric surface, where X_5 can be thought as of a S^1 fibration over this space. Toric geometry provides a simple framework for describing and constructing these surfaces, encoded in a combinatorial object called a toric

²In particular, the abelian orbifolds \mathbb{C}^3/Γ for $\Gamma = \mathbb{Z}_n$ or $\Gamma = \mathbb{Z}_n \times \mathbb{Z}_m$ already fall in this category.

fan. In particular, in physics, we describe the same data using a toric diagram Δ , a convex lattice polytope in 2 dimensions.

The D3-brane stack setup on a singular toric cone preserves (at least) $\mathcal{N} = 1$ supersymmetry in four dimensions. Finding the quiver (matter content) and superpotential for a general singularity is usually a difficult task. However, this data is related to the holomorphic (complex) structure of the Calabi-Yau 3-fold and independent of the symplectic structure (encoded in the Kähler potential), thus it can be computed in the resolved singularity [19, 25, 37–39].

Brane tilings [40–44], also known as dimer models in the statistical mechanics and probability literature [45, 46], provide an alternative to encode the quiver and the superpotential of the $\mathcal{N} = 1$ quiver gauge theory that arises from D3-branes probing toric CY 3-folds. The brane tiling is represented as a periodic bipartite graph on a two-dimensional torus \mathbb{T}^2 , where each edge maps to an arrow (bifundamental field) in the quiver and each face in the tiling corresponds to a node/circle in the quiver (gauge group). The tiling also encodes the superpotential, as each loop surrounding a white or black node in the tiling corresponds to a term in the superpotential with a specific sign, determined by the orientation of the loop.

The combinatorial structure of the brane tiling provides a simpler way to obtain the geometric data (toric diagram), via the forward algorithm [40, 41]. Conversely, obtaining quivers from a toric diagram is known as the inverse algorithm [43, 47], which is generally more complicated as the correspondence is one-to-many. A toric diagram may give rise to more than one quiver gauge theory, related by toric-Seiberg duality, known as the different toric phases of the geometry [48–52].

The brane tiling is itself a physical system composed of D5 and NS5-branes in a type-IIB string theory background. This background is twice T-dual to the D3 stack probing the toric CY manifold. Under the double T-duality, the D3-branes are mapped to D5-branes, and the toric CY 3-fold geometry is mapped to an NS5-brane wrapping a holomorphic surface defined by the zero locus of the Newton polynomial

$$P(z, w) = \sum_{(a,b) \in \Delta} c_{a,b} z^a w^b \quad (1.21)$$

associated with the toric diagram Δ . Here, the parameters $c_{a,b}$ encode the symplectic structure moduli of the original CY manifold. This configuration is summarized in the brane setup in table 1.4. The D5-branes span the (0123) directions, while wrapping the (57)-coordinates of the 2-torus, while the holomorphic surface Σ is embedded in a $(\mathbb{C}^\times)^2$ with complex coordinates $z = e^{x_4 + ix_5}$, $w = e^{x_6 + ix_7}$.

In this configuration, the D5 stack wraps the 2-torus and the NS5 brane intersects the D5-brane along various cycles, whose directions on the torus match the outward normals of the toric diagram facets (see fig. 1.3). The NS5-brane can also run parallel to the N stack of D5-branes, subdividing the torus into regions of bound states of $(N, 0)$ and $(N, \pm 1)$ of D5/NS5-branes.

	0	1	2	3	4	5	6	7	8	9
D5	○	○	○	○		○		○		
NS5	○	○	○	○	— Σ —					

TABLE 1.4: 5-brane configuration in 9+1 dimensions in IIB string theory, equivalent to D3-branes probing a toric Calabi-Yau singularity after T-dualizing the 2 circles on the 57-directions. NS5-brane wraps a Riemann surface Σ .

Massless open strings extend between the $(N, 0)$ 5-branes, giving rise to the quiver structure, where the $(N, 0)$ regions match the gauge groups, *i.e.* the faces in the tiling. The bipartite nature of the dimer manifest itself by interpreting the $(N, \pm 1)$ regions as corresponding to white and black nodes, respectively, in the tiling.

A more modern interpretation [43] of the brane tiling is as the skeleton graph of the coamoeba projection of the spectral curve defining Σ . This projection is defined by taking the surface Σ and mapping it onto the 2-torus via

$$\text{Arg} : (\mathbb{C}^\times)^2 \rightarrow \mathbb{T}^2 \quad (z, w) \mapsto (\text{Arg}(z), \text{Arg}(w)) \quad (1.22)$$

When varying the moduli $c_{(a,b)} \in \mathbb{C}^\times$ defining the shape of Σ , the coamoeba can take different skeleton structures, which corresponds to going to a new toric phase. On the other hand,

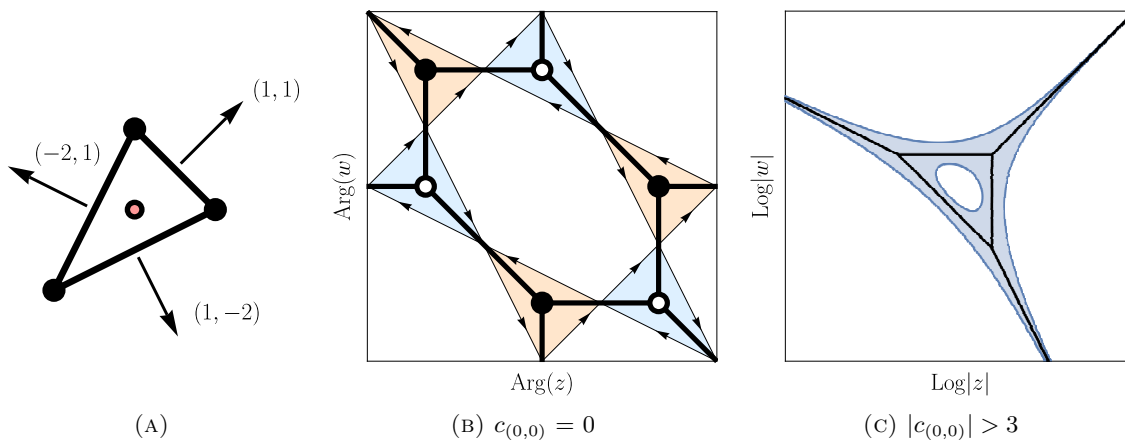


FIGURE 1.3: Toric diagram (a), coamoeba (b) and amoeba (c) projections of the Σ curve for orbifold geometry $\mathbb{C}^3/\mathbb{Z}_3$. Normals of the toric diagram (a) map to NS5 cycle intersection that wrap \mathbb{T}^2 , as well as defining the (p, q) -legs in (c). Brane tiling in (b) is obtained by mapping $(N, \pm 1)$ regions (blue/orange) to white/black nodes.

the skeleton (or tropicalization) of the amoeba projection, where $(z, w) \in \Sigma$ is mapped to $(\text{Log}(z), \text{Log}(w))$, has the physical interpretation of a web of (p, q) 5-branes in type IIB string theory [53, 54].

1.2 Thesis outline

In this section, we summarize the structure of the thesis. The remaining chapters are organized as follows:

In chapter 2, we review mathematical concepts and results in algebraic geometry, toric geometry, and quiver representation theory, which arm the reader with the tools behind the computations and algorithms presented in this work. We begin with a discussion on rings, ideals, and varieties, explaining the structure of polynomial rings, ideals, and their geometric interpretations as algebraic sets, specifically affine varieties. The chapter then moves to toric varieties, describing (with examples) how they can be constructed using combinatorial data like cones and fans. This section concludes with a discussion of toric Calabi-Yau affine cones and their associated toric diagrams. In the second section, we provide a concise introduction to the structure and properties of quiver representations and quiver path algebras, which are crucial for understanding the moduli of toric quiver gauge theories. Using quiver data, we explore the construction of moduli spaces via Geometric Invariant Theory (GIT) and symplectic reduction, which are related by the famous Kempf-Ness theorem. Finally, we define the stability of quiver representations using the θ -stability criterion, which is heavily used in a later chapter.

In chapter 3, we explore quiver gauge theories from the perspective of 4d $\mathcal{N} = 1$ supersymmetric gauge theories and their representation through quiver diagrams and brane tilings. It presents the basics of supersymmetric gauge theory and reviews how brane tilings encode the quiver and the superpotential. We then describe the various components of the moduli space of vacua of quiver gauge theory, as well as the fast-forward method that quickly obtains the toric data ($U(1)^3$ mesonic charges). Finally, we examine dualities of brane tilings, such as toric-Seiberg and specular dualities, which relate different quiver theories and provide insights into the moduli spaces of these theories.

In chapter 4, we delve into superpotential deformations in D3-brane worldvolume theories on (pseudo) del Pezzo geometries. We define the zig-zag operator, uniquely defined by a zig-zag path. This operator parametrizes a one-parameter family of deformations of the toric quiver gauge theory, which preserve $U(1)^2$ symmetry for generic values of the deformation parameter, and interpolate between two toric endpoints. In particular, we focus on the study of geometries with reflexive toric diagrams, whose deformations are summarized in fig. 1.4 and details in appendix A. Leveraging specular duality of brane tilings (related to Mirror Symmetry), we establish a connection between zig-zag deformations and toric-Seiberg dualities.

In chapter 5, we continue the study of zig-zag deformations, exploring the consequences of the deformation in crepant resolutions instead of the of singular Calabi-Yau cones. We explain how different resolutions of these singularities are in correspondence with Kähler chambers, which are convex conical regions of the valid (stable moduli) real-valued Fayet-Iliopoulos (FI)

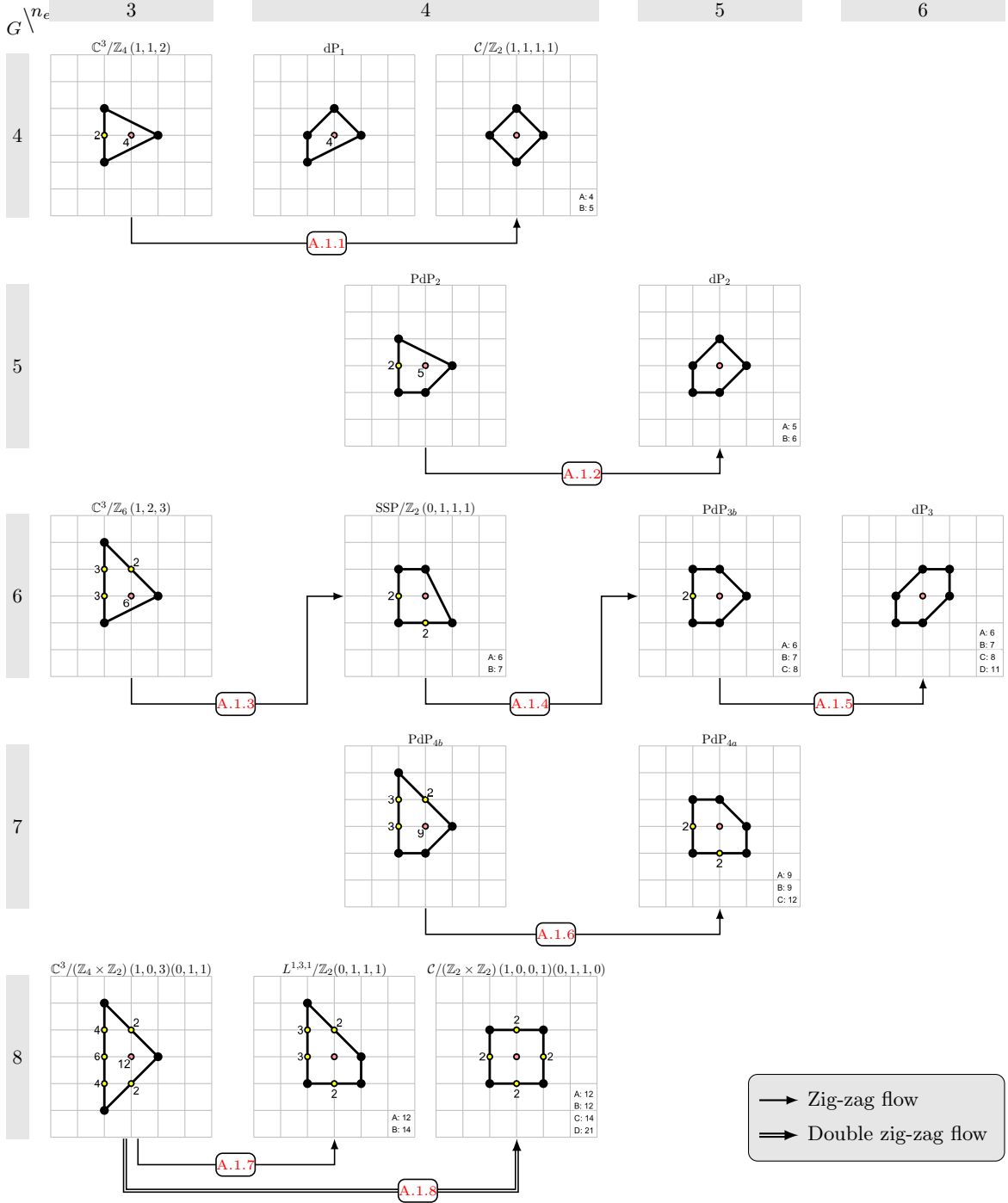


FIGURE 1.4: Toric-to-toric 4d $\mathcal{N} = 1$ RG flows, connecting geometries with reflexive toric diagrams via zig-zag deformations. Rows and columns are organized by the number of nodes G in the quiver and the number of extremal points n_e in the polytope, following [55]. Links in the arrows point to details in appendix A.

parameters in that resolution. The chapter further delves into the use of dimer models and perfect matchings to construct these resolutions, offering detailed examples for del Pezzo surfaces. Finally, we describe how zig-zag deformations in the brane tiling are related to Hanany-Witten moves in the corresponding (p, q) -webs.

In chapter 6, we extend the ideas of the zig-zag deformation to other 4d $\mathcal{N} = 1$ quiver gauge theories whose mesonic moduli are described by a non-reflexive polytope. We elaborate on the conditions on which we can still obtain a flows to a toric dimer model. We explain the algorithms that explicitly find the field redefinition that explicitly recovers the toric F-term condition of the IR theory, and also find all toric phases. We apply these algorithms to find the map all 1-parameter deformations between toric phases of quiver gauge theories described by toric diagrams with 2 internal points.

Chapter 7 includes discussion about the results and possible future directions.

1.3 Code developed

Brane tilings on abelian orbifolds have sufficient structure in the quiver to allow computations to be performed manually. However, as we move on to toric diagrams with one or more internal points, these computations become prohibitively complex and prone to human error. Therefore, during this thesis, we developed a comprehensive set of modules (Mathematica [56] packages) to assist with and greatly automate operations related to brane tilings and dimer models:

- **QuiverGaugeTheory** [2]: During this work, we needed to regularly compute all sort of properties based on the dimer model/brane tiling (\mathcal{Q}, W) in question. This package is a collection of methods to extract and compute properties of dimer models. The package contains algorithms for obtaining toric diagram, chiral rings, mesonic generators, toric phases, full resolutions (polytope triangulations), Kähler chambers, dual cones, along many other properties. Graphically, it contains methods that generate brane tilings and quiver from a superpotential input and (p, q) -webs from a polytope triangulation data.
- **InterfaceM2** [3]: This is a small interface with Mathematica and Macaulay2 [57], a command line interface (CLI) program for computational algebraic geometry. The core code evaluates commands and interprets the output from a Macaulay2 process running in the background. On top this functionality, the package has a limited set of specific methods that access relevant algorithms not present in Mathematica. For *e.g.*, the method `PrimaryDecompositionM2` allows the primary decomposition of an ideal by generating the necessary code to be sent via the interface, in which the output is converted back the original representation in Mathematica.

Furthermore, collaboration with my supervisor and F. Carta on the superconformal index of del Pezzo quivers was not included in the thesis. From this collaboration a Mathematica package with relevant applications in the theoretical physics community was developed.

- **LieACh** [4]: LieART [58] is a recognized package in the Physics community designed for Mathematica, which facilitates calculations commonly encountered within the domain of Lie algebras and Lie algebra representation theory. It allows the decomposition of tensor products, root systems of Lie algebras, weight systems and the branching of irreducible representations into subalgebras. The LieACh package is built on top of LieART to provide support for 1-dimensional representations of Lie algebras, *i.e.*, character representations. Many computations in the theoretical physics and field theory lead to large polynomial expressions that help count states and/or operators (*e.g.* superconformal indices or Hilbert series). These states/operators are organized into characters of representations of a semisimple Lie algebra, *i.e.*, as a formal sum of irreducible representations (irreps):

$$\mathcal{I}(z_1, \dots, z_r) = \sum_{\Lambda} a_{\Lambda} \chi_{\Lambda}(z_1, \dots, z_r)$$

Using known Lie algebra representation theory [59], we were able to implement a fast method that extracts the (Λ, a_{Λ}) pairs with the highest weight that classifies the irrep and the associated coefficient a_{Λ} .

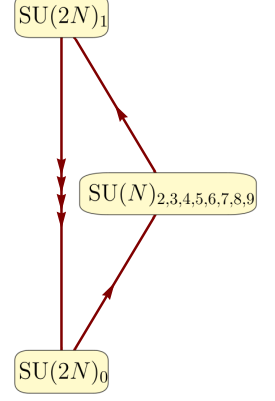
We utilized the LieACh package to track dibaryon states of *del Pezzo* quivers. Briefly explained,³ this counting is achieved via the superconformal index [60–64], a Witten index traced over the Hilbert space of the radially quantized theory on S^{d-1} . Canceling out nonzero energy states enables us to derive the 4d $\mathcal{N} = 1$ index on $S^3 \times S^1$,

$$\mathcal{I}(p, q, \mu_i) = \text{Tr} (-1)^F p^{\frac{R}{2} + J_1^3 + J_2^3} q^{\frac{R}{2} + J_1^3 - J_2^3} \prod_i z_i^{C_i} . \quad (1.23)$$

Here, R represents the generator of the $U(1)$ superconformal R-charge, and $J_{1,2}^i$ are the generators of the $\mathfrak{su}(2)_1 \times \mathfrak{su}(2)_2$ Lorentz symmetry. Additionally, C_i denotes the Cartan generators of the global symmetries. This trace can be written in a closed form: chiral and vector multiplets contribute to the index through infinite products, via the use of elliptic gamma functions $\Gamma(p, q; z)$. The result is then often expanded in a series of the fugacity $t = (pq)^{\frac{1}{2}}$, which captures the charges of $R + 2J_1^3$. We obtained high order expansions for *del Pezzo* n quivers (degree $9 - n$), where the baryonic symmetry enhances to the exceptional family $E_{3 \leq n \leq 8}$, where $E_3 = A_2 \times A_1$, $E_4 = A_4$, and $E_5 = D_5$. For *e.g.*, the index for the *del Pezzo* 7 quiver for nodes with $N = 2$ is given by

³Not in the scope of the thesis.

$$\begin{aligned}
\mathcal{I}_{\text{dP}_7}^{N=2} = & 1 + (10 + [0000010]_z)t^2 + [0000010]_z[1]_u t^3 \\
& + \left(43 + [1000000]_z \right. \\
& \quad \left. + 8[0000010]_z + [0000020]_z + [0000010]_z[2]_u \right)t^4 \\
& + \left(19[1]_u - [1000000]_z[1]_u + [0000100]_z[1]_u \right. \\
& \quad \left. + 9[0000010]_z[1]_u + [0000020]_z[1]_u + [0000010]_z[3]_u \right)t^5 \\
& + O(t^6) ,
\end{aligned}$$



where $u = p/q$ represents the $\mathfrak{su}(2)_2$ fugacity, and $z = (z_1, \dots, z_7)$ are the fugacities of the exceptional E_7 baryonic symmetry. For instance, in the term, $[0 \dots 010]_z t^{2N/(9-n)}$ we observe the dibaryons associated to (-1) -degree rational curves in the del Pezzo surface. This example is a few thousand terms long but utilizing the aforementioned package we managed to simplify the expression into irreducible characters of the Lie algebra $E_7 \times A_1$. We note that we reproduced representations of the exceptional symmetry group using the quiver gauge theory with superpotential, with no need to postulate a completion of *incomplete* representations as suggested in [65].

Part I

Review of concepts

Chapter 2

Mathematical preliminaries

2.1 Toric geometry

2.1.1 Rings, ideals and varieties

A commutative *ring* [66, 67] is a set of elements R equipped with addition $+$: $R \times R \rightarrow R$ and multiplication \cdot : $R \times R \rightarrow R$, both associative operations, such that $(R, +)$ forms an abelian group and multiplication is commutative, *i.e.*, $a \cdot b = b \cdot a$, for all $a, b \in R$. Contrary to a field, non-zero elements do not need to be units (that is, have a multiplicative inverse).

Let k be an algebraically closed field, for example \mathbb{C} . A *polynomial ring* $k[x]$ is an extension of the ring k by an element x , defined as the set of expressions¹

$$a_0 + a_1x + \cdots + a_dx^d, \quad d \in \mathbb{N} \tag{2.1}$$

where $a_0, a_1, \dots, a_d \in k$, with appropriate addition and multiplication operations. Inductively, we can define a multivariate polynomial ring $k[x_1, \dots, x_n] = k[x_1, \dots, x_{n-1}][x_n]$. The polynomial ring $R = k[x_1, \dots, x_n]$ is also an associative k -algebra, meaning it has a vector space multiplication by scalars $k \times R \rightarrow R$.²

An *ideal* I of a ring R is a subset of elements, $I \subseteq R$, such that $(I, +)$ forms a subgroup of $(R, +)$ and is closed under multiplication; that is, for $b \in I$, then $a \cdot b \in I$, for all $a \in R$. It is worth noting that every subring of R naturally contains the multiplicative identity $1 \in R$, so if $1 \in I$, then the ideal is the ring itself, $I = R$.

Given an ideal of a polynomial ring $I \subseteq R = k[x_1, \dots, x_n]$, it can be expressed as

$$I = \langle f_1, \dots, f_m \rangle = Rf_1 + \cdots + Rf_m, \tag{2.2}$$

¹We use the convention $\mathbb{N} = 0, 1, 2, \dots$ to denote the semigroup of nonnegative numbers.

²We will use the terms "ring" and " k -algebra" loosely, assuming the underlying rings have a vector space structure over some base/ground ring/field k .

for some set of generators $f_1, \dots, f_m \in R$. This ideal has an intuitive interpretation in terms of the system of polynomial equations $f_1 = \dots = f_m = 0$. We can build further relations $h_1 f_1 + \dots + h_m f_m \in I$, given $h_1, \dots, h_m \in R$, which also vanish as a consequence of the first set of equations. Furthermore, with an ideal $I = \langle f_1, \dots, f_m \rangle$ we can define the quotient ring R/I by defining an equivalence relation $f \sim g \iff f - g \in I$, for $f, g \in R$, with equivalence classes $[f] = \{f + h \mid h \in I\} = f + I$.

Verifying if an element of $R = k[x_1, \dots, x_n]$ is in some ideal $I = \langle f_1, \dots, f_m \rangle$ can be a daunting task, especially for a larger number of variables. Usually it starts by performing the polynomial division algorithm such that

$$f = q_1 f_1 + \dots + q_m f_m + r, \quad (2.3)$$

for some quotients $q_1, \dots, q_m \in R$ and a remainder $r \in R$. However, while the condition $r = 0$ is sufficient to guarantee that $f \in I$, we still might get nonzero remainders where f is an element of the ideal, when dividing by the above set. Computationally, this ambiguity is solved by determining a *reduced Gröbner basis* [66] of the ideal I , which is an ordered tuple $G = (b_1, \dots, b_s)$ that still generates the initial ideal $I = \langle G \rangle = \langle b_1, \dots, b_s \rangle$. When f is divided by a Gröbner basis G , the remainder is called the *normal form* \bar{f}^G , which is unique with respect to G and has the property that its leading term is not divisible by the leading term of any polynomial in the basis.³ A Gröbner basis provides a way to test membership in the ideal, *i.e.*, by checking $\bar{f}^G = 0$, but also simplifies systems of polynomial equations and performs other computations more efficiently than using the original generators of the ideal.

By Hilbert's basis theorem, polynomial algebras $R = k[x_1, \dots, x_n]$ are noetherian, which implies that every ideal is finitely generated, as in eq. (2.2). This constraint is equivalent to ensuring that ideals obey the Ascending Chain Condition (ACC): for a chain of ideals $I_1 \subseteq I_2 \subseteq I_3 \subseteq \dots$, we require that

$$I_1 \subseteq I_2 \subseteq \dots \subseteq I_N = I_{N+1} = \dots, \quad (2.4)$$

meaning that for all $j \geq N$ in the ideal chain, $I_j = I_N$. In other words, after a certain point, all the ideals in the chain are the same, and the chain doesn't keep growing indefinitely. This implies that every ideal of a polynomial ring is contained in a *maximal ideal* $\mathfrak{m} \subsetneq R$. Maximal ideals are defined such that there is no other proper ideal $J \subsetneq R$ where \mathfrak{m} is also a proper subset of J , *i.e.*, $\mathfrak{m} \subsetneq J$. The set of maximal ideals of a ring R is denoted as the *maximal spectrum* $\text{Specm } R$.

Given a polynomial algebra $R = k[x_1, \dots, x_n]$, the set of k -algebra homomorphisms can be identified with the affine space k^n , by identifying $a \in k^n$ with evaluation morphisms

³The division and Gröbner basis on $k[x_1, \dots, x_n]$ assume a given monomial ordering $x^\alpha < x^\beta \iff \alpha < \beta$, for $\alpha, \beta \in \mathbb{N}^n$, in order to determine the leading terms of the form $x^\alpha = x_1^{\alpha_1} \dots x_n^{\alpha_n}$.

$\text{ev}_a \in \text{Hom}_{k\text{-Alg}}(k[x_1, \dots, x_n], k)$, defined by $\text{ev}_a(f) = f(a_1, \dots, a_n)$. The kernel of ev_a is the maximal ideal

$$\mathfrak{m}_a = \{f \in k[x_1, \dots, x_n] \mid f(a) = 0\} = \langle x_1 - a_1, \dots, x_n - a_n \rangle. \quad (2.5)$$

From the isomorphism theorem follows that every maximal ideal $\mathfrak{m} \subset k[x_1, \dots, x_n]$ with $k[x_1, \dots, x_n]/\mathfrak{m} = k$ corresponds to a unique $a \in k^n$ such that $\mathfrak{m} = \mathfrak{m}_a$. Note that not all maximal ideals are of the form described in eq. (2.5). Sometimes, the set of maximal ideals \mathfrak{m} of any k -algebra R with $R/\mathfrak{m} = k$ is called the k -spectrum of R and is denoted by $k\text{-Spec } R \subseteq \text{Specm } R$ [67].

The requirement for k to be an algebraically closed field is crucial for the equality $k\text{-Spec } R = \text{Specm } R$. An arbitrary maximal ideal \mathfrak{m} can be easily identified by the property that the quotient R/\mathfrak{m} must be a field (a finite field extension of k), but not necessarily the base field k . This fails already for a \mathbb{R} -algebra.

Example 2.1. Consider $R = \mathbb{R}[x]$. The ideal $\langle x^2 + 1 \rangle$ is maximal under $\mathbb{R}[x]$ but not under $\mathbb{C}[x]$. Therefore, $\mathbb{R}[x]/\langle x^2 + 1 \rangle = \mathbb{R}[i] = \mathbb{C}$ is a field. For $\mathbb{R}[x]$, $\langle x - a \rangle$ with $a \in \mathbb{R}$ are maximal ideals, but we have also maximal ideals $\langle x^2 - (\alpha + \bar{\alpha})x + \alpha\bar{\alpha} \rangle$ for conjugate pairs $\alpha, \bar{\alpha} \in \mathbb{C} \setminus \mathbb{R}$. Thus, we can conclude that the maximal spectrum is the closure of the upper half of the complex plane, $\text{Specm } \mathbb{R}[x] = \overline{\mathbb{H}} = \{z \in \mathbb{C} \mid \text{Im } z \geq 0\}$. In general, for n variables, the maximal spectrum of $\mathbb{R}[x_1, \dots, x_n]$ is given by \mathbb{C}^n by identifying points under the action of $\{\text{id}_{\mathbb{C}^n}, z \mapsto \bar{z}\} \cong \mathbb{Z}_2$. As a result,

$$\text{Specm } \mathbb{R}[x_1, \dots, x_n] = \mathbb{R}^n \times (\mathbb{R}^n / \{\pm \text{id}_{\mathbb{R}^n}\}) = \mathbb{R}^n \times C_{\mathbb{R}}(\mathbb{RP}^{n-1}), \quad (2.6)$$

where $C_{\mathbb{R}}(\mathbb{RP}^{n-1})$ denotes the real cone over the real projective space \mathbb{RP}^{n-1} , and the real space $\mathbb{R}^n = \mathbb{R}\text{-Spec } \mathbb{R}[x_1, \dots, x_n]$ matches the tip of the cone.

Affine varieties [66, 68] are sets of solutions to systems of polynomial equations over a field, typically considered within a space k^n . For any set of elements S in a polynomial ring $R = k[x_1, \dots, x_n]$ over a field k , the affine variety

$$\mathbb{V}(S) = \{a \in k^n \mid f(a) = 0, \text{ for all } f \in S\} \quad (2.7)$$

is defined as the set of points in k^n satisfying the vanishing of the polynomials in I . This generalizes for subsets that are ideals. For a given element $f \in R$, then $\mathbb{V}(f)$ is the hypersurface in k^n defined by the zero set of the function f . Any affine variety of a finite set $f_1, \dots, f_m \in R$ can be seen as an intersection of hyperspaces: $\mathbb{V}(f_1, \dots, f_m) = \mathbb{V}(\langle f_1, \dots, f_m \rangle) = \mathbb{V}(f_1) \cap \dots \cap \mathbb{V}(f_m)$. Similarly, we can define the *vanishing ideal* of an affine variety $X \subseteq k^n$,

$$\mathbb{I}(X) = \{f \in R \mid f(a) = 0, \text{ for all } a \in X\}, \quad (2.8)$$

which includes all polynomials in R that vanish at every point in X . For an algebraically closed field k , the *coordinate ring* of a variety X is defined simply as $k[X] = R/\mathbb{I}(X)$, which is the k -algebra of k -valued polynomial functions on X .

The space k^n is endowed with the *Zariski topology* (usually denoted by \mathbb{A}^n), where closed sets are the $\mathbb{V}(I)$ and open sets are the complements

$$U_I = k^n \setminus \mathbb{V}(I) = (k^n \setminus \mathbb{V}(f_1)) \cup \dots \cup (k^n \setminus \mathbb{V}(f_m)) = U_{f_1} \cup \dots \cup U_{f_m} \quad , \quad (2.9)$$

of a finitely generated ideal $I = \langle f_1, \dots, f_m \rangle$, where the

$$U_f = \{a \in k^n \mid f(a) \neq 0\} \quad (2.10)$$

are the basic open sets. In particular, these open sets have an algebraic connection with the localization R_f , for $U_f = \text{Specm}(R_f)$. A *localization* [68] of an integral domain R allows us to define quotients of R by elements of some multiplicative closed set $S \subset R$. It is defined as the quotient $S^{-1}R = (R \times S)/\sim$, where $(p, q) \sim (p', q')$ if and only if there exists $u \in S$ such that $u(pq' - p'q) = 0$. The sum and multiplication on $S^{-1}R$ are defined as expected. An example of localization is the *field of rational functions* $k(X)$, which is the localization of $R = k[X]$ by all non-zero elements $S = k[X] \setminus \{0\}$. Similarly, the localization by a single element $f \in R$ is the ring $R_f = \{g/f^\ell \in k(X) \mid \ell \in \mathbb{N}\}$, where the quotient set is $S = \{f^\ell \mid \ell \in \mathbb{N}\}$.

The vanishing ideal \mathbb{I} and zero set \mathbb{V} act almost complementary. Note that $\mathbb{I}(X)$ constitutes the maximal subset of appropriate functions that vanish on X , thus $\mathbb{V}(\mathbb{I}(X)) = X$. On the other hand, composing the relation in the opposite direction, $\mathbb{I}(\mathbb{V}(I)) \subseteq I$, does not necessarily recover the initial ideal $I \subset R$. The main reason for this is that a variety cannot distinguish if the defining relation arises from $f = 0$ or $f^p = 0$ for some $p > 1$. Equivalently, we have $\mathbb{V}(I) = \mathbb{V}(\sqrt{I})$, where $\sqrt{I} = \{f \in R \mid f^p \in I, p > 0\}$ is the *radical ideal* of I . Hilbert's *Nullstellensatz* is a foundational theorem linking algebraic (ideals) and geometric (varieties) structures,

$$\mathbb{I}(\mathbb{V}(I)) = \sqrt{I} \quad , \quad (2.11)$$

which captures exactly the fact that $\mathbb{V}(I)$ may forget some information about I .

An affine variety can be decomposed into *irreducible components*. That is, a variety X can be written as a unique decomposition of irreducible affine varieties,

$$X = X_1 \cup X_2 \cup \dots \cup X_s \quad , \quad (2.12)$$

such that $X_i \not\subseteq X_j$ for all $i \neq j$. If X is an irreducible variety, then $\mathbb{I}(X) \subseteq R$ must be prime. A *prime ideal* $\mathfrak{p} \subseteq R$ is defined such that if the product $gh \in \mathfrak{p}$, for some $g, h \in R$, then either $g \in \mathfrak{p}$ or $h \in \mathfrak{p}$. If $\mathbb{I}(X)$ were not prime, then we could pick two elements $f_1, f_2 \notin \mathbb{I}(X)$ with

$X \subseteq \mathbb{V}(f_1 f_2) = \mathbb{V}(f_1) \cup \mathbb{V}(f_2)$, and we would have components $X \cap \mathbb{V}(f_i) \subsetneq X$, thus X would be reducible. The *prime spectrum* is simply denoted as $\text{Spec } R$. Note that every maximal ideal is also a prime ideal, $\text{Specm } R \subseteq \text{Spec } R$, but $\text{Spec } R$ includes a much larger structure and is in one-to-one correspondence with irreducible affine varieties of $\mathbb{V}(0) = k^n$ (e.g., algebraic curves).

It is possible to obtain a unique decomposition of ideals, revealing their constituent components in a manner analogous to prime factorization. A *primary ideal* Q is very similar to a prime ideal, but relaxes the defining condition of prime ideals as follows: if the product $gh \in Q$, then either $g \in Q$ or $h^p \in Q$ for some $p \in \mathbb{N}$. Prime ideals have $p = 1$. Any ideal I of a noetherian ring R has a minimal *primary decomposition* [66]

$$I = Q_1 \cap Q_2 \cap \dots \cap Q_s \quad (2.13)$$

into an intersection of primary ideals Q_i , such that the decomposition is irredundant, i.e., $\bigcap_{j \neq i} Q_j \not\subseteq Q_i$. From the definition, the radicals $\mathfrak{p}_i = \sqrt{Q_i}$ are prime ideals (*associated primes* of I). While a minimal primary decomposition might not be unique, the radicals of the primaries \mathfrak{p}_i are all different and uniquely determined by I . Since eq. (2.13) implies

$$\mathbb{V}(I) = \mathbb{V}(\mathfrak{p}_1) \cup \dots \cup \mathbb{V}(\mathfrak{p}_s), \quad (2.14)$$

where $\mathbb{V}(\mathfrak{p}_i)$ are irreducible components, the primary decomposition is an extremely powerful algebraic algorithm that allows us to identify irreducible varieties from a set of equations I .

In the affine world, we can summarize the bijections provided by algebraic geometry as follows (k algebraic closed):

Algebra, ring R	Geometry, affine space X
radical ideals, $I = \sqrt{I} \subset R$	varieties $\mathbb{V}(I) \subseteq X$
prime ideals, $\mathfrak{p} \in \text{Spec } R$	irreducible varieties $\mathbb{V}(\mathfrak{p}) \subseteq X$
maximal ideals, $\mathfrak{m}_a \in \text{Specm } R$	points $a \in X$

2.1.2 Toric varieties, cones and fans

A *toric variety* [68] is an irreducible affine variety V containing the algebraic torus $T \cong (\mathbb{C}^\times)^n$ as a Zariski open subset, $T \subseteq V$, such that the action on itself extends to all V by an algebraic group action $T \times V \rightarrow V$.

The torus T inherits an algebraic group structure from $(\mathbb{C}^\times)^n$ and has a lattice M of characters $\chi^m(t) = \prod_{i=1}^n t_i^{m_i} \in \text{Hom}(T, \mathbb{C}^\times)$, which is a free abelian group of rank r , isomorphic to \mathbb{Z}^n . Similarly, the dual lattice $N = \text{Hom}_{\mathbb{Z}}(M, \mathbb{Z})$, is the lattice of co-characters $\lambda^u(t) = (t^{u_1}, \dots, t^{u_n})$, $u \in N$. The group isomorphism to the torus T determines a basis in M and

dual basis in N , such that we have the natural pairing

$$\begin{aligned} \langle -, - \rangle : M \times N &\rightarrow \text{Hom}_{\mathbb{Z}}(\mathbb{Z}, \mathbb{Z}) \xrightarrow{\cong} \mathbb{Z} \\ (m, u) &\mapsto \chi^m \circ \lambda^u \mapsto m \cdot u \end{aligned} \quad (2.15)$$

The latter lattice defines one-parameter subgroups of the toric variety torus algebraic group $T = T_N$, where

$$T_N = N \otimes_{\mathbb{Z}} \mathbb{C}^\times \quad (2.16)$$

The previous equation means that the torus is just the union of all the images $\{\lambda^u(t) \mid t \in \mathbb{C}^\times\}$, for all $u \in N$. The union of the Zariski closure of the one-parameter subgroups images generate the Zariski closure of T_N , *i.e.*, the full toric variety.

We can use different combinatorial approaches to construct affine toric varieties. Let \mathcal{A} be a fixed subset of elements $\{m_1, \dots, m_s\} \subseteq M$. Then, we can define a monomial map,

$$\Phi_{\mathcal{A}} : T \rightarrow \mathbb{C}^s \quad t \mapsto (\chi^{m_1}(t), \dots, \chi^{m_s}(t)) . \quad (2.17)$$

The Zariski closure of its image is a toric variety $Y_{\mathcal{A}} = \overline{\text{im } \Phi_{\mathcal{A}}} \subseteq \mathbb{C}^s$ whose dense torus has the character lattice $\mathbb{Z}_{\mathcal{A}} = \{\sum_{i=1}^s a_i m_i \mid a_i \in \mathbb{Z}\} \subseteq M$. The dimension of the variety is simply $\dim Y_{\mathcal{A}} = \text{rank}(\mathbb{Z}_{\mathcal{A}})$.

An algebraic approach is to construct the vanishing ideal $\mathbb{I}(X_{\mathcal{A}}) \subset \mathbb{C}[x_1, \dots, x_s]$ defining the coordinate ring $\mathbb{C}[X_{\mathcal{A}}]$. Given the monomial map $\Phi_{\mathcal{A}}$ we can induce⁴ the map $\widehat{\Phi}_{\mathcal{A}} : \mathbb{Z}^s \rightarrow M$, $\ell \mapsto \sum_{i=1}^s \ell_i m_i$. For $\alpha, \beta \in \mathbb{N}^s$ such that $\alpha - \beta \in \ker \widehat{\Phi}_{\mathcal{A}}$, then we have that $\chi^{\sum_{i=1}^s \alpha_i m_i}(t) - \chi^{\sum_{i=1}^s \beta_i m_i}(t) = 0$. We can define the *toric ideal*

$$I_A = \langle x^\alpha - x^\beta \mid \alpha, \beta \in \mathbb{N}^s, \alpha - \beta \in \ker(A) \rangle , \quad x^\alpha = \prod_{i=1}^s (x_i)^{\alpha_i} , \quad (2.18)$$

for a general matrix A . Therefore, the vanishing ideal defining the affine toric variety is $\mathbb{I}(X_{\mathcal{A}}) = I_{\widehat{\Phi}_{\mathcal{A}}}$. By assigning a generator $x_i = \chi^{m_i}$ to each element in $m_i \in \mathcal{A}$, the linear relations between elements of \mathcal{A} are captured by the multiplicative relations (binomials) in the toric ideal.

Another approach is to use the affine semigroup $S = \mathbb{N}_{\mathcal{A}}$ generated by the set $\mathcal{A} \subseteq M$, for which its ring is given by

$$\mathbb{C}[S] = \bigoplus_{m \in S} \mathbb{C} \chi^m = \mathbb{C}[\chi^{m_1}, \dots, \chi^{m_s}] \quad (2.19)$$

⁴We can view $\Phi_{\mathcal{A}}$ as a group homomorphism of tori $(\mathbb{C}^\times)^n \rightarrow (\mathbb{C}^\times)^s$ and noting that moving to character lattices $\text{Hom}(-, \mathbb{C}^\times)$ is a contravariant operation (functor).

with the expected multiplication rule $\chi^m \chi^{m'} = \chi^{m+m'}$. We can verify that $\mathbb{C}[\mathbf{S}]$ indeed matches the coordinate ring $\mathbb{C}[X_{\mathcal{A}}]$ via the pullback⁵ of the monomial map

$$\Phi_{\mathcal{A}}^* : \mathbb{C}[x_1, \dots, x_s] \rightarrow \mathbb{C}[M] \quad x_i \mapsto \chi^{m_i} . \quad (2.20)$$

Note that for a basis $e_1, \dots, e_n \in M$, as a semigroup the lattice M is generated by $\{\pm e_1, \dots, \pm e_n\}$, which implies $\mathbb{C}[M]$ is given by Laurent polynomials in $\mathbb{C}[t_1^{\pm}, \dots, t_n^{\pm}]$. From the isomorphism theorem, $\mathbb{C}[x_1, \dots, x_s] / \mathbb{I}(X_{\mathcal{A}}) = \mathbb{C}[x_1, \dots, x_s] / \ker(\Phi_{\mathcal{A}}^*) \cong \text{im}(\Phi_{\mathcal{A}}^*) = \mathbb{C}[\mathbf{S}]$. Its maximal spectrum recovers the affine toric variety, $X_{\mathcal{A}} = \text{Specm } \mathbb{C}[\mathbf{S}]$.

Example 2.2. The *conifold* $\mathbb{V}(xy - zw) \subset \mathbb{C}^4$ is an affine toric variety and is generated by the elements $\mathcal{A} = \{(1, 0, 0), (0, 1, 0), (0, 0, 1), (1, 1, -1)\}$ of a rank 3 lattice, generating the semigroup $\mathbf{S} = \mathbb{N}\mathcal{A}$. The semigroup algebra generates the coordinate ring

$$\mathbb{C}[\mathbf{S}] = \mathbb{C}[t_1, t_2, t_3, t_1 t_2 (t_3)^{-1}] = \mathbb{C}[x, y, z, w] / \langle xy - zw \rangle . \quad (2.21)$$

Note that $\ker(\widehat{\Phi}_{\mathcal{A}}) = \text{span}_{\mathbb{Z}}\{(1, 1, -1, -1)\}$ describes the monomial relations in the toric ideal (2.18) of conifold.

Affine toric varieties are closely interconnected with the discrete geometry of rational convex polyhedral cones. A given affine semigroup \mathbf{S}_{σ} is generated by a finite number of elements and spans a region in M , which can be described by a cone σ in $N_{\mathbb{R}} = N \otimes_{\mathbb{Z}} \mathbb{R}$. A cone $\sigma \subseteq N_{\mathbb{R}} \cong \mathbb{R}^n$ can be further characterized by additional properties:

- σ is *strongly convex* $\Leftrightarrow \sigma \cap (-\sigma) = \{0\} \Leftrightarrow \dim \sigma^{\vee} = n$
- σ is *rational* \Leftrightarrow elements in the finite set S belong to the lattice N (instead of $N_{\mathbb{R}}$)

A strongly convex rational cone is generated by a finite set S ,

$$\sigma = \text{Cone}(S) = \left\{ \sum_{u \in S} \lambda_u u \mid \lambda_u \in \mathbb{R}_{\geq 0} \right\} \subseteq N_{\mathbb{R}} . \quad (2.22)$$

Also set $\text{Cone}(\emptyset) = \{0\}$. Furthermore, a strongly convex rational polyhedral cone σ can be minimally described by its rays. A *ray* ρ is a semi-infinite edge of the cone, and since ρ is itself a 1-dimensional rational cone, there exists a primitive generator $u_{\rho} \in \rho \cap N$ such that $\rho = \text{Cone}(u_{\rho})$. The set of rays forms the minimal generators of the cone σ .

The construction of \mathbf{S}_{σ} uses the *dual cone* of a polyhedral cone $\sigma \subseteq N_{\mathbb{R}}$, defined as

$$\sigma^{\vee} = \{m \in M_{\mathbb{R}} \mid \langle m, u \rangle \geq 0, \forall u \in \sigma\} \subseteq M_{\mathbb{R}} . \quad (2.23)$$

⁵Now going to $\text{Hom}_{\mathbb{C}\text{-Alg}}(-, \mathbb{C})$.

The dual cone is described by the intersection of half-spaces with normal vectors in σ . Since $(\sigma^\vee)^\vee = \sigma$, a similar description exists where face normals are mapped to generators of σ^\vee . If $\{m_1, \dots, m_s\}$ are the rays generators of the dual cone σ^\vee , then it is easy to check that

$$\sigma = H_{m_1}^+ \cap \dots \cap H_{m_s}^+, \quad (2.24)$$

where $H_m^+ = \{u \in N_{\mathbb{R}} \mid \langle m, u \rangle \geq 0\}$ are closed supporting half-spaces of the polyhedral cone σ . The boundary of the half-spaces, $H_m = \{u \in N_{\mathbb{R}} \mid \langle m, u \rangle = 0\}$ defines a supporting hyperplane, where m is the (inward) normal of the hyperplane. A *face* of the polyhedral cone σ is a $\tau = H_m \cap \sigma$ for some $m \in \sigma^\vee$, written $\tau \preceq \sigma$. We denote the set of n -dimensional faces of a cone as $\sigma(n) = \{\tau \preceq \sigma \mid \dim \tau = n\}$. The cone σ is a face of itself, $\sigma \preceq \sigma$, for element $m = 0$. Faces $\tau \prec \sigma$ are called proper, meaning $\tau \neq \sigma$.

We can construct an affine semigroup from a rational polyhedral cone $\sigma \subseteq N_{\mathbb{R}}$ by

$$\mathbf{S}_\sigma = \sigma^\vee \cap M, \quad (2.25)$$

which is finitely generated. Then, $X_\sigma = \text{Specm } \mathbb{C}[\mathbf{S}_\sigma]$ is an affine toric variety as defined above. In general, the semigroup generators do not match the cone generators of σ^\vee . The unique minimal generating set of \mathbf{S}_σ is called the *Hilbert basis* \mathcal{H} , which is composed of non-zero irreducible elements that generate \mathbf{S}_σ . These are elements $m \in \mathbf{S}_\sigma \setminus \{0\}$ such that if $m = m_1 + m_2$, for $m_1, m_2 \in \mathbf{S}_\sigma$, then either $m_1 = 0$ or $m_2 = 0$.

Let $X_\sigma = \text{Specm } \mathbb{C}[\mathbf{S}_\sigma]$, for a strongly convex rational polyhedral cone $\sigma = \text{Cone}(S)$, with $\{u_\rho \mid \rho \in \sigma(1)\}$ being the primitive ray generators of σ :

- X_σ is *smooth* $\Leftrightarrow \sigma$ is *smooth/regular* $\Leftrightarrow \{u_\rho\}_\rho$ forms part of the \mathbb{Z} -basis of N .
- X_σ is \mathbb{Q} -*factorial*, *i.e.* a finite quotient of a smooth affine variety (is an orbifold) $\Leftrightarrow \sigma$ is *simplicial* $\Leftrightarrow \{u_\rho\}_\rho$ are linearly independent over \mathbb{R} .
- X_σ is \mathbb{Q} -*Gorenstein* \Leftrightarrow there exists $m \in M_{\mathbb{Q}}$ such that $\langle m, u_\rho \rangle = 1$ for all $u_\rho, \rho \in \sigma(1)$. The minimal integer $q > 0$ such that $qm \in M$ is the Gorenstein degree of X_σ .

At this point, we have been discussing affine varieties generated by a single cone. However, we can construct abstract toric varieties by gluing together affine toric pieces X_σ . A *fan* $\Sigma \subseteq N_{\mathbb{R}}$ is a finite collection of cones such that:

- All $\sigma \in \Sigma$ are strongly convex rational polyhedral cones.
- Every face τ of a cone $\sigma \in \Sigma$, $\tau \preceq \sigma$, is also a cone in the fan, $\tau \in \Sigma$.
- Any two $\sigma_1, \sigma_2 \in \Sigma$ intersect at a common face $\tau = \sigma_1 \cap \sigma_2 \in \Sigma$.

We denote by $\Sigma(n)$ the collection of n -dimensional cones (note that 0 is included as the 0-dimensional cone). A normal toric variety X_Σ for a given fan Σ is still toric in the same sense as above, *i.e.* contains a torus T_N with a toric action that extends itself to the algebraic action $T_N \times X_\Sigma \rightarrow X_\Sigma$.

Fixing a fan $\Sigma \subseteq N_{\mathbb{R}}$, we can explain how it encodes the gluing data for the toric variety X_Σ . A face $\tau \preceq \sigma$ of a cone $\sigma \in \Sigma$ can be written as $\tau = \sigma \cap H_m$ for $m \in M$. Firstly, any face of σ defines an open affine subset of U_σ , given that the inclusion $S_\tau \hookrightarrow S_\sigma$ induces the open injection of $U_\tau \hookrightarrow U_\sigma$. Restricting to the image, we also have a bijection⁶ $U_\tau \xrightarrow{\cong} (U_\sigma)_{\chi^m}$ for the normal $m \in M$, where the open subset $(U_\sigma)_{\chi^m}$ is a localization defined above in eq. (2.10). Secondly, for each pair of cones $\sigma_1, \sigma_2 \in \Sigma$ with a common face $\tau = \sigma_1 \cap \sigma_2 = \sigma_1 \cap H_m = \sigma_2 \cap H_m$, where $m \in \sigma_1^\vee \cap (-\sigma_2)^\vee \cap M$, there exists an isomorphism

$$U_{\sigma_1} \supset (U_{\sigma_1})_{\chi^m} \cong U_\tau \cong (U_{\sigma_2})_{\chi^{-m}} \subset U_{\sigma_2} . \quad (2.26)$$

The rational transition functions $g_{\sigma_2, \sigma_1} : (U_{\sigma_1})_{\chi^m} \dashrightarrow (U_{\sigma_2})_{\chi^{-m}}$,⁷ as well as the affine patches $\{U_\sigma\}_{\sigma \in \Sigma}$ where these are defined, constitute the gluing data of X_Σ .

Example 2.3. Let's describe explicitly how the abstract theory introduced above is realized for the \mathbb{P}^2 fan, defined in $N = \mathbb{Z}^2$, shown in fig. 2.1. This fan contains minimal ray generators

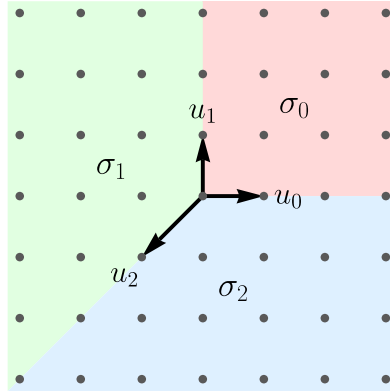


FIGURE 2.1: Fan of \mathbb{P}^2 .

$u_0 = (1, 0)$, $u_1 = (0, 1)$, $u_2 = (-1, -1)$, where we take the standard basis in N to be $e_1 = (1, 0)$ and $e_2 = (0, 1)$. The maximal cones of fan have duals:

$$\begin{aligned} \sigma_0^\vee &= \text{Cone}((1, 0), (0, 1)) \\ \sigma_1^\vee &= \text{Cone}((-1, 0), (-1, 1)) \\ \sigma_2^\vee &= \text{Cone}((1, -1), (0, -1)) \end{aligned} \quad (2.27)$$

⁶For $\tau = \sigma \cap H_m$, we have $S_\tau = S_\sigma + \mathbb{N}(-m)$, which implies that $\mathbb{C}[S_\tau] = \mathbb{C}[S_\sigma]_{\chi^m}$ matches the localization of $\mathbb{C}[S_\sigma]$ by the monomial χ^m . The bijection follows from taking $\text{Specm}(-)$.

⁷The arrow \dashrightarrow is often used for birational map, *i.e.*, isomorphisms that are well-defined rational maps in both directions.

Let's focus on the rational transition function between U_{σ_0} and U_{σ_1} . The intersection of these affine patches is associated to the common ray $\tau_{01} = \text{Cone}((0, 1))$, with dual cone $\tau_{01}^\vee = \text{Cone}(\pm(1, 0), (0, 1))$. Choosing $m = (1, 0) \in \tau_{01}^\vee \cap \sigma_0^\vee \cap (-\sigma_1)^\vee$, we note that

$$\begin{aligned} (U_{\sigma_0})_{\chi^m} &= \text{Specm} \left(\mathbb{C}[\chi^{(1,0)} = t_0, \chi^{(0,1)} = s_0]_{t_0} \right) = \{(t_0, s_0) \in \mathbb{C}^2 \mid t_0 \neq 0\}, \\ (U_{\sigma_1})_{\chi^{-m}} &= \text{Specm} \left(\mathbb{C}[\chi^{(-1,0)} = t_1, \chi^{(-1,1)} = s_1]_{t_1} \right) = \{(t_1, s_1) \in \mathbb{C}^2 \mid t_1 \neq 0\}, \end{aligned} \quad (2.28)$$

where we assign distinct pairs of variables (t_i, s_i) to the minimal generators of the affine patches U_{σ_i} . We can derive the birational relation between the variables from the monomial representation, for *e.g.*, $s_1 = \chi^{(-1,1)} = \chi^{(-1,0)}\chi^{(0,1)} = s_0 t_0^{-1}$. The transition function is

$$\begin{aligned} g_{10} : (U_{\sigma_0})_{\chi^m} &\dashrightarrow (U_{\sigma_1})_{\chi^{-m}} \\ (t_0, s_0) &\mapsto (t_0^{-1}, s_0 t_0^{-1}) \end{aligned} \quad (2.29)$$

which is well-defined for $\chi^m = t_0 \neq 0$. We recover the standard patches of \mathbb{P}_2 in terms of homogeneous coordinates (x_0, x_1, x_2) , by sending $t_0 \mapsto x_1/x_0$ and $s_0 \mapsto x_2/x_0$, where these can be written as $U_{\sigma_i} = \{[x_0 : x_1 : x_2] \mid x_i \neq 0\} \cong \mathbb{C}^2$.

Let X_Σ be a normal toric variety defined by a fan $\Sigma \subseteq \mathbb{N}_\mathbb{R}$. There is a dictionary between properties of a toric variety and its fan:

- X_Σ is a smooth variety $\Leftrightarrow \Sigma$ is smooth \Leftrightarrow every cone $\sigma \in \Sigma$ is smooth (regular).
- X_Σ is an orbifold $\Leftrightarrow \Sigma$ is *simplicial* \Leftrightarrow every cone $\sigma \in \Sigma$ is simplicial.
- X_Σ is compact in the classical topology $\Leftrightarrow \Sigma$ is *complete* \Leftrightarrow the fan is supported in the entire $N_\mathbb{R}$, *i.e.* $\text{supp}(\Sigma) = \bigcup_{\sigma \in \Sigma} \sigma = N_\mathbb{R}$.

2.1.3 Homogeneous coordinate ring of a toric variety

We introduced one of the ways we can build a toric variety from a fan Σ , by gluing multiple affine open patches U_σ , for $\sigma \in \Sigma$. Instead, a more physical and convenient construction due to Cox [68] is to build toric varieties as the total homogeneous coordinate space \mathbb{C}^s minus a base locus Z_Σ , quotiented by a reductive algebraic group G . Fix $n = \dim X_\Sigma = \text{rank}(N)$.

A concept at the heart of this quotient is the idea of divisors, which capture information about the zeroes and poles of rational functions on a variety. A *Weil divisor* D is an element which can be written as a formal sum $D = \sum_i a_i D_i \in \text{Div}(X)$, with coefficients $a_i \in \mathbb{Z}$. The generators of the free abelian group $\text{Div}(X)$ are prime divisors D_i , which are similar to codimension 1 hypersurfaces in the sense that locally they can be defined as the zero locus of a single equation.⁸ Furthermore, given an invertible rational function $f \in \mathbb{C}(X)^\times$ we can

⁸For an affine variety this is true globally, $D_i = \mathbb{V}(\mathfrak{p}_i)$ for some prime $\mathfrak{p}_i \subset \mathbb{C}[X]$. In general, for each prime divisor there is a local ring \mathcal{O}_{X, D_i} with a unique (prime) maximal ideal that describes the local behavior.

associate to it a divisor

$$\operatorname{div}(f) = \sum_i \operatorname{ord}_{D_i}(f) D_i, \quad (2.30)$$

where $\operatorname{ord}_{D_i} : \mathbb{C}(X)^\times \rightarrow \mathbb{Z}$ defines the order⁹ of the zeros/poles in the subvarieties D_i . Elements written as in (2.30) are referred to as *principal divisors*, which define a closed subgroup $\operatorname{Div}_0(X) \subseteq \operatorname{Div}(X)$.

In particular, for a toric variety X_Σ torus-invariant prime divisors are easy to identify. The cone-orbit correspondence tells us that there exists a bijection between cones $\sigma \in \Sigma$ and T_N -invariant orbits $O(\sigma) \subseteq X_\Sigma$. The closure of an orbit $V(\tau) = \overline{O(\tau)} = \bigcup_{\sigma \supseteq \tau} O(\sigma)$ is a toric subvariety with torus $T_{N(\tau)} = O(\tau)$ as an open subset and with $\dim V(\tau) = \dim X_\Sigma - \dim \tau$. Thus, rays of the fan $\rho \in \Sigma(1)$ give rise to codimension 1 orbits, whose closure is a T_N -invariant prime divisor $D_\rho = V(\rho)$. These form the basis of the toric divisor group

$$\operatorname{Div}_{T_N}(X_\Sigma) = \bigoplus_{\rho \in \Sigma(1)} \mathbb{Z}D_\rho \cong \mathbb{Z}^{\Sigma(1)} \quad (2.31)$$

Note that not all Weil divisors are principal. This mismatch is captured in the divisor class group $\operatorname{Cl}(X) = \operatorname{Div}(X) / \operatorname{Div}_0(X)$. The quotient is defined by an equivalence relation, such that two divisors $D, E \in \operatorname{Div}(X)$ are equivalent if and only if there exists a rational function f in X such that $D \sim E \Leftrightarrow D - E = \operatorname{div}(f) \in \operatorname{Div}_0(X)$.

The divisor class group is usually not easy to calculate. However, in the case of toric varieties $\operatorname{Cl}(X_\Sigma)$ pops out from the combinatorial structure of the fan Σ . Consider the ray map,

$$r : \operatorname{Div}_{T_N}(X_\Sigma) \rightarrow N, \quad D_\rho \mapsto u_\rho, \quad (2.32)$$

which maps toric divisors (standard basis elements of $\mathbb{Z}^{\Sigma(1)}$) to the minimal generator of the rays $\rho \in \Sigma(1)$. Going to the dual lattice, we can obtain the exact sequence

$$0 \longrightarrow M \xrightarrow{r^*} \bigoplus_\rho \mathbb{Z}D_\rho \longrightarrow \operatorname{Cl}_{T_N}(X_\Sigma) \longrightarrow 0 \quad (2.33)$$

where the dual map is defined by $r^*(m) = \operatorname{div}(\chi^m)$,

$$\operatorname{div}(\chi^m) = \sum_{\rho \in \Sigma(1)} \langle m, u_\rho \rangle D_\rho. \quad (2.34)$$

⁹For example, take the divisor $D = \{0\} \subset \mathbb{C}$. Given a rational $f \in \mathbb{C}(x)^\times$ we can write

$$f(x) = x^k \frac{h(x)}{g(x)} \quad g, h \in \mathbb{C}[x], \quad g(0) \neq 0, h(0) \neq 0,$$

where $\operatorname{ord}_D(f) = k \in \mathbb{Z}$. The divisor D is associated to the prime ideal $\langle x \rangle \subset \mathbb{C}[x]$.

The sequence is exact since the monomials χ^m are precisely the rational functions on $T_N \subset X_\Sigma$, invariant under the torus action. The character lattice M is one-to-one with the T_N -invariant principal divisors, which are mapped to the zero class $[\text{div}(\chi^m)] = 0$ in the class group. This is the divisor sequence that defines the quotient $\text{Cl}_{T_N}(X_\Sigma) = \text{coker}(r^*) = \mathbb{Z}^{\Sigma(1)} / \text{im}(r^*)$.

Acting with the contravariant $\text{Hom}(-, \mathbb{C}^\times)$, we obtain the group sequence

$$1 \longleftarrow T_N \xleftarrow{\phi} (\mathbb{C}^\times)^{\Sigma(1)} \longleftarrow G \longleftarrow 1 \quad (2.35)$$

with $\phi(t) = \left(\prod_\rho t_\rho^{\langle e_1^*, u_\rho \rangle}, \dots, \prod_\rho t_\rho^{\langle e_n^*, u_\rho \rangle} \right) \in T_N$, where e_1^*, \dots, e_n^* are basis elements of M . In the same way M is the character lattice of the torus group T_N , we have a reductive algebraic group $G = \text{Hom}_{\mathbb{Z}}(\text{Cl}_{T_N}(X_\Sigma), \mathbb{C}^\times)$ that has the divisor class group as its character group. Then, the kernel of ϕ defines,

$$G = \left\{ t \in (\mathbb{C}^\times)^{\Sigma(1)} \mid \prod_\rho t_\rho^{\langle m, u_\rho \rangle} = 1, \forall m \in M \right\}, \quad (2.36)$$

which acts on $(\mathbb{C}^\times)^{\Sigma(1)}$ via coordinate multiplication. From the sequence, we see that the torus T_N is the group quotient $(\mathbb{C}^\times)^{\Sigma(1)} / G$. Since T_N is itself isomorphic to a torus group, then $G \cong (\mathbb{C}^\times)^\ell \times \Gamma$, with $\ell = |\Sigma(1)| - \text{rank}(N)$, and where Γ is a finite abelian group.

A Weyl divisor D on a normal variety X is a *Cartier divisor* if it is locally principal. For a Cartier divisor, D there exists a finite open cover $\{U_\alpha\}_{\alpha \in I}$ such that $D|_{U_\alpha} = \text{div}(f_\alpha)|_{U_\alpha}$, for all $\alpha \in I$. We say that $\{(U_\alpha, f_\alpha)\}_{\alpha \in I}$ is its local data. Similar to the class group $\text{Cl}(X)$, we can define the *Picard group* as $\text{Pic}(X) = \text{CDiv}(X) / \text{Div}_0(X)$. In general, global sections defined on a Weyl divisor are

$$H^0(X, \mathcal{O}_X(D)) = \{f \in \mathbb{C}(X)^\times \mid \text{div}(f) + D \geq 0\} \cup \{0\}. \quad (2.37)$$

Thanks to the locality data of the Cartier divisors we are allowed to define rational transition functions $s_{\alpha\beta} = f_\alpha / f_\beta$, regular in $U_\alpha \cap U_\beta$, transforming sections defined on U_β to sections defined on U_α . Intuitively, (2.37) implies that sections $f \in \Gamma(X, \mathcal{O}_X(D))$ can have poles which are, in the worst case scenario, the same order as zeros defining D . Since the transition functions obey,

$$s_{\alpha\beta} s_{\beta\alpha} = 1 \quad s_{\alpha\beta} s_{\beta\gamma} s_{\gamma\alpha} = 1, \quad (2.38)$$

then $\mathcal{O}_X(D)$ is a line bundle.¹⁰ A sum of two divisors defines a line bundle which is the tensor product of the respective line bundles, *i.e.* $\mathcal{O}_X(D + E) = \mathcal{O}_X(D) \otimes \mathcal{O}_X(E)$. Isomorphism between bundles $\mathcal{O}_X(D) \cong \mathcal{O}_X(E)$ comes from linear equivalence between divisors $D \sim E$. Thus, the Picard group is also the group of isomorphism classes of line bundles on X .

¹⁰In the language of sheaves, we say $\mathcal{O}_X(D)$ is invertible.

We have seen how the torus $T_N \subset X_\Sigma$ arises from the larger $(\mathbb{C}^\times)^{\Sigma(1)} \subset \mathbb{C}^{\Sigma(1)}$. Note that at this point G and $\mathbb{C}^{\Sigma(1)}$ only depend on the rays of the fan. To construct the full toric variety X_Σ we need an object that encodes the information of all cones in the Σ . Let the total coordinate (Cox) ring be

$$R = \mathbb{C}[x_\rho \mid \rho \in \Sigma(1)] , \quad (2.39)$$

where $\mathbb{C}^{\Sigma(1)} = \text{Specm}(R)$ and x_ρ is a homogeneous coordinate associated to each toric divisor D_ρ . In this picture, the toric prime divisors are codimension 1 subvarieties defined by $D_\rho = \mathbb{V}_{X_\Sigma}(x_\rho)$. It is important to note that $x_\rho \in R$ is not a rational function of X_Σ . By definition, a monomial $x^a = \prod_\rho (x_\rho)^{a_\rho}$ defines a principal divisor iff it has zero degree, *i.e.*, $\deg(x^a) = [\sum_\rho a_\rho D_\rho] \in \text{Cl}(X_\Sigma)$ maps to the zero class.

Then, we can define the *irrelevant ideal*

$$\text{Irr}_\Sigma = \left\langle \prod_{\rho \in \Sigma(1) \setminus \sigma(1)} x_\rho \mid \sigma \in \Sigma \right\rangle . \quad (2.40)$$

The minimal generators of Irr_Σ are obtained by only considering the monomials in (2.40) for the maximal cones of Σ . The *exceptional set* is simply $Z_\Sigma = \mathbb{V}(\text{Irr}_\Sigma)$. From here, it is possible to show that

$$X_\Sigma = (\mathbb{C}^{\Sigma(1)} \setminus \mathbb{V}(\text{Irr}_\Sigma)) // G . \quad (2.41)$$

This effectively constitutes an affine Geometric Invariant Theory (GIT) [68] quotient with the projection $\pi : \mathbb{C}^{\Sigma(1)} \setminus Z_\Sigma \rightarrow X_\Sigma$. In this construction, two points map to the same class $\pi(x) = \pi(y)$ if and only if the closure of their G -orbits intersect, $\overline{G \cdot x} \cap \overline{G \cdot y} \neq \emptyset$.¹¹ In practice, the stronger condition that x and y belong to the same closed G -orbit holds for almost all points $x, y \in \mathbb{C}^{\Sigma(1)} \setminus Z_\Sigma$ that map to the same point in X_Σ .

Example 2.4. Let $N = \mathbb{Z}^2$ and the fan Σ contain the rays generators $u_0 = (2, -1)$, $u_1 = (-1, 2)$, $u_2 = (-1, -1)$, splitting $N_\mathbb{R}$ into 3 maximal cones (see fig. 2.1). The irrelevant ideal for this fan is simply $\text{Irr}_\Sigma = \langle x_0, x_1, x_2 \rangle$, which removes the origin from the total space \mathbb{C}^3 in the quotient construction. By representing the ray map as the linear action $\begin{bmatrix} 2 & -1 & -1 \\ -1 & 2 & -1 \end{bmatrix}$, the sequence (2.33) simplifies to

$$0 \longrightarrow \mathbb{Z}^2 \xrightarrow{\begin{bmatrix} 2 & -1 \\ -1 & 2 \end{bmatrix}} \mathbb{Z}^3 \xrightarrow{[1 \ 1 \ 1]} \mathbb{Z}^1 \longrightarrow 0 \quad (2.42)$$

The cokernel of the dual ray map tells us that there exists a \mathbb{C}^\times acting on $\mathbb{C}^3 \setminus \{0\}$, which wrongly points to the quotient being \mathbb{P}^2 . However, X_Σ does not have smooth \mathbb{C}^2 as the affine

¹¹This condition is known as the categorical quotient condition. The geometric quotient additionally requires all G -orbits of $\mathbb{C}^{\Sigma(1)} \setminus Z_\Sigma$ to be closed, *i.e.* $\pi(x) = \pi(y) \Leftrightarrow x$ and y lie in the same closed G -orbit.

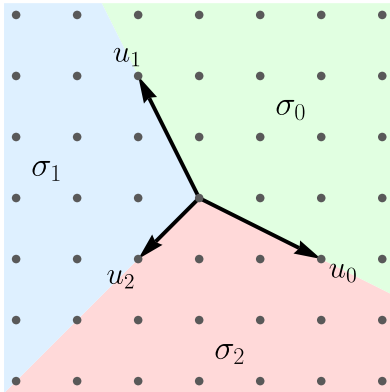


FIGURE 2.2: Fan of $\mathbb{P}^2/\mathbb{Z}_3(0, 1, 2)$, with lattice $N = \mathbb{Z}^2$.

patches like \mathbb{P}^2 (see fig. 2.1). A quick computation tells us that the Hilbert basis of $\sigma_0^\vee \cap M$ is $\mathcal{H} = \{(2, 1), (1, 1), (1, 2)\}$. By the symmetry of the fan, we can use this basis to derive that all maximal cones generate

$$U_{\sigma_i} = \text{Specm}(\mathbb{C}[x, y, z]/\langle xz - y^3 \rangle) = \mathbb{V}_{\mathbb{C}^3}(xz - y^3). \quad (2.43)$$

These patches are orbifolds with a singular fixed point of type A_2 , which implies that the group has torsion $\Gamma \subset G$. This torsion can be interpreted as follows. Consider the usual fan

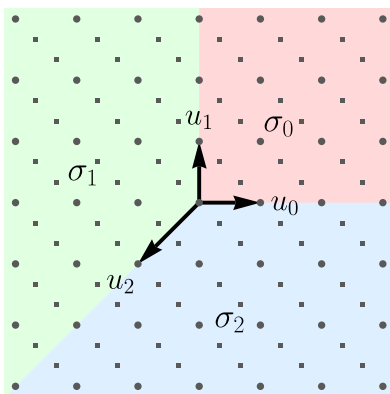


FIGURE 2.3: Fan of $\mathbb{P}^2/\mathbb{Z}_3(0, 1, 2)$, with lattice $N' = \{(a/3, b/3) \mid a + b \equiv 0 \pmod{3}\}$.

for \mathbb{P}^2 in fig. 2.1, with standard lattice $N = \mathbb{Z}^2$. By keeping the fan fixed but changing the lattice to $N' \supset N$ (see fig. 2.3), the quotient $\Gamma = N'/N$ defines the isomorphism between the two affine patches

$$\mathbb{C}[\sigma_i^\vee \cap M'] = \mathbb{C}[\sigma_i^\vee \cap M]^\Gamma \iff U_{\sigma_i, N'} = U_{\sigma_i, N}/\Gamma. \quad (2.44)$$

This relation allows us to derive that $U_{\sigma_i, N'} = \mathbb{C}^2/\mathbb{Z}_3$, with action $\zeta \cdot (s, t) = (\zeta s, \zeta^{-1}t)$, from the simpler patches of \mathbb{P}^2 , where $U_{\sigma_i, N} = \mathbb{C}^2$. In particular, the ring of \mathbb{Z}_3 -invariants under this action simplifies to $\mathbb{C}[s, t]^{\mathbb{Z}_3} = \mathbb{C}[s^3, st, t^3]$, matching the result from (2.43).

Due to the presence of affine orbifold patches, the group G in the quotient description also contains a finite abelian component. From eq. (2.36),

$$\frac{(t_1)^2}{t_2 t_3} = 1, \frac{(t_2)^2}{t_1 t_3} = 1 \Rightarrow \left(\frac{t_2}{t_1}\right)^3 = 1 \Rightarrow t_2 = \zeta t_1, \zeta \in \mathbb{Z}_3 \quad (2.45)$$

which leads to $G = \{(t, \zeta t, \zeta^2 t) \mid t \in \mathbb{C}^\times, \zeta \in \mathbb{Z}_3\}$. The resulting toric variety X_Σ is usually denoted as $\mathbb{P}^2/\mathbb{Z}_3(0, 1, 2)$, where the latter triplet of integers is the charges under which the homogeneous coordinates transform.¹²

In general, an A_{k-1} -type singularity [68] appears as the singular fixed point in the quotient

$$\mathbb{V}_{\mathbb{C}^3}(xz - y^k) = \mathbb{C}^2/\mathbb{Z}_k, \quad (2.46)$$

with action given by $\zeta \cdot (z_0, z_1) = (\zeta z_0, \zeta^{k-1} z_1)$. Such a singularity is often associated with a cone $\sigma = \text{Cone}((1, 0), (1, k))$. These fall in the larger class of singularities (rational double points) lying in orbifolds \mathbb{C}^2/Γ , where $\Gamma \subset \text{SU}(2)$ is a finite subgroup given by the ADE classification. The naming convention comes from the bijection with the simply laced Dynkin diagrams of families A_k , D_k and E_6 , E_7 , E_8 . Finite groups of DE-type are nonabelian, therefore such singular points do not appear in the toric context.

2.1.4 Calabi-Yau affine cones, toric diagrams and crepant resolutions

In string theory, the study of Calabi-Yau (CY) manifolds are particularly important [69, 70]. Toric geometry allows us to define and generate a large class of noncompact CY whose geometric properties are encoded by combinatorial objects. The toric variety of a Σ is an affine CY n -fold if and only if the primitive vectors generating the one-dimensional cones $\{u_\rho \mid \rho \in \Sigma(1)\}$ all lie in the same affine hyperplane, *i.e.*, exists a $m \in M$ such that $\langle m, u_\rho \rangle = 1$ for all $\rho \in \Sigma(1)$. We say such a toric variety X_Σ is *Gorenstein*, as the previous condition implies the cones $\sigma \in \Sigma$ are \mathbb{Q} -Gorenstein of degree 1. Noncompactness is an immediate consequence of a noncomplete fan, since the primitive generators do not span $N_{\mathbb{R}} = \mathbb{R}^n$.

Since the generators are coplanar a convenient way to describe a toric CY 3-fold is by a *toric diagram* Δ , a convex lattice polygon usually placed in the standard 2-dimensional lattice \mathbb{Z}^2 . We will denote these affine toric CY cones as \mathcal{Y}_Δ . From a toric diagram we can generate a fan with a single maximal convex polyhedron cone σ_Δ by placing the vertices of the toric diagram at height 1 and spanning the cone from the origin,

$$\sigma_\Delta = \text{Cone}((v, 1) \mid v \in \Delta) \subset N_{\mathbb{R}} = \mathbb{R}^3. \quad (2.47)$$

¹²Following notation in [55].

Similarly, the toric diagram of a Gorenstein X_{σ_Δ} can be obtained by projecting the cone slice $\sigma_\Delta \cap H_m = \text{Conv}(\{u_\rho \mid \rho \in \sigma_\Delta(1)\})$ down to the 2-dimensional lattice.

Particularly, we will focus mostly on \mathcal{Y}_Δ which are described by *reflexive* toric diagrams. These polytopes possess a unique interior lattice point, which we will always assume that is placed at the origin. Then, a relevant property of reflexive polytopes is that its *polar dual*

$$\Delta^\circ = \{m \in \mathbb{Z}^2 \mid \langle m, \mathbf{v} \rangle \geq -1, \forall \mathbf{v} \in \Delta\} \quad (2.48)$$

is itself reflexive. Note this operation is an involution, $(\Delta^\circ)^\circ = \Delta$, therefore reflexive polytopes come in pairs (Δ, Δ°) . In section 3.6, we will see how the two associated geometries are related via Mirror Symmetry in the context of quiver gauge theory [69]. Furthermore, from the definition (2.23) it is possible to show that generators of the semigroup S_σ are in one-to-one with the points of the polar dual. The Hilbert basis is precisely the lattice points $\mathcal{H} = \Delta^\circ \times \{1\} \subset \mathbb{Z}^3$, which makes reflexive Gorenstein cones such as (2.47) simpler to work with.

A 3-dimensional CY \mathcal{Y}_Δ from a reflexive toric diagram can be thought as the “complex cone” over 2-dimensional Gorenstein Fano variety $X_{\Sigma(\Delta)}$, where the 2-dimensional fan is constructed as follows:¹³

- A vertex \mathbf{v} of the polytope corresponds to a ray of the fan $\rho_{\mathbf{v}} = \text{Cone}(\mathbf{v}) \in \Sigma(\Delta)(1)$.
- A facet F of the polytope defines a maximal cone $\sigma_F = \text{Cone}(u \mid u \in F) \in \Sigma(\Delta)(2)$, taking the apex of these cones to align with the interior point of the polytope.

The fan subdivision is self-evident by comparing the affine subvarieties from the CY 3-fold \mathcal{Y}_Δ and the affine patches of $X_{\Sigma(\Delta)}$. Let N be a rank 3 lattice and $\tau = \text{Cone}((u, 1) \mid u \in F)$ be the codimension 1 cone facet of the affine CY cone $\sigma_\Delta \succ \tau$. There exists a choice of a rank-2 lattice $N_\tau \subset N$ such that N_τ is the minimal saturated sublattice containing the generators of $\tau \subset (N_\tau)_\mathbb{R}$. Furthermore, we can obtain the orthogonal lattice to τ as the abelian group quotient $N(\tau) = N/N_\tau$.¹⁴ This choice, $N = N_\tau \oplus N(\tau)$, induces an algebra decomposition

$$\mathbb{C}[\tau^\vee \cap M] = \mathbb{C}[\tau^\vee \cap M_\tau] \otimes \mathbb{C}[M(\tau)] \quad \Rightarrow \quad U_{\tau, N} = U_{\tau, N_\tau} \times \mathbb{C}^\times \subset \mathcal{Y}_\Delta, \quad (2.49)$$

where $M(\tau)$ is the dual lattice to $N(\tau)$, and $U_{\tau, N_2} = U_{\sigma_F}$ is precisely the affine patch of $X_{\Sigma(\Delta)}$ for the cone span of the polytope facet $F \subset \Delta$. Note that $M(\tau)$ is a torsionless free abelian group of rank 1 ($\cong \mathbb{Z}$), with affine spectrum $\text{Specm}(\mathbb{C}[M(\tau)]) = \text{Specm}(\mathbb{C}[t^\pm]) = \mathbb{C}^\times$.

Example 2.5. Let Δ be the toric diagram in fig. 2.4a. Above, from the generators of the \mathbb{P}^2 ,

¹³It is important to note that the toric diagram lives in the cocharacter lattice N , so $\Sigma(\Delta)$ is not the normal fan of Δ .

¹⁴A lattice is the same thing as a finitely generated free abelian group.

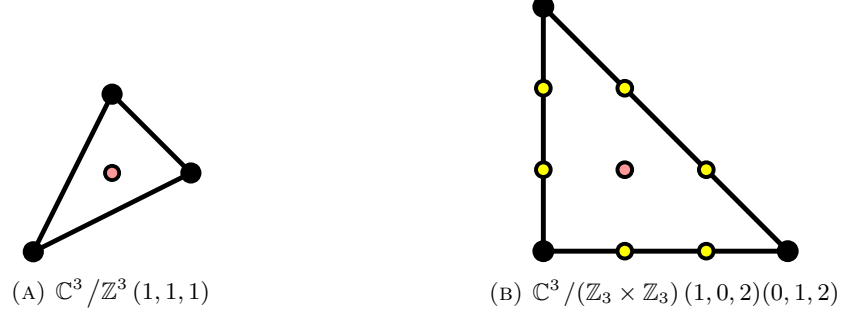


FIGURE 2.4: Reflexive toric diagrams. Black dots are vertices, red is for the origin (internal). Yellow dots are non-vertex points in facets revealing the presence of an A_n -type singularities.

we derived that the group action elements obey $t_i = t_j = t$, for all $1 \leq i, j \leq 3$. By placing the generators in a hyperplane at height 1, we have the additional condition,

$$t_1 t_2 t_3 = 1 \implies t^3 = 1. \quad (2.50)$$

This restricts \mathbb{C}^\times the action of $G = \{(\zeta, \zeta, \zeta) \mid \zeta \in \mathbb{Z}_3\}$ on the total space \mathbb{C}^3 . Note that in the quotient construction of the affine CY cone the origin is not removed. While \mathbb{P}^2 is a smooth toric variety, its complex cone $\mathbb{C}^3 / \mathbb{Z}_3 (1, 1, 1)$ is an affine variety with an orbifold singularity at the origin. The toric ideal $\mathbb{I}(\mathcal{Y}_\Delta) = I_A$ of the singular CY 3-fold is

$$\begin{aligned} \mathbb{I}(\mathcal{Y}_\Delta) = \langle & z_5 z_9 - z_7 z_8, z_5 z_6 - z_9^2, z_4 z_9 - z_6 z_8, z_4 z_7 - z_9^2, z_4 z_5 - z_8 z_9, z_3 z_9 - z_6 z_7, \\ & z_3 z_8 - z_9^2, z_3 z_5 - z_7 z_9, z_3 z_4 - z_6 z_9, z_2 z_9 - z_4 z_8, z_2 z_7 - z_8 z_9, z_2 z_6 - z_4^2, \\ & z_2 z_5 - z_8^2, z_2 z_3 - z_6 z_8, z_1 z_9 - z_5 z_7, z_1 z_8 - z_5^2, z_1 z_6 - z_7 z_9, z_1 z_4 - z_7 z_8, \\ & z_1 z_3 - z_7^2, z_1 z_2 - z_5 z_8, z_0 z_9 - z_3 z_6, z_0 z_8 - z_6 z_9, z_0 z_7 - z_3^2, z_0 z_5 - z_6 z_7, \\ & z_0 z_4 - z_6^2, z_0 z_2 - z_4 z_6, z_0 z_1 - z_3 z_7 \rangle, \end{aligned} \quad (2.51)$$

with generators of the base ring matching the lattice points of polar dual polytope 2.4b,

$$A = \begin{bmatrix} z_0 & z_1 & z_2 & z_3 & z_4 & z_5 & z_6 & z_7 & z_8 & z_9 \\ 2 & -1 & -1 & 1 & 0 & 1 & 1 & 0 & -1 & 0 \\ -1 & 2 & -1 & 0 & -1 & 1 & -1 & 1 & 0 & 0 \\ 1 & 1 & 1 & 1 & 1 & 1 & 1 & 1 & 1 & 1 \end{bmatrix}. \quad (2.52)$$

With some patience, we can write down all the 27 relations above from linear relations between the generators (columns in (2.52)). The equations define the image under the Veronese embedding $X_{\Sigma(\Delta)} \hookrightarrow \mathbb{P}^9$, where (z_0, \dots, z_9) are the homogeneous coordinates of \mathbb{P}^9 . The affine 3-fold cone \mathcal{Y}_Δ follows from an embedding in \mathbb{C}^{10} , obeying the same relations. A similar story occurs starting from the toric diagram in fig. 2.4b, where it describes the CY 3-fold $\mathcal{Y}_\Delta = \mathbb{C}^3 / (\mathbb{Z}_3 \times \mathbb{Z}_3) (1, 0, 2)(0, 1, 2)$, whereas the Fano toric variety is $X_{\Sigma(\Delta)} = \mathbb{P}^2 / \mathbb{Z}_3 (0, 1, 2)$, with the fan in fig. 2.2.

A toric surface X_Σ is *Fano* if its anticanonical divisor

$$-K_{X_\Sigma} = \sum_{\rho \in \Sigma(1)} D_\rho \quad (2.53)$$

is an ample \mathbb{Q} -Cartier divisor, *i.e.* there exists an integer $\ell > 0$ such that ℓK_{X_Σ} is Cartier. Alternatively, a simpler way to check that a divisor is ample using combinatorics of polytopes. Following directly from (2.37), global sections of a toric divisor $D = \sum_\rho a_\rho D_\rho$,

$$H^0(X_\Sigma, \mathcal{O}_{X_\Sigma}(D)) = \bigoplus_{m \in P_D \cap M} \mathbb{C} \chi^m, \quad (2.54)$$

can be described as combinations of monomials at integral points of the divisor polyhedron

$$P_D = \{m \in M_{\mathbb{R}} \mid \langle m, u_\rho \rangle + a_\rho \geq 0, \forall \rho \in \Sigma(1)\}. \quad (2.55)$$

The divisor D is *ample* if there exists a Gorenstein index ℓ such that ℓD is *very ample*, *i.e.* the toric variety generated by the monomial basis $\mathcal{A} = P_{\ell D} \cap M$ matches the original X_Σ (see eq. (2.20)). The smallest such index ℓ is called the Gorenstein index of X_Σ . Toric varieties $X_{\Sigma(\Delta)}$ from reflexive diagrams Δ are precisely the case where the toric divisors of the $\Sigma(\Delta)$ define a very ample ($\ell = 1$) anticanonical divisor whose polytope matches the polar dual of the toric diagram, $P_{-K_{\Sigma(\Delta)}} \cap M = \Delta^\circ$.

Listing the possible Fano toric surfaces corresponds to classifying all reflexive toric diagrams [71, 72]. Shifting the polytope or applying a \mathbb{Z}^n lattice automorphisms does change the resulting Fano variety. In 2 dimensions, the classification of all $\text{GL}(2, \mathbb{Z})$ -inequivalent yielded a total of 16 reflexive polytope, listed in figs. 1.4 and 2.4 [55]. There is a slight abuse of notation, in which dP_n refers simultaneously to the *del Pezzo surface* of degree $9 - n$ and the affine Calabi–Yau from taking the complex cone over it. The del Pezzo surfaces dP_n for $n \leq 8$ are blow-ups of $\text{dP}_0 = \mathbb{P}^2$ at n generic points. For $n \leq 3$, we can translate the blow-ups to fixed points of toric action. As such, dP_n surfaces for $0 \leq n \leq 3$, together with *Hirzebruch surface* $\mathbb{F}_0 = \mathbb{P}^1 \times \mathbb{P}^1$ make up the 5 smooth toric Fano varieties. The other 11 Fano varieties $X_{\Sigma(\Delta)}$ containing non-isolated *A*-type singularities are abelian orbifolds or so-called *Pseudo del Pezzo surfaces* PdP_n . Similarly, we can obtain the latter singular geometries from blow-ups on smooth Fano varieties at specific points.

As all CY 3-folds we discussed here (and even some Fano toric surfaces defining them) are singular, we will need to resort to the concept of smoothing of the *singular locus* X_{sing} . A *resolution* of a variety X is the tuple (ϕ, \tilde{X}) ,

$$\phi : \tilde{X} \rightarrow X, \quad (2.56)$$

such that the restriction of ϕ to the complement of the *exceptional locus* $\text{Exc}(\phi) = \phi^{-1}(X_{\text{sing}})$ defines an isomorphism $\tilde{X} \setminus \phi^{-1}(X_{\text{sing}}) \cong X \setminus X_{\text{sing}}$. In the case of toric singularities, resolutions can be determined in terms of a fan refinement $\Sigma \rightarrow \tilde{\Sigma}$. This is a process of subdividing the cones of a fan into “smaller” cones, in a way that the resulting collection still forms a fan. If all cones in a refined $\tilde{\Sigma}$ are smooth we refer to $(\phi, X_{\tilde{\Sigma}})$ as a full resolution, otherwise it is aptly named partial.

In the context of string theory,¹⁵ the resolutions $\phi : \mathcal{Y}_{\tilde{\Sigma}} \rightarrow \mathcal{Y}_{\Delta}$ of CY 3-folds must be *crepant*. Resolutions may introduce toric divisors associated with new rays from $\tilde{\Sigma}(1) \supseteq \sigma_{\Delta}(1)$, thereby generally breaking the Gorenstein condition. Given the unique normal $m \in M$ that defines the Gorenstein hyperplane of σ_{Δ} , a resolution is crepant if and only if $\langle m, u_{\rho} \rangle = 1$ for all $\rho \in \tilde{\Sigma}(1)$. Thus, to ensure the CY condition in the resolved geometry $\mathcal{Y}_{\tilde{\Sigma}}$ the new rays $\rho \in \tilde{\Sigma}(1) \setminus \sigma_{\Delta}(1)$ must originate from non-vertex points of the toric diagram Δ . We can refine $\sigma_{\Delta} \rightarrow \tilde{\Sigma}$ by introducing additional segments between rays, as exemplified in fig. 2.5. Furthermore, by intersecting $\tilde{\Sigma}$ with the Gorenstein hyperplane, it becomes apparent that we can identify all possible full resolutions with the fine triangulations T_{Δ} ¹⁶ of the toric diagram.

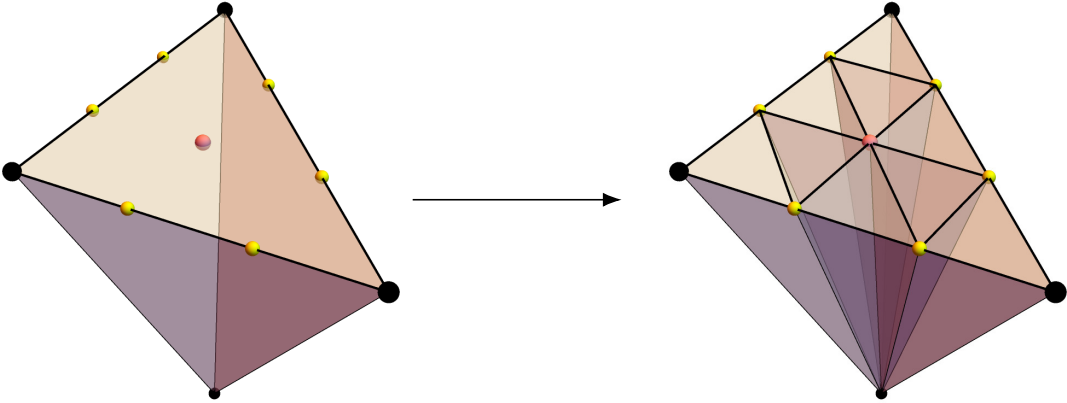


FIGURE 2.5: A full resolution $\sigma_{\Delta} \rightarrow \tilde{\Sigma}$ of the cone $\sigma_{\Delta} = \text{Cone}(\Delta \times \{1\})$ describing the singular Calabi-Yau 3-fold $\mathbb{C}^3 / (\mathbb{Z}_3 \times \mathbb{Z}_3) (1, 0, 2)(0, 1, 2)$ to a smooth fan $\tilde{\Sigma}$.

From the structure of the refined fan $\tilde{\Sigma}$ it is possible to obtain the geometry of the exceptional locus. Under the resolution $\phi : \mathcal{Y}_{\tilde{\Sigma}} \rightarrow \mathcal{Y}_{\Delta}$ the irreducible components of the exceptional locus are given by the orbit closures

$$\text{Exc}(\phi) = V(\tilde{\sigma}_1) \cup \dots \cup V(\tilde{\sigma}_r), \quad (2.57)$$

where $\tilde{\sigma}_1, \dots, \tilde{\sigma}_r$ are the irreducible/minimal cones of the refined fan $\tilde{\Sigma}$ that intersect with the relative interior of σ_{Δ} , $\text{Relint}(\sigma_{\Delta})$.

We can identify the geometry of the subvariety $V(\tau)$ as follows. For a decomposition $N = N_{\tau} \oplus N(\tau)$, where $N_{\tau} \subset N$ is the minimal saturated sublattice containing $\tau \subset (N_{\tau})_{\mathbb{R}}$, there

¹⁵For backgrounds $\mathbb{R}^{1,3} \times \mathcal{Y}_{\tilde{\Sigma}}$ without fluxes.

¹⁶In a fine triangulation T_{Δ} , all points of Δ are involved.

exists a projection $\pi : N_{\mathbb{R}} \rightarrow N(\tau)_{\mathbb{R}} = (N/N_{\tau})_{\mathbb{R}}$. Then, the fan [68]

$$\text{Star}(\tau) = \{\pi(\sigma) \subseteq N(\tau)_{\mathbb{R}} \mid \sigma \in \Sigma, \tau \preceq \sigma\} \quad (2.58)$$

defines a toric variety $X_{\text{Star}(\tau)}$ isomorphic to the orbit closure $V(\tau)$. The cone τ is collapsed to the origin and the adjacent cones $\sigma \succeq \tau$ are projected to $N(\tau)_{\mathbb{R}}$. As a consequence, we have the following equivalence for full resolutions of 3-dimensional CY_3 cones:

- $\tau \in \tilde{\Sigma}(2)$ with $\tau \cap \text{Relint}(\sigma_{\Delta}) \neq \emptyset \iff$ internal segment of $T_{\Delta} \iff$ blow-up $V(\tau) \cong \mathbb{P}^1$
- $\tau \in \tilde{\Sigma}(2)$ with $\tau \cap \text{Relint}(\sigma_{\Delta}) = \emptyset \iff$ boundary segments of $T_{\Delta} \iff V(\tau) \cong \mathbb{C}$
- $\rho \in \tilde{\Sigma}(1)$ with $\rho \cap \text{Relint}(\sigma_{\Delta}) = \emptyset \iff$ nonvertex boundary point of $\Delta \iff$ noncompact toric divisor D_{ρ} .

Furthermore, internal points in the toric diagram whose corresponding rays are in the relative interior of σ_{Δ} define the *exceptional compact divisors* D_{ρ} , whose fan $\text{Star}(\rho)$ matches with a smooth refinement of a 2-dimensional Fano variety fan. For *e.g.*, the internal ray in fig. 2.5 $\rho = \mathbb{R}_{\geq 0} \cdot (0, 0, 1)$ defines the exceptional divisor D_{ρ} , which matches the smooth geometry with 2-dimensional fan describing the *del Pezzo 3* surface (dP_3 in fig. 1.4).

2.2 Quiver representation theory

A quiver \mathcal{Q} is a multidigraph, a directed graph where multiple edges between two vertices and loops are allowed. The data defining the quiver \mathcal{Q} consists of a set of vertices \mathcal{Q}_0 , a set of edges \mathcal{Q}_1 , and two mappings $s, t : \mathcal{Q}_1 \rightarrow \mathcal{Q}_0$ defined as the “source” and “tail” of an edge. Formally, \mathcal{Q} is the ordered tuple $(\mathcal{Q}_0, \mathcal{Q}_1, s, t)$.

In this section, we provide a (very) short introduction to quiver representations, with particular focus on stability of quiver representations moduli (check [73–75] for a larger review). From now on, we assume the quivers are finite, implying that \mathcal{Q}_0 and \mathcal{Q}_1 as sets are finite.

2.2.1 Quiver representations and path algebras

A representation V of a quiver \mathcal{Q} is a realization of the quiver diagram in the category of \mathbb{C} vector spaces. Equivalently, a representation is an assignment of a \mathbb{C} -vector space V_i for each vertex $i \in \mathcal{Q}_0$, and a collection of linear maps $\phi_e : V_{t(e)} \rightarrow V_{s(e)}$ for every edge $e \in \mathcal{Q}_1$. A finite-dimensional representation V has a dimension vector $\alpha \in (\mathbb{N})^{\mathcal{Q}_0}$, where $\alpha_i = \dim V_i$.

Many of the notions of linear algebra can be extended to quiver representations. Given two representations $V = (\{V_i\}_{i \in \mathcal{Q}_0}, \{\phi_e\}_{e \in \mathcal{Q}_1})$ and $W = (\{W_i\}_{i \in \mathcal{Q}_0}, \{\psi_e\}_{e \in \mathcal{Q}_1})$, a morphism between quiver representations $f : S \rightarrow R$ is a collection of linear maps $f_i : W_i \rightarrow V_i$ such

that $f_{s(e)} \psi_e = \phi_e f_{t(e)}$ for all edges $e \in \mathcal{Q}_1$. Two representations V and W are isomorphic if f is bijective. A *subrepresentation* $W \subset V$ of a representation of \mathcal{Q} consists of subspaces $W_i \subset V_i$ and arrows $\{\psi_e\}_{e \in \mathcal{Q}_1}$ such that $\phi_e|_{W_{t(e)}} = \psi_e$. In this case, we can find an injective morphism f between representations.

It is evident that for two representations of a quiver \mathcal{Q} to be isomorphic, they must share the same dimension vector. Consequently, the vector α is always assumed to be predetermined and fixed in subsequent discussions. We denote the set of representations of \mathcal{Q} with dimension vector α by

$$\text{Rep}(\mathcal{Q}, \alpha) \cong \prod_{e \in \mathcal{Q}_1} \text{Hom}(V_{t(e)}, V_{s(e)}) . \quad (2.59)$$

The later equality is trivial, as a representation is fully specified by the linear maps ϕ_e . If we are considering representations in coordinate spaces, $V_i \cong \mathbb{C}^{\alpha_i}$, then $\text{Rep}(\mathcal{Q}, \alpha)$ has the structure of an affine space. The group $G(\alpha) = \prod_{i \in \mathcal{Q}_0} \text{GL}(V_i)$ produces a natural action on $\text{Rep}(\mathcal{Q}, \alpha)$, by a change of basis at each vertex:

$$g \cdot V = \{g_{t(e)} \phi_e g_{s(e)}^{-1} \mid e \in \mathcal{Q}_1\} , \quad (2.60)$$

for $V = (\phi_e)_{e \in \mathcal{Q}_1} \in \text{Rep}(\mathcal{Q}, \alpha)$ and $g = (g_i)_{i \in \mathcal{Q}_0} \in G(\alpha)$. Orbits of $G(\alpha)$ are isomorphism classes of quiver representations.

Path algebras encapsulate the essence of quiver representations in an algebraic framework, offering a versatile tool for probing deeper into the underlying structure of quivers. The path algebra of \mathcal{Q} over a field k , usually denoted as $k\mathcal{Q}$, is an associative k -algebra where the basis elements u_p are given by paths in the quiver \mathcal{Q} . For the complex field, the elements of the path algebra can be separated into elements of $S = \mathbb{C}^{\mathcal{Q}_0}$ and $A = \mathbb{C}^{\mathcal{Q}_1}$. For each vertex $i \in \mathcal{Q}_0$, there is a length-zero trivial path (no edge) with algebra element $\mathbb{1}_i \in S$. Similarly, for each $e \in \mathcal{Q}_1$ we have an element $u_e \in A$, with multiplication equivalent to the concatenation of paths,

$$u_{e_1} u_{e_2} = \begin{cases} u_{e_1 e_2} & t(e_1) = s(e_2) \\ 0 & \text{otherwise} \end{cases} . \quad (2.61)$$

For $\mathbb{1}_i \in S$, $u_e \in A$, then $\mathbb{1}_i u_e = u_e$ if $s(e) = i$ and $u_e \mathbb{1}_i = u_e$ if $t(e) = i$, otherwise vanishing. Vertex elements are idempotent, $\mathbb{1}_i(\mathbb{1} - \mathbb{1}_i) = 0$, with identity element $\mathbb{1} = \sum_{i \in \mathcal{Q}_0} \mathbb{1}_i$. Thus, S is a finite dimensional commutative \mathbb{C} -algebra, and A is a finite-dimensional S -bimodule. The path algebra can be decomposed as [73, 74]

$$\mathbb{C}\mathcal{Q} = \bigoplus_{d=0}^{\infty} A^{\otimes_S d} = S \oplus A \oplus (A \otimes_S A) \oplus (A \otimes_S A \otimes_S A) \oplus \cdots \quad (2.62)$$

Note that we can further decompose the path algebra of any length d into algebras of paths starting at vertex i and ending at j , $A^{\otimes s d} = \bigoplus_{i,j \in \mathcal{Q}_0} \mathbb{1}_i A^{\otimes s d} \mathbb{1}_j$, since the trivial path elements $\mathbb{1}_i$ act as a projection.

We can jump between representations of \mathcal{Q} and modules (representations) over the path algebra $\mathbb{C}\mathcal{Q}$ since we can establish a bijection between the two.¹⁷ For a quiver representation V , a path $p = e_1 \dots e_\ell$ defines a linear map $\phi_p : V_{t(e_\ell)} \rightarrow V_{s(e_1)}$, given by $\phi_p = \phi_{e_1} \phi_{e_2} \dots \phi_{e_\ell}$. Thus, we can trivially define a $\mathbb{C}\mathcal{Q}$ -module structure on $\bigoplus_{i \in \mathcal{Q}_0} V_i$, meaning

$$u_p v = \begin{cases} \phi_p(v) & v \in V_{t(p)} \\ 0 & \text{otherwise} \end{cases} . \quad (2.63)$$

On the other hand, if V is a $\mathbb{C}\mathcal{Q}$ -module, we can define the vector subspaces $V_i = \mathbb{1}_i V$. Additionally, for each edge $e \in \mathcal{Q}_1$ we can define edge maps $\phi_e : V_{t(e)} \rightarrow V_{s(e)}$ as $\phi_e(v) = u_e v$. Therefore, $(\{V_i\}, \{\phi_e\})$ is a representation of \mathcal{Q} .

Now that we have established a connection between the affine space $\text{Rep}(\mathcal{Q}, \alpha)$ with modules of the path algebra $\mathbb{C}\mathcal{Q}$, we can generalize the same ideas for a given path subalgebra, in particular for quotient subalgebras defined by a quiver potential. A potential W is an element of trace space $\text{Tr}(\mathbb{C}\mathcal{Q}) = \mathbb{C}\mathcal{Q}/[\mathbb{C}\mathcal{Q}, \mathbb{C}\mathcal{Q}]$, in which elements in the path algebra $\mathbb{C}\mathcal{Q}$ are equivalent up to commutators of paths. For any open path $u_{p_1 p_2} = u_{p_1} u_{p_2}$ the commutator is $[u_{p_1}, u_{p_2}] = u_{p_1 p_2}$, since $t(p_2) \neq s(p_1)$, which implies all open paths in the trace algebra are in the zero equivalence class. In general¹⁸, potentials will be of the form [74, 76]

$$W = \sum_c \alpha_c u_c , \quad \text{with } s(c) = t(c) , \quad (2.64)$$

meaning c is a cycle in the quiver and $\alpha_c \in \mathbb{C}$. Additionally, the potential can be restricted to have a fixed degree n in the tensor algebra (fixed cycle length), $W \in \text{Tr}(A^{\otimes n})$, or with fixed degree in some other grading.

For every element $u \in A$, we can define the cyclic derivative $\partial_u \in A^*$ is the continuous \mathbb{C} -linear map acting on cyclic paths by [74, 76]

$$\partial_u(u_{e_1} u_{e_2} \dots u_{e_d}) = \sum_p \partial_u(u_{e_p}) u_{e_{p+1}} \dots u_{e_d} u_{e_1} \dots u_{e_{p-1}} . \quad (2.65)$$

Similarly, there exists a dual basis $\{\partial_{u_e}\}_{e \in \mathcal{Q}_1}$ such that $\partial_{u_e}(u_{e'}) = \delta_{ee'}$. Abbreviate $\partial_e \equiv \partial_{u_e}$. The *Jacobian ideal* $J(W) = \langle \partial_e W \mid e \in \mathcal{Q}_1 \rangle \subseteq \mathbb{C}\mathcal{Q}$ [73, 74] is the ideal generated by the

¹⁷We say that the abelian category of finite dimensional representations of \mathcal{Q} is the same as the category of modules over the path algebra, $\mathbb{C}\mathcal{Q}\text{-Mod}$, *i.e.* the category of finite dimensional representations of $\mathbb{C}\mathcal{Q}$.

¹⁸We will only consider finite potentials. Therefore, we are avoiding discussing the complete path algebra $\widehat{\mathbb{C}\mathcal{Q}} = \prod_{d=0}^{\infty} A^{\otimes s d}$, and the closure of the commutator algebra, which includes infinite paths.

relations $\partial_e W = 0$ for all $e \in \mathcal{Q}_1$. We call the quotient [74, 76]

$$\mathcal{A}_{\mathcal{Q},W} = \mathbb{C}\mathcal{Q}/\langle \partial_e W \mid e \in \mathcal{Q}_1 \rangle \quad (2.66)$$

the *Jacobian algebra* of W . This algebra obeys the *cancellation* property, meaning that if for every arrow $e \in \mathcal{Q}_1$ and any two path elements $u_p, u_q \in \mathcal{A}_{\mathcal{Q},W}$, with $t(e) = h(p) = h(q)$, then if $u_e u_p = u_e u_q \Rightarrow u_p = u_q$.

From the categorical equivalency established above, points (representations) of a $G(\alpha)$ -invariant affine space $\text{Rep}(\mathcal{Q}; \alpha)$ are associated to modules of the free path algebra (zero potential). By the same token, a module of the subalgebra $\mathcal{A}_{\mathcal{Q},W} \subseteq \mathbb{C}\mathcal{Q}$ is associated to a given representation in $\text{Rep}(\mathcal{Q}; \alpha)$ such that its edge maps are compatible with the relations provided by the Jacobian ideal. We denote this subvariety as $\text{Rep}(\mathcal{Q}, W; \alpha)$, which is obviously is contained within $\text{Rep}(\mathcal{Q}; \alpha)$ [73, 77]:

$$\begin{aligned} \text{Rep}(\mathcal{Q}; \alpha) &\leftrightarrow \mathbb{C}\mathcal{Q} \\ \text{Rep}(\mathcal{Q}, W; \alpha) &\leftrightarrow \mathbb{C}\mathcal{Q}/J(W) \end{aligned}$$

We will use the space $\text{Rep}(\mathcal{Q}, W; \alpha)$ to build moduli spaces, by constructing appropriate quotients by $G(\alpha)$.

Given a strongly connected quiver \mathcal{Q} and a potential W , we can enlarge the quiver by disjoint sets of cycles $\mathcal{Q}_2 = \mathcal{Q}_2^+ \sqcup \mathcal{Q}_2^-$, such that the potentials follow $W = \sum_{c \in \mathcal{Q}_2^+} u_c - \sum_{c \in \mathcal{Q}_2^-} u_c$. This defines a *dimer model* (\mathcal{Q}, W) [78]. Every edge e must be contained exactly once in one cycle in \mathcal{Q}_2^+ and \mathcal{Q}_2^- . Additionally, the incidence graph of the cycles and arrows meeting a given vertex is connected. Thus, for every $e \in \mathcal{Q}_1$, relations are $\partial_e W = u_{p^+} - u_{p^-}$, $p^\pm e \in \mathcal{Q}_2^\pm$, which imply that every cycle in \mathcal{Q}_2 is equivalent in the Jacobi algebra $\mathcal{A}_{\mathcal{Q},W}$. Given a dimer model characterized by (\mathcal{Q}, W) , we can embed it in a compact orientable surface with an Euler characteristic $\chi_{\mathcal{Q}} = |\mathcal{Q}_0| - |\mathcal{Q}_1| + |\mathcal{Q}_2|$, such that the cycles in \mathcal{Q}_2^+ and \mathcal{Q}_2^- are oriented oppositely, with one set being clockwise.

In the realm of physics, dimer models are often discussed as a framework for understanding certain aspects of string theory and gauge theories [41]. A brane tiling is conceptualized starting from the dual of graph (\mathcal{Q}, W) as defined above, which involves embedding a bipartite graph on a surface of Euler characteristic $\chi_{\mathcal{Q}}$, where the nodes correspond to \mathcal{Q}_2 , the edges to \mathcal{Q}_1 , and the cycles (faces) to \mathcal{Q}_0 . In physics parlance, the terms brane tiling and dimer model (or dual of), are often used interchangeably. We will dive deeper into brane tilings, from a more physical perspective, in a later chapter.

2.2.2 Moduli of quiver representations

Viewing quiver representations as an affine variety, we can construct moduli by taking quotients by a group action. We will focus on two approaches to construct moduli that

appear in supersymmetry gauge theory. The first approach involves Geometric Invariant Theory (GIT) [79], where we consider an algebraic quotient of the complex $\text{Rep}(\mathcal{Q}, W; \alpha)$ by the action of the complex reductive Lie group $G(\alpha)$. The second approach involves a set-theoretic quotient [80, 81], which is derived as level-set of the space of representations as a (real) symplectic manifold identified by orbits of the compact real Lie group $K(\alpha)$, such that $G(\alpha) = K(\alpha)_{\mathbb{C}}$. These are related, since every compact connected Lie group has a reductive algebraic complexification. Then, by the celebrated theorem of Kempf and Ness [82], as long as the complex variety is projective the symplectic quotient is in fact homeomorphic to the algebraic quotient, when considered as a complex analytic variety.

2.2.2.1 Proj GIT quotient

Let \mathcal{Z} be a complex variety, G be a reductive algebraic group, and we will appropriately take $k = \mathbb{C}$ to be our algebraic closed base field. The group action on \mathcal{Z} by the group is an algebraic map $G \times \mathcal{Z} \rightarrow \mathcal{Z}$, where we will denote the image of (g, z) by $g \cdot z$. A morphism $f : \mathcal{Z} \rightarrow \mathcal{X}$ is G -invariant if $f(g \cdot z) = f(z)$ for all g and z . For instance, if \mathcal{Z}, \mathcal{X} are affine then we are considering invariant functions on \mathcal{Z} , which form a subring $\mathbb{C}[\mathcal{Z}]^G \subseteq \mathbb{C}[\mathcal{Z}]$ of the coordinate ring of \mathcal{Z} .

In GIT, we can lift the action of the group to a linearized trivial line bundle $\mathcal{Z} \times \mathbb{C} \rightarrow \mathcal{Z}$, by a character $\chi \in \text{Hom}(G, \mathbb{C}^{\times})$. The action $G \times (\mathcal{Z} \times \mathbb{C}) \rightarrow \mathcal{Z} \times \mathbb{C}$ is defined as

$$g \cdot (z, t) \mapsto (g \cdot z, \chi(g)^n t) \quad (2.67)$$

In the coordinate ring of the trivial bundle, $\mathbb{C}[\mathcal{Z} \times \mathbb{C}]$, the group acts as $(g \cdot f)(z, t) = f(g^{-1} \cdot z, \chi(g)^{-n} t)$, which can be rewritten as

$$g \cdot f(z, t) = g \cdot \sum_{n \geq 0} f_n(z) t^n = \sum_{n \geq 0} f_n(g^{-1} \cdot z) \chi(g)^{-n} t^n, \quad (2.68)$$

since $\mathbb{C}[\mathcal{Z} \times \mathbb{C}] = \mathbb{C}[\mathcal{Z}] \otimes \mathbb{C}[t]$. Thus, for f to be G -invariant, we must have $g \cdot f_n = \chi(g)^n f_n$ for all n . We call such functions $f_n \in \mathbb{C}[\mathcal{Z}]$ as χ^n -semi-invariants, which defines a \mathbb{N} -grading on the polynomials of the fiber bundle

$$R = \mathbb{C}[\mathcal{Z} \times \mathbb{C}]^G = \bigoplus_{n \in \mathbb{N}} \mathbb{C}[\mathcal{Z}]^{\chi^n}, \quad (2.69)$$

where $\mathbb{C}[\mathcal{Z}]^{\chi^n}$ is a ring of semi-invariants.

The GIT quotient [79] is the quasi-projective variety corresponding to the closed points of

$$\mathcal{Z} //_{\chi} G = \text{Proj } \mathbb{C}[\mathcal{Z} \times \mathbb{C}]^G. \quad (2.70)$$

The closed points of $\text{Proj } R$, for a graded ring $R = \bigoplus_{n \geq 0} R_n$, are naturally in correspondence with the homogeneous (under the induced grading) maximal ideals that do not contain the *irrelevant ideal* $R_+ = \bigoplus_{n > 0} R_n$ [83].

There is a way to understand the points of $\mathcal{Z} //_{\chi} G$ instead of looking at ideals of $\mathbb{C}[\mathcal{Z} \times \mathbb{C}]^G$, using the idea of χ -semistability. A point $z \in \mathcal{Z}$ is χ -*semistable* if for some $n > 0$ there exists a nonvanishing semi-invariant $f \in \mathbb{C}[\mathcal{Z}]^{\chi^n}$ such that $z \in \mathcal{Z}_f \equiv \{w \in \mathcal{Z} \mid f(w) \neq 0\}$. Thus, the set of all χ -semistable points are defined as

$$\mathcal{Z}_{\chi}^{\text{ss}} = \bigcup_{f \in R_+} \{z \in \mathcal{Z} \mid f(z) \neq 0\}. \quad (2.71)$$

If, in addition, \mathcal{Z}_f is closed under the action of G and the stabilizer G_z is finite, then we say that z is χ -*stable*.

Two points in $z_1, z_2 \in \mathcal{Z}_{\chi}^{\text{ss}}$ are called *S-equivalent* if and only if the intersection of the closure of the G -orbits is nonempty in the set of semistable points, meaning that [84]

$$\overline{G \cdot z_1} \cap \overline{G \cdot z_2} \cap \mathcal{Z}_{\chi}^{\text{ss}} \neq \emptyset. \quad (2.72)$$

For each point in $z \in \mathcal{Z}$, we can define a maximal ideal $\mathfrak{m}_z = \{f \in R \mid f(z) = 0\}$, and in particular if z is χ -semistable then \mathfrak{m}_z is also homogeneous and does not contain the irrelevant ideal R_+ . Moreover, we have that $\mathfrak{m}_{z_1} = \mathfrak{m}_{z_2}$ for two S-equivalent points z_1, z_2 . Therefore, the GIT quotient $\mathcal{Z} //_{\chi} G$ is a variety whose points are in natural bijection with the S-equivalence classes of χ -semistable points of \mathcal{Z} [79].

Example 2.6. Consider the construction of \mathbb{P}^n via action of $G = \mathbb{C}^{\times}$ on \mathbb{C}^{n+1} , defined as $\lambda \cdot (z_0, \dots, z_n) = (\lambda z_0, \dots, \lambda z_n)$, together with choice of character $\chi(\lambda) = \lambda^{-1}$. For this choice, χ^n -semi-invariants are just the homogeneous polynomials of degree n . Therefore, $R_{\chi} = \mathbb{C}[z_0, \dots, z_n]$, with the standard \mathbb{N} -grading, for which $\mathbb{P}^n = \text{Proj } \mathbb{C}[z_0, \dots, z_n]$. The origin is the only point that is not χ -semistable, since all polynomials of degree $n > 0$ vanish at 0. From the construction above, $\mathfrak{m}_0 = \{f \in R \mid f(0) = 0\}$ contains (is exactly) the irrelevant ideal R_+ , and therefore we need to exclude the origin from the semistable set. For $z \neq 0$, we can identify maximal ideals $\mathfrak{m}_z = \mathfrak{m}_{\lambda \cdot z}$, since any homogeneous f obeys $f(\lambda \cdot z) = \lambda^n f(z)$. The closure of orbits of \mathbb{C}^{\times} are lines going through the origin and are in one-to-one with S-equivalence classes of orbits as they intersect outside $(\mathbb{C}^{n+1})_{\chi}^{\text{ss}} = \mathbb{C}^{n+1} \setminus \{(0, \dots, 0)\}$.

2.2.2.2 Symplectic reduction

To define the symplectic reduction one must study the action of a real compact Lie group K on a manifold M with a closed nondegenerate 2-form $\omega \in \Gamma(\wedge^2 T^*M)$. A symplectic manifold (M, ω) provides a geometric canvas for the expression of the phase space of Hamiltonian dynamics, which can be thought as being parametrized by coordinates x_i and its conjugate

momentum p_i . The form ω allows us to connect a position and momentum coordinates via the contraction $\iota_X \omega \in \Gamma(T^*M)$ for some direction $X \in \Gamma(TM)$. Locally, this relation becomes more clear, as it has the form $dp_i = \iota_{\partial_{x_i}} \omega$. Moreover, a general vector field X_H is called hamiltonian if $\iota_{X_H} \omega = dH$ is an exact form, and it has an associated hamiltonian function H , which is preserved along its flow lines [85].

A compact Lie group K with a free and proper action, defines a class of diffeomorphisms $\psi : G \rightarrow \text{Diff}(M)$, $g \mapsto \psi_g$, for all $g \in K$, which we can also denote as $\psi_g(p) = g \cdot p$. We also require that this action respects the symplectic structure on M , which can be written as $(\psi_g)^* \omega = \omega$ (ψ_g is symplectomorphic). A Lie algebra element $\zeta \in \mathfrak{k}$ induces a vector field at some point $p \in M$ by the infinitesimal action

$$(X^\zeta)_p = \frac{d}{dt} \left[\psi_{\exp(i\zeta t)}(p) \right]_{|t=0} \quad (2.73)$$

The compatibility of the action with the symplectic structure is equivalent to $\iota_{X^\zeta} \omega$ being closed for all $\zeta \in \mathfrak{k}$ (X^ζ is called symplectic). This action has a *moment map*

$$\mu : M \rightarrow \mathfrak{k}^* , \quad (2.74)$$

where the ζ -component $\mu^\zeta : M \rightarrow \mathbb{R}$, defined by $\mu^\zeta(p) = \langle \mu(p), \zeta \rangle$, is a hamiltonian function for the vector field X^ζ ,

$$d\mu^\zeta + \iota_{X^\zeta} \omega = 0 . \quad (2.75)$$

Additionally, the moment map is required to be K -equivariant, more formally written as

$$\mu(g \cdot p) = \text{Ad}_g^* \mu(p) , \quad \forall g \in K , \quad (2.76)$$

where $\text{Ad}^* : K \rightarrow \text{Aut}(\mathfrak{k}^*)$ is the coadjoint representation. Due to the latter property, orbits of the coadjoint stabilizer $K^\xi = \{g \in K \mid \text{Ad}_g^* \xi = \xi\}$ have the same level under the moment map.

Now we can define the symplectic reduction of a hamiltonian space (M, ω, K, μ) . Let $\xi \in \mathfrak{k}^*$ be a regular value of μ . This is equivalent to requiring that K acts freely on $\mu^{-1}(\xi)$, *i.e.* the stabilizer $K_p = \{g \in K \mid g \cdot p = p\}$ is trivial for all $p \in \mu^{-1}(\xi)$. Then, the *symplectic reduction* at ξ is the smooth manifold (space of orbits) [80]

$$M //_\xi K = \mu^{-1}(\xi) / K^\xi \quad (2.77)$$

and there is a unique symplectic form inherited from (M, ω) . The level-set is quotiented by the entire group if ξ is central, $K^\xi = K$.¹⁹ However, we can bypass the central assumption by

¹⁹All levels $\xi \in \mathfrak{k}^*$ are central if K is abelian.

considering the coadjoint orbit $O^\xi = \text{Ad}_K^* \xi \subseteq \mathfrak{k}^*$. We can lift the symplectic structure onto $M \times O^\xi$ and the diagonal action of K is hamiltonian with the shifted moment map

$$\tilde{\mu} : M \times O^\xi \rightarrow \mathfrak{k}^* \quad (p, \eta) \mapsto \mu(p) - \eta. \quad (2.78)$$

Additionally, K acts freely on $\mu^{-1}(\xi)$ iff K also acts freely on $\tilde{\mu}^{-1}(0)$. In this case, $M //_\xi K$ and $(M \times O^\xi) //_0 K$ are well-defined and symplectomorphic.

While considering coadjoint orbits can simplify assumptions, a more physically valid approach is to relax the condition that K must act freely on $\mu^{-1}(0)$. As long as K_p is discrete and finite for $p \in \mu^{-1}(0)$ and K is a torus, then the quotient $\mu^{-1}(0)/K$ is still trackable, resulting in a space with singularities, often with the structure of an orbifold.

Example 2.7. We can repeat the example of \mathbb{P}^n , now via symplectic reduction on \mathbb{C}^{n+1} with the standard symplectic structure $\omega = \frac{i}{2} \sum_{i=0}^n dz_i \wedge d\bar{z}_i$. In this case, we have the compact Lie group $K = \text{U}(1)$, with action $e^{i\theta} \cdot (z_0, \dots, z_n) = (e^{i\theta} z_0, \dots, e^{i\theta} z_n)$. The vector field generated by $\theta \in \mathfrak{u}(1)$ is given by $X^\theta = i\theta \sum_{i=0}^n (z_i \partial_i - \bar{z}_i \bar{\partial}_i)$, and obeys

$$\iota_{X^\theta} \omega = -\theta \sum_{i=0}^n (z_i d\bar{z}_i + \bar{z}_i dz_i) = -d\mu^\theta = -\theta d\mu \quad (2.79)$$

with the moment map given by

$$\mu : \mathbb{C}^n \rightarrow \mathfrak{u}(1)^* = \mathbb{R} \quad (z_0, \dots, z_n) \mapsto \sum_{i=0}^n |z_i|^2. \quad (2.80)$$

Then, $\mu^{-1}(1) \cong S^{2n+1} \subset \mathbb{C}^{n+1}$ and the symplectic quotient is $S^{2n+1}/\text{U}(1) = \mathbb{P}^n$. Note that \mathbb{C}^\times is the complexification of $K = \text{U}(1)$, which plays an important role in relating this quotient with section 2.2.2.1.

2.2.2.3 Kempf-Ness theorem

In this work, we will often use the previous quotient constructions to build moduli of quiver representations. Recall that we defined the $\mathcal{Z} = \text{Rep}(\mathcal{Q}, W; \alpha)$ as the representation space of the quiver \mathcal{Q} , consistent with relations ∂W . Taking $V_i \cong \mathbb{C}^{\alpha_i}$, this space is complex with a natural algebraic action of the complex reductive Lie group $G(\alpha)$. We will see later that we can mostly focus on representations with the unit dimension vector, so we will take $\alpha = \mathbb{1}$.

For quiver representations with general vector dimension α , characters are given by $\chi^\theta = \prod_{i \in \mathcal{Q}_0} \det^{-\theta_i}$, since each element in the product $\det^{-\theta_i} : \text{GL}(\alpha_i, \mathbb{C}) \rightarrow \mathbb{C}^\times$ is the most general 1-dimensional representation. For unit dimension vector, the character is simply $\chi^\theta(t) = \prod_{i \in \mathcal{Q}_0} (t_i)^{-\theta_i}$. These are completely determined by choice of integers $\theta \in \mathbb{Z}^{\mathcal{Q}_0}$, for

which we can define the GIT quotient as

$$\mathcal{M}(\mathcal{Q}, W; \theta)_{\text{GIT}} = \text{Rep}(\mathcal{Q}, W; \alpha) //_{\chi^\theta} G(\alpha) . \quad (2.81)$$

Turning now to the symplectic reduction, we can endow the complex variety $\text{Rep}(\mathcal{Q}, W; \alpha)$ with the standard symplectic structure. Additionally, the largest compact real Lie group in $G(\alpha)$ is $K(\alpha) = \prod_{i \in \mathcal{Q}_0} \text{U}(1)$ and defines a hamiltonian action with a moment map. In this case, the symplectic reduction defines a quotient

$$\mathcal{M}(\mathcal{Q}, W; \xi)_{\text{K}} = \text{Rep}(\mathcal{Q}, W; \alpha) //_{\xi} K(\alpha) . \quad (2.82)$$

These two quotients are connected through the *Kempf–Ness theorem* [82]

$$\mathcal{M}(\mathcal{Q}, W; \xi)_{\text{K}} \cong \mathcal{M}(\mathcal{Q}, W; \theta)_{\text{GIT}} , \quad \text{for } \xi = \theta \in \mathbb{Z}^{\mathcal{Q}_0} , \quad (2.83)$$

via a homeomorphism of complex analytic varieties. Note that, while the symplectic reduction is defined for real levels of the moment map, in the GIT quotient the space of characters that produces the \mathbb{N} -grading in the ring of functions in the line bundle of quiver representations is equivalent to $\mathbb{Z}^{\mathcal{Q}_0}$.

2.2.3 θ -stability of quiver representations

Building upon the foundations laid by the GIT quotient and the Kempf–Ness theorem above, we will explore how θ -stability serves as a way to distinguish between stable, semistable, and unstable representations in the context of quiver representations. These notions can be generally be understood via the study of the group action and classification of orbits, but this can be simplified by the *Hilbert–Mumford criterion* [79] and a theorem by King [77].

We need to start by better understanding the characters and one-parameter subgroups of $G(\alpha)$. A one-parameter subgroup λ is an element of $\text{Hom}(\mathbb{C}^\times, G(\alpha))$, while a character χ is an element of $\text{Hom}(G(\alpha), \mathbb{C}^\times)$. We can define the inner-product

$$\langle -, - \rangle : \text{Hom}(\mathbb{C}^\times, G(\alpha)) \times \text{Hom}(G(\alpha), \mathbb{C}^\times) \rightarrow \mathbb{Z} . \quad (2.84)$$

This is possible since the composition of the two elements $\chi \circ \lambda \in \text{Hom}(\mathbb{C}^\times, \mathbb{C}^\times)$, which is group-isomorphic to \mathbb{Z} via the map $t^n \mapsto n$.

Let $G(\alpha)$ be the reductive group acting on the affine variety \mathcal{Z} . A point $z \in \mathcal{Z}$ is χ -semistable if and only if for any one-parameter subgroup λ such that $\lim_{t \rightarrow \infty} \lambda(t) \cdot z$ exists we have $\langle \lambda, \chi \rangle \geq 0$. If the inequality is strict for any nontrivial such λ , then z is χ -stable.

For unframed quivers like the ones we focus on, each point of $\text{Rep}(\mathcal{Q}, \alpha)$ has a nontrivial subgroup $\Gamma \cong \mathbb{C}^\times$ ²⁰ contained in its stabilizer. Therefore, we must include the condition that $\chi(\Gamma) = 1$ in the semistability condition.

As we have seen above, when $\alpha = \mathbf{1}$, a character χ of $G(\alpha) = (\mathbb{C}^\times)^{\mathcal{Q}_0}$ is fully determined by a $\theta \in \mathbb{Z}^{\mathcal{Q}_0}$, which we can explicitly write as $\chi(t_1, \dots, t_{|\mathcal{Q}_0|}) = \prod_{i \in \mathcal{Q}_0} (t_i)^{-\theta_i}$. Similarly, a one-parameter subgroup must be of the form $\lambda(t) = (t^{\beta_1}, \dots, t^{\beta_{|\mathcal{Q}_0|}})$, for $\beta \in \mathbb{Z}^{\mathcal{Q}_0}$. So the inequality for quivers can be simply be written as

$$\langle \lambda, \chi \rangle \geq 0 \quad \Leftrightarrow \quad \theta \cdot \beta \leq 0. \quad (2.85)$$

Note that $\chi(\Gamma) = 1$ requires χ to be a character of $\mathbb{P}G(\alpha)$. This is equivalent to $\theta \cdot \alpha = 0$.

The definition of θ -(semi)stability follows from this criterion. Given $\theta \in \mathbb{R}^{\mathcal{Q}_0}$, a representation V of the quiver \mathcal{Q} with (nonzero) dimension vector α is called θ -semistable if $\theta \cdot \alpha = 0$ and for any subrepresentation $W \subset V$ with dimension vector β we have $\theta \cdot \beta \leq 0$. We say that V is θ -stable if under the previous assumptions $\theta \cdot \beta < 0$ for any nontrivial proper subrepresentation $W \subset V$ with dimension vector β .

These results can be tied together with a theorem by King [77]. Let \mathcal{Q} be a quiver, and let $\theta \in \mathbb{Z}^{\mathcal{Q}_0}$. Let $\alpha \in \mathbb{N}$ be a dimension vector such that $\theta \cdot \alpha = 0$. Then, any $V \in \text{Rep}(\mathcal{Q}, \alpha)$ is χ_θ -semistable (resp. χ_θ -stable) if and only if V is θ -semistable (resp. θ -stable).

²⁰This corresponds to the complexification of the trivially acting diagonal $U(1)$ in the quiver gauge theory.

Chapter 3

Quiver gauge theories and Brane Tilings

3.1 4d $\mathcal{N} = 1$ supersymmetric gauge theory

We aim to recap the minimal supersymmetric gauge theory in 4-dimensions, enumerating representations of the supersymmetry algebra and how to formulate the lagrangian description of a theory [86].

It is well-known that the Lorentz symmetry in 1+3 dimensions is parametrized by pure rotations and boosts $M_{\mu\nu}$. From this set, we can construct two sets of $\mathfrak{su}(2)$ generators. However, since we started by using real parameters for the transformation (angles and rapidity), these two sets are complex conjugates and therefore not really independent. The trick here is to consider complex representations of the complexified algebra

$$\mathfrak{so}(1, 3)_{\mathbb{C}} = \mathfrak{sl}(2, \mathbb{C}) \oplus \mathfrak{sl}(2, \mathbb{C}) , \quad (3.1)$$

and, to obtain regular (bosonic) representations of $\mathrm{SO}^{\uparrow}(1, 3)$, we restrict to representations (a, b) , where $a + b \in \mathbb{Z}$. The correct way of interpreting the latter is as representations of the double cover $\mathrm{Spin}^{\uparrow}(1, 3) = \mathrm{SL}(2, \mathbb{C})$, where these can have labels such that $a + b \in \frac{1}{2}\mathbb{Z}$ (bosonic and fermionic). Some examples are: scalar representation $(0, 0)$, vector representation $(\frac{1}{2}, \frac{1}{2})$, symmetric traceless representation $(1, 1)$, Dirac representation $(\frac{1}{2}, 0) \oplus (0, \frac{1}{2})$, Weyl spinors $(\frac{1}{2}, 0)$ or $(0, \frac{1}{2})$.

The supersymmetric algebra in 4 dimensions consists of extending the Poincaré algebra into a \mathbb{Z}_2 -graded superalgebra, $\mathfrak{g} = \mathfrak{g}_0 \oplus \mathfrak{g}_1$, which includes the generators $M_{\mu\nu}$, P_{μ} and additional sets of supercharges. For $\mathcal{N} = 1$ supersymmetry, we have 4 supercharges Q_{α} and $\bar{Q}_{\dot{\alpha}}$, transforming as fundamental/anti-fundamental representations $(\frac{1}{2}, 0)$ and $(0, \frac{1}{2})$, respectively, of the complexified Lorentz algebra. It is easy to check that the Lorentz action

on $Q_\alpha, \bar{Q}_{\dot{\alpha}}$ together with the graded Jacobi identities completely fix the algebra, up to normalizations.

$$\begin{aligned} \{Q_\alpha, \bar{Q}_{\dot{\alpha}}\} &= 2(\sigma^\mu)_{\alpha\dot{\alpha}} P_\mu \\ [M^{\mu\nu}, Q_\alpha] &= i(\sigma^{\mu\nu})_\alpha{}^\beta Q_\beta, \\ [M^{\mu\nu}, \bar{Q}_{\dot{\alpha}}] &= i(\bar{\sigma}^{\mu\nu})^{\dot{\alpha}}{}_{\dot{\beta}} \bar{Q}^{\dot{\beta}} \end{aligned} \quad (3.2)$$

where $\sigma^\mu = (\mathbb{1}, -\sigma_i)$ and $\sigma^{\mu\nu} = \frac{1}{4}(\sigma^\mu \bar{\sigma}^\nu - \sigma^\nu \bar{\sigma}^\mu)$. For $\mathcal{N} = 1$ SUSY, we may still have¹ a U(1) R -symmetry which acts as a rotation on supercharges

$$[R, Q_\alpha] = -Q_\alpha, \quad [R, \bar{Q}_{\dot{\alpha}}] = \bar{Q}_{\dot{\alpha}}. \quad (3.3)$$

The charges Q_α and $\bar{Q}_{\dot{\alpha}}$ live in the fundamental/anti-fundamental representation of the R -symmetry, with charges ± 1 .

Theories involving the minimal $\mathcal{N} = 1$ supersymmetry and its supermultiplets can be constructed using the notion of superspace and superfield. This space includes the usual spacetime coordinates together with a set of conjugate Grassmann variables θ_α and $\bar{\theta}^{\dot{\alpha}}$. A general superfield is a field on this superspace and due to the properties of the Grassmann algebra, any superfield can be expanded as

$$\begin{aligned} Y(x, \theta, \bar{\theta}) &= \phi(x) + \theta \psi(x) + \bar{\theta} \bar{\chi}(x) + \theta\theta M(x) + \bar{\theta}\bar{\theta} N(x) + (\theta\sigma^\mu\bar{\theta}) A_\mu(x) \\ &\quad + (\theta\theta) \bar{\theta} \bar{\lambda}(x) + (\bar{\theta}\bar{\theta}) \theta \rho(x) + \theta\theta \bar{\theta}\bar{\theta} D(x), \end{aligned} \quad (3.4)$$

where $\theta\theta = \varepsilon_{\alpha\beta} \theta^\alpha \theta^\beta$ corresponds to the usual $\text{SL}(2, \mathbb{C})$ contraction (similar for $\bar{\theta}$). These will be transformed under pure supertranslations generated by the superalgebra as

$$\delta_{\epsilon, \bar{\epsilon}} Y(x^\mu, \theta_\alpha, \bar{\theta}^{\dot{\alpha}}) = Y(x^\mu + i(\theta\sigma^\mu\bar{\epsilon}) - i(\epsilon\sigma^\mu\bar{\theta}), \theta_\alpha + \epsilon_\alpha, \bar{\theta}^{\dot{\alpha}} + \bar{\epsilon}^{\dot{\alpha}}) \quad (3.5)$$

A general superfield corresponds to a reducible representation of SUSY, but we can impose constraints leading to fields that are indeed irreducible. The most relevant for gauge theories are chiral/anti-chiral superfields, which later will constitute the matter content. These are defined as,

$$\bar{D}_{\dot{\alpha}} \Phi = 0, \quad (3.6)$$

where the supercovariant derivative is given by $D_\alpha = \partial_\alpha + i(\sigma^\mu \bar{\theta})_\alpha \partial_\mu$ and $\bar{D}_{\dot{\alpha}} = (D_\alpha)^\dagger$. The chiral constraint reduces the degrees of freedom, and we can rewrite the superfield to be

¹It can be broken by superpotential interactions.

independent of $\bar{\theta}$

$$\begin{aligned}\Phi(y, \theta) &= \phi(y) + \sqrt{2}\theta\psi(y) - \theta\theta F(y) \\ &= \phi(x) + \sqrt{2}\theta\psi(x) - \theta\theta F(x) + i\theta\sigma^\mu\bar{\theta}\partial_\mu\phi(x) \\ &\quad - \frac{i}{\sqrt{2}}\theta\theta\partial_\mu\psi(x)\sigma^\mu\bar{\theta} - \frac{1}{4}\theta\theta\bar{\theta}\bar{\theta}\partial_\mu\partial^\mu\phi(x)\end{aligned}\tag{3.7}$$

where $y^\mu = x^\mu + i\theta\sigma^\mu\bar{\theta}$.

With chiral fields, we can construct supersymmetric actions by incorporating two types of terms resulting from different Berezin integrals:

- *D-terms* of the form $\int d^2\theta d^2\bar{\theta} K(\Phi, \bar{\Phi}) = K(\Phi, \bar{\Phi})|_{\theta\theta\bar{\theta}\bar{\theta}}$, *e.g.* the Kähler (real) potential.
- *F-terms* of the form $\int d^2\theta W(\Phi) = W(\Phi)|_{\theta\theta}$ plus its hermitian conjugate, *e.g.* the chiral superpotential, which is a holomorphic function of a chiral superfields.

Another relevant superfield representation is the real vector superfield $V = V^\dagger$, as this will encode the gauge field. As in any gauge theory, each vector superfield transforms under the adjoint representation,

$$e^{2V} \rightarrow e^{i\bar{\Lambda}} e^{2V} e^{-i\Lambda}, \tag{3.8}$$

where Λ is some chiral field, element of $\mathfrak{g} = \bigoplus_A \mathfrak{g}_A$. The supersymmetric gauge invariant field strength W_α is called the gaugino superfield for the top component $\bar{\theta}\bar{\theta}\theta^\alpha\lambda_\alpha$ of V and can be expanded as

$$W_\alpha = -\frac{1}{8}\bar{D}^2 (e^{-2V} D_\alpha e^{2V}) = -i\lambda_\alpha + \theta_\alpha D + i(\sigma^{\mu\nu}\theta)_\alpha F_{\mu\nu} + \theta\theta [\nabla_\mu, (\sigma^\mu\bar{\lambda})_\alpha], \tag{3.9}$$

where again all fields are functions of y , and we used the Wess-Zumino gauge, which eliminates the bottom components of V . In the later equality we have the gauge-covariant derivative $\nabla_\mu = \partial_\mu - iA_\mu$ and $F_{\mu\nu} = [\nabla_\mu, \nabla_\nu]$ is the field-strength.

Quiver gauge theories are Yang-Mills theories composed by a gauge group with several components

$$G = \prod_A G_A, \tag{3.10}$$

where G_A is a simple Lie group. Since the gaugino superfield is chiral, each simple component will have a Yang-Mills term resulting from an F-term. We introduce a complexified gauge coupling

$$\tau_A = \frac{\Theta_A}{2\pi} + \frac{4\pi i}{g_A^2} \tag{3.11}$$

for each factor. Then, the general super Yang-Mill action for the vector superfields is given by

$$S_{\text{YM}} = \text{Im} \left(\sum_A \int d^4x d^2\theta \frac{\tau_A}{8\pi} \text{Tr}_A (W^{A\alpha} W_\alpha^A) \right), \quad (3.12)$$

which results both the in conventional kinetic term $-\frac{1}{4g_A^2} \text{Tr} (F^{A\mu\nu} F_{\mu\nu}^A)$, and the instanton density $\frac{\Theta_A}{32\pi^2} \text{Tr} (F^{A\mu\nu} \tilde{F}_{\mu\nu}^A)$, for each factor G_A .

On the other hand, matter content can be described by several chiral multiplets, where each superfield can be transformed under a different representation R of the Lie algebra

$$\Phi \rightarrow e^{i\Lambda} \Phi, \quad \bar{\Phi} \rightarrow \bar{\Phi} e^{-i\bar{\Lambda}}, \quad \Lambda = \sum_A \sum_{a=1}^{\dim G_A} \Lambda_A^a T_{A,R}^a. \quad (3.13)$$

The full action for the matter content will include a kinetic term that is consistent with SUSY gauge transformations, together with an F-term (and its conjugate) for the chiral superpotential $W(\Phi)$

$$S_{\text{m}} = \sum_i \int d^4x d^2\theta d^2\bar{\theta} \bar{\Phi}^i e^{(2\sum_{A,a} V_A^a T_{A,R_i}^a)} \Phi^i \quad (3.14)$$

$$S_W = \int d^4x d^2\theta W(\Phi) + \text{h. c.} \quad (3.15)$$

For every factor $G_A = \text{U}(1)$, the vector superfield is abelian, and it transforms as $V \rightarrow V - \frac{i}{2}(\Lambda - \bar{\Lambda})$. Since Λ and $\bar{\Lambda}$ are chiral fields, we can add to the action the gauge invariant term,

$$S_{\text{FI}} = \sum_{A|G_A=\text{U}(1)} \xi_A \int d^4x d^2\theta d^2\bar{\theta} V, \quad (3.16)$$

where the real constants ξ_A are the Fayet-Iliopoulos (FI) parameters.

Combining all the terms in the action we obtain the usual terms for the dynamical superpartners and couplings between usual fields, *i.e.* a gauge vector A_μ , complex scalar ϕ and Weyl spinor ψ , but also the gaugino λ_α . More importantly, new non-dynamical fields appear in the action, originating from the top components of the chiral and vector multiplets, respectively. The equations of motion for these fields are algebraic and lead to the *F-term* and *D-term equations*,

$$\bar{F}_i = \frac{\partial W}{\partial \phi^i} = \partial_i W, \quad (3.17)$$

$$D_A^a = -g_A^2 \left(\sum_i \bar{\phi}_i T_{A,R_i}^a \phi^i - \xi_A \right) \equiv -g_A^2 \mu_A^a(\bar{\phi}, \phi), \quad (3.18)$$

where $\mu_A(\bar{\phi}, \phi)$ is a moment map associated with the Lie algebra of the group G_A . Recall that $\xi_A = 0$ for nonabelian factors in the gauge group. Integrating out these fields, the scalar

potential takes the form

$$\begin{aligned} V(\bar{\phi}, \phi) &= \sum_i \bar{F}^i F_i + \sum_A \frac{1}{2g_A^2} \text{Tr}_A(D_A^2) \\ &= \sum_i |\partial_i W(\phi)|^2 + \sum_A \frac{g_A^2}{2} \sum_{a=1}^{\dim G_A} \mu_A^a(\bar{\phi}, \phi)^2 \end{aligned} \quad (3.19)$$

Note that the potential is of the form $V \sim (\text{F-terms})^2 + (\text{D-terms})^2$, so the supersymmetric vacua will be obtained by setting $F_i(\phi) = 0$ and $D_A^a(\bar{\phi}, \phi) = 0$, where $\phi \in \mathbb{C}^n$ represents the vacuum expectation (VEV) of the scalar component of Φ . Thus, the *moduli space* of supersymmetric vacua is simply given by

$$\mathcal{M} = \{(\bar{\phi}, \phi) \mid \partial_i W(\phi) = 0, \bar{\partial}_i \bar{W}(\bar{\phi}) = 0, \mu_A^a(\bar{\phi}, \phi) = 0\} / G . \quad (3.20)$$

Note that this description is the same as the Kähler quotient (symplectic reduction) previously introduced in section 2.2.2.2, where the moduli are the preimage of a moment map at some regular value with identification of orbits of G . From the Kempf–Ness theorem, it is well-known to be equivalent to a holomorphic description where we instead quotient by the complexified gauge group [87]

$$\mathcal{M} = \{\phi \mid \partial_i W(\phi) = 0\} // G_{\mathbb{C}} . \quad (3.21)$$

From the point of view of supersymmetry, this holomorphic description follows from considering chiral superfields and their (superfield) gauge transformations (3.13), while the symplectic reduction follows from the component formalism. For example, for a $G = \text{U}(1)^r$ linear sigma model with $n + 1$ chiral fields, the moduli space of vacua is of the form

$$\left(\mathbb{C}[\phi^0, \dots, \phi^n] / \langle \partial_1 W, \dots, \partial_n W \rangle \right) // (\mathbb{C}^\times)^r , \quad \phi^i \sim \prod_{a=1}^r \lambda_a^{q_a^i} \phi^i , \quad \lambda_a \in \mathbb{C}^\times . \quad (3.22)$$

Note that the moduli space \mathcal{M} is not necessarily a set of isolated points and, in many cases, we might have potential with flat directions, where we can continuously change the value of the expectation value and still maintain the scalar potential $V = 0$. In section 2.2.2.1, we have an example computed for a single $\text{U}(1)$, acting with charges $q_1^i = 1$ and no relations, $W = 0$, resulting in $\mathcal{M} = \mathbb{P}^n$.

In non-supersymmetric theories, the renormalization of the potential will generally change the form of the effective scalar potential, with RG flow both changing the values of the couplings in the original potential and possibly generation a series of new, higher order interactions. Normally, flat directions are lifted by these quantum corrections, so the study of the classical vacuum moduli space is of little interest. However, in supersymmetric theories, by the Seiberg non-renormalization theorems [88], the superpotential does not receive perturbative

corrections. However, in $\mathcal{N} = 1$ gauge theories the superpotential may be renormalized by non-perturbative effects such as instantons. But for our purposes, we need not be concerned about having new terms, so we can think of the supersymmetric moduli space of vacua of the classical and quantum theories as the same.

Quiver gauge theories are Yang-Mills theories with a gauge group consisting of several factors, generally multiple $U(N)$ or $SU(N)$, in which the matter content transforms as a bi-fundamental representation of two simple factors. The term *quiver* corresponds to the directed graph that specifies the matter content, the field representations and the structure of the gauge groups. The directed edges connect two different vertices, say (a, b) , which represent the different gauge groups, for example, $SU(N)_a$ and $SU(N)_b$. Each of the quiver graph corresponds to a $\mathcal{N} = 1$ chiral multiplet, Φ_{ab} , which transforms under the bi-fundamental representation $\bar{N} \otimes \bar{N}$ of $SU(N)_a \times SU(N)_b$. In terms of the fields, this corresponds to a transformation

$$\Phi_{ab} \rightarrow e^{i\Lambda_a} \Phi_{ab} e^{-i\Lambda_b} . \quad (3.23)$$

The usual quiver graph does hold the all the information to define superpotential $W(X)$, which is necessary to specify the $\mathcal{N} = 1$ theory. The superpotential must be composed of gauge-invariant operators and these can be obtained from the cycles available in the quiver, which correspond to traces of a string of chiral multiplets.² The terms in the superpotential must also be invariant under any global symmetries.

In this work, we will focus on a special class of $\mathcal{N} = 1$ superconformal quiver gauge theories in 4 dimensions. These admit a mesonic $U(1)^3$ global symmetry, one of the factors being the SUSY R -symmetry $U(1)_R$. The mesonic branch of the moduli space of these theories are described as toric varieties for which the geometry data can be encoded into a convex lattice polytope, also known as the toric diagram of the Calabi-Yau singularity. The properties of the superpotential allow us to graphically encode the theory by embedding a bipartite graph in a torus, called a brane tiling.

3.2 Brane tilings

A *brane tiling* [40–44] is a bipartite graph on a 2-torus \mathbb{T}^2 which encodes quiver and superpotential of a so *toric* supersymmetric gauge theory with four supercharges (4d $\mathcal{N} = 1$ and dimensional reductions thereof). This is the low energy field theory on the worldvolume of N D-branes probing a CY_3 cone \mathcal{Y} with $U(1)^3$ isometry. The graph consists of 0-dimensional vertices (or nodes), 1-dimensional edges connecting a pair of vertices, and 2-dimensional faces bounded by edges. The graph is bipartite, meaning that vertices are

²These are so-called mesonic operators. For $SU(N)$ gauge factors one can also write baryonic operators built using epsilon tensor. These operators are irrelevant for large enough N , therefore we will ignore this possibility.

colored black or white and edges connect vertices of different colors. The coloring encodes a counterclockwise/clockwise ordering of the edges incident to a vertex.

The data of a brane tiling and its field theory interpretation are given by:

- **Faces** correspond to $U(N)_i$ group factors,³ for $i \in \{1, \dots, g\}$, where g denotes the number of unitary gauge group factors (sometimes F for the number of faces).
- **Edges** between two faces i and j represent chiral superfields X_{ij}^a , which transform in the bifundamental representation of $U(N)_i \times U(N)_j$. If $i = j$, the chiral superfield is in the adjoint representation. The direction of the arrow in the quiver diagram is determined by the orientation of the distinct-colored vertices that the corresponding edge connects to in the tiling. We write E for the number of chiral superfields/edges.
- **Vertices** \circ/\bullet represent toric superpotential terms. Each superpotential term is the single trace of the product of bifundamentals chiral superfields associated to the incoming edges of the corresponding vertex, ordered clockwise/counterclockwise and with a $+/-$ sign according to the white/black color of the vertex.

The bipartite nature of the graph guarantees that each bifundamental chiral superfield appears exactly once in exactly two superpotential monomials with opposite signs. This is known as the *toric condition* and leads to F-term equations of the form

$$\frac{\partial W}{\partial X_{ij}} = 0 \quad \Rightarrow \quad X_{j,c_1} \cdots X_{c_r,i} = X_{j,d_1} \cdots X_{d_s,i} , \quad (3.24)$$

for two specific connected paths (c_1, \dots, c_r) and (d_1, \dots, d_s) in the brane tiling/quiver.

The dual graph of the brane tiling is the *periodic quiver diagram* [41]: it consists of 0-dimensional vertices (or nodes) representing unitary gauge groups, 1-dimensional directed edges (or arrows) representing bifundamental chiral superfields, and 2-dimensional oriented faces whose boundaries represent (positive or negative) superpotential terms. The usual quiver graph refers only to the 1-skeleton structure and encodes the gauge group and matter content of the gauge theory. The quiver data is encoded in the *incidence matrix* $d \in \mathbf{M}_{g \times E}(\mathbb{Z})$ of the graph:

$$d_{ie} = \delta_{i,s(e)} - \delta_{i,t(e)} = \begin{cases} +1 & t(e) = i \\ -1 & s(e) = i \\ 0 & \text{else} \end{cases} \quad (3.25)$$

where $t(e)$ and $s(e)$ denote the nodes at the tail and head of the arrow (or directed edge) e . In the quiver gauge theory, we associate to each edge e a chiral superfield X_e in the bifundamental

³In four dimensions the low energy gauge groups are special unitary, since central $U(1)$ factors are massive or decoupled. Considering unitary gauge groups is nevertheless useful to study mesonic moduli space of vacua, which we focus on in this paper. Baryonic branches can also be studied, by relating baryonic VEVs to FI parameters (see chapter 5). See [89] and references therein for a comprehensive discussion.

representation of $U(N)_{t(e)} \times U(N)_{s(e)}$. By an abuse of notation, we will interchangeably denote a chiral superfield as X_e according to the corresponding edge in the graph or as X_{ij}^a according to the nodes $i = t(e)$ and $j = s(e)$ it connects. The superscript a labels the A_{ij} bifundamentals between nodes i and j in the quiver.

Toric quiver gauge theories are generically chiral, hence there is a non-trivial condition for cancellation of gauge anomalies. In the most general case, where the gauge group is

$$G = \prod_{i=1}^g U(N_i) , \quad (3.26)$$

the four-dimensional $SU(N_i)$ gauge anomaly cancellation⁴ condition reads [91]

$$\sum_j (a_{ij} - a_{ji}) N_j = 0 , \quad (3.27)$$

where $a \in \mathbf{M}_{g \times g}(\mathbb{Z})$ is the adjacency matrix of the quiver, with entry a_{ij} counting the number of arrows from node i to node j .

3.2.1 Perfect matchings

When considering brane tilings as bipartite graphs, a *perfect matching* p_α [40, 41], or dimer collection, is a set of edges, sometimes called “dimers”, which connect each vertex of the brane tiling exactly once. The collection of perfect matchings is summarized in the *perfect matching matrix* $P \in \mathbf{M}_{E \times c}(\mathbb{Z})$, with entries

$$P_{e\alpha} = \begin{cases} 1 , & X_e \in p_\alpha \\ 0 , & X_e \notin p_\alpha \end{cases} . \quad (3.28)$$

Obtaining all perfect matchings is a combinatorial problem that can be solved via the *Kasteleyn matrix* [40, 41]. For brane tilings, this is just the node connectivity matrix of the bipartite graph, with the caveat of also including the winding number information

$$h(X_e) = \left(h_z(X_e), h_w(X_e) \right) \quad (3.29)$$

of the edge. To define it we need to pick a fundamental domain on the \mathbb{T}^2 we choose two primitive winding cycles (γ_z, γ_w) . This choice is $GL(2, \mathbb{Z})$ invariant. By fixing the bipartite orientation of the edges to be directed from the white to black nodes, we have that $h_{z,w}$ equals $+1/-1$ if the edge X_e crosses the cycle $\gamma_{z,w}$ in the positive/negative direction, and 0 if no

⁴The central $U(1)_i \subset U(N_i)$ generically also have (mixed) gauge anomalies, which are cancelled in string theory by Stückelberg terms that make the corresponding gauge bosons massive [89, 90]. Anomaly-free central $U(1)_i$ factors decouple in the infrared and become non-anomalous baryonic symmetries.

crossing occurred. Therefore, the Kasteleyn matrix takes the form

$$K_{ij}(z, w) = \sum_{e \in B_i \cap W_j} a_e z^{h_z(X_e)} w^{h_w(X_e)}, \quad (3.30)$$

where $B_i \cap W_j$ denotes the set of tiling edges that connect to both node B_i and node W_j , and a_e is an *edge weight*. As a convention, we index the row and columns of the Kasteleyn matrix as black and white nodes, respectively. If we just take all $a_e = 1$, the resulting permanent will list the multiplicities of the perfect matchings for each monomial $z^a w^b$. Keeping the a_e edge weight general, we can keep track of which edge e belongs to a particular perfect matching.

It turns out that the combinatorics evolved in finding the perfect matchings is the same found in determinant methods of the Kasteleyn matrix. The permanent of a Kasteleyn matrix is a sum where each term in the expansion is associated to a unique perfect matching,

$$\text{perm } K(z, w) = \sum_{\alpha=1}^c z^{h_z(p_\alpha)} w^{h_w(p_\alpha)} \prod_{X_e \in p_\alpha} a_e, \quad (3.31)$$

with the winding number given by

$$h(p_\alpha) = \sum_{X_e \in p_\alpha} h(X_e). \quad (3.32)$$

Similarly, we could have used a determinant and introduced the appropriate -1 factors. The winding numbers of perfect matchings in brane tilings have a deep connection to the toric diagram Δ of the underlying geometry, a lattice polytope representation of a toric Calabi-Yau threefold. Remarkably, the signed intersection numbers $h(p_\alpha)$ correspond to the coordinates of the toric diagram.

The number of perfect matchings can be larger, the number of coordinates of the toric diagram. Perfect matchings are *extremal* when their winding number is mapped to vertices of the convex hull of Δ . Consistency of the brane tiling requires these to have multiplicity equal to 1 [47]. Perfect matchings along the hull boundary of Δ are *non-extremal* and reveal the presence of a non-isolated singularities in the affine toric Calabi-Yau. Perfect matchings are *internal* otherwise.

3.2.2 Zig-zag paths

A *zig-zag path* η is a special type of closed oriented path in a brane tiling, which forms a homology cycle on \mathbb{T}^2 [47]. By definition, it is a map $\eta : Z \rightarrow \mathcal{Q}_1$ such that, $h \circ \eta_n = t \circ \eta_{n+1}$, for each $n \in \mathbb{Z}$. Additionally, η_{2n} and η_{2n+1} are both in the boundary of the same black node and, η_{2n-1} and η_{2n} are both in the boundary of the same white node. A zig-zag path follows the edges of the brane tiling, making a maximal left turn at each white node and a maximal

right turn at each black node, following this rule until the path closes in \mathbb{T}^2 . A convenient way to depict a zig-zag path is to deform it slightly so that it crosses in the middle of each of the edges that it follows, keeping the black vertex on the left and the white vertex on the right as we do when we go from the tiling to the dual periodic quiver.

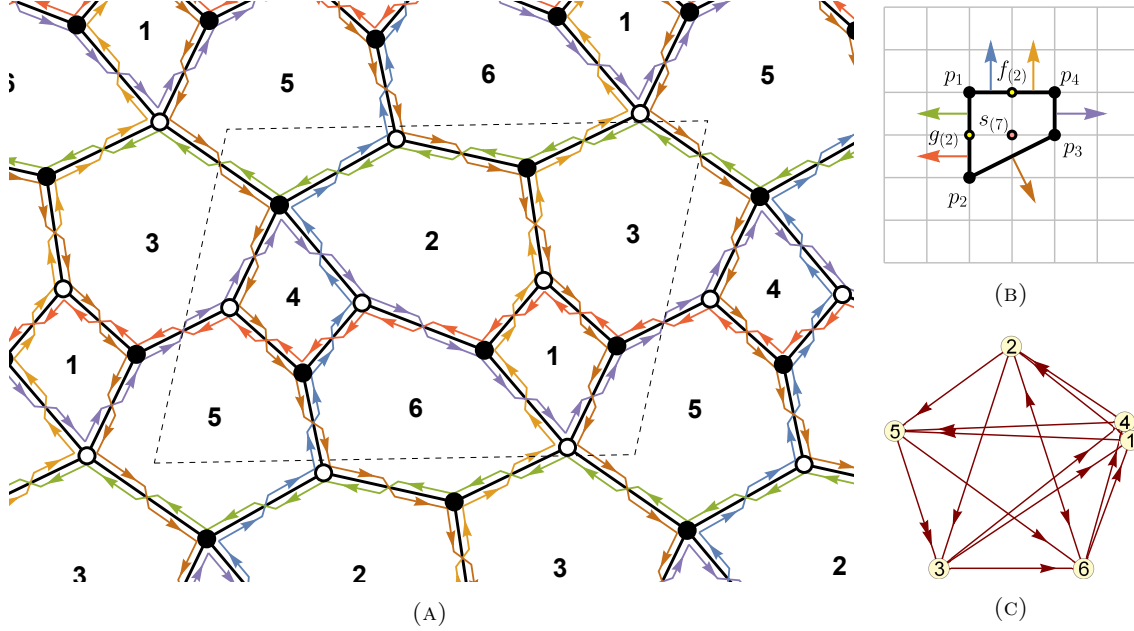


FIGURE 3.1: Model PdP_{3c} Phase B [55]: (a) brane tiling decorated with zig-zag paths; (b) toric diagram with normal vectors (p, q) associated to zig-zags; (c) quiver diagram.

From the description above, we can work out how a brane tiling edge is oriented regarding a given zig-zag η : we define a *zig* to be an edge that goes from a black to white node along η , otherwise we call it a *zag*. A given edge is exactly a zig and a zag of two different zig-zag paths.

The zig-zag paths form a collection of loops on the torus, with winding numbers $h(\eta_i)$ in terms of the homology basis of the reference fundamental domain, similar to eq. (3.32). From these we can reconstruct the data of the singular toric geometry: winding numbers of zig-zag paths form a set of vectors in \mathbb{Z}^2 , which represent the outward pointing normals of the toric diagram (compare fig. 3.1b with fig. 3.1a).

For consistency of the dimer model, we require the Calabi-Yau condition to hold. This statement can be restated in various different ways [78]. In terms of zig-zags, consistency implies that if we have a brane tiling edge e where two zig-zag paths η^+, η^- start, then the only time the zig-zag paths intersect on the torus is at $\eta_0^+ = \eta_0^- = X_e$. In terms of the covering space $\mathbb{R}^2 \rightarrow \mathbb{R}^2/\mathbb{Z}^2 = \mathbb{T}^2$, this condition implies that the extended paths do not self-intersect.

3.3 Master space and other moduli

The moduli space of supersymmetric vacua \mathcal{M} of a 4d $\mathcal{N} = 1$ low energy quiver gauge theory on the worldvolume of regular D3-branes consists of various components (or *branches*).

The first go-to tool for studying the moduli of quiver gauge theories is the master space \mathcal{F}^\flat [92–95]. The master space is a toric variety of dimension $3N + g - 1$ and is defined as the space of solutions to the F-term equations, given the chiral fields as matrices, quotiented by $SU(N)^g$, since only the nonabelian part of $G = U(N)^g$ couples in the IR. In particular, for the abelian theory on the worldvolume of a single D3-brane, \mathcal{F}^\flat is the same as the full moduli space of the quiver theory, of dimension $g + 2$. The master space \mathcal{F}^\flat often decomposes into multiple irreducible components: the non-trivial top component referred as the *coherent component* ${}^{\text{Irr}}\mathcal{F}^\flat$ and multiple pieces lower-dimensional pieces, usually linear affine components (no relations).

In general, we can write the master space as

$$\mathcal{F}^\flat = \text{Specm} \left((\mathbb{C}[X_{e_1}, \dots, X_{e_E}] / \langle \partial_X W \rangle)^{SU(N)_{\mathbb{C}}^g} \right) . \quad (3.33)$$

By $R^{SU(N)_{\mathbb{C}}^g}$, we mean the algebraic invariants of the ring R under the complexified nonabelian quiver symmetry $SU(N)_{\mathbb{C}}^g = SL(N, \mathbb{C})^g$, *i.e.* traces (mesons) and determinants (baryons). These invariants form the spectrum of chiral BPS operators and their vacuum expectation values (VEVs) parametrize two components of the moduli spaces, the *mesonic branch* and the *baryonic branch*.

Any cycle in \mathcal{Q} can be concatenated with itself any number of times to obtain larger cycles. However, \mathcal{F}^\flat is finitely generated even though it seems that we have an infinite number of generators. Therefore, we expected these larger composite generators must be subjected to additional relations, *i.e.* via Cayley–Hamilton theorem.

3.3.1 Geometric and baryonic branches

If the Calabi-Yau 3-fold cone \mathcal{Y} only has an isolated singularity at the tip of the cone, the two branches are:

- *Mesonic branch = Geometric branch* $\mathcal{M}^{\text{mes}} = \mathcal{M}^{\text{geom}}$ [89, 93, 94, 96]: it describes N regular D3-branes probing the Calabi-Yau 3-fold cone \mathcal{Y} . It is an affine variety parametrized by the VEVs of mesonic operators (henceforth often referred to simply as mesons), *i.e.* traces of products of chiral superfields which are associated to cycles in the quiver:

$$M_i = \text{tr} (X_{e_1} \cdots X_{e_\ell}) . \quad (3.34)$$

In general, we have that $\mathcal{M}^{\text{geom}} = \text{Sym}^N(\mathcal{Y})$ with dimension $3N$. If $N = 1$, the moduli $\mathcal{M}^{\text{geom}} = \mathcal{Y}$ reproduce the affine Calabi-Yau geometry, hence the name geometric branch.

- *Baryonic branch* \mathcal{M}^{bar} [35, 97]: it describes N regular D3-branes probing different (partial) resolutions $\tilde{\mathcal{Y}}_\xi$ of the singular Calabi-Yau 3-fold cone \mathcal{Y} . It is parametrized by VEVs of dibaryonic operators (or simply dibaryons) of the schematic type

$$B_j = \det(X_{e_1} \dots X_{e_m}) , \quad (3.35)$$

where (e_1, \dots, e_m) are open paths in the quiver. Geometrically, the full moduli space of vacua ${}^{\text{Irr}}\mathcal{F}^{\text{b}}$ can be thought as the total space of the fibration $\tilde{\mathcal{Y}}_\xi$ over a complexified $(g-1)$ -dimensional Kähler moduli space of \mathcal{Y} parametrized by a vector ξ . The fiber directions are mesonic, while the base directions are baryonic. In the gauged linear sigma model (GLSM) that describes the toric geometry of $\tilde{\mathcal{Y}}_\xi$, the Kähler moduli $\text{Re}(\xi)$ are realized by Fayet-Iliopoulos (FI) parameters.

If we gauge the central $U(1)^g \subset U(N)^g$, the baryonic branch disappears and the moduli space of vacua consists of the mesonic branch only.

3.3.2 $\mathcal{N} = 2$ Coulomb branches

In this work we are interested in Calabi-Yau cones \mathcal{Y} which have lines of non-isolated singularities, which are of A -type since we assume that \mathcal{Y} is toric. Then there are additional mesonic components of the moduli space of vacua on top of the geometric branch:

- $\mathcal{N} = 2$ *Coulomb branch* $\mathcal{M}^{\mathcal{N}=2}$: for each non-isolated singularity of \mathcal{Y} , locally of A_{k-1} type, this extra mesonic component of the moduli space of vacua describes kN $\mathcal{N} = 2$ fractional D3-branes [98] probing the locus of the non-isolated A_{k-1} singularity. For $N = 1$ and for each A_{k-1} singularity, this branch is parametrized by VEVs of k independent chiral mesons, which take identical VEVs on $\mathcal{M}^{\text{geom}}$. The intersection of a $\mathcal{N} = 2$ Coulomb branch and the geometric branch is a locus of non-isolated singularity of the latter. A regular D3-brane on a non-isolated singularity of \mathcal{Y} can marginally decay into k different $\mathcal{N} = 2$ fractional branes which separately probe the singular locus. Conversely, k coincident $\mathcal{N} = 2$ fractional branes of different type can recombine into a regular D3-brane, which is free to explore the whole Calabi-Yau \mathcal{Y} .

This naming convention arises from the fact that if $\mathcal{Y} = \mathbb{C}^2/\Gamma \times \mathbb{C}$, with $\Gamma \subset \text{SU}(2)$ a finite subgroup [22], this is literally the Coulomb branch of a $\mathcal{N} = 2$ theory. The physics of the fractional branes and the geometry of this component of the moduli space of vacua is largely determined by the local geometry of \mathcal{Y} near the singularity, hence the name for the type of

fractional branes and for the branch of the moduli space. The latter is a misnomer, as there is no Coulomb branch for $\mathcal{N} = 1$ gauge theories, but we stick to it for the sake of brevity.

The full mesonic moduli space of vacua is then the union of the geometric branch and the $\mathcal{N} = 2$ Coulomb branches: $\mathcal{M}^{\text{mes}} = \mathcal{M}^{\text{geom}} \cup \mathcal{M}^{\mathcal{N}=2}$. We will use $f(M_i, \dots) \simeq 0$ to indicate relations in the full chiral ring, while we will use \sim to denote relations which only hold on the geometric component, but not on $\mathcal{N} = 2$ Coulomb branches.⁵

3.4 A-maximization and conformal invariance

A-maximization [99–101] is a technique used in the study of supersymmetric gauge theories to determine the exact superconformal R -symmetry at an infrared fixed point, which is part of the superconformal algebra. It plays a crucial role in understanding relevant and marginal (chiral) operators and by extension the dynamics of the quiver gauge theory.

Before initiating the discussion on how to find the conformal $U(1)_R$ charge, there are certain restrictions arising from conformal invariance, which these charges must obey. Recall that for a 1 + 3-dimensional $\mathcal{N} = 1$ supersymmetric gauge theory with gauge group $SU(N)$ the 1-loop beta function for the $1/g^2$ coupling is given by the exact NSVZ formula [102, 103]

$$\beta_{\frac{1}{g^2}} = \frac{1}{8\pi} \frac{3c_2[\mathcal{R}_{\text{adj}}] - \sum_{\phi} d[\mathcal{R}_{\phi}](1 - \gamma_{\phi})}{1 - \frac{g^2}{8\pi} c_2[\mathcal{R}_{\text{adj}}]} . \quad (3.36)$$

The sum in eq. (3.36) is over the matter fields of the gauge theory and $d[\mathcal{R}_{\phi}]$ is the Dynkin index of the representation \mathcal{R}_{ϕ} , which is defined by $\text{Tr}(T_{\mathcal{R}_{\phi}}^a T_{\mathcal{R}_{\phi}}^b) = d[\mathcal{R}_{\phi}] \delta^{ab}$.⁶ Similarly, $c_2[\mathcal{R}_{\text{adj}}]$ represents the Casimir factor for the adjoint. Furthermore, in superconformal field theories the anomalous dimension γ_{ϕ} of the chiral superfield ϕ is related to the conformal scaling dimension

$$\Delta_{\phi} = 1 + \frac{1}{2}\gamma_{\phi} = \frac{3}{2}R[\phi] , \quad (3.37)$$

and the conformal R -charge $R[\phi]$. In the IR conformal fixed point, we must have $\beta_{\frac{1}{g^2}} = 0$, which can be written as

$$N = \sum_{\phi} d[\mathcal{R}_{\phi}] (1 - R[\phi]) \quad (3.38)$$

In the context of quiver gauge theories, we can have many configurations of BPS (fractional, or wrapped) D-branes at a toric singularity, leading to a general gauge group of the form

⁵Note that the presence of additional components in \mathcal{F}^b does not immediately imply $\mathcal{N} = 2$ Coulomb branches, since isolated singularities can still produce reducible master spaces.

⁶This does not uniquely define the Dynkin index. In physics, we also take the convention of $d[\mathcal{R}_{\phi}] = 1/2$ for ϕ in the fundamental representation of $SU(N)$.

$G = \prod_{i=1}^g \text{SU}(N_i)$. Matter fields arise from strings stretching from a D-brane of a given type and either ending on a different or same type of D-brane (respectively), and transform in bi-fundamental representations, X_{ij} . For a quiver \mathcal{Q} we can simplify the general formula (3.36) to

$$\begin{aligned} N_i + \sum_{\substack{e \in \mathcal{Q}_1 \\ h(e)=i}} \frac{1}{2} N_{t(e)} (R[X_e] - 1) + \sum_{\substack{e \in \mathcal{Q}_1 \\ t(e)=i}} \frac{1}{2} N_{h(e)} (R[X_e] - 1) &= 0 \\ \Rightarrow N_i^2 + \sum_{e \in \mathcal{Q}_1 | i \in \partial e} N_{t(e)} N_{h(e)} (R[X_e] - 1) &= 0 \end{aligned} \quad , \quad \forall i \in \mathcal{Q}_0 . \quad (3.39)$$

Note that the above includes matter in the adjoint representation, since adjoints have $h(e) = t(e) = i$, which receive a contribution $(N_{h(e)} + N_{t(e)})/2$ matching the expected Dynkin index $d[\Phi_i] = N_i$. Additionally, every term in the superpotential has total R -charge 2

$$-2 + \sum_{e \in \partial c} R[X_e] = 0 \quad , \quad \forall c \in \mathcal{Q}_2 . \quad (3.40)$$

We can see this condition as conformal invariance $\beta_{\lambda_c} = 0$ for a coupling λ_c for each chiral gauge invariant operator $\lambda_c \text{Tr}[X_{c_1} X_{c_2} \dots X_{c_n}]$ in the superpotential, where $c \in \mathcal{Q}_2 = \mathcal{Q}_2^+ \sqcup \mathcal{Q}_2^-$ is an oriented cycle in the dimer model/superpotential. But note that only some oriented cycles in the quiver might appear in the superpotential.

These conditions are fairly weak and, in most general case, we still have a continuous family $R(s)$ of non-anomalous $U(1)_R$ symmetries with generator (or R -charge)

$$R(s) = R_0 + \sum_I s^I F^I \quad (3.41)$$

where $\{F^I\}$ are conserved charges for global non-anomalous $U(1)$ symmetries,⁷ and R_0 is a non-anomalous R -symmetry. It was shown by Intriligator and Wecht [99] that the true conformal R symmetry is the one that minimizes the 4-dimensional central charge

$$a = \frac{3}{32} (3 \text{Tr} R^3 - \text{Tr} R) \quad (3.42)$$

among all trial R -charges of the form (3.41). This expression matches a triangle anomaly, where the trace is taken over the fermions in the chiral and vector multiplets of the theory. Bifundamental chiral fields X_e between gauge groups of ranks $N_{h(e)}$ and $N_{t(e)}$ contribute with $N_{h(e)} N_{t(e)}$ fermions (adjoints have $N_{h(e)} = N_{t(e)}$). Each fermion has an R -charge shifted by -1 compared to its scalar component, $R[X_e] - 1$, since in the chiral multiplet X_e the fermion appears with $\psi_e \cdot \theta$. For each gauge group, $\text{SU}(N_i)$ there are $N_i^2 - 1$ gauginos, which all

⁷As emphasized in [89, 100, 104] the baryonic symmetries decouple from the maximization procedure, so we can restrict the parameters s^I to vary over the 2-dimensional subspace of mesonic flavor symmetries in a-maximization.

have R -charge 1. We can greatly simplify $\text{Tr } R = 0$ using eq. (3.39) for anomaly free quiver gauge theories, leading to

$$a = \frac{9}{32} \left(-\frac{2g}{3} + \sum_{i \in \mathcal{Q}_0} N_i^2 + \sum_{e \in \mathcal{Q}_1} N_{h(e)} N_{t(e)} (R[X_e] - 1)^3 \right), \quad (3.43)$$

where $g = \sum_{i \in \mathcal{Q}_0} 1$ is the number of simple components in G . The correct choice of superconformal R -symmetry $R(s_0)$ corresponds to the value of the parameter s_0 where $a(s)$ has a local maximum, restricted by eqs. (3.39) and (3.40).

3.5 Fast-forward algorithm

The *toric diagram* Δ [40, 41, 54] of the CY_3 cone $\mathcal{Y} = \mathcal{M}^{\text{geom}}$ can be obtained from the winding numbers of differences of perfect matchings and a reference perfect matching. These form the lattice points of a convex lattice polygon $\Delta \subset \mathbb{Z}^2$, which we consider modulo $\text{SL}(2, \mathbb{Z})$ transformations and lattice translations. Alternatively, the perfect matching technology gives the toric diagram directly via the *fast-forward* algorithm [26, 51]:

- To each perfect matching p_α , we associate a field in an abelian $U(1)^c$ gauged linear sigma model (GLSM) [26, 105], which we call a *perfect matching variable* and also denote by p_α , with a slight abuse of notation. Expressing the bifundamentals in terms of perfect matching variables as

$$X_e = \prod_{\alpha=1}^c (p_\alpha)^{P_{e\alpha}} \quad (3.44)$$

solves the F-term equations automatically,

$$\bar{F}_e = \frac{\partial W}{\partial X_e} = 0, \quad (3.45)$$

at the expense of introducing an abelian gauge symmetry that leaves each bifundamental in (3.44) invariant. The charges of perfect matching variables under this gauge symmetry are encoded in a charge matrix $Q_F \in \mathbf{M}_{(c-g-2) \times c}(\mathbb{Z})$, defined as

$$Q_F P^T = 0 \quad \Rightarrow \quad Q_F = (\ker P)^T. \quad (3.46)$$

We remark that we can bypass the brane tiling construction step and still obtain P by grouping superpotential terms. While we lose the edge-winding information of the fundamental domain ($z = w = 1$ in (3.31)), the same combinatorics that allows us to obtain the perfect matchings is still present.

- There are D-terms for each of the $U(1)$ factors in the quiver, which take the form

$$D_i = -g_i^2 \left(\sum_e d_{ie} |X_e|^2 - \xi_i \right), \quad (3.47)$$

where $\xi \in \mathbb{R}^g$ are Fayet-Iliopoulos (FI) parameters. The D-term charge matrix $Q_D \in \mathbf{M}_{(g-1) \times c}(\mathbb{Z})$ is obtained by solving the matrix equation,

$$Q_D P^T = \hat{d}, \quad (3.48)$$

where we define the *reduced incidence matrix* $\hat{d} \in \mathbf{M}_{(g-1) \times E}(\mathbb{Z})$ by subtracting all remaining rows of d by one of the rows, e.g. $\hat{d}_{ie} = d_{ie} - d_{Ge}$, $i \in \{1, \dots, g-1\}$. This matrix encodes the charges of the bifundamentals under the faithfully acting gauge group of the quiver $U(1)^g/U(1)$.

- We can combine Q_F and Q_D in a total charge matrix $Q_t \in \mathbf{M}_{(c-3) \times c}(\mathbb{Z})$

$$Q_t = \begin{pmatrix} Q_F \\ Q_D \end{pmatrix}. \quad (3.49)$$

Then, the $3 \times c$ matrix

$$G_t = (\ker Q_t)^T \quad (3.50)$$

gives a collection of c lattice points in \mathbb{Z}^3 representing the charges of the perfect matching variables under the $U(1)^3$ toric symmetries. For the model to describe D3-branes probing a toric Calabi-Yau the lattice points must be coplanar, so that it can be projectivized to obtain the toric diagram $\Delta \subset \mathbb{Z}^2$.

The geometric branch of the moduli space $\mathcal{M}^{\text{geom}}$ of the 4d $\mathcal{N} = 1$ supersymmetric gauge theory with abelian gauge group $U(1)^g$ coincides with the classical moduli space of the GLSM introduced above. This is the Kähler quotient by the abelian gauge group with the total charge matrix Q_t

$$\mathcal{M}^{\text{geom}} = \mathbb{C}^c // U(1)_{Q_t}^{c-3} \quad (3.51)$$

at level $\xi = 0$, which results in a toric CY_3 cone \mathcal{Y} . In general, the fast-forward algorithm allows us to change the basis of fields in such a way that we transform the F-terms into D-term with zero FI parameters. As a result, a resolution of the cone \mathcal{Y} is given by the symplectic quotient by the moment map

$$\mu(p_\alpha)_i = \sum_{\alpha=1}^c (Q_t)_{i\alpha} |p_\alpha|^2, \quad \text{at some level} \quad \Xi = \begin{pmatrix} 0 \\ \xi \end{pmatrix}. \quad (3.52)$$

We stress that while the perfect matching technology is very useful to extract the geometric branch, it does not provide a general solution of the F -term equations and does not capture $\mathcal{N} = 2$ Coulomb branches.

3.6 Dualities of brane tilings

3.6.1 Toric-Seiberg duality

Often, different quiver gauge theories, represented by different brane tilings, are related by a so-called *toric duality* [50, 52]. This is just a form of $\mathcal{N} = 1$ Seiberg duality [48] for theories with toric moduli spaces.

A Seiberg duality on a quiver node of rank N_c defines a mutation to a new (dual) node of rank $N_f - N_c$, with $N_f = \sum_{i \neq c} N_i A_{ic} = \sum_{j \neq c} A_{cj} N_j$ guaranteed by the gauge anomaly cancellation.

In general, Seiberg duality relates an infinite tree of quiver gauge theories duals by allowing the mutation of any sequence of nodes in the quiver. But in order to guarantee that the Seiberg dual model is also toric, the ranks $N_i = N$ of the gauge groups in the worldvolume theory of N regular D3-branes probing a toric CY 3-fold singularity must be unchanged. The mutated node i that obeys this condition has $N_f = 2N$, and it corresponds to a square in the brane tiling. The result of Seiberg duality on square faces is graphically represented in fig. 3.2.

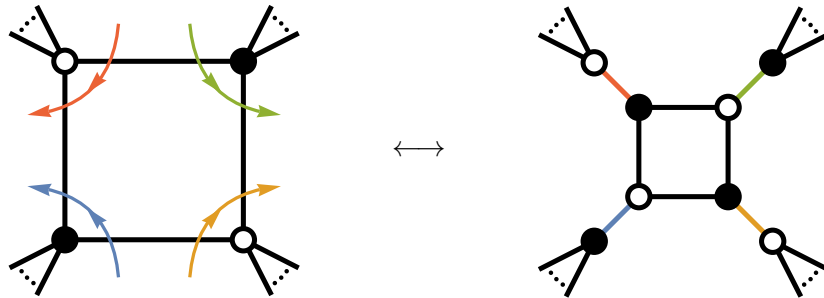


FIGURE 3.2: Toric (Seiberg) duality as an operation on the brane tiling. Colored arrows represent chiral superfield products. Often, one must integrate out massive fields by shrinking pairs of edges which share a bivalent vertex.

Toric duality connects brane tilings with different field content and superpotential but identical mesonic moduli space \mathcal{M}^{mes} . The associated toric diagrams are $\text{SL}(2, \mathbb{Z})$ equivalent. However, the multiplicities of internal points are not the same and this leads to a different $\text{Irr } \mathcal{F}^b$ due to anomalous $\text{U}(1)$ baryonic symmetries. But these can become equivalent if we restrict to non-anomalous charges [95]. We refer to toric dual brane tilings as *toric phases* of the same geometry \mathcal{Y} .

3.6.2 Specular duality

Specular duality [43, 106] is an application of mirror symmetry to brane tilings. It is a correspondence between a brane tiling on \mathbb{T}^2 and a brane tiling defined on the mirror curve Σ of the toric 3-fold \mathcal{Y} . A toric \mathcal{Y} , which can be specified by a convex integer polytope $\Delta \subset \mathbb{Z}^2$, has a mirror geometry \mathcal{W} defined by the double fibration over the Z plane,

$$Z = P(z, w) = \sum_{(p,q) \in \Delta} c_{p,q} z^p w^q, \quad (3.53)$$

$$Z = uv$$

for $z, w \in \mathbb{C}^\times$ and $u, v \in \mathbb{C}$. The complex coefficients $c_{p,q}$ parametrize the complex structure deformations of \mathcal{W} are mirror dual to the Kähler moduli of \mathcal{Y} [27]. The mirror curve Σ_Z is a Riemann surface defined by the first equation $P(z, w) - Z = 0$ and encodes all the toric geometry information in the *Newton polynomial* $P(z, w)$ of Δ .

The fiber at the origin, $P(z, w) = 0$, which we denote simply by Σ , is of particular relevance as it can be related to the brane tiling on \mathbb{T}^2 via the *untwisting map* [43], exemplified graphically by fig. 3.3.

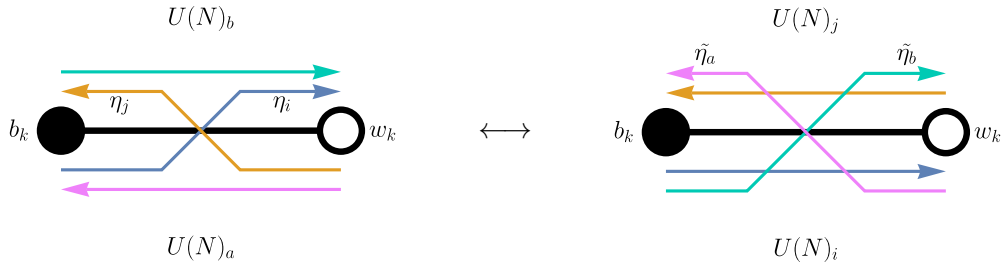


FIGURE 3.3: Untwisting map, followed by the identification of punctures with gauge groups.

In the untwisting map, the number of edges and vertices in the tiling remain the same. A given edge X_{ab} crossed by a zig η_i and a zag η_j is relabeled as X_{ij} . The map acts on the boundary of a face (gauge group $U(N)_a$), turning it into a zig-zag path $\tilde{\eta}_a$, which has non-trivial homology on the new tiling. On the other hand, the original zig-zag paths η_i become closed polygon cycles that wind around punctures γ_i of the Riemann surface Σ . The number of punctures of Σ_Z is given by the number of external points B of Δ , which is the same as the number of zig-zag paths. By itself, the untwisting map leads to closed polygon cycles winding punctures γ_i of Σ , usually referred to as a shiver. We need to map the punctures γ_i with gauge groups $U(N)_i$ to obtain a consistent brane tiling. This is summarized in table 3.1.

Note that the specular duality exchanges B zig-zag paths with g face boundaries and vice versa, while keeping the number of nodes and edges in the tiling. From Pick's theorem,

brane tiling on \mathbb{T}^2	brane tiling on Σ
zig-zag path η_i	face/gauge group $U(N)_i$
face/gauge group $U(N)_a$	zig-zag path $\tilde{\eta}_a$
node/term w_k, b_k	node/term w_k, b_k
edge/field X_{ab}	edge/field X_{ij}

TABLE 3.1: Specular duality mapping

$g = 2 \text{Area}(\Delta) = B + 2I - 2$, it is easy to show that

$$g(\Sigma) = g(\mathbb{T}^2) - \frac{B - g}{2} = I, \quad (3.54)$$

i.e. the new consistent tiling is embedded in a Riemann surface of genus equal to the number of internal points I in the toric diagram Δ of the original model. In this paper, we will consider only models with reflexive toric diagrams, with $g(\mathbb{T}^2) = g(\Sigma) = 1$, a special case where specular duals also have reflexive toric diagrams (see [106] for the full web of duals).

Part II

Study of del Pezzo geometries

Chapter 4

Zig-zag deformation of toric (pseudo) del Pezzo theories

The focus of this work is to classify and study a special class of superpotential deformations which relate worldvolume theories of D3-branes probing local toric (pseudo) del Pezzo geometries [107], which have reflexive toric diagrams [55]. To do so, we perform a series of operations on the brane tiling, which encodes the effect of relevant (or marginal, in one case) superpotential deformations. The deformation violates the toric condition, breaking the $U(1)^3$ mesonic symmetry to a $U(1)^2$ subgroup. The extra term δW in the deformed superpotential

$$W_{\text{def}} = W + \delta W \tag{4.1}$$

have UV superconformal R-charge, $R_{\text{sc}}[\delta W] \leq 2$ so that the deformation is relevant or marginal. We are mostly interested in special deformations which have an extra emergent $U(1)$ symmetry in the infrared, restoring the full toric $U(1)^3$ symmetry.

We present a general framework for deformations of brane tiling models by an operator \mathcal{O}_η fully defined by a zig-zag path η . We call \mathcal{O}_η a *zig-zag operator* and the superpotential deformation a *zig-zag deformation*. Firstly, we will work through some examples of relevant deformations of this type by manipulating the gauge theory, integrating out any fields which become massive after the deformation and finding field redefinitions which lead to a new toric superpotential. We will also give an interpretation of the zig-zag deformation in terms of brane tilings, extending [108], as well as analyze it from the perspective of the chiral ring and the moduli space of vacua. Finally, we will present the main argument, which holds for all \mathcal{O}_η of zig-zag paths η of length 4. This is verified for all reflexive geometries. The full details can be found in fig. 1.4 and appendix A.

4.1 Zig-zag operator

The chiral ring of mesonic operators, and the mesonic branch of the moduli space of vacua which is obtained by replacing chiral operators by their VEVs, are important for finding the operators that trigger deformations that lead to new toric models. We reviewed in the previous section the notions of geometric branch of the moduli space, which is isomorphic to the geometry \mathcal{Y} probed by a regular brane, and of $\mathcal{N} = 2$ Coulomb branches emanating from loci of non-isolated singularities of \mathcal{Y} , which are probed by $\mathcal{N} = 2$ fractional branes.

In the brane tiling, $\mathcal{N} = 2$ fractional branes are associated to strips of faces in the tiling bounded by zig-zag paths with the same homology class [98]. If \mathcal{Y} has a non-isolated A_k singularity ($k \geq 1$), there is a subset of zig-zags $\{\eta_0, \eta_1, \dots, \eta_k\}$ in the same homology class, which divide the brane tiling into $k + 1$ strips, corresponding to $k + 1$ $\mathcal{N} = 2$ fractional branes that a regular brane can split into. For each strip, we have a mesonic operator in the chiral ring, which is a loop in the tiling with opposite winding numbers to the zig-zag paths at the boundary of the strip. In all the tilings we consider (and presumably in general) it is always possible to find a place along the strip where it is exactly one face wide. Taking that face as a start and end point of a path winding along the strip, and using that homotopic open paths are F-term equivalent [109], it follows that for each strip there is exactly one meson generator in the chiral ring with mesonic charges equal and opposite to the winding numbers of the boundary zig-zags. Thus, for each A_k singularity, there are $k + 1$ inequivalent mesons $\{M_0, M_1, \dots, M_k\}$ in the chiral ring, since by the zig-zag path construction there are no F-terms connecting them. This is exemplified in fig. 4.1.

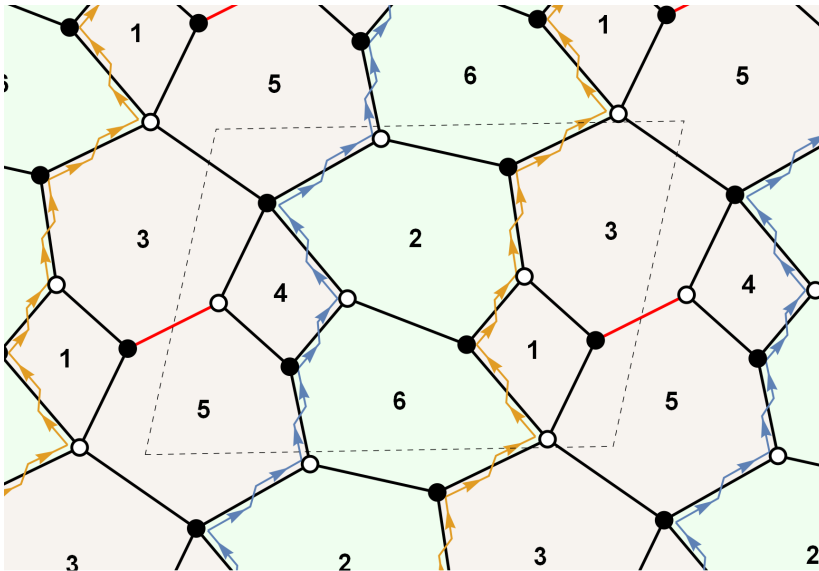


FIGURE 4.1: Tiling of PdP_{3c} phase B, focusing on the two parallel zig-zag paths and $\mathcal{N} = 2$ fractional branes strips associated to the most relevant (lowest R_{sc}) zigzag deformation. The red edge, X_{53}^2 , indicates the F-term equation that relates the two non-zero winding mesons of the strip in the chiral ring, i.e. $X_{31}X_{15}X_{53}^1 \simeq X_{34}X_{45}X_{53}^1$.

For each zig-zag path separating two strips, say η , there are two inequivalent mesonic generators $\mathcal{O}_\eta^L \not\sim \mathcal{O}_\eta^R$ in the chiral ring which have the same charges:

$$\mathcal{O}_\eta^L = X_{e_{i_1}} \cdots X_{e_{i_r}} , \quad \mathcal{O}_\eta^R = X_{e_{j_1}} \cdots X_{e_{j_s}} , \quad (4.2)$$

where $c^L = e_{i_1} \cdots e_{i_r}$ and $c^R = e_{j_1} \cdots e_{j_s}$ correspond to the 1-cycles in the tiling running through all the edges on the immediate left and right sides of the oriented zig-zag path η . The mesonic operators $\mathcal{O}_{\eta_j}^L$ and $\mathcal{O}_{\eta_j}^R$ take equal VEV in the geometric branch $\mathcal{M}^{\text{geom}}$ (we write $\mathcal{O}_{\eta_j}^L \sim \mathcal{O}_{\eta_j}^R$), but different VEVs in a $\mathcal{N} = 2$ Coulomb branch $\mathcal{M}^{\mathcal{N}=2}$ (hence $\mathcal{O}_{\eta_j}^L \not\sim \mathcal{O}_{\eta_j}^R$). Additionally, for a set of zig-zag paths in the same homology class $\{\eta_0, \eta_1, \dots, \eta_k\}$, ordered by adjacency in the brane tiling, we have $\mathcal{O}_{\eta_j}^R \simeq \mathcal{O}_{\eta_{j+1}}^L (\simeq M_{j+1})$. These two chiral mesons can be forced to become equivalent in the chiral ring by turning on a superpotential deformation

$$\delta W_\eta = \mu (\mathcal{O}_\eta^L - \mathcal{O}_\eta^R) \equiv \mu \mathcal{O}_\eta . \quad (4.3)$$

We remark that the zig-zag operator \mathcal{O}_η can be written as

$$\mathcal{O}_\eta \equiv \prod_{k=n}^1 \frac{\partial^2 W}{\partial \eta_{2k} \partial \eta_{2k-1}} - (-1)^n \prod_{k=n}^1 \frac{\partial^2 W}{\partial \eta_{2k+1} \partial \eta_{2k}} , \quad (4.4)$$

where $\eta_i = \eta_{(i \bmod 2n)}$ are the $2n$ chiral fields that represent the zig-zag closed path. In this definition, we assume that η_1 is an edge that goes from a black to white node along η . The operation $\frac{\partial}{\partial \eta_i}$ is a *cyclic derivative* with respect to paths in the quiver, defined as

$$\begin{aligned} \frac{\partial}{\partial X_{e_i}} \text{Tr}(X_{e_1} \cdots X_{e_n}) &= X_{e_{i+1}} \cdots X_{e_n} X_{e_1} \cdots X_{e_{i-1}} , \\ \frac{\partial}{\partial X_{e_i}} X_{e_1} \cdots X_{e_n} &= X_{e_{i+1}} \cdots X_{e_{i-1}} \quad \text{if } i = 1, n , \end{aligned} \quad (4.5)$$

otherwise undefined. The $(-1)^n$ factor on eq. (4.4) takes into account that the right-side second derivative acts on black nodes in the tiling. Note that the chiral mesons defining \mathcal{O}_η are oriented in the opposite direction to η .

In a theory with four supercharges, a chiral operator \mathcal{O} which acquires a VEV in the full supersymmetric moduli space cannot be nilpotent in the chiral ring, because VEVs of chiral operators factorize. For a theory with a $U(1)_R$ symmetry and a superpotential $W_{\text{def}} \equiv W + \delta W \equiv W + \mu \mathcal{O}$, where $\frac{\partial}{\partial \mu} W = 0$, one can show that

$$\left\langle \frac{\partial}{\partial \mu} W_{\text{def}} \right\rangle = \langle \mathcal{O} \rangle = 0 , \quad (4.6)$$

where $\langle \cdot \rangle$ is the expectation value in a supersymmetric vacuum. In the chiral ring of the deformed theory the operator \mathcal{O} must be nilpotent, *i.e.*, $\mathcal{O}^n \simeq 0$ for some nilpotency index n .

This argument was made for SCFTs with marginal deformations in [110], but it extends to any theory with a $U(1)_R$ preserving deformation, marginal or not.

In our case, we have that $\langle \mathcal{O}_\eta^L \rangle = \langle \mathcal{O}_\eta^R \rangle$ after the deformation, some $\mathcal{N} = 2$ fractional brane moduli are lifted, and the order of non-isolated A_k singularity decreases. For the toric theories that we study in this paper, the deformed F-terms force $\mathcal{O}_\eta^L \simeq \mathcal{O}_\eta^R$ in the chiral ring, which means that the nilpotency index is 1.

4.2 Mesonic moduli from chiral rings

In this section we consider the mesonic branch of the moduli space \mathcal{M}^{mes} , hence we take abelian gauge group $U(1)^g$ with vanishing FI parameters, and we focus in particular on its geometric component $\mathcal{M}^{\text{geom}}$, which describes the Calabi-Yau cone \mathcal{Y} . Since we are interested in deformations that violate toricity, we will not use the fast-forward algorithm or plethystics [94, 111], and instead derive the algebraic description explicitly. For this description, it is convenient to study the parent space obtained by relaxing the D-term constraints, *i.e.*, the master space \mathcal{F}^\flat of the abelian theory [92–95]. Geometrically, this is a non-compact CY_{g+2} cone, which consists of 3-dimensional resolved Calabi-Yau cones $\tilde{\mathcal{Y}}_\xi$ fibered over a $(g-1)$ -dimensional base space parameterized by FI parameters ξ (with $\sum_{i=1}^g \xi_i = 0$). The fiber at $\xi = 0$ is the singular cone \mathcal{Y} . Algebraically, the master space is described by the zero locus of a set of homogeneous polynomials in an ambient affine space. For $N = 1$, eq. (3.33) is simply

$$\mathcal{F}^\flat = \text{Specm} \left(k[X_{e_1}, \dots, X_{e_E}] / \langle \partial_X W \rangle \right), \quad (4.7)$$

where $k = \mathbb{C}$ or $k = \mathbb{C}[\mu^\pm]$, for a deformation parameter μ .

To obtain the mesonic moduli, we still need to quotient by $G = U(1)^g$. We will do so by constructing the *chiral ring* of the abelian theory, *i.e.* the quotient $k[M_{c_1}, \dots, M_{c_s}] / I_{\text{chiral}}$ of the polynomial ring of a finite set of mesonic generators $\{M_c\}$, modulo the chiral ideal I_{chiral} . The ideal I_{chiral} captures F-term equations in the $G_{\mathbb{C}}$ -invariant sector of the master space coordinate ring $k[X_{e_1}, \dots, X_{e_E}] / \langle \partial_X W \rangle$. The chiral ring can be obtained via

$$I_{\text{chiral}} = \ker \left(\Phi_W : k[M_{c_1}, \dots, M_{c_s}] \rightarrow k[X_{e_1}, \dots, X_{e_E}] / \langle \partial_X W \rangle \right), \quad (4.8)$$

where the homomorphism Φ_W is trivially constructed by assigning a mesonic generator M_c (no relations) to a cycle $c = e_1 e_2 \dots e_n$ in the quiver

$$\Phi_W(M_c) = X_{e_1} X_{e_2} \dots X_{e_n}, \quad (4.9)$$

If $W = 0$, the image $\text{im}(\Phi_W)$ is just the ring of $G_{\mathbb{C}}$ -invariants $k[X_{e_1}, \dots, X_{e_E}]^{G_{\mathbb{C}}}$ and $\ker(\Phi_W) = I_{\text{chiral}}$ consists of relations due to compositions of cycles, which follow purely from gauge

invariance. In the general case, Φ_W is trivially defined by the inclusion $k[X_{e_1}, \dots, X_{e_E}]^{G_C} \hookrightarrow k[X_{e_1}, \dots, X_{e_E}]$, mapping generators to quiver cycles that descend to equivalence classes in $\text{im}(\Phi_W) \subsetneq k[X_{e_1}, \dots, X_{e_E}]/\langle \partial_X W \rangle$. The kernel¹ of Φ_W is an ideal I_{chiral} that contains all the relations between cycles in the abelian quiver up to F-terms. Alternatively, this can be computed via the elimination of chiral superfield variables $\{X_e\}$ in an ideal composed of the F-term relations and the map Φ_W that encodes the complexified gauge group orbits, sitting in the larger base ring $k[M_{c_1}, \dots, M_{c_s}, X_{e_1}, \dots, X_{e_E}]$, i.e.

$$I_{\text{chiral}} = \langle \partial_X W, M_{c_1} - \Phi_W(M_{c_1}), \dots, M_{c_s} - \Phi_W(M_{c_s}) \rangle \cap k[M_{c_1}, \dots, M_{c_s}]. \quad (4.10)$$

This construction is particularly useful if the toric CY₃ cone \mathcal{Y} has lines of non-isolated A_{k-1} singularities. As we reviewed, in this case the moduli space includes additional $\mathcal{N} = 2$ Coulomb branches, which account for the regular D3-brane splitting into $\mathcal{N} = 2$ fractional D3-branes which separately probe the locus of non-isolated singularities. For this reason, the variety associated to the chiral ring $k[M_i]/I_{\text{chiral}}$ may be the union of several irreducible components, including the three-fold $\mathcal{M}^{\text{geom}} = \mathcal{Y}$ and several other varieties. These additional components can be detected via the *primary decomposition*,

$$I_{\text{chiral}} = I_{\text{geom}} \cap J_1 \cap \dots \cap J_\ell, \quad (4.11)$$

where the top non-trivial component I_{geom} is denoted as the *geometric ideal*. Generally,² each component J_i is associated to a single non-isolated A_{k-1} singularity, which is freely generated by k chiral mesons with no relations. These give rise to affine varieties \mathbb{C}^k , which intersect \mathcal{Y} at 1-dimensional singular loci. We can identify the geometric branch with the quotient ring associated to the 3-dimensional non-trivial component of the primary decomposition

$$\mathcal{M}^{\text{geom}} = \text{Specm} \left(k[M_{c_1}, \dots, M_{c_s}] / I_{\text{geom}} \right). \quad (4.12)$$

This algorithm is a distilled version of the affine GIT quotient [87, 89, 112], adapted to quiver gauge theories. We crucially used the fact that for a quiver with $G = \text{U}(1)^g$ the typical unruliness of the chiral ring is kept in check by the commutativity and finiteness of the mesonic generators.

4.3 RG flows between toric del Pezzos

The superpotential deformed by relevant terms violates the toric condition and breaks the mesonic and R -symmetries down to a $\text{U}(1)^2$ subgroup. We will be mostly interested in RG

¹This can be easily obtained via computational algebraic geometry software, e.g. Macaulay2 [57].

²One brane tiling, PdP₅ phase B [55], is found to have an additional branch, parametrized by chiral mesons with opposite winding in the tiling. We conjecture that this is related to the fact that this tiling contains two oppositely oriented strips, one of which contains the other.

flows with toric endpoints, namely with an emergent $U(1)^3$ symmetry in the IR (we will discuss an IR endpoint which is a marginal deformation of a toric model in section 4.4). By construction, the deformation does not change the number of non-anomalous and anomalous baryonic symmetries (of the $SU(N)^g$ theory). If the IR endpoint of the RG flow is toric, its toric diagram must have the same number of internal points I and external points E as the toric diagram of the undeformed UV theory, since the rank of the anomalous baryonic symmetry is $2I$ and the rank of the non-anomalous baryonic symmetry is $E - 3$ for toric models [35, 36, 94, 100]. In geometric terms, the deformation does not change the degree of the del Pezzo surface.

We first integrate out any massive bifundamentals appearing in superpotential terms of the form $\mu X_{ab} X_{ba}$, by imposing the F-term equations

$$\frac{\partial W_{\text{def}}}{\partial (X_{ab}, X_{ba})} = 0, \quad (4.13)$$

which modifies the superpotential as follows:

$$\mu X_{ab} X_{ba} + X_{ab} g_{ba}(X) - f_{ab}(X) X_{ba} + \dots \mapsto \frac{1}{\mu} f_{ab}(X) g_{ba}(X) + \dots \quad (4.14)$$

The resulting superpotential does not usually make manifest the toric symmetry, but a particular set of field redefinitions may restore the toric condition. For the case of gauge theories resulting from reflexive polytopes, we were able to restore the desired form by field redefinitions of degree up to 2,

$$X_{ij}^k = \sum_m \alpha_{ij}^m \tilde{X}_{ij}^m + \sum_{l,m,n} \beta_{ilj}^{knm} \tilde{X}_{il}^m \tilde{X}_{lj}^n, \quad (4.15)$$

for some coefficients $\alpha_{ij}^m, \beta_{ilj}^{knm}$ such that $\alpha_{ij}^k \neq 0$. The coefficients in the non-trivial field redefinitions are proportional to $1/\mu$, and the Jacobian of this change of variables obeys (up to an overall sign)

$$\det \left(\frac{\partial X}{\partial \tilde{X}} \right) = \mu^{(E_i - E_f - V_f)/2}, \quad (4.16)$$

where E_i is the number of bifundamentals of the initial model and V_f, E_f denote respectively the number of superpotential terms and bifundamentals of the final model after integrating out massive degrees of freedom. The resulting low-energy superpotential can be written as

$$W_{\text{low}}(X) = \frac{1}{\mu} W'(\tilde{X}), \quad (4.17)$$

with W' toric. The remaining power of μ can be cancelled by a complexified $U(1)_R$ transformation $\tilde{X}_e \mapsto \mu^{R[\tilde{X}_e]/2} \tilde{X}_e$ on all bifundamentals, which cancels the $\mu^{-V_f/2}$ factor in the Jacobian. Note that the power of μ in the combined Jacobian is given by $(E_i - E_f)/2$.

4.3.1 PdP_{3c} to PdP_{3b}

Take for example one of the toric phases of the *Pseudo del Pezzo 3c* model (phase B in [55]), with superpotential

$$\begin{aligned} W_{\text{PdP}_{3c}}^{(B)} = & X_{12}X_{23}X_{31} + X_{25}X_{56}X_{62} + X_{26}X_{64}X_{42} + X_{34}X_{45}X_{53}^2 \\ & + X_{15}X_{53}^1X_{36}X_{61} - X_{12}X_{26}X_{61} - X_{15}X_{53}^2X_{31} - X_{23}X_{36}X_{62} \\ & - X_{45}X_{56}X_{64} - X_{25}X_{53}^1X_{34}X_{42} , \end{aligned} \quad (4.18)$$

and with tiling, quiver and toric diagram in fig. 3.1. It is useful to list the generators of the mesonic branch by enumerating all the chiral mesons³ in the quiver, along with their mesonic $U(1)^3$ charges, and organize them by their GSLM decomposition using eq. (3.44). This leads to table 4.1. Many chiral mesons are F-term equivalent, so we can pick one representative of

Gen. (p_α)	Generator (X_e)	$U(1)^2$	$U(1)_{R_{\text{sc}}}$
$p_2^2 p_3 g s$	$X_{26}X_{62} \sim X_{31}X_{15}X_{53}^1 \simeq X_{34}X_{45}X_{53}^1$	(0, -1)	1.577...
$p_3^2 p_4 f s$	$X_{15}X_{56}X_{61} \sim X_{23}X_{34}X_{42}$	(1, 0)	1.690...
$p_1 p_2 p_3 p_4 f g s$	$X_{12}X_{23}X_{31} \simeq X_{25}X_{56}X_{62} \simeq X_{25}X_{53}^1X_{34}X_{42} \simeq$ $X_{34}X_{45}X_{53}^2 \simeq X_{12}X_{26}X_{61} \simeq X_{15}X_{53}^1X_{36}X_{61} \simeq$ $X_{15}X_{53}^2X_{31} \simeq X_{23}X_{36}X_{62} \simeq X_{45}X_{56}X_{64} \simeq X_{26}X_{64}X_{42}$	(0, 0)	2
$p_1^2 p_2^2 f g^2 s$	$X_{36}X_{64}X_{45}X_{53}^1 \simeq X_{36}X_{62}X_{25}X_{53}^1 \simeq X_{31}X_{12}X_{25}X_{53}^1$	(-1, 0)	2.309...
$p_1^2 p_3 p_4^2 f^2 g s$	$X_{23}X_{36}X_{64}X_{42} \simeq X_{25}X_{56}X_{64}X_{42} \simeq X_{25}X_{53}^2X_{34}X_{42} \simeq$ $X_{15}X_{53}^2X_{36}X_{61} \simeq X_{12}X_{23}X_{36}X_{61} \simeq X_{12}X_{25}X_{56}X_{61}$	(0, 1)	2.422...
$p_1^3 p_2 p_4 f^2 g^2 s$	$X_{36}X_{64}X_{45}X_{53}^2 \simeq X_{25}X_{53}^2X_{36}X_{62} \simeq X_{12}X_{25}X_{53}^2X_{31} \simeq$ $X_{25}X_{53}^1X_{36}X_{64}X_{42} \simeq X_{12}X_{25}X_{53}^1X_{36}X_{61}$	(-1, 1)	2.732...
$p_1^4 p_4^3 f^3 g^2 s$	$X_{25}X_{53}^2X_{36}X_{64}X_{42} \simeq X_{12}X_{25}X_{53}^2X_{36}X_{61}$	(-1, 2)	3.154...

TABLE 4.1: Table of generators of the mesonic moduli space for PdP_{3c} phase B, where $f = \prod_{i=1}^2 f_i$, $g = \prod_{i=1}^7 g_i$ and $s = \prod_{i=1}^7 s_i$ (perfect matchings on fig. 3.1). The superconformal R-charge $U(1)_R$ can be obtained via a-maximization [99–101].

each equivalence class and define the map Φ_W as

$$\begin{aligned} A_1 : X_{26}X_{62} & & B_2 : X_{31}X_{15}X_{53}^1 & & B_8 : X_{15}X_{56}X_{61} \\ B_5 : X_{23}X_{34}X_{42} & & B_1 : X_{45}X_{56}X_{64} & & C_1 : X_{36}X_{64}X_{45}X_{53}^1 \\ C_4 : X_{25}X_{56}X_{64}X_{42} & & C_2 : X_{36}X_{64}X_{45}X_{53}^2 & & D_3 : X_{25}X_{53}^2X_{36}X_{64}X_{42} \end{aligned} \quad (4.19)$$

The affine cone over PdP_{3c} contains two non-isolated A_1 singularities. The corresponding zig-zag deformations are triggered by differences of relevant chiral mesons in the first two rows of table 4.1, which can be further corroborated by the primary decomposition of the

³For $N = 1$, this corresponds to all indecomposable paths. For $N > 1$ these are single trace operators.

chiral ideal $I_{\text{chiral}} = I_{\text{geom}} \cap J_1 \cap J_2$,

$$\begin{aligned}
I_{\text{geom}} &= \langle B_5 - B_8, A_1 - B_2, C_2^2 - C_1 D_3, C_2 C_4 - B_1 D_3, B_1 C_2 - B_2 D_3, C_4^2 - B_8 D_3, \\
&\quad C_1 C_4 - B_2 D_3, B_1 C_4 - B_8 C_2, B_8 C_1 - B_2 C_4, B_1 C_1 - B_2 C_2, B_1^2 - B_2 C_4 \rangle \\
J_1 &= \langle D_3, C_2, C_4, C_1, B_1, B_5, B_8 \rangle \\
J_2 &= \langle D_3, C_2, C_4, C_1, B_1, A_1, B_2 \rangle .
\end{aligned} \tag{4.20}$$

As expected, the two components associated to the ideals J_1 and J_2 are parameterized by the chiral mesons that define the $\mathcal{N} = 2$ fractional brane strips, which intersect the geometric branch at $B_5 = B_8$ and $A_1 = B_2$, respectively.

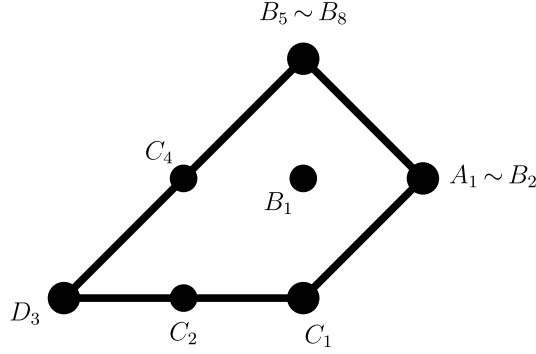


FIGURE 4.2: Lattice of the $U(1)^2$ mesonic flavor charges of the generators of PdP_{3c} phase B (see table 4.1).

Of the two relevant deformations only the most relevant (smaller R_{sc}) leads to a new toric model in the IR.⁴ A quick inspection of the tiling in fig. 4.1 or table 4.1 reveals that we have two zig-zag deformations

$$\begin{aligned}
\mathcal{O}_{\eta_5} &= X_{26} X_{62} - X_{31} X_{15} X_{53}^1 \\
\mathcal{O}_{\eta_6} &= X_{34} X_{45} X_{53}^1 - X_{26} X_{62} ,
\end{aligned} \tag{4.21}$$

which are equivalent due to chiral relations, $\mathcal{O}_{\eta_5} + \mathcal{O}_{\eta_6} \simeq 0$. Therefore, we can just pick the RG flow triggered by the superpotential deformation

$$\delta W = \mu \mathcal{O}_{\eta_5} = \mu (X_{26} X_{62} - X_{31} X_{15} X_{53}^1) . \tag{4.22}$$

Adding this term modifies the F-term equations, forcing the relation $A_1 \simeq B_2$ in the chiral ring. The deformation lifts the component J_1 and removes the A_1 singularity which is intersected

⁴The deformation by the next relevant zig-zag operator $\mathcal{O}_\eta = X_{15} X_{56} X_{61} - X_{23} X_{34} X_{42}$ does not lead to a toric IR fixed point. Nevertheless, it fits into a more general picture that relates zig-zag deformations of two toric models, see section 4.5.

by it. The chiral ring is now given by the relations $I'_{\text{chiral}} = I'_{\text{geom}} \cap J'_2$, where

$$\begin{aligned}
J'_{\text{mes}} = & \langle B_5 - B_8, C_2 C_4 - B_1 D_3, C_1 C_4 - B_2 D_3, C_2^2 - C_1 D_3, B_1 C_2 - B_2 D_3, \\
& B_1 C_1 - B_2 C_2, B_1^2 - B_2 C_4, C_4^2 - B_8 D_3 + \mu B_1 C_4, \\
& B_8 C_2 - B_1 C_4 - \mu B_2 C_4, B_2 C_4 - B_8 C_1 + \mu B_1 B_2 \rangle \\
J'_2 = & \langle D_3, C_4, C_2, C_1, B_2, B_1 \rangle .
\end{aligned} \tag{4.23}$$

There is a slight abuse of notation here. While the relations hold for the choice of representatives in eq. (4.19), there is a splitting in the F-term equivalence classes and the generators of the chiral ring are now given by

$$\begin{aligned}
B_2 : & X_{26} X_{62} \simeq X_{53}^1 X_{34} X_{45} \simeq X_{15} X_{53}^1 X_{31} \\
B_1 : & X_{56} X_{64} X_{45} \simeq X_{53}^2 X_{34} X_{45} \simeq X_{26} X_{64} X_{42} \simeq X_{25} X_{56} X_{62} \simeq \\
& \simeq X_{15} X_{53}^2 X_{31} \simeq X_{25} X_{53}^1 X_{34} X_{42} \\
C_4 : & X_{25} X_{56} X_{64} X_{42} \simeq X_{25} X_{53}^2 X_{34} X_{42} \\
B_1 + \mu B_2 : & X_{23} X_{36} X_{62} \simeq X_{12} X_{26} X_{61} \simeq X_{12} X_{23} X_{31} \simeq X_{15} X_{53}^1 X_{36} X_{61} \\
C_4 + \mu B_1 : & X_{23} X_{36} X_{64} X_{42} \simeq X_{15} X_{53}^2 X_{36} X_{61} \simeq X_{12} X_{25} X_{56} X_{61} \\
C_4 + 2\mu B_1 + \mu^2 B_2 : & X_{12} X_{23} X_{36} X_{61}
\end{aligned} \tag{4.24}$$

and

$$\begin{aligned}
C_1 : & X_{53}^1 X_{36} X_{64} X_{45} \simeq X_{25} X_{53}^1 X_{36} X_{62} \simeq X_{12} X_{25} X_{53}^1 X_{31} \\
C_2 : & X_{53}^2 X_{36} X_{64} X_{45} \simeq X_{25} X_{53}^2 X_{36} X_{62} \simeq X_{12} X_{25} X_{53}^2 X_{31} \simeq \\
& \simeq X_{25} X_{53}^1 X_{36} X_{64} X_{42} \\
D_3 : & X_{25} X_{53}^2 X_{36} X_{64} X_{42} \\
C_2 + \mu C_1 : & X_{12} X_{25} X_{53}^1 X_{36} X_{61} \\
D_3 + \mu C_2 : & X_{12} X_{25} X_{53}^2 X_{36} X_{61} .
\end{aligned} \tag{4.25}$$

The generators B_5 and B_8 remain represented by the same quiver cycles in (4.19). Note that, from the point of view of the PdP_{3c} theory, the mixing of mesonic generators upon deformation occurs in the direction of the winding number (1, 0) of the zig-zag η_5 . This matches the mesonic charges of the spurionic parameter μ in the superpotential deformation $\mu(A_1 - B_2)$, which determine the pattern of global symmetry breaking.⁵

If we integrate out the massive fields X_{26} and X_{62} , by imposing their F-term equations,

$$X_{26} = \frac{1}{\mu} (X_{23} X_{36} - X_{25} X_{56}) , \quad X_{62} = \frac{1}{\mu} (X_{61} X_{12} - X_{64} X_{42}) , \tag{4.26}$$

⁵Indeed, μ has $U(1)^3$ charges (1, 0, 0), where the first two charges are mesonic, and the last is the R -charge under the $U(1)_R$ symmetry that assigns charge 2 to all mesonic generators. The R -charge is forgotten when the lattice of generators is projected from \mathbb{Z}^3 to \mathbb{Z}^2 as in fig. 4.2.

the result is not explicitly toric, but we can make it so (up to an overall $1/\mu$) by the field redefinitions

$$\begin{aligned} X_{31} &\mapsto -\frac{1}{\mu}X_{31} + \frac{1}{\mu}X_{36}X_{61} & X_{53}^1 &\mapsto \frac{1}{\mu}X_{53}^1 - \frac{1}{\mu}X_{53}^2 \\ X_{45} &\mapsto \frac{1}{\mu}X_{45} - \frac{1}{\mu}X_{42}X_{25} \end{aligned} \quad (4.27)$$

as described in (4.15). Using the methods described previously, we can identify the final result as toric phase B of the cone over the *Pseudo del Pezzo 3b* [55], with superpotential

$$\begin{aligned} W_{\text{PdP}_{3b}}^{(B)} &= X_{15}X_{53}^1X_{31} + X_{34}X_{45}X_{53}^2 + X_{12}X_{25}X_{56}X_{61} + X_{23}X_{36}X_{64}X_{42} \\ &\quad - X_{12}X_{23}X_{31} - X_{45}X_{56}X_{64} - X_{15}X_{53}^2X_{36}X_{61} - X_{25}X_{53}^1X_{34}X_{42} . \end{aligned} \quad (4.28)$$

We can use the fast-forward method and zig-zag paths to read off the changes in the toric diagram. The removal/reduction of the order of the non-isolated singularity is reflected in the fact that the number of points in the side of the toric diagram orthogonal to the zig-zag's external (p, q) -leg is reduced by one. Consequently, the number of extremal points in the toric diagram increases by one.

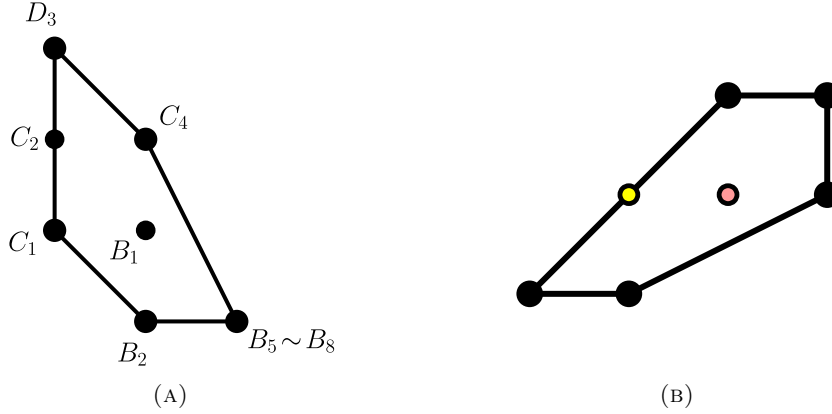


FIGURE 4.3: (a) Lattice of $U(1)^2$ mesonic flavor charges of the generators and (b) toric diagram of PdP_{3b} .

The top coherent primary component I'_{mes} does not manifest a $U(1)^3$ toric symmetry like in (4.20) but, similarly to above, we can find a redefinition that makes the toric symmetry manifest. We can use (4.27) to construct the ring isomorphism,

$$\begin{aligned} B_1 &\mapsto \frac{B_1 - C_4}{\mu} & B_2 &\mapsto \frac{B_2 - 2B_1 + C_4}{\mu^2} \\ C_2 &\mapsto \frac{C_2 - D_3}{\mu} & C_1 &\mapsto \frac{C_1 - 2C_2 + D_3}{\mu^2} \end{aligned} \quad (4.29)$$

which is defined for $\mu \neq 0$. Then the relations among mesonic moduli take the toric form

$$I'_{\text{geom}} = \langle B_8 - B_5, B_1^2 - B_5 C_2, B_1 C_4 - B_5 D_3, B_1 B_2 - B_5 C_1, B_2 C_4 - B_5 C_2, \\ C_1 C_4 - B_1 C_2, C_2 C_4 - B_1 D_3, B_2 D_3 - B_1 C_2, B_2 C_2 - B_1 C_1, C_2^2 - C_1 D_3 \rangle . \quad (4.30)$$

From the superpotential (4.28), we can find the geometric component of the moduli space of the complex cone over PdP_{3b} , which is isomorphic to I'_{geom} (as ring quotients). We can assign $U(1)^2$ charges to each generator consistently with the toric relations in I'_{geom} , obtaining the lattice diagram in fig. 4.3a. Note that for geometries described by reflexive polytopes the lattice of generators is polar dual to the toric diagram.

Zig-zag move in the brane tiling

It is also possible to obtain the final brane tiling by a graph deformation of the initial brane tiling. This builds on [108], where it was understood that a specific degenerate move of the vertices and edges of the tiling along a zig-zag path described the effect of a mass deformation of Klebanov-Witten type [22]. The definition of that move required all the vertices on the zig-zag path associated to the deformation to be trivalent. In order to apply the same move to the more general deformations that we consider in this paper, we need to resolve the vertices on the zig-zag path so that they become trivalent, which makes the tiling locally similar to that of $\mathbb{C}^2/\mathbb{Z}_k \times \mathbb{C}$, in a neighborhood of the zig-zag path. This is possible by *integrating in* fields [113], *i.e.* introducing pairs of bifundamental fields with a superpotential mass term, which upon imposing their F-term equations (or “integrating out” as in (4.14)) leads back to the original model. In the brane tiling, this corresponds to replacing a white/black node with a total of $k + l > 3$ incident edges by two white/black nodes with $k + 1$ and $l + 1$ incident edges, connected by a 2-valent black/white node in between. We can always arrange to have $k = 2$ (or $l = 2$) for the vertices that remain on the zig-zag path after this process, after which the brane tiling move of [108] can be applied.

For example, in the case of PdP_{3c} phase B in fig. 4.1 and the zig-zag path associated to the deformation (4.22), we only need to resolve one of the nodes in the zig-zag path, which has the following local effect on the superpotential

$$X_{15} X_{53}^1 X_{36} X_{61} \mapsto -X'_{13} X'_{31} + X_{15} X_{53}^1 X'_{31} + X'_{13} X_{36} X_{61} \quad , \quad (4.31)$$

where primed fields X'_{13} , X'_{31} have been integrated in. In the new tiling (fig. 4.4), we see that this introduces a new meson $X'_{13} X_{31}$ in the “ $\mathcal{N} = 2$ fractional brane strip”, which is made of massive chirals and is F-term equivalent to $X_{31} X_{15} X_{53}^1 \simeq X_{34} X_{45} X_{53}^1$ (see table 4.2).

Gen. (p_α)	Generator (X_e)	$U(1)^2$	$U(1)_R$
$p_2^2 p_3 g s$	$X_{26} X_{62} \sim X'_{13} X_{31} \simeq X_{31} X_{15} X_{53}^1 \simeq X_{34} X_{45} X_{53}^1$	(1, 0)	1.577...

TABLE 4.2: Partial table of generators of the mesonic moduli space for the integrated in PdP_{3c} phase B model.

This allows us to rewrite the deformation (4.22) as the superpotential mass deformation

$$\delta W' = \mu (X_{26} X_{62} - X'_{13} X_{31}) . \quad (4.32)$$

We can follow the same procedure as before and restore the $U(1)^3$ toric symmetry by the field redefinitions

$$X_{45} \mapsto \frac{1}{\mu} X_{45} - \frac{1}{\mu} X_{42} X_{25} , \quad X_{53}^1 \mapsto \frac{1}{\mu} X_{53}^1 - \frac{1}{\mu} X_{53}^2 , \quad (4.33)$$

which leads to the same superpotential as (4.28), with the relabelling $X'_{31} \leftrightarrow X_{31}$.

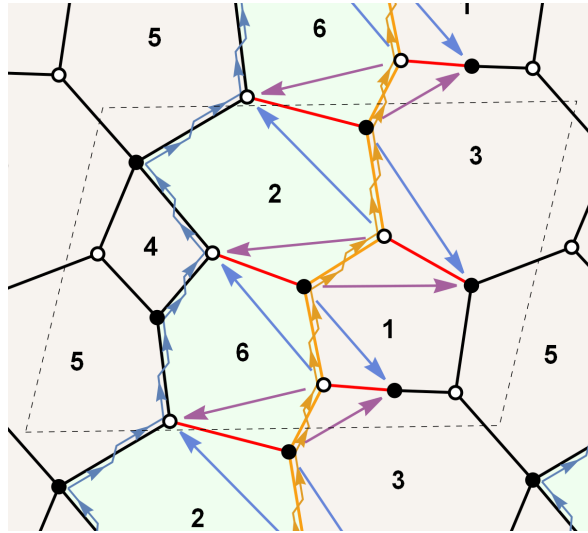


FIGURE 4.4: Tiling of PdP_{3c} phase B with integrated-in node along the deformation zig-zag (yellow), highlighting the two possible (purple/blue) zig-zag moves that realize the deformation.

The result of the deformation and field redefinitions can be visualized in the brane tiling as the folding of the edges involved in the deformation onto the zig-zag path $\eta = X_{12} X_{23} X_{36} X_{61}$. To perform the move that leads to the endpoint tiling, we select alternating edges of a zig-zag path (after integrating in if necessary to ensure that all vertices are trivalent). Then, every pair of edges directly connected to the zig-zag edge on each side are folded onto it by identifying nodes of the same color, and consequently edges, as indicated by the arrows in figure 4.4. We call this operation on the brane tiling a *zig-zag move*.

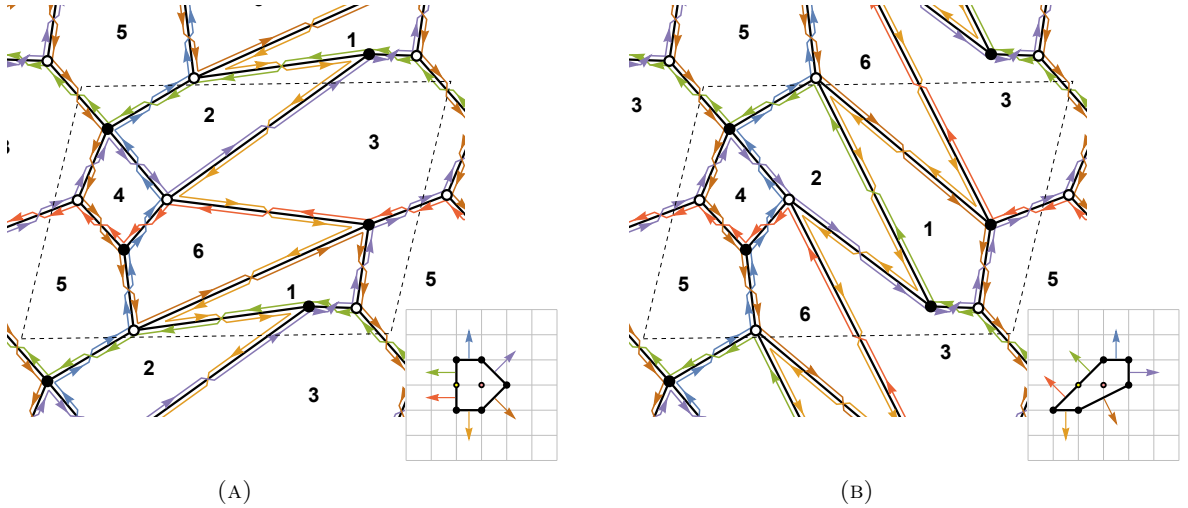


FIGURE 4.5: Tilings and toric diagrams of PdP_{3b} phase B, obtained by applying to the tiling of figure 4.4 the zig-zag move depicted by the purple arrows (a) and blue arrows (b), keeping the original fundamental domain fixed.

There are two ways to do this, which lead to equivalent results which differ by a $\text{SL}(2, \mathbb{Z})$ transformation, see fig. 4.4 and fig. 4.5. The zig-zag path reverses its direction (fig. 4.5) because all the edges that enter the mass deformation (4.32) in the brane tiling are integrated out [108]. A key observation is the fact that the zig-zag path itself is unchanged as a cycle in the quiver, but it reverses its winding on \mathbb{T}^2 .⁶ Additionally, all zig-zags parallel to the one triggering the deformation also remain unaffected.

4.3.2 Higher order non-isolated singularities

Up to this point, we established a solid example of a toric-to-toric flow triggered by a zig-zag deformation of the form (4.3), with mesonic operators M_0, M_1 , given by nonhomotopic paths on the immediate sides of a single zig-zag path in the brane tiling. For geometries with non-isolated singularities of higher order k , we can generalize to

$$\delta W = \mu \sum_{i \in I} \mathcal{O}_{\eta_i} \quad \text{s.t.} \quad \sum_{i=0}^k \mathcal{O}_{\eta_i} \simeq 0. \quad (4.34)$$

For A_1 singularities, the two possible choices for a zig-zag deformation only differ by a sign. The deformation removes the non-isolated singularity and lifts the associated $\mathcal{N} = 2$ fractional brane component from the moduli. For A_2 singularities, we may have three orientations to choose based on the zig-zags $\{\eta_0, \eta_1, \eta_2\}$, but all choices still amount to deforming along a single operator \mathcal{O}_{η_i} . However, the same is not true for $k > 2$.

Specifically for reflexive toric geometries, there is a single example where an A_3 singularity is present: the orbifold $\mathbb{C}^3/(\mathbb{Z}_4 \times \mathbb{Z}_2)$ quotiented with action $(1, 0, 3)(0, 1, 1)$. When a regular D3-

⁶This works for length 4 zig-zags and is a pattern throughout this work.

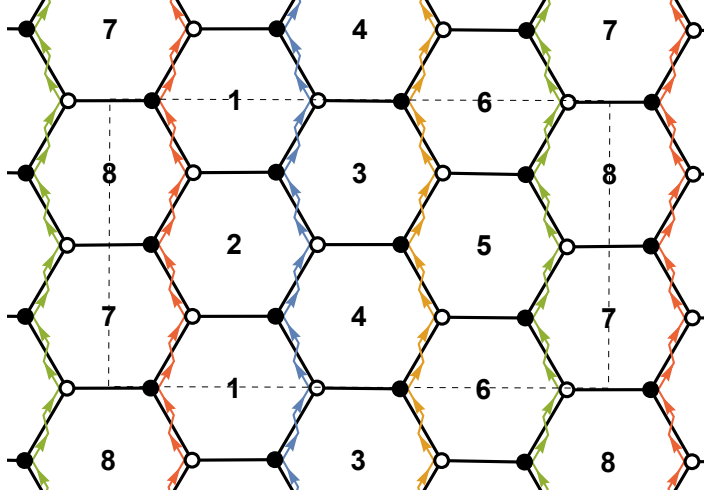


FIGURE 4.6: Tiling of $\mathbb{C}^3/(\mathbb{Z}_4 \times \mathbb{Z}_2)$ $(1, 0, 3)(0, 1, 1)$, with emphasis on the zig-zag paths associated to the non-isolated A_3 singularity.

brane is on the locus of the A_3 singularity, it can split into four $\mathcal{N} = 2$ fractional branes which individually probe the non-isolated singularity. In the worldvolume theory, this fractional brane branch is parameterized by the expectation value of four mesonic operators. By the correspondence between zig-zag paths and superpotential deformations, we have the relevant zig-zag operators

$$\begin{aligned} \mathcal{O}_{\eta_5} &= X_{12}X_{21} - X_{34}X_{43} & \mathcal{O}_{\eta_7} &= X_{56}X_{65} - X_{78}X_{87} \\ \mathcal{O}_{\eta_6} &= X_{34}X_{43} - X_{56}X_{65} & \mathcal{O}_{\eta_8} &= X_{78}X_{87} - X_{12}X_{21} \end{aligned}, \quad (4.35)$$

with all conformal R-charges equal, $R_{\text{sc}}[\mathcal{O}_\eta] = 4/3$. Taking any one of these operators as the deformation δW will trigger a flow to the toric phase A of $L^{1,3,1}/\mathbb{Z}_2$ $(0, 1, 1, 0)$ (detailed in appendix A.1.7), which is expected from effects of a single zig-zag deformation on the initial tiling topology.

We can also trigger a *double* zig-zag deformation of $\mathbb{C}^3/(\mathbb{Z}_4 \times \mathbb{Z}_2)$ by reversing two parallel zig-zag paths in the tiling simultaneously. This leads to the different toric phases of PdP₅ (flows A.1.8). If we reverse two non-adjacent zig-zag paths, we obtain phase A of PdP₅ [55]. There are two possible combinations that lead to the same operator, up to an overall sign,

$$\begin{aligned} \delta W &= \mu (\mathcal{O}_{\eta_5} + \mathcal{O}_{\eta_7}) \\ &= \mu (X_{12}X_{21} - X_{34}X_{43} + X_{56}X_{65} - X_{78}X_{87}) \end{aligned} \quad (4.36)$$

The resulting superpotential from this deformation, after integrating out massive fields, immediately obeys the toric conditions, up to a $1/\mu$ factor that can be removed by a complexified R-symmetry transformation of the fields. From the original tiling, it is possible to perform the two zig-zag moves simultaneously as zig-zag paths (and adjacent edges) do not overlap, as described previously in fig. 4.4. The simultaneous reflection of the zig-zag paths of

the same homology through a double deformation splits an A_3 -type singularity splits into two of A_1 -type with associated zig-zags of opposite homology class.

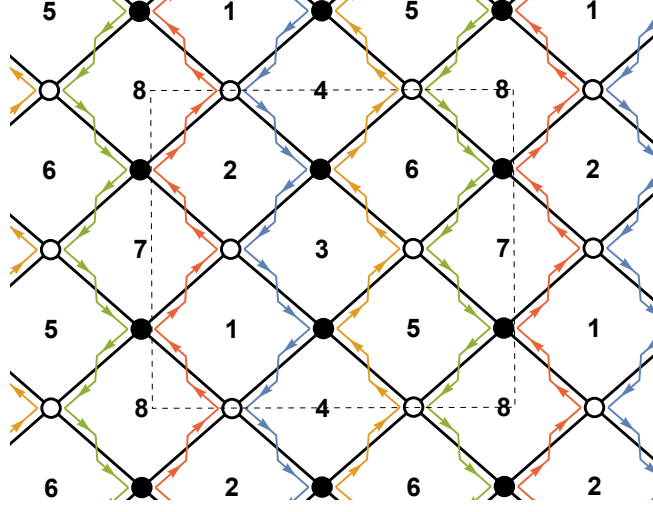


FIGURE 4.7: Brane tiling of PdP_5 phase A, showcasing the zig-zag paths of the parent model in fig. 4.6 and the reversed zig-zag paths after the deformation.

On the other hand, if we reverse two adjacent parallel zig-zag paths, we obtain phase B of PdP_5 . The four possible combinations result in two possible deformations:

$$\delta W = \mu (\mathcal{O}_{\eta_5} + \mathcal{O}_{\eta_6}) = \mu (X_{12}X_{21} - X_{56}X_{65}) \quad (4.37)$$

$$\delta W = \mu (\mathcal{O}_{\eta_6} + \mathcal{O}_{\eta_7}) = \mu (X_{34}X_{43} - X_{78}X_{87}) \quad (4.38)$$

Contrasting with the previous deformation, PdP_5 phase B still contains 2-cycles in the quiver. After integrating the massive fields in the deformed superpotential we still need to apply a field redefinition to these vector-like pairs in order to restore the $U(1)^3$ toric symmetry. For the first deformation in (4.37), we apply

$$\begin{aligned} X_{34} &\mapsto -\frac{1}{\mu}X_{34} + \left(\frac{1}{\mu} - \beta_1\right) X_{31}X_{14} + \beta_1 X_{36}X_{64} \\ X_{43} &\mapsto -\frac{1}{\mu}X_{43} + \left(\frac{1}{\mu} - \beta_1\right) X_{45}X_{53} + \beta_1 X_{42}X_{23} \\ X_{78} &\mapsto \frac{1}{\mu}X_{78} + \left(-\frac{1}{\mu} - \beta_2\right) X_{72}X_{28} + \beta_2 X_{75}X_{58} \\ X_{87} &\mapsto \frac{1}{\mu}X_{87} + \left(-\frac{1}{\mu} - \beta_2\right) X_{86}X_{67} + \beta_2 X_{81}X_{17} \end{aligned}, \quad (4.39)$$

where the parameters $\beta_1, \beta_2 \in \mathbb{C}$ are free, as they cancel out in the superpotential. A similar redefinition applies for the second case (4.38). The mesonic moduli and $\mathcal{N} = 2$ fractional branes for both deformations are isomorphic to the phase A case.

We note that for double zig-zag deformations that are adjacent in the tiling we need an addendum to our prescription for the brane tiling move: besides requiring that the nodes on

the zig-zag are 3-valent as before, we must also ensure that adjacent edges do not overlap for the multiple zig-zags involved in the deformation. We can do so by integrating in fields to replace an edge in the tiling by three edges connected via bivalent nodes, as exemplified in fig. 4.8a. After resolving the overlaps, the same zig-zag move as before can be performed. In

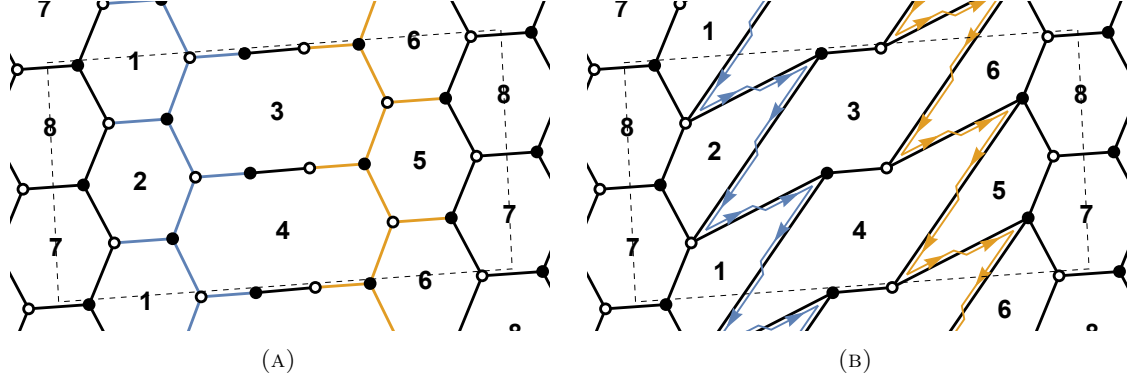


FIGURE 4.8: Zig-zag move to obtain PdP5 Phase B (b) from the integrated-in edges $\mathbb{C}^3/(\mathbb{Z}_4 \times \mathbb{Z}_2)$ model (a).

particular, the result of the deformation (4.37) and the move described above results in the tiling in fig. 4.8b.

4.4 RG flow to a nontoric geometry: from $L^{1,3,1}/\mathbb{Z}_2$ to a marginal deformation of PdP₅

Another possibility for deformations is a flow triggered by a relevant zig-zag operator, which flows not to a toric fixed point but to an exactly marginal deformation thereof. We discuss this case since it reveals the general theory of deformations interpolating between toric quiver gauge theories.

In the previous section, the geometry of the real cone over $L^{1,3,1}/\mathbb{Z}_2$ $(0, 1, 1, 0)$ was reached by triggering a single zig-zag deformation of $\mathbb{C}^3/(\mathbb{Z}_4 \times \mathbb{Z}_2)$ $(1, 0, 3)(0, 1, 1)$. This deformation lifts one $\mathcal{N} = 2$ Coulomb branch modulus, flowing to a geometry with an A_2 singularity. We have also seen that adding a pair of zig-zag operators to the orbifold superpotential the field theory flows to PdP₅, this time lifting the non-isolated A_3 singularity into two A_1 singularities. We would then expect that, by turning on a relevant zig-zag operator of $L^{1,3,1}/\mathbb{Z}_2$, we would be able to flow to PdP₅.

The $L^{1,3,1}/\mathbb{Z}_2$ model has 3 relevant zig-zag operators associated to its A_2 non-isolated singularity, with $R_{\text{sc}} = (10 - 2\sqrt{7})/3$. In the toric phase A in fig. 4.9a, they take the form

$$\begin{aligned}
 \mathcal{O}_{\eta_6} &= X_{78}X_{87} - X_{14}X_{42}X_{23}X_{31} & \eta_6 &= X_{17}X_{72}X_{28}X_{81} \\
 \mathcal{O}_{\eta_7} &= X_{14}X_{42}X_{23}X_{31} - X_{56}X_{65} & \eta_7 &= X_{36}X_{64}X_{45}X_{53} \cdot \\
 \mathcal{O}_{\eta_8} &= X_{56}X_{65} - X_{78}X_{87} & \eta_8 &= X_{58}X_{86}X_{67}X_{75}
 \end{aligned} \tag{4.40}$$

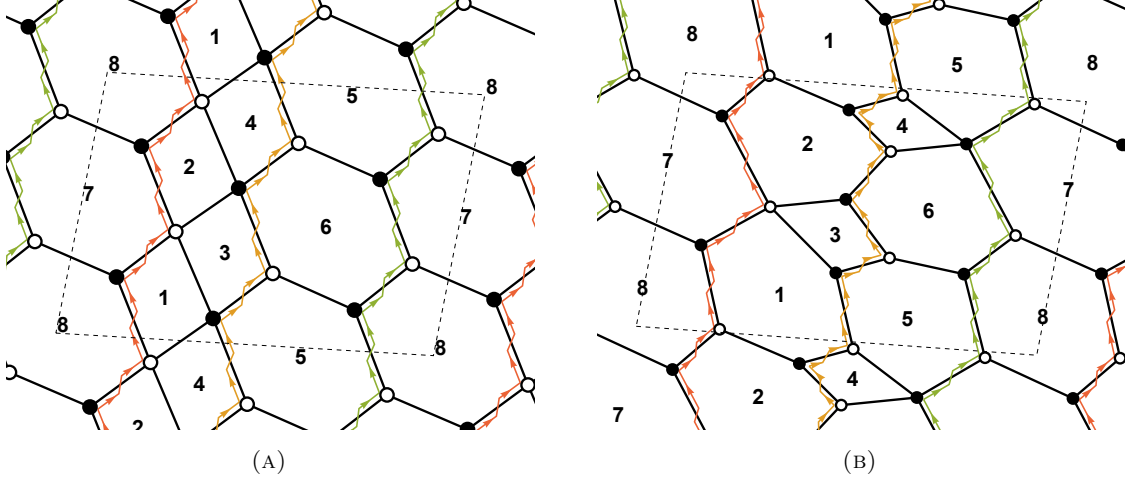


FIGURE 4.9: Brane tilings of phase A (a) and phase B (b) of $L^{1,3,1}/\mathbb{Z}_2$ (0, 1, 1, 0). The two tilings are Seiberg dual by mutating node 4.

The obvious first choice is the deformation \mathcal{O}_{η_8} , which according to our aforementioned zig-zag move should end up in PdP₅ phase A, in fig. 4.7. By integrating out the massive fields $\{X_{56}, X_{65}, X_{78}, X_{87}\}$ and redefining $\{X_{75}, X_{86}\} \rightarrow \{\mu X_{75}, \mu X_{86}\}$, the resulting superpotential is

$$W_{\text{PdP}_5}^{(A)} + \frac{1}{\mu} \mathcal{O}'_{\eta_8}, \quad (4.41)$$

where $\mathcal{O}'_{\eta_8} = X_{17}X_{72}X_{28}X_{81} - X_{36}X_{64}X_{45}X_{53}$ is the operator generated by the reversed zig-zag η_8 (same), now obtained from the superpotential $W_{\text{PdP}_5}^{(A)}$. We conclude that the deformation leads to an exactly marginal deformation of the PdP₅ phase A brane tiling, since all its zig-zag operators \mathcal{O}'_{η} have $R_{\text{sc}} = 2$ and are easily seen to be exactly marginal (*e.g.* by computing the single trace contribution to the superconformal index [114]). Only in the limit, $\mu \rightarrow \infty$ we reach a point in the conformal manifold describing a toric SCFT. Similarly, the relevant deformations by operators $\mathcal{O}_{\eta_6}, \mathcal{O}_{\eta_7}$ also flow to a marginal deformations $\mathcal{O}'_{\eta_6}, \mathcal{O}'_{\eta_7}$ of PdP₅ phase B. Note that $\{\eta_6, \eta_7, \eta_8\}$ are the same paths before and after the deformation, no matter which zig-zag we choose to reverse.

For $L^{1,3,1}/\mathbb{Z}_2$ (0, 1, 1, 0) phase B, the zig-zag operators \mathcal{O}_{η} in fig. 4.9b

$$\begin{aligned} \mathcal{O}_{\eta_6} &= X_{78}X_{87} - X_{12}X_{23}X_{31} \\ \mathcal{O}_{\eta_8} &= X_{46}X_{65}X_{54} - X_{78}X_{87} \end{aligned} \quad (4.42)$$

both trigger flows to marginal deformations of PdP₅ phase C. An interesting case is the deformation associated to the zig-zag η_7

$$\mathcal{O}_{\eta_7} = X_{12}X_{23}X_{31} - X_{46}X_{65}X_{54} \quad \eta_7 = X_{15}X_{53}X_{36}X_{62}X_{24}X_{41}, \quad (4.43)$$

since we were not able to apply the previous techniques to find a way to classify the endpoint of this flow as a toric fixed point or a marginal deformation thereof. Note that, contrary to all other deformations in $L^{1,3,1}/\mathbb{Z}_2$ (0, 1, 1, 0) phase A (and all other shown above), this zig-zag path η_7 has length 6 instead of 4 due to the toric/Seiberg duality. We will see this difference play a crucial role in the classification of zig-zag deformations.

4.5 Zig-zag deformation under Mirror Symmetry

Now that we have considered what happens for all possible zig-zag deformations of reflexive models, we will make a general statement to summarize the results, and we will also present how these are connected to the mirror geometries, more specifically, to the tilings of the mirror curve Σ obtain by specular duality [106], making connection with the work of [115].

In the previous section and in appendix A, we studied all possible deformations by zig-zag operators \mathcal{O}_η of toric quiver gauge theories associated to reflexive toric diagrams, with emphasis on relevant and exactly marginal deformations. The common threads we found can be summarized as follows:

- Whenever the zig-zag η generating a relevant \mathcal{O}_η had length 4, we could relate the deformation of the given toric quiver gauge theory (\mathcal{Q}, W) with quiver \mathcal{Q} and superpotential W , to another toric model (\mathcal{Q}', W') in this class (or an exactly marginal deformation thereof).⁷
- The zig-zag η is reversed in the endpoint model (\mathcal{Q}', W') , and is described by the same closed path in the quiver. However, the latter is a coincidence of length 4 zig-zags. If we consider $\text{PdP}_{3c}/\mathbb{Z}_2$ by extending the tiling in fig. 4.4 along the zig-zag, the brane tiling move still reverses the zig-zag, but leads to a different cycle η' in \mathcal{Q}' .
- Deforming a UV toric model (\mathcal{Q}, W) by a relevant zig-zag operator \mathcal{O}_η triggers an RG flow that approaches another toric model (\mathcal{Q}', W') in the IR from an irrelevant/marginal direction $\mathcal{O}'_{\eta'}$. For example, in the previously discussed deformation of PdP_{3c} phase B for the choice of zig-zag path $\eta_5 = X_{12}X_{23}X_{36}X_{61} = \eta'_5$, we can find field redefinitions such that

$$W_{\text{PdP}_{3c}^{(B)}} + \mu \mathcal{O}_{\eta_5} \xrightarrow{\begin{array}{l} X_{31} \mapsto -\frac{1}{\mu} X_{31} + X_{36} X_{61} \\ X_{23} \mapsto \mu X_{23}, X_{61} \mapsto \mu X_{61} \end{array}} W_{\text{PdP}_{3b}^{(B)}} + \frac{1}{\mu} \mathcal{O}'_{\eta'_5} \quad (4.44)$$

We were able to find additional field redefinitions resulting in the toric fixed point in (4.27) because the zig-zag operator $\mathcal{O}'_{\eta'_5} = X_{15}X_{53}^2X_{31} - X_{25}X_{56}X_{64}X_{42} \simeq 0$ under the

⁷Recall that for the deformation (4.43) of $L^{1,3,1}/\mathbb{Z}_2$ (0, 1, 1, 0) phase B, associated to a zig-zag path of length 6, we could not match the result to a zig-zag marginal deformation of a toric phase for PdP_5 , as expected from phase A result, though we were able to match the deformed geometries on the two sides.

IR F-terms. In contrast, if the reversed zig-zag path is parallel to another zig-zag path, signalling a non-isolated singularity of the IR geometry, as in section 4.4, the deformation $\mathcal{O}'_{\eta'}$ is non-trivial in the chiral ring and cannot be absorbed by a field redefinition.

In order to relate to the mirror (or specular dual) geometry, the first key insight is that the zig-zag path η that triggers the flow must be of length 4. Under specular duality, a zig-zag path η_i becomes the boundary of a face in the tiling representing the gauge group $U(N)_i$, and vice versa. Thus, from the perspective of the specular dual, we need to consider operations that “reverse” the cycle associated to square faces. This operation is exactly the toric-Seiberg duality on the node $U(N)_i$. Therefore, it is natural to expect that the specular dual of the UV toric fixed point is toric-Seiberg dual to the specular dual to the IR toric fixed point of the zig-zag flow. Indeed, this was first proposed in [115],⁸ where the quiver obtained by specular duality was dubbed *twin quiver*, and mutations of (generalized) toric polytopes were related to mutations of twin quivers. This is depicted in the bottom half of fig. 4.10. The main contribution of this paper is to complete fig. 4.10 by adding the top half: in the special case where the two geometries are toric (not generalized toric) and the reversed zig-zag path has length 4, we give a systematic prescription for finding the deformations of the superpotential that relate the two toric models (\mathcal{Q}, W) and (\mathcal{Q}', W') . We have checked that this expectation is correct for the brane tilings associated to reflexive polygons (and more, see [116]). We also note that the zig-zag deformation operators \mathcal{O}_η which play a crucial role in our story do not map to gauge invariant mesonic (single trace) operators in the twin (or specular dual) models. This is perhaps unsurprising, since specular duality is not a quantum field theory duality, but rather a duality of graphs.

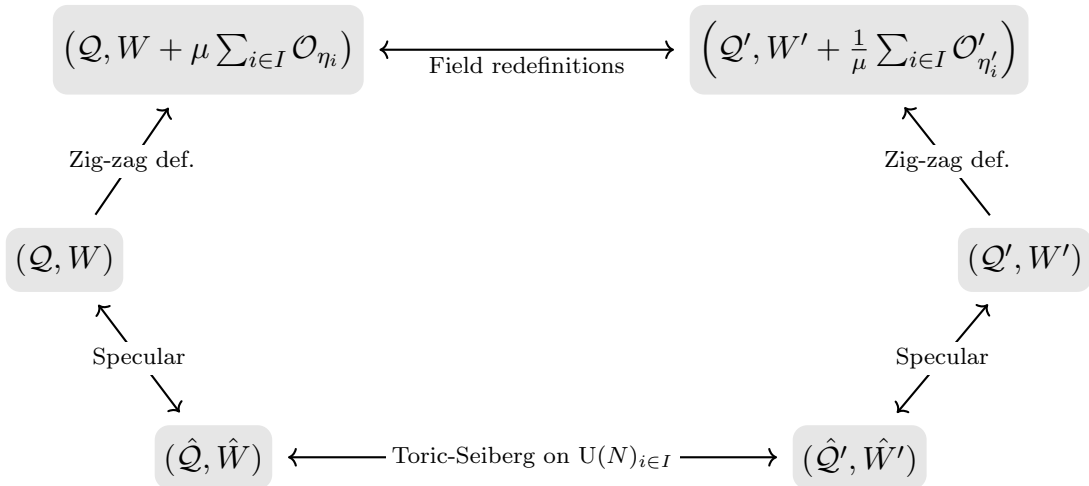


FIGURE 4.10: Diagram representing the connection between length 4 zig-zag deformations and Seiberg duality on the specular dual models.

The deformation parameter μ can be viewed as the inhomogeneous coordinate of a base \mathbb{P}^1 , which has a quiver with deformed superpotential as fibers. The two toric models correspond

⁸This point was also realized independently by JS.

to the two poles. Each zig-zag deformation of a toric model describes how the fiber varies over a patch of \mathbb{P}^1 , which excludes the other pole. On the overlap of the two patches, we can find field redefinitions relating the two deformed quivers and superpotentials: these are the transition functions for the fiber.

In this thesis, we considered relevant zig-zag deformations of UV toric models and matched them to trivial/irrelevant/marginal zig-zag deformations of IR toric models, so there is a clear RG flow direction. It turns out however that fig. 4.10 describes more generally 1-parameter families of deformations relating a pair of toric models, with no reference to an RG flow direction. This structure and the underlying geometry will be explored in future work [117].

The relation to specular duality and (toric) Seiberg duality which was appreciated in [115] also explains why triggering different or multiple zig-zag deformations associated to the same non-isolated singularity may lead to different models. Take for example the reflexive model $\mathbb{C}^3/(\mathbb{Z}_4 \times \mathbb{Z}_2)(1, 0, 3)(0, 1, 1)$, which is specular dual to model PdP₅ phase D. This geometry has a non-isolated A_3 singularity, as manifested by the 4 zig-zag paths with the same winding in its brane tiling. The specular dual of these zig-zags are represented by 4 square polygons symmetrically placed around an octagon in PdP₅ phase D, also shown in fig. 4.11b. The

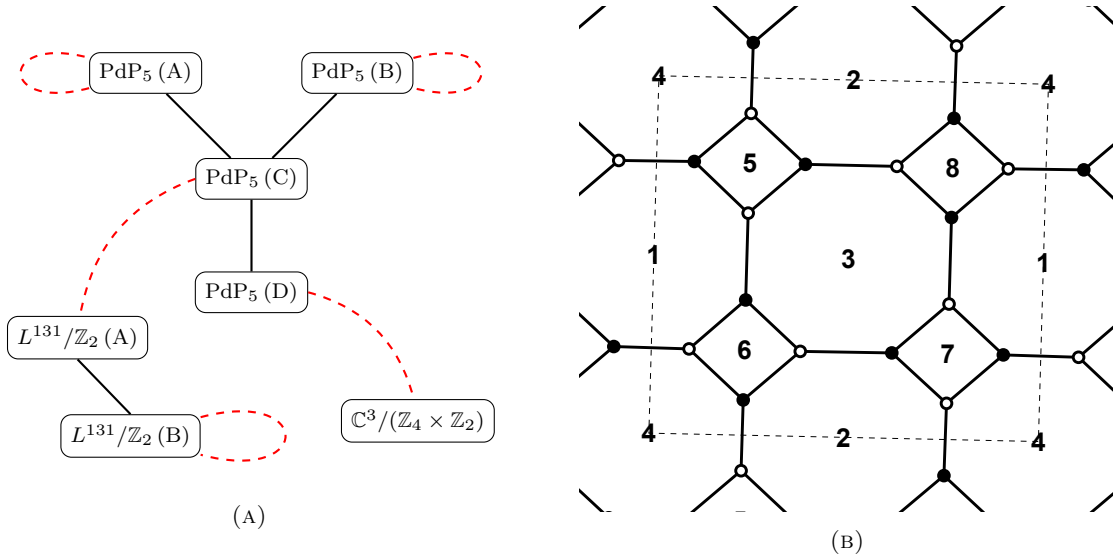


FIGURE 4.11: (a) Graph with toric-Seiberg dualities (solid black edges) and specular dualities (dashed red edges) of $g = 8$ reflexive models. (b) Brane tiling of PdP₅ phase D, specular dual to the model $\mathbb{C}^3/(\mathbb{Z}_4 \times \mathbb{Z}_2)(1, 0, 3)(0, 1, 1)$.

symmetry of PdP₅ (D) tiling means that no matter the $\mathbb{C}^3/(\mathbb{Z}_4 \times \mathbb{Z}_2)$ zig-zag deformation chosen, the model flows to L^{131}/\mathbb{Z}_2 phase A, since PdP₅ phase D is connected to phase C by a single toric-Seiberg duality, which in turn is specular dual to L^{131}/\mathbb{Z}_2 phase A (fig. 4.11a). On the other hand, double deformations of $\mathbb{C}^3/(\mathbb{Z}_4 \times \mathbb{Z}_2)$ flow to either of the 2 specular self-dual phases of PdP₅, depending on the pair of zig-zag operators that trigger the flow: the pairs $\{\eta_5, \eta_7\}$, $\{\eta_6, \eta_8\}$ flow to phase A, while $\{\eta_5, \eta_6\}$, $\{\eta_6, \eta_7\}$, $\{\eta_7, \eta_8\}$, $\{\eta_8, \eta_5\}$ flow to phase B. By the argument above, the split among the possible pairs occurs because applying

toric-Seiberg dualities on opposite squares faces in the octagon in fig. 4.11a leads to a different tiling from the brane tiling resulting from dualizing adjacent square faces.

Additionally, the flows from $L^{1,3,1}/\mathbb{Z}_2(0, 1, 1, 0)$ to marginal deformations of PdP₅ can also be understood using fig. 4.11a. Listing the possible paths from these two geometries

$$\begin{array}{ccccccc}
L^{1,3,1}/\mathbb{Z}_2(\text{A}) & \xrightarrow{\text{spec.}} & \text{PdP}_5(\text{C}) & \xrightarrow{\text{Seib.}} & \text{PdP}_5(\text{A}) & \xrightarrow{\text{spec.}} & \text{PdP}_5(\text{A}) \\
L^{1,3,1}/\mathbb{Z}_2(\text{A}) & \xrightarrow{\text{spec.}} & \text{PdP}_5(\text{C}) & \xrightarrow{\text{Seib.}} & \text{PdP}_5(\text{B}) & \xrightarrow{\text{spec.}} & \text{PdP}_5(\text{B}) \\
L^{1,3,1}/\mathbb{Z}_2(\text{B}) & \xrightarrow{\text{spec.}} & L^{1,3,1}/\mathbb{Z}_2(\text{B}) & \xrightarrow{\text{Seib.}} & L^{1,3,1}/\mathbb{Z}_2(\text{A}) & \xrightarrow{\text{spec.}} & \text{PdP}_5(\text{C})
\end{array} \tag{4.45}$$

we see these correspond exactly to all the possible flows in the previous section (and appendix A.2.1).

Chapter 5

Zig-zag deformation and resolutions

In this section, we study the interplay between the zig-zag deformations discussed previously and crepant resolutions $\tilde{\mathcal{Y}}$ of singular Calabi-Yau cones \mathcal{Y} .

5.1 Minimal GLSM

A four-dimensional $\mathcal{N} = 1$ quiver gauge theory with abelian gauge group \mathcal{G} , quiver \mathcal{Q} and superpotential W is the low energy worldvolume description of a regular D3-brane probing the cone \mathcal{Y} . Resolutions of the singular cone can be viewed as fibers $\tilde{\mathcal{Y}}$ in the master space

$$\mathcal{F} = \{(X_e)_e \mid \partial W = 0\} . \quad (5.1)$$

Algebraically, \mathcal{Y} is fully reproduced by the moduli space of the abelian gauge theory with $\mathcal{G} = \mathrm{U}(1)^G$. Similarly, resolving the cone $\tilde{\mathcal{Y}}$ corresponds to turning on Fayet-Iliopoulos terms in the action. The FI parameters affect D-term equations, leading to non-zero levels for the moment map $\mu : \mathcal{F} \rightarrow \mathfrak{g}^* \cong (\mathbb{C}^\times)^G$

$$\mu_i(X) = \sum_e d_{ie} |X_e|^2 , \quad (5.2)$$

where $d_{ie} = \delta_{i,s(e)} - \delta_{i,t(e)}$ is the incidence matrix of the quiver \mathcal{Q} . The Kähler quotient description of the moduli space $\mathcal{M}(\mathcal{Q}, W; \xi)_\mathbb{K}$ is thus given by¹

$$\mathcal{F} //_\xi \mathcal{G} \equiv \mu^{-1}(\xi) / \mathcal{G} . \quad (5.3)$$

For toric quiver gauge theories, we can exploit dimer model technology and perfect matchings. We can introduce a GLSM (3.44) with no superpotential, that trivializes the F-term equations

¹For ξ a regular value of μ . More generally, if \mathcal{G} is nonabelian, one has to quotient by the co-adjoint stabilizer at the level ξ , given by $\mathcal{G}_\xi = \{g \in \mathcal{G} \mid \mathrm{Ad}_g^*(\xi) = \xi\}$.

$\partial W = 0$. Since this description is redundant, it comes at a cost of extra D-term equations of a spurious $U(1)^{c-G-2}$ gauge symmetry, with charges Q_F defined in (3.46). These additional gauge symmetries do not have FI parameters, as they only serve as connection between the GLSM and the toric variety. Similarly, in the basis of perfect matchings $\{p_\alpha\}$, we can obtain the charges Q_D from the incidence matrix using (3.48). We can group all the D-terms as in table 5.1. Each perfect matching p_α corresponds to a point in the toric diagram Δ of the

	p_1	\dots	p_c	FI
$U(1)_i^F$	$(Q_F)_i^1$	\dots	$(Q_F)_i^c$	0
$U(1)_j^D$	$(Q_D)_j^1$	\dots	$(Q_D)_j^c$	ξ_j

TABLE 5.1: Description of the D-terms for the GLSM associated to a toric model.

singular \mathcal{Y} . Multiple perfect matchings are associated to non-extremal points in Δ . It is possible to eliminate some p_α in the D-term equations such that exactly one variable remains per point in Δ . Because all perfect matchings appear in the D-terms as linear combinations of $|p_\alpha|^2$, each choice of a single p.m. per point in the toric diagram determines an *open string Kähler chamber* in FI parameter space [112]. Conversely, a generic choice of FI parameters ξ falls in the interior of a Kähler chamber, which determines a p.m. variable for each point in the toric diagram.

	p_{x_1}	\dots	p_{x_ℓ}	FI
$U(1)_a$	Q_a^1	\dots	Q_a^ℓ	$\zeta_a(\xi)$

TABLE 5.2: Minimal GLSM, with one p.m. variable per lattice point in Δ . The resolution parameter $\zeta_a(\xi)$ control the Kähler volumes of a basis of holomorphic 2-cycles, which depend linearly on the FI parameters in each open string Kähler chamber.

In order to visualize the Kähler chambers of a toric model let us look at the example of the *pseudo del Pezzo 1* ($\mathcal{Y} = \mathbb{C}^3 / \mathbb{Z}_4(1, 1, 2)$) model, with superpotential

$$\begin{aligned}
W = & X_{13}X_{34}^1X_{41}^2 + X_{24}X_{41}^1X_{12}^2 + X_{31}X_{12}^1X_{23}^2 + X_{42}X_{23}^1X_{34}^2 \\
& - X_{13}X_{34}^2X_{41}^1 - X_{24}X_{41}^2X_{12}^1 - X_{31}X_{12}^2X_{23}^1 - X_{42}X_{23}^2X_{34}^1.
\end{aligned} \tag{5.4}$$

The perfect matchings are

$$\begin{aligned}
p_1 &= \{X_{12}^1, X_{23}^1, X_{34}^1, X_{41}^1\} & s_1 &= \{X_{12}^1, X_{12}^2, X_{13}, X_{42}\} \\
p_2 &= \{X_{13}, X_{24}, X_{31}, X_{42}\} & s_2 &= \{X_{13}, X_{23}^1, X_{23}^2, X_{24}\} \\
p_3 &= \{X_{12}^2, X_{23}^2, X_{34}^2, X_{41}^2\} & s_3 &= \{X_{24}, X_{31}, X_{34}^1, X_{34}^2\} \\
f_1 &= \{X_{12}^1, X_{12}^2, X_{34}^1, X_{34}^2\} & s_4 &= \{X_{31}, X_{41}^1, X_{41}^2, X_{42}\} \\
f_2 &= \{X_{23}^1, X_{23}^2, X_{41}^1, X_{41}^2\}
\end{aligned} \tag{5.5}$$

and their associated perfect matching variables are shown in the toric diagram in table 5.3. From this, we can extract the perfect matching matrix P and rewrite the bifundamentals in terms of the GLSM fields $\{p_\alpha\}$, so that all F-term equations hold. From the perfect matching matrix and D-terms of the toric model, we obtain (recall eqs. (3.46) and (3.48)) a GLSM with charges and FI parameters given in table 5.3.

	p_1	p_2	p_3	f_1	f_2	s_1	s_2	s_3	s_4	FI
$U(1)_1^F$	-1	-1	-1	1	0	0	1	0	1	0
$U(1)_2^F$	0	-1	0	-1	0	1	0	1	0	0
$U(1)_3^F$	-1	0	-1	1	1	0	0	0	0	0
$U(1)_1^D$	-1	-1	-1	1	0	1	1	0	0	ξ_1
$U(1)_2^D$	0	0	0	0	0	-1	1	0	0	ξ_2
$U(1)_3^D$	0	1	0	1	0	-1	-1	0	0	ξ_3
$U(1)_4^D$	1	0	1	-2	0	1	-1	0	0	ξ_4

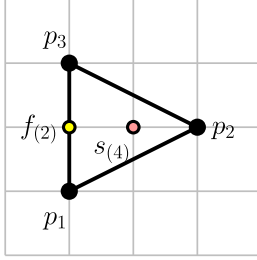


TABLE 5.3: Table encoding D-term equations of the GLSM and toric diagram of PdP₁.

The GLSM fields associated to extremal points on the toric diagram are unique by consistency. We can eliminate those and obtain D-terms with the remaining fields of higher multiplicity. In the PdP₁ case, we have

$$|s_2|^2 - |s_1|^2 = \xi_2 \quad |s_3|^2 - |s_2|^2 = \xi_3 \quad |s_4|^2 - |s_3|^2 = \xi_4 \quad (5.6)$$

$$|f_2|^2 - |f_1|^2 = \xi_4 + \xi_2 \quad (5.7)$$

subject to the condition $\xi_1 + \xi_2 + \xi_3 + \xi_4 = 0$, coming from the decoupled center-of-mass $U(1)$. From these D-terms, we can choose p.m. variables $(p_{(-1,0)}, p_{(0,0)})$ for the points $(-1, 0), (0, 0)$ to obtain the conditions that define the corresponding open string Kähler chamber. For example, the choice $p_{(-1,0)} = f_1$ requires that $\xi_2 + \xi_4 \geq 0$, because in that case f_2 can be solved for in terms of f_1 , while $p_{(0,0)} = s_1$ requires $\xi_2 \geq 0 \wedge \xi_2 + \xi_3 \geq 0 \wedge \xi_2 + \xi_3 + \xi_4 \geq 0$. By repeating this process for all choices of perfect matching variables, we obtain conditions that divide the FI parameter space \mathbb{R}^3 into 8 polyhedral cones that intersect at the origin $\xi = 0$. This particular example allows us to visualize open string Kähler chambers using the stereographic projection (fig. 5.1).

Eliminating the redundant D-term equations and GLSM fields using eqs. (5.6) and (5.7) onto the original D-terms in table 5.3 we obtain the minimal GLSM in table 5.4, by fixing the same $U(1)$ charges for all Kähler chambers.

The singularity $\mathbb{C}^3/\mathbb{Z}_4(1, 1, 2)$ is a fairly simple example that allows visualization of the Kähler chambers, but it misses the complication of compatibility of the Kähler chambers with different triangulations of the toric diagram. We will describe an elegant and more systematic

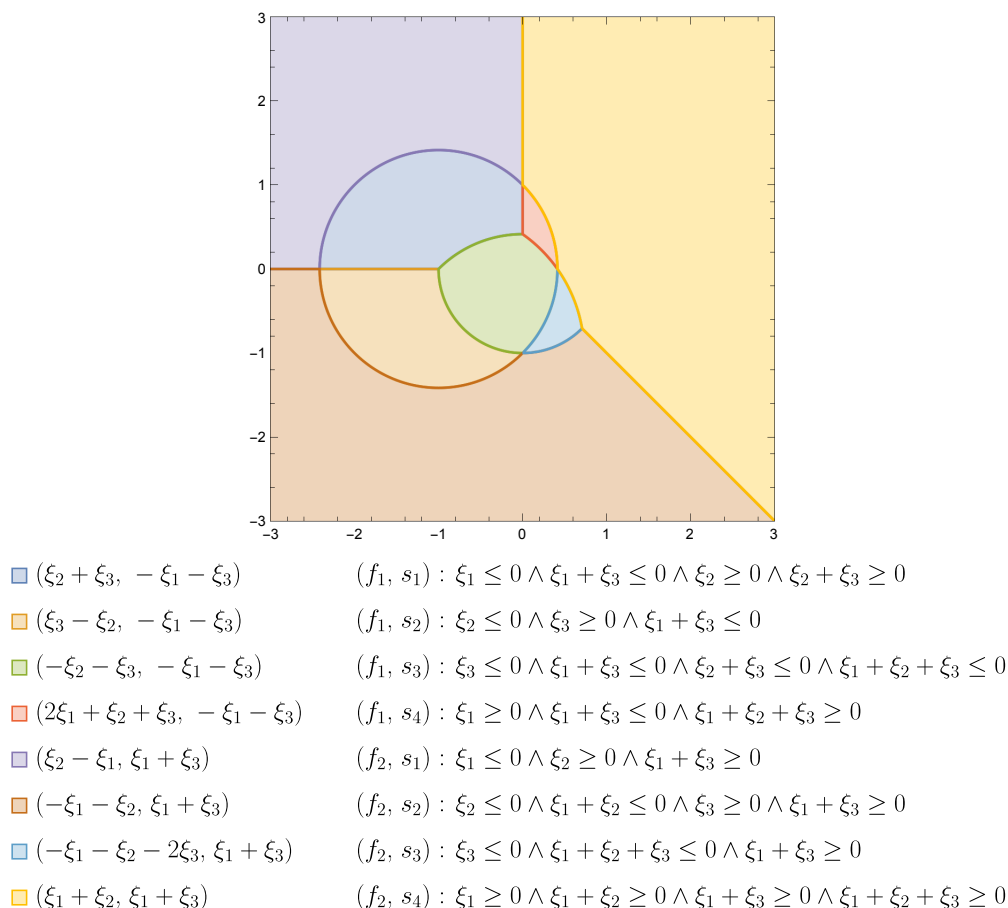


FIGURE 5.1: Region plot of open string Kähler chambers for PdP_1 , using stereographic projection of (ξ_1, ξ_2, ξ_3) . Swatch legend shows the resolution parameters (ζ_1, ζ_2) as piecewise linear functions of the FI parameters for each of the choices of $(p_{(-1,0)}, p_{(0,0)})$.

	$p_{(-1,-1)}$	$p_{(1,0)}$	$p_{(-1,1)}$	$p_{(-1,0)}$	$p_{(0,0)}$	FI
$\text{U}(1)_1$	0	1	0	1	-2	$\zeta_1(\xi)$
$\text{U}(1)_2$	1	0	1	-2	0	$\zeta_2(\xi)$

TABLE 5.4: Minimal GLSM for PdP_1 , with $\zeta_a(\xi)$ given in fig. 5.1.

way of obtaining these wedge regions in the FI parameter space, using the fact that Kähler chambers stem from the quiver \mathcal{Q} and modules of a path subalgebra of $\mathbb{C}\mathcal{Q}$.

5.2 Kähler chambers from θ -stability

The stability condition for the orbits of the complexified gauge group $\mathcal{G}_{\mathbb{C}}$ needed to construct a given resolution divides the moduli space of resolutions into chambers as before. We now construct the possible open string Kähler chambers from the perspective of quiver representations of a quiver \mathcal{Q} , with path relations encoded in the superpotential W .

Through the Kempf–Ness theorem, the Kähler quotient (5.3) is related to the moduli space of quiver representations computed via the GIT quotient,

$$\mathcal{M}(\mathcal{Q}, W; \xi)_K = \mathcal{M}(\mathcal{Q}, W; \theta)_{\text{GIT}}, \quad \text{for } \xi = \theta \in \mathbb{Z}^G. \quad (5.8)$$

Following results of section 2.2.3, closed points of $\mathcal{M}(\mathcal{Q}, W; \theta)_{\text{GIT}}$ are in correspondence with semistable representations of the quiver \mathcal{Q} . We are interested in the representation space $\text{Rep}(\mathcal{Q}, \alpha)$ with dimension vector $\alpha = \mathbf{1}_G = (1, \dots, 1)$. For a given $\theta \in \mathbb{R}^G$, a representation V of \mathcal{Q} with nonzero dimension vector α is called θ -semistable if $\theta \cdot \alpha = 0$ and for any proper subrepresentation $W \subset V$, with dimension vector $\beta = \dim W$, we have $\theta \cdot \beta \leq 0$. We say that V is θ -stable if under the previous assumptions $\theta \cdot \beta < 0$ for any nontrivial proper subrepresentation $W \subset V$.

A choice of Kähler chamber K corresponds to a choice of a perfect matching for each point x in the toric diagram Δ , denoted by K_x . We can restrict to the exceptional divisor for this resolution by vanishing the corresponding field in the GLSM, thus setting $X_e = 0$ for all $X_e \in K_x$. We define the subquiver \mathcal{Q}_{K_x} as the quiver \mathcal{Q} with edges not in the perfect matching K_x , $\{e \in \mathcal{Q}_1 \mid X_e \notin K_x\}$. A representation V of \mathcal{Q}_{K_x} with dimension α is also a subrepresentation of the quiver \mathcal{Q} , with

$$X_e = 0 \quad \forall X_e \in K_x. \quad (5.9)$$

The intersection of the θ -semistability² conditions for a general module in all the subquiver representation spaces $\text{Rep}(\mathcal{Q}_p, \alpha)$, $p \in K$, defines the region of compatibility in the resolutions space, $\xi = \theta$, for the chamber K . More concretely, we can write this as

$$\mathcal{R}(K) = \bigcap_{x \in \Delta} \mathcal{R}(\mathcal{Q}_{K_x}) \quad (5.10)$$

with

$$\mathcal{R}(\mathcal{Q}) = \{\xi \in \mathbb{R}^G \mid \xi \cdot \dim V \leq 0, \xi \cdot \alpha = 0, \forall V \in \text{Rep}(\mathcal{Q}, \alpha)\}. \quad (5.11)$$

Take the example of PdP_1 in section 5.1. For the choice $(f_{(-1,0)}, s_{(0,0)}) = (f_1, s_1)$, we obtain the subquivers in fig. 5.2. Quiver subrepresentations correspond to quiver subdiagrams which are invariant under outward flow. For example, the subquiver \mathcal{Q}_{f_1} has a single proper subrepresentation with dimension $\beta = (1, 0, 1, 0)$. \mathcal{Q}_{s_1} has proper subrepresentations with dimensions $\beta \in \{(1, 0, 1, 1), (1, 0, 0, 1), (1, 0, 0, 0)\}$. Together with $0 = \alpha \cdot \xi = \xi_1 + \xi_2 + \xi_3 + \xi_4$, the semistability conditions become $\xi_2 + \xi_4 \geq 0$ and $\xi_2 \geq 0 \wedge \xi_2 + \xi_3 \geq 0 \wedge \xi_2 + \xi_3 + \xi_4 \geq 0$ respectively, matching the result obtained above.

²Note that saturating the θ -semistability lands us on the boundary between multiple open string Kähler chambers. Thus, full resolutions are obtained by considering θ -stability.

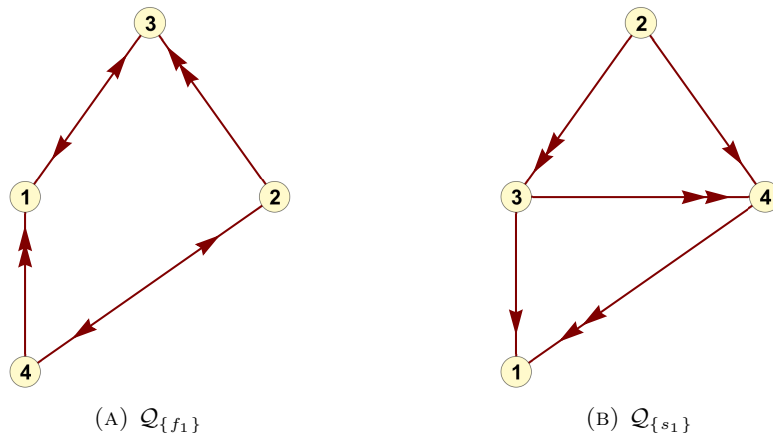


FIGURE 5.2: Subquivers of PdP_1 obtained by deleting edges from the perfect matching of the chamber $(f_{(-1,0)}, s_{(0,0)}) = (f_1, s_1)$.

5.3 (p, q) -webs, 2-cycles and zig-zags

A crepant resolution of a toric Calabi-Yau singularity \mathcal{Y} to $\tilde{\mathcal{Y}}$ consists of a “blow-up” of multiple \mathbb{P}^1 . There are only a few ways to resolve the singularity consistently with the toric structure. Each toric crepant (partial) resolution is encoded in a (p, q) -web diagram.

(p, q) -webs are a geometric representation of 5-brane configurations in type IIB string theory, which engineer 5-dimensional field theories. In this context, we are allowed to create bound states of D5-branes and NS5-branes, which we assign charges $(1, 0)$ and $(0, 1)$ respectively. If the 5-branes worldvolumes share $4 + 1$ dimensions, in order to preserve eight supercharges the remaining worldvolume directions form segments in a 2d plane (x, y) oriented according to the brane charges, *i.e.* $\Delta x + i\Delta y \parallel p + \tau q$ for the axio-dilaton $\tau = C_0 + ie^{-\Phi}$ of type IIB string theory. As is customary, we depict all web diagrams at $\tau = i$, so that D5/NS5 pure states align with the horizontal/vertical axis: the effect of changing τ is to perform a general linear transformation in the (x, y) plane. The balance of forces requires RR-NSNS charge conservation at each vertex: if all fivebranes are incoming,

$$\sum_i (p_i, q_i) = (0, 0) . \quad (5.12)$$

The toric Calabi-Yau 3-folds studied in this paper are affine toric varieties given by a complex cone over a compact toric surface. The mesonic toric action $U(1)^2 \subset U(1)^3$ acts naturally on a torus fiber \mathbb{T}^2 over the complex plane. The (p, q) -web associated to this geometry is given by a set of segments and vertices, in which one or both S^1 in the fibration shrink to a point, respectively. Resolving a toric singularity corresponds to blowing up a point and replacing it by a \mathbb{P}^1 , *i.e.*, replacing a vertex in the (p, q) -web by a segment (with S^1 fiber).

Given a complete triangulation of the toric diagram of \mathcal{Y} , we can construct a consistent (p, q) -web of a fully resolved toric singularity. Every unit triangle in the triangulation of the

toric diagram is dual to a 3-valent vertex in the (p, q) -web, in such a way that every connected line is perpendicular to the triangle edges, which automatically satisfy eq. (5.12). Edges of the boundary of the toric diagram are dual to the semi-infinite external legs of the web, and represent non-compact holomorphic 2-cycles. Internal edges are dual to finite segments on the web, which represent holomorphic 2-cycles with a finite volume.

The volume of holomorphic 2-cycles can be quickly computed from the GLSM. Recall that a toric Calabi-Yau 3-fold has a collection of toric divisors D_{p_α} , defined by setting

$$p_\alpha = 0 \tag{5.13}$$

in the GLSM in table 5.1. Toric curves, which are \mathbb{P}^1 , arise as transverse intersection of two toric divisors. The volume of a holomorphic 2-cycle $\mathcal{C} = D_{p_\alpha} \cdot D_{p_\beta} \in H_2(\mathcal{Y}, \mathbb{Z})$ is

$$\text{vol}(\mathcal{C}) = \int_{\mathcal{C}} \omega = \int_{\tilde{\mathcal{Y}}} \text{PD}(D_{p_\alpha}) \wedge \text{PD}(D_{p_\beta}) \wedge \omega , \tag{5.14}$$

where $\text{PD}(D_{p_\alpha})$ is the Poincaré dual in $H^2(\tilde{\mathcal{Y}}, \mathbb{Z})$ to the divisor D_{p_α} and ω is the Kähler form. The result is a positive linear combination of the resolution parameters. By setting to zero the variables in the GLSM associated to the intersecting divisors, $p_\alpha = p_\beta = 0$, from a linear combination of the D-term equations of the GLSM we can obtain an equation

$$|p_N|^2 + |p_S|^2 = \text{vol}(\mathcal{C}) , \tag{5.15}$$

where the GLSM fields p_N, p_S vanish on the toric divisors that intersect \mathcal{C} at the poles.

For any triangulation T_Δ of the toric diagram, we can find the tuples $(p_\alpha, p_\beta, p_N, p_S)$ associated to each internal edge. Furthermore, the positivity condition

$$\int_{\mathcal{C}} \omega \geq 0 , \tag{5.16}$$

for all the holomorphic 2-cycles for a given fully resolved singularity $\tilde{\mathcal{Y}}$, gives us the compatibility conditions for the associated triangulated toric diagram T_Δ , which are a set of inequalities for the FI parameters in the GLSM. The quiver representation machinery also allows us to quickly obtain these regions in FI parameter space. A triangulation T_Δ is *compatible* with an open string Kähler chamber K if the semistability condition for all subquivers \mathcal{Q}_{K_x, K_y} and \mathcal{Q}_{K_x} , defined by

$$\mathcal{R}(T_\Delta, K) = \bigcap_{(x,y) \in T_\Delta} \mathcal{R}(\mathcal{Q}_{K_x, K_y}) \cap \mathcal{R}(K) \tag{5.17}$$

results in a region of codimension 0, where $\mathcal{R}(K)$ and $\mathcal{R}(\mathcal{Q})$ are defined in eq. (5.10) and (5.11). The union of all $\mathcal{R}(T_\Delta, K)$ for all open string Kähler chambers K is equivalent to the positivity conditions (5.16) for the effective curves.

Take, for example, the complex cone over the *del Pezzo 1* surface, with toric diagram $\Delta = \text{Conv}(\{(-1, 0), (1, -1), (0, 1), (-1, 1)\}) \cap \mathbb{Z}^2$. Using p.m. variables from the brane tiling

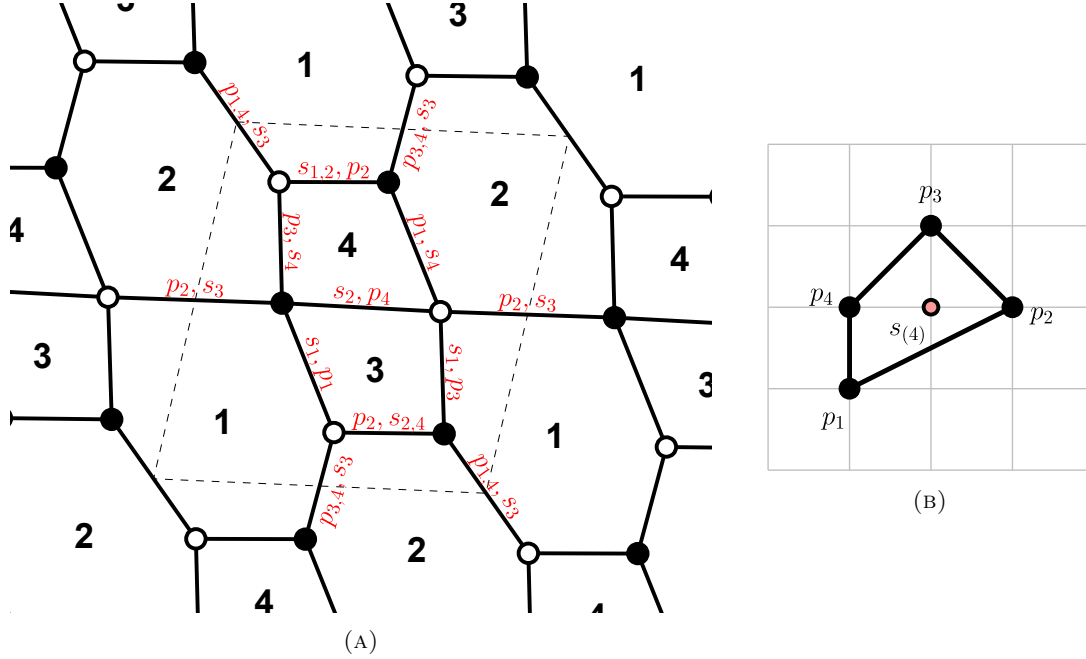


FIGURE 5.3: (a) Brane tiling of dP_1 , with each edge labelled with perfect matching it belongs to. (b) Toric diagram of dP_1 .

in fig. 5.3a, we find a GLSM with D -term equations

$$\begin{aligned}
 |p_1|^2 + |p_2|^2 + |p_3|^2 - |s_1|^2 - |s_3|^2 - |s_4|^2 &= 0 \\
 |p_2|^2 + |p_4|^2 - |s_2|^2 - |s_3|^2 &= 0 \\
 |s_1|^2 - |s_3|^2 &= \xi_1 \\
 |s_3|^2 - |s_4|^2 &= \xi_2 \\
 |s_2|^2 - |s_1|^2 &= \xi_3 \\
 |s_4|^2 - |s_2|^2 &= \xi_4
 \end{aligned} \tag{5.18}$$

This model has four open string Kähler chambers, corresponding to the choice of perfect matching variable for the internal point in the toric diagram, $K_i = \{s_i\}$, $1 \leq i \leq 4$. Triangulations of the toric diagram are associated to two complete resolutions, represented along with their dual (p, q) -webs in fig. 5.4. The triangulations can be defined by the single internal segment where a flop transition is possible, thus we have $T_{\Delta}^{(1)} = \{((-1, 0), (0, 1))\}$ and $T_{\Delta}^{(2)} = \{((0, 0), (-1, 1))\}$. For definiteness, let's choose the Kähler chamber such that $p_{(0,0)} = s_3$, for which we obtain

$$\mathcal{R}(\{s_3\}) = \{\xi_1 \geq 0, \xi_2 \leq 0, \xi_1 + \xi_3 \geq 0\}. \tag{5.19}$$

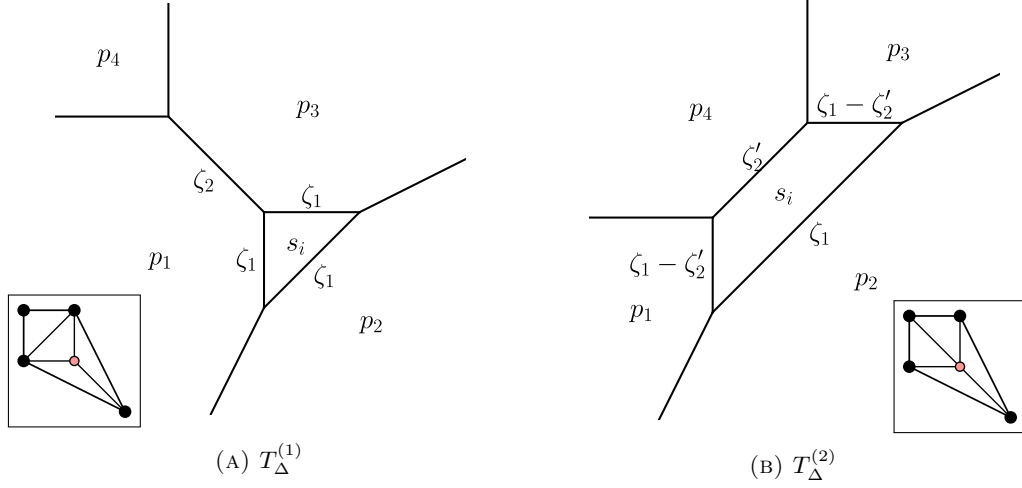


FIGURE 5.4: (p, q) -webs associated to the two resolutions of the complex cone over $d\mathbb{P}_1$, related by a flop transition (at $\zeta_2' = -\zeta_2 = 0$). For the choice of $p_{(0,0)} = s_3$, we have $\zeta_1 = \xi_1 - \xi_2$ and $\zeta_2 = -\zeta_2' = \xi_2 + \xi_3$.

After eliminating the redundant p.m. variables, we obtain the minimal GLSM

$$\begin{aligned} |p_4|^2 + |s_3|^2 - |p_1|^2 - |p_3|^2 &= \xi_2 + \xi_3, \\ |p_2|^2 + |p_4|^2 - 2|s_3|^2 &= \xi_1 + \xi_3 \end{aligned} \quad (5.20)$$

that describes the geometry. In this FI parameter region, we can obtain the holomorphic 2-cycles $D_{p_\alpha} \cdot D_{p_\beta}$, where D_p is the toric divisor associated to the GLSM fields p , by setting $p_\alpha = p_\beta = 0$ in the D -term equations of the GLSM. For the resolution associated with $T_{\Delta}^{(1)}$, which describes a finite size \mathbb{P}^2 intersecting \mathbb{P}^1 , the holomorphic 2-cycles have volumes

$$\begin{aligned} \text{vol}(D_{p_1} \cdot D_{s_3}) &= \text{vol}(D_{p_3} \cdot D_{s_3}) = \text{vol}(D_{p_2} \cdot D_{s_3}) = \xi_1 - \xi_2, \\ \text{vol}(D_{p_1} \cdot D_{p_3}) &= \xi_2 + \xi_3. \end{aligned} \quad (5.21)$$

On the other hand, for the resolution associated with $T_{\Delta}^{(2)}$, which has a finite size $d\mathbb{P}_1$,

$$\begin{aligned} \text{vol}(D_{p_2} \cdot D_{s_3}) &= \xi_1 - \xi_2, \\ \text{vol}(D_{p_4} \cdot D_{s_3}) &= -\xi_2 - \xi_3, \\ \text{vol}(D_{p_1} \cdot D_{s_3}) &= \text{vol}(D_{p_3} \cdot D_{s_3}) = \xi_1 + \xi_3. \end{aligned} \quad (5.22)$$

In the chamber $\mathcal{R}(\{s_3\})$, the parameter $\xi_2 + \xi_3$ can be positive/negative and its sign determines two resolutions in fig. 5.4, related by the flop transition

$$D_{p_1} \cdot D_{p_3} \longleftrightarrow D_{p_4} \cdot D_{s_3}. \quad (5.23)$$

If $\xi_2 + \xi_3 > 0$, we lie on the resolution $T_{\Delta}^{(1)}$, otherwise for $\xi_2 + \xi_3 < 0$ we land in $T_{\Delta}^{(2)}$, consistently with the positivity conditions of the volumes of $D_{p_1} \cdot D_{p_3}$ and $D_{p_4} \cdot D_{s_3}$ respectively. If $\xi_2 + \xi_3 = 0$

the singularity is not fully resolved. Note that for the curve $D_{p_1} \cdot D_{s_3}$, either $(p_N, p_S) = (p_2, p_3)$ or (p_2, p_4) , since $|p_4|^2 - |p_3|^2 = \xi_2 + \xi_3$ for $p_1 = s_3 = 0$. A similar result holds for $D_{p_3} \cdot D_{s_3}$. Compatibility conditions of the resolution $T_\Delta^{(1)}$ with the Kähler chamber $K = \{s_3\}$ can be directly obtained from the θ -stability of representation of \mathcal{Q}_{p_1, p_3} , from which we have the proper subrepresentation with dimension vector $(0, 1, 1, 0)$. For the subquiver \mathcal{Q}_{p_4, s_3} , we have the complementary dimension vector $(1, 0, 0, 1)$. These determine

$$\begin{aligned} \mathcal{R}(T_\Delta^{(1)}, \{s_3\}) &= \{\xi_2 + \xi_3 \geq 0\} \cap \mathcal{R}(\{s_3\}) , \\ \mathcal{R}(T_\Delta^{(2)}, \{s_3\}) &= \{\xi_2 + \xi_3 \leq 0\} \cap \mathcal{R}(\{s_3\}) . \end{aligned} \tag{5.24}$$

Semi-infinite legs of fivebrane webs are related to zig-zag paths in the tiling, by matching (p, q) charges with homology classes (up to $\text{SL}(2, \mathbb{Z})$). Moreover, by taking successive counterclockwise differences of perfect matchings $p_i - p_{i+1}$ along the boundary of Δ , we can reconstruct the zig-zag using edges X_e alternating from the matchings p_i and p_{i+1} with opposite orientation.³ For isolated toric singularities, these ordered pairs of external matchings are in one-to-one correspondence to the zig-zag paths [44, 118, 119]. The case of non-isolated singularities is more interesting, since the corresponding toric diagrams have external perfect matchings of higher multiplicity.

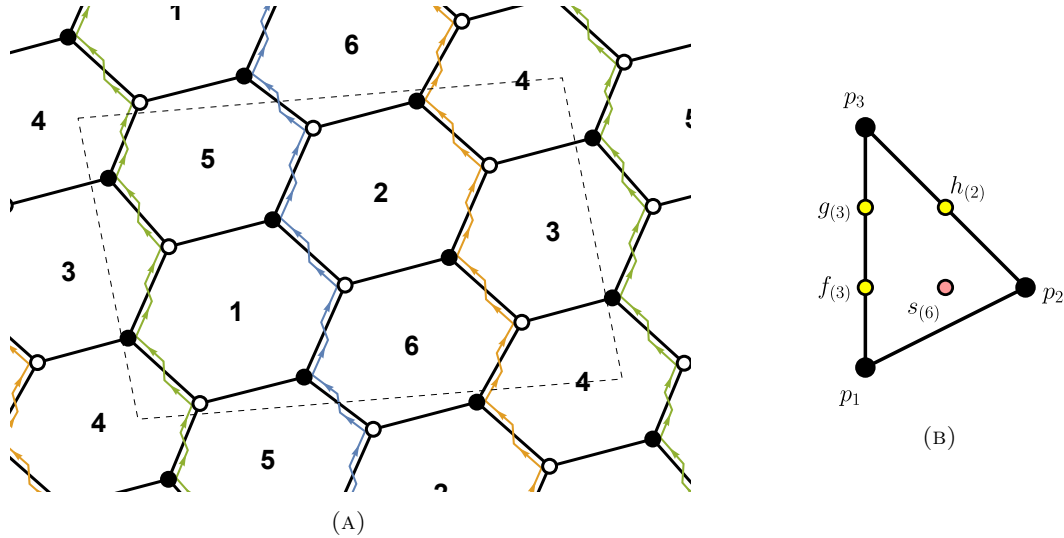


FIGURE 5.5: Brane tiling and toric diagram for $\mathbb{C}^3/\mathbb{Z}_6(1, 2, 3)$, highlighting the three parallel zig-zag paths associated to the A_2 singularity.

For instance, the complex cone over *pseudo del Pezzo 3a* ($\mathcal{Y} = \mathbb{C}^3/\mathbb{Z}_6(1, 2, 3)$) has an A_2 singularity, as signalled by the length 3 side in its toric diagram, see fig. 5.5. The PdP_{3a} theory flows to another toric quiver gauge theory by the deformation associated to any of the

³Edges present in the both p_i and p_{i+1} will cancel, so only X_e in the symmetric difference of the matching sets will form the path.

parallel zig-zag paths normal to the side:

$$\begin{aligned}
\eta_4 = X_{12}X_{25}X_{56}X_{61} & : \{p_3 - g_1, g_2 - f_1, g_3 - f_2, f_3 - p_1\} \\
\eta_5 = X_{24}X_{46}X_{63}X_{32} & : \{p_3 - g_2, g_1 - f_1, g_3 - f_3, f_2 - p_1\} \\
\eta_6 = X_{13}X_{35}X_{54}X_{41} & : \{p_3 - g_3, g_1 - f_2, g_2 - f_3, f_1 - p_1\}
\end{aligned} \tag{5.25}$$

We can infer the p.m. differences in (5.25) from the perfect matching submatrix (5.26) for the relevant matchings and bifundamentals:

$$\left(\begin{array}{c|cccccccccccc}
& X_{12} & X_{13} & X_{24} & X_{25} & X_{32} & X_{35} & X_{41} & X_{46} & X_{54} & X_{56} & X_{61} & X_{63} \\
\hline
p_3 & 0 & 1 & 0 & 1 & 1 & 0 & 0 & 1 & 1 & 0 & 1 & 0 \\
\hline
g_1 & 1 & 1 & 0 & 0 & 1 & 0 & 0 & 1 & 1 & 1 & 0 & 0 \\
g_2 & 0 & 1 & 1 & 1 & 0 & 0 & 0 & 0 & 1 & 0 & 1 & 1 \\
g_3 & 0 & 0 & 0 & 1 & 1 & 1 & 1 & 1 & 0 & 0 & 1 & 0 \\
\hline
f_1 & 1 & 1 & 1 & 0 & 0 & 0 & 0 & 0 & 1 & 1 & 0 & 1 \\
f_2 & 1 & 0 & 0 & 0 & 1 & 1 & 1 & 1 & 0 & 1 & 0 & 0 \\
f_3 & 0 & 0 & 1 & 1 & 0 & 1 & 1 & 0 & 0 & 0 & 1 & 1 \\
\hline
p_1 & 1 & 0 & 1 & 0 & 0 & 1 & 1 & 0 & 0 & 1 & 0 & 1
\end{array} \right) \tag{5.26}$$

For non-isolated singularities, the multiplicity of external non-extremal perfect matchings leads to multiple successive boundary pairs that construct the same zig-zag path. A choice of Kähler chamber fixes the perfect matching variables for each lattice point in Δ and selects unique boundary pairs. However, some chambers do not have compatible resolutions. For incompatible chambers, we may have multiple differences $p_i - p_{i+1}$ which give rise to the same path or one which describes a disconnected set of paths in the brane tiling. In the example above, zig-zag paths cannot be constructed by differences of boundary matchings when any of the pairs (g_3, f_1) , (g_2, f_2) , (g_1, f_3) are chosen for the points $(-1, -1), (-1, 0) \in \Delta$. This is consistent with the fact that the open string Kähler chambers

$$\{g_3, f_1, h_i, s_j\}, \quad \{g_2, f_2, h_i, s_j\}, \quad \{g_1, f_3, h_i, s_j\}, \tag{5.27}$$

for $1 \leq i \leq 2$ and $1 \leq j \leq 6$, are incompatible with all five possible triangulations of fig. 5.5b. We can visualize the region of resolution parameters in which the p.m.s of an A_k singularity side are compatible as the total space of a fibration, with the fiber given by the perfect matchings. In particular, for PdP_{3a} we can represent the regions and boundaries in a plane (see fig. 5.6).

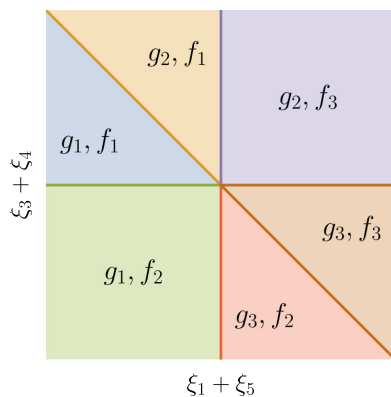


FIGURE 5.6: Regions formed by the stability of reps. of $Q_{g_i}, Q_{f_j}, Q_{g_i, f_j}$ in the PdP_{3a} quiver.

Using the data from the GLSM and subquiver representation stability, we obtain the volumes of 2-cycles in terms of FI parameters and associate external legs of the fivebrane web to zig-zag paths in the brane tiling, and hence chiral operators in the gauge theory. Geometrically, we can apply the zig-zag deformation to the quiver gauge theory with FI parameters, therefore it should be possible to map Kähler chambers between UV and IR toric models. We analyze this problem next.

5.4 Zig-zag deformation as a Hanany-Witten move

We have seen that for a zig-zag deformation \mathcal{O}_η associated to a zig-zag path η of length 4, the deformed UV toric theory flows to another toric gauge theory in the IR, which has η reversed relative to the original brane tiling. The UV geometry has at least one non-isolated A_k singularity, $k \geq 1$, meaning that the tiling has $k + 1$ parallel zig-zags of the same homology (p, q) . At the IR endpoint of the deformation, each reversed zig-zag has homology $(-p, -q)$. The other parallel zig-zag paths are unaffected in the tiling, while some other zig-zag paths are rearranged and have different homology, as seen by comparing fig. 3.1 and fig. 4.5.

Translating the zig-zag move in the brane tiling to the (p, q) -web suggests that the deformation is described by a Hanany-Witten move for a 7-brane on which the 5-brane associated to the deformation zig-zag ends.⁴ Indeed, an external (p, q) fivebrane can terminate on a $[p, q]$ 7-brane, which is a point in the plane of the fivebrane web [120]. By using $\text{SL}(2, \mathbb{Z})$, we can assume without loss of generality that the external legs associated to the relevant parallel zig-zags are D5-branes with charge $(-1, 0)$. We can now end one of the aforementioned D5-branes on a D7-brane, which we then move along the line of the D5-brane, until it ends on the opposite side of the (p, q) web diagram. This corresponds to reversing the orientation of the zig-zag path.

Every time the D7 (or $[1, 0]7$) brane crosses a $(r, s)5$ -brane, by the Hanany-Witten effect a number $|s|$ of $(1, 0)5$ -branes are created, which are suspended between the crossed 5-brane

⁴We thank Michele Del Zotto for this suggestion.

and the D7-brane. For the reflexive geometries studied in this paper, reversing the D7-brane horizontally to the opposite side has it cross exactly two fivebranes with NSNS charge $|s| = 1$: the first HW transition annihilates the original $(-1, 0)$ 5-brane, while the second HW transition creates a new $(1, 0)$ 5-brane. We then can take the limit of the 7-brane going to infinity in the opposite direction to recover a new toric geometry.⁵ We will provide precise evidence that the resulting fivebrane web describes the fully resolved toric geometry obtained at the endpoint of the Klebanov-Witten deformation.

The 7-brane sources a $SL(2, \mathbb{Z})$ monodromy which affects the rest of the web. We can take the monodromy cut to extend from the 7-brane to infinity along the line of the 5-brane we attached it to. As we slide the 7-brane to the opposite end of the line, we also need to rotate the monodromy cut by ± 180 degrees to the opposite side, so that the cut disappears when the 7-brane goes to infinity in the opposite direction. Every time the monodromy cut of a $[p, q]$ 7-brane crosses a 5-brane, the charge of the 5-brane is acted upon by the $SL(2, \mathbb{Z})$ monodromy matrix

$$M_{p,q} = \begin{pmatrix} 1 - pq & p^2 \\ -q^2 & 1 + pq \end{pmatrix}. \quad (5.28)$$

If the branch cut is moved counterclockwise then we apply $M_{p,q}$ to the affected segments, otherwise we act with $M_{p,q}^{-1}$ moving the cut clockwise. Rotating the monodromy cut by 180 degrees clockwise or counterclockwise and sending the 7-brane to infinity, the two resulting (p, q) -webs are equivalent up to a $SL(2, \mathbb{Z})$ transformation. This matches exactly the choice of tiling move in fig. 4.4 for the zig-zag of homology $(0, 1)$, which results either in fig. 4.5a (clockwise) or fig. 4.5b (anticlockwise). Similarly to the zig-zag deformation, parallel D5-branes of the same charge as the (p, q) 7-brane are unaffected by the monodromy.

It is straightforward to see that zig-zag deformations which relate fully resolvable toric geometries with a single exceptional divisor can be generalized to non-reflexive toric geometries if and only if the lattice width w of the toric diagram normal to the (p, q) 5-brane being reversed is exactly 2.⁶ Infinite families of these deformations have already been verified, for example from $(\mathbb{C}^2/\mathbb{Z}_n \times \mathbb{C})/\mathbb{Z}_2$ to $L_{1,n-1,1}/\mathbb{Z}_2$, for all $n \geq 2$ [108], and more examples will be provided in [116].

We can show that the Hanany-Witten move is consistent with the quiver gauge theory analysis for the regions $\mathcal{R}(T_\Delta, K)$, defined in eq. (5.17), of the field theories involved in the zig-zag deformation. In figs. 5.7 and 5.8, we have (p, q) -webs associated to the triangulated toric diagram T_Δ in which we perform a Hanany-Witten move for two different parallel 5-branes.

⁵It is natural to interpret the position of the 7-brane along the line of the 5-branes as a monotonic function of $|\mu|$ which tends to $\mp\infty$ at the two ends of the line (for example, $\log|\mu|$). We will derive this fact and elaborate on the precise relation in [117].

⁶If $w > 2$, at the endpoint of the Hanany-Witten move the D7 brane would become attached to $w - 1 > 1$ coincident D5 branes, leading to a toric geometry with frozen resolutions, which is described by a *generalized toric diagram* (or *polytope*) [121–123]. We will study those situations in a companion paper [117].

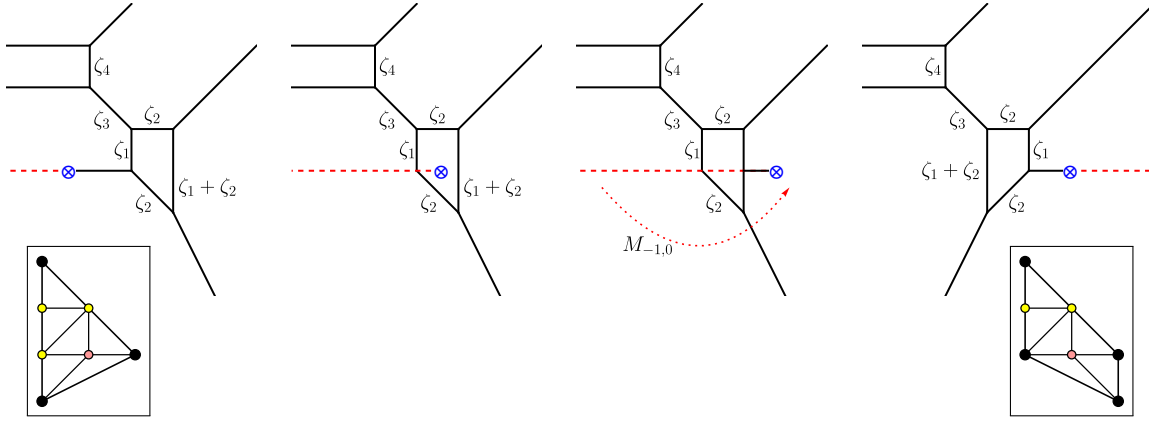


FIGURE 5.7: Hanany-Witten move mapping resolution T_Δ of PdP_{3a} to $T_\Delta^{(2)}$ of PdP_{3c} . 5-branes are in black, 7-branes are in blue, and monodromy cuts in dashed red. Volumes of holomorphic cycles ζ_a are superimposed.

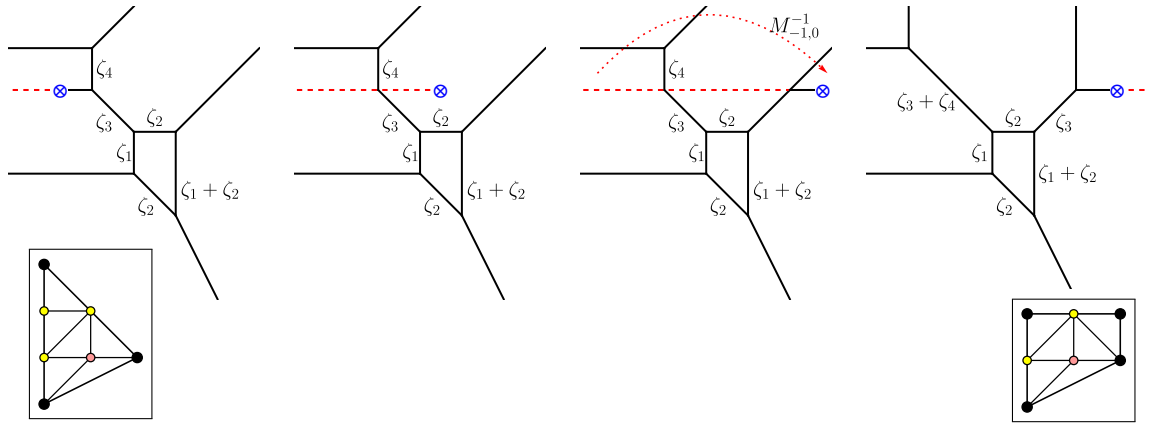


FIGURE 5.8: Hanany-Witten move mapping resolution T_Δ of PdP_{3a} to $T_\Delta^{(1)}$ of PdP_{3c} . Volumes of holomorphic cycles ζ_a are superimposed.

The resulting (p, q) -webs are dual to the triangulated toric diagrams $T_{\Delta'}^{(1)}$ or $T_{\Delta'}^{(2)}$ of PdP_{3c} , as expected.

For any open string Kähler chamber, we know exactly which zig-zag path corresponds to which semi-infinite 5-brane. We can therefore identify which 5-brane we need to reverse to match the zig-zag deformation. The result of the Hanany-Witten move can then be compared with resolved geometry obtained from the quiver gauge theory analysis.

In the first move represented in fig. 5.8, there exist multiple pairs of open string Kähler chambers $K_1^{(1)}, K_2^{(1)}$ such that the chosen zig-zag η corresponds to either of the top two parallel 5-branes. As a result,

$$\mathcal{R} \left(T_\Delta, K_1^{(1)} \right) \cup \mathcal{R} \left(T_\Delta, K_2^{(1)} \right) = \mathcal{R} \left(T_{\Delta'}^{(1)}, K'^{(1)} \right). \quad (5.29)$$

For example, for the reversal of $\eta_4 = X_{12}X_{25}X_{56}X_{61}$ in PdP_{3a} ($\mu \rightarrow 0$), see A.7, the two regions

$$\begin{aligned}\mathcal{R}(T_\Delta, \{g_1, f_1, h_2, s_2\}) &= \{\xi_3 \leq 0, \xi_1 \leq 0, \xi_2 + \xi_5 \geq 0, \xi_1 + \xi_3 + \xi_4 \geq 0, \xi_1 + \xi_3 + \xi_4 + \xi_5 \leq 0\} \\ \mathcal{R}(T_\Delta, \{g_2, f_1, h_2, s_2\}) &= \{\xi_3 \leq 0, \xi_1 \leq 0, \xi_2 + \xi_5 \geq 0, \xi_5 \leq 0, \xi_1 + \xi_3 + \xi_4 + \xi_5 \geq 0\}\end{aligned}\quad (5.30)$$

join into the single region

$$\mathcal{R}(T_{\Delta'}^{(1)}, \{f'_2, g'_1, s'_2\}) = \{\xi_5 \leq 0, \xi_3 \leq 0, \xi_1 \leq 0, \xi_2 + \xi_5 \geq 0, \xi_1 + \xi_3 + \xi_4 \geq 0\}, \quad (5.31)$$

for phase A of PdP_{3c} ($\mu \rightarrow \infty$). In these subregions, the volumes of 2-cycles (see figs. 5.7 and 5.8) can be written as

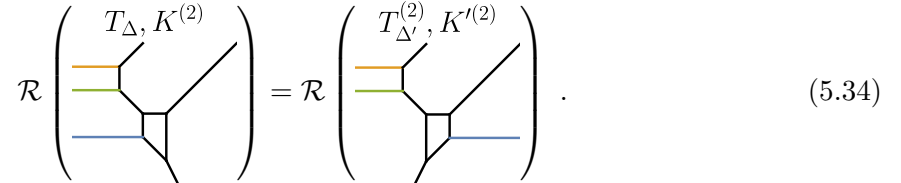
$$\begin{aligned}\zeta_1 &= -\xi_1 & \zeta_3 &= -\xi_5 + \min(0, \xi_1 + \xi_3 + \xi_4 + \xi_5) \\ \zeta_2 &= \xi_2 - \xi_3 + \xi_5 & \zeta_4 &= |\xi_1 + \xi_3 + \xi_4 + \xi_5|\end{aligned}\quad (5.32)$$

The intersection between the two regions in eq. (5.30) corresponds to the θ -stability conditions for subquiver \mathcal{Q}_{g_1, g_2} , which is when the volume $\zeta_4(\xi)$ vanishes, or equivalently when the two parallel 5-branes coincide.

In general, each resolution partitions the k parallel external legs of the nonisolated A_{k-1} singularity into groups of k_1, \dots, k_m parallel 5-branes. Moving a parallel 5-brane from a given partition to another requires a flop transition, thus moving us to another triangulation. For a given resolution T_Δ , we have

$$\bigcup_{i=1}^{k_a} \mathcal{R}(T_\Delta, K_i^{(a)}) = \mathcal{R}(T_{\Delta'}^{(a)}, K'^{(a)}) \quad \text{for } a \in \{1, \dots, m\}, \quad (5.33)$$

for $T_{\Delta'}^{(a)}$ and $K'^{(a)}$ triangulations and open string Kähler chambers of the $\mu \rightarrow \infty$ geometry. The move represented in fig. 5.7 is when the zig-zag corresponds to an external leg in a $k_a = 1$ partition, in which case

$$\mathcal{R}\left(T_\Delta, K^{(2)}\right) = \mathcal{R}\left(T_{\Delta'}^{(2)}, K'^{(2)}\right). \quad (5.34)$$


Using the technology of quiver representation theory, we have been able to map the various open string Kähler chambers of any two (pseudo-)del Pezzo theories related by a zig-zag deformation, listed in appendix A and fig. 1.4. For readers interested in the details, an ancillary file is available upon request (appendix C). Fixing the zig-zag η and mapping regions

$\mathcal{R}(T_\Delta, K)$ and volumes ζ_a from both models, we have verified that the (resolution of) the final toric geometry is precisely the one dual to the (p, q) -web obtained by reversing the external leg associated to η .

Part III

Beyond reflexive polytopes

Chapter 6

Zig-zag deformations of geometries from non-reflexive polytopes

6.1 Zig-zag operator generalized

As introduced before [1], for dimer models with toric geometric moduli encapsulated by a reflexive polytope we can define a zig-zag operator \mathcal{O}_η , for a zig-zag path η in the brane tiling. Given such an operator we can deform the moduli space by modifying the superpotential W of the dimer model (\mathcal{Q}, W) , with quiver \mathcal{Q} , by

$$W_{\text{def}} = W + \mu \sum_{\eta \in S} \mathcal{O}_\eta . \quad (6.1)$$

Often these deformations are trivial in the chiral ring. However, in the presence of A_{k-1} -type non-isolated singularities in the geometry, we can choose a subset of zig-zag paths $\eta \in S$ from a group of k parallel zig-zag paths, which yield a non-trivial deformation. As such, the geometric branch (the top component of the mesonic moduli of the abelian theory on the worldvolume of a regular D-brane) is deformed and the non-isolated singularity in question is partially or fully lifted. Furthermore, the directions on the $\mathcal{N} = 2$ Coulomb branch parametrized by the mesonic operators present in $\sum_{\eta \in S} \mathcal{O}_\eta$ are also lifted by the deformation.

We recall that the zig-zag operator \mathcal{O}_η was defined as¹

$$\mathcal{O}_\eta = \mathcal{O}_\eta^L - \mathcal{O}_\eta^R , \quad (6.2)$$

$$\mathcal{O}_\eta^L = \prod_{k=n}^1 \frac{\partial^2 W}{\partial \eta_{2k} \partial \eta_{2k-1}} , \quad \mathcal{O}_\eta^R = (-1)^n \prod_{k=n}^1 \frac{\partial^2 W}{\partial \eta_{2k+1} \partial \eta_{2k}} ,$$

where $\eta_i = \eta_{(i \bmod 2n)}$ are the $2n$ chiral multiplets that represent the zig-zag closed path. The deformation breaks the $U(1)^3$ mesonic flavor symmetry (toric condition) in the undeformed

¹We assume that η_1 is an edge that goes from a black to white node along η in the brane tiling representation.

theory to a $U(1)^2$ subgroup. However, it has been shown it is often possible to recover an emergent toric $U(1)^3$ symmetry in the infrared. In the case of reflexive polytopes, by turning a zig-zag deformation (6.1) with zig-zag paths $\eta \in S$ being cycles of length 4 in the quiver it is possible to flow to a new toric quiver gauge theory in the $\mu \rightarrow \infty$ limit, described by a new brane tiling (\mathcal{Q}', W') . The model (\mathcal{Q}', W') can be obtained from the original brane tiling at $\mu = 0$ by a graph deformation in which nodes and edges are merged and, more importantly, each zig-zag path $\eta \in S$ in the deformation is reversed to zig-zags $\eta' \in S'$. Here S' is the set of zig-zag paths at $\mu = \infty$ with opposite \mathbb{T}^2 -homology from those in S (at $\mu = 0$). Each zig-zag path reversed matches an outward pointing normal vector to an edge of the toric diagram also being reversed, resulting in a polytope mutation. From the point of view of the dual (p, q) -web, the set of parallel external legs associated to the corresponding zig-zag paths are also reversed via a Hanany-Witten move for a 7-brane that crosses the (p, q) -web in the direction of the reversed 5-brane.

The deformation parameter μ can be thought of as the base coordinate on a \mathbb{P}^1 bundle whose fibers are a family of deformed moduli. It has been shown that, for $\mu \in \mathbb{C}^\times$, it is possible to find an isomorphism

$$\mathcal{M}^{\text{mes}} \left(\mathcal{Q}, W + \mu \sum_{\eta \in S} \mathcal{O}_\eta \right) \cong \mathcal{M}^{\text{mes}} \left(\mathcal{Q}', W' + \frac{1}{\mu} \sum_{\eta' \in S'} \mathcal{O}'_{\eta'} \right). \quad (6.3)$$

The poles of \mathbb{P}^1 are the toric geometries of the dimer models (\mathcal{Q}, W) and (\mathcal{Q}', W') , at the limits $\mu = 0$ and $\mu = \infty$. The flow to another toric geometry is when the isomorphism matches at $\mu = \infty$ and a field redefinition that fully recovers W' is possible. This can occur when:

- $|S'| = 1$, $\eta' \in S'$ is associated to an isolated singularity of the (\mathcal{Q}', W') moduli $\Rightarrow \mathcal{O}'_{\eta'} \simeq 0$
- $|S'| = k > 1$, $\eta' \in S'$ correspond to *all* the zig-zag paths associated to an A_{k-1} non-isolated singularity in the (\mathcal{Q}', W') moduli $\Rightarrow \sum_{\eta' \in S'} \mathcal{O}'_{\eta'} \simeq 0$

The above scenarios fail to be realized when the initial model (\mathcal{Q}, W) contains any zig-zag paths with opposite \mathbb{T}^2 -homology to the parallel zig-zag paths $\eta \in S$ defining the initial deformation. If so, we obtain a $\mu = \infty$ theory (\mathcal{Q}', W') deformed by a non-trivial operator $\sum_{\eta' \in S'} \mathcal{O}'_{\eta'}$ for which we were not able to find a chiral field redefinition.

In the following sections, we intend to generalize the zig-zag deformation for dimer models of toric geometries other than ones defined by reflexive polytopes.

6.1.1 Revisiting the conifold

The deformation of $\mathbb{C}^2/\mathbb{Z}_2 \times \mathbb{C}$ to the conifold $\mathcal{C} = \mathbb{V}_{\mathbb{C}^4}(xy - zw)$, as discussed in the seminal paper by Klebanov and Witten [22], was the first known example of a toric-to-toric deformation being studied. The quiver gauge theory on the worldvolume of D3-branes probing

the $\mathbb{C}^2/\mathbb{Z}_2 \times \mathbb{C}$ orbifold is a 4d $\mathcal{N} = 1$ SYM theory with $U(N)_1 \times U(N)_2$ gauge symmetry, with two fields Φ_1, Φ_2 on the adjoint representation of each factor and two chiral multiplets. See quiver in fig. 6.1. Usually, placing a stack of D3-branes on a canonical Gorenstein singularity

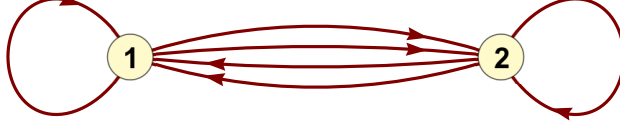


FIGURE 6.1: Quiver of the $\mathbb{C}^2/\mathbb{Z}_2 \times \mathbb{C}$ theory

breaks the $\mathcal{N} = 4$ supersymmetry to $\mathcal{N} = 1$. However, as $\mathbb{C} \times \mathbb{C}^2/\mathbb{Z}_{n+1}$ orbifolds are the simplest A_n -type abelian CY singularities, it turns out that this worldvolume theory preserves $\mathcal{N} = 2$ SUSY, where $\Phi_{1,2}$ are part of $\mathcal{N} = 2$ vector multiplets (for each factor) and with hypermultiplets (X_{12}^k, X_{21}^l) . The superpotential defining the theory is (trace is implicit)

$$\begin{aligned} W &= \Phi_1(X_{12}^1 X_{21}^2 - X_{12}^2 X_{21}^1) + \Phi_2(X_{21}^1 X_{12}^2 - X_{21}^2 X_{12}^1) \\ &= \epsilon_{ab} \Phi_1 X_{12}^a X_{21}^b + \epsilon_{ab} \Phi_2 X_{21}^a X_{12}^b . \end{aligned} \quad (6.4)$$

The moduli space of supersymmetric vacua of the associated 4d $\mathcal{N} = 1$ quiver gauge theory contains a mesonic moduli branch \mathcal{M}^{mes} , parametrized by the of mesonic operators Φ_1, Φ_2 and also $A_{ab} = X_{12}^a X_{21}^b$, with indices labelling the doublet representation of the mesonic flavor symmetry $SU(2)$, along with the $SU(2)_R \times U(1)_r$ R-symmetry of $\mathcal{N} = 2$ SCFTs. These operators are related in the chiral ring of the abelian theory by

$$A_{12} = A_{21} \quad (A_{12})^2 = A_{11} A_{22} \quad \Phi_1 A_{ab} = A_{ab} \Phi_2 \quad (6.5)$$

The relations define two irreducible components: the expected affine toric CY 3-fold cone being probed by a single D3-brane, parametrized by A_{ab} , $a, b = 1, 2$, and a $\mathcal{N} = 2$ branch parametrized freely by Φ_1, Φ_2 . The latter can be lifted by deforming the superpotential with the relevant term

$$\frac{\mu}{2} \left((\Phi_1)^2 - (\Phi_2)^2 \right) , \quad (6.6)$$

Simply integrating out the fields Φ_1 and Φ_2 we obtain the superpotential

$$W' = \frac{1}{\mu} \left(X_{12}^1 X_{21}^1 X_{12}^2 X_{21}^2 - X_{12}^1 X_{21}^2 X_{12}^2 X_{21}^1 \right) . \quad (6.7)$$

By completing the F-term $\mu \frac{\partial W'}{\partial X_{12}^1}$ with X_{12}^1 , we obtain the conifold binomial relation

$$xy - zw = 0 , \quad (6.8)$$

matching the determinant of $(A_{ab}) = \begin{pmatrix} z & x \\ y & w \end{pmatrix}$.

At this point, we did not connect this known deformation to our story of the zig-zag deformation. Let's examine the brane tiling of the $\mathbb{C}^2/\mathbb{Z}_2$ theory (see fig. 6.2). We see this model contain 4

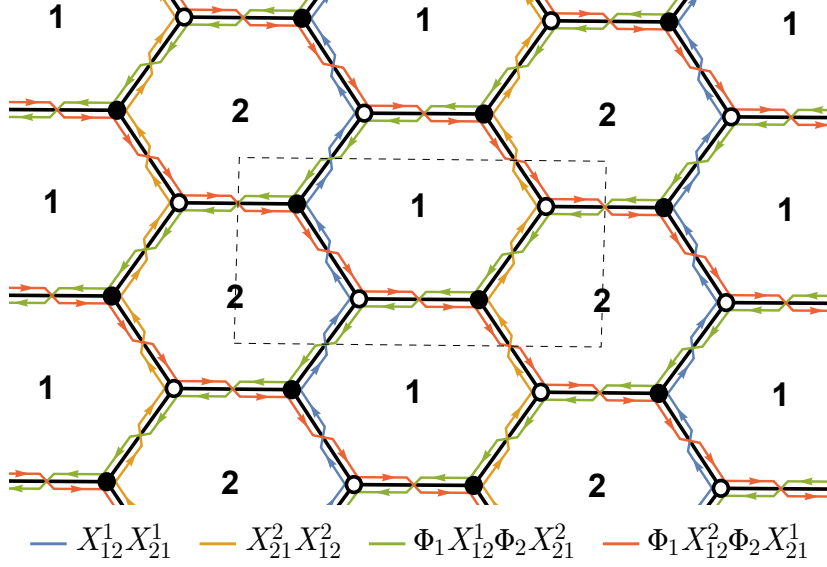


FIGURE 6.2: Brane tiling of the $\mathbb{C}^2/\mathbb{Z}_2 \times \mathbb{C}$ theory.

zig-zag paths

$$\begin{aligned}
 \eta_1 &= X_{12}^1 X_{21}^1 & \eta_3 &= \Phi_1 X_{12}^1 \Phi_2 X_{21}^2 \\
 \eta_2 &= X_{12}^2 X_{21}^2 & \eta_4 &= \Phi_1 X_{12}^2 \Phi_2 X_{21}^1
 \end{aligned} \tag{6.9}$$

Given the presence of an A_1 -type singularity, the zig-zag paths η_1 and η_2 are parallel. As such, we expect the turning the zig-zag deformation associated to one of these yield eq. (6.6). However, contrary to the reflexive toric diagram cases studied before, these zig-zags only have length 2 and their zig-zag operator (as defined above) is

$$\mathcal{O}_{\eta_2} = \Phi_1 - \Phi_2 = -\mathcal{O}_{\eta_1} . \tag{6.10}$$

This does not match the quadratic deformation (6.6), but rather it is a linear (complex) FI deformation, which preserves $\mathcal{N} = 2$ supersymmetry. In fact, turning on a deformation $\delta W = \mu(\Phi_1 - \Phi_2)$ leads to mesonic moduli

$$\Phi_1 = \Phi_2 \quad A_{12} - A_{21} = \mu \quad A_{11} A_{22} = A_{12}(A_{12} + \mu) \tag{6.11}$$

where the $\mathcal{N} = 2$ branch in eq. (6.5) is again lifted (by the 1st equation). Letting $x = A_{11}$, $y = A_{22}$, $z = A_{12} + \mu/2$ and $w = \Phi_1$, the moduli can be rewritten as

$$xy - z^2 = \left(\frac{\mu}{2}\right)^2, \quad w \in \mathbb{C} \tag{6.12}$$

We can view this as complex structure deformation of only $\mathbb{C}^2/\mathbb{Z}_2$, which makes the cone smooth. As such, the D3-brane now probes a smooth point and at low energy the field theory is simply $\mathcal{N} = 4$ SYM.

The deformation that recovers the toric conifold is obtained from the operator by concatenating the zig-zag path twice, *i.e.*, $(\eta_2)^2 = \eta_2\eta_2 = X_{12}^2 X_{21}^2 X_{12}^2 X_{21}^2$. In fig. 6.2 this path is still a closed zig-zag but now winds twice vertically the brane tiling. Recall that \mathcal{O}_η^L and \mathcal{O}_η^R are the chiral mesons given by the 1-cycles in the tiling running through all the edges on the immediate left and right sides of the oriented zig-zag path η . As such, these 1-cycles will be again twice as long, implying

$$\mathcal{O}_{\eta_2\eta_2}^L = (\mathcal{O}_{\eta_2}^L)^2 = (\Phi_1)^2, \quad \mathcal{O}_{\eta_2\eta_2}^R = (\mathcal{O}_{\eta_2}^R)^2 = (\Phi_2)^2. \quad (6.13)$$

The obvious generalization would be to define

$$\mathcal{O}_{\eta,r} = \frac{1}{r} \left[(\mathcal{O}_\eta^L)^r - (\mathcal{O}_\eta^R)^r \right], \quad (6.14)$$

where again a single trace is implied, as the zig-zag operator for a zig-zag simple cycle η concatenated r -times. In the next section, we explore the geometrical consequences of deforming the dimer model with $\mathcal{O}_{\eta,r}$.

6.1.2 Hanany-Witten move of a 7-brane “bound” state

It was observed that the zig-zag deformation between two geometries associated to triangulated toric diagrams of the $\mu = 0$ and $\mu = \infty$ are related to a polytope mutation. The triangulated diagram here describes a set of resolution parameters in which the toric Calabi-Yau singularity take a specific resolution. In a given resolution, we were able to map a zig-zag paths to specific 5-branes in the dual (p, q) -web.

The (p, q) -web [53, 121] is a web of 5-dimensional branes in Type IIB String Theory. The web structure correspond to lines in the (56) plane, while the 5-branes span the (01234) directions and sit at a point in the other directions. The slope of each 5-brane is determined by its (p, q) charges, mutually coprime, which must obey charge conservation at every web junction. External legs of the web can terminate on a $[p, q]$ 7-brane that are pointlike in the (56) plane, while extending in the other directions. Each 7-brane comes with a $\text{SL}(2, \mathbb{Z})$ monodromy cut on the plane that are often pointed radially outwards. We can neglect the curvature corrections from the 7-branes by taking the limit of the external legs to be semi-infinite, making the 7-branes very separated.

The zig-zag deformations \mathcal{O}_η studied before are equivalent to deforming the position of a $[1, 0]$ 7-brane attached to a specific $(1, 0)$ 5-brane.² We showed that is possible to differentiate the k

²We can apply a $\text{SL}(2, \mathbb{Z})$ transformation so the parallel 5-branes we wish to reverse have charges $(1, 0)$.

parallel external 5-brane legs, dual to a toric diagram side that describes an A_{k-1} singularity. By turning on FI parameters in the toric quiver gauge theory (and in the associated GLSM) and fully resolving the web, each external leg can be mapped to a zig-zag path in the dimer model. Adding a relevant deformation \mathcal{O}_η in the 4d $\mathcal{N} = 1$ quiver gauge theory triggers maps to RG flow to an IR effective theory equivalent to sliding the D7-brane in the plane, along the line of the 5-brane. As the $[1, 0]$ 7-brane crosses other (a, b) 5-branes, the Dirac paring

$$\left| \det \begin{pmatrix} 1 & a \\ 0 & b \end{pmatrix} \right| = |s| \quad (6.15)$$

tells us how many $(1, 0)$ 5-branes are created at the crossing and attached to the D7-brane, by the Hanany-Witten (HW) effect. We showed for the reflexive geometries that reversing the D7-brane horizontally to the opposite side has it cross exactly two 5-branes with charge $|b| = 1$ for deformations initiated from zig-zags of the highest A_k nonisolated singularity (most relevant). As a result, the first HW transition annihilates the original $(1, 0)$ 5-brane, the second HW transition creates a new $(1, 0)$ 5-brane. By rotating $\pm 180^\circ$ the $\text{SL}(2, \mathbb{Z})$ monodromy cut, that extends from infinity in $(1, 0)$ -direction to the 7-brane, we can take the limit of the 7-brane going to infinity in the opposite direction to recover a new toric geometry. The polytope mutation on the original diagram is a direct result of sliding the monodromy cut across part of the (p, q) -web. If the branch cut is rotated counterclockwise, then we apply

$$M_{p,q} = \begin{pmatrix} 1 - pq & p^2 \\ -q^2 & 1 + pq \end{pmatrix}, \quad (6.16)$$

to the affected segments, otherwise we act with $M_{p,q}^{-1}$ moving the cut clockwise. The two resulting (p, q) -webs are equivalent up to a $\text{SL}(2, \mathbb{Z})$ transformation.

For the $\mathbb{C}^2/\mathbb{Z}_2 \times \mathbb{C}$ geometry, we note that its toric diagram $\Delta = \text{Conv}\{(0, 0), (1, 0), (0, 2)\} \cap \mathbb{Z}^2$ does not have internal points and any full resolution does not contain a compact 4-cycle. As a consequence, when we couple a single $[1, 0]$ 7-brane to one of the two $(1, 0)$ 5-branes in the dual web and move it horizontally as described above, the D7-brane only crosses a single NS5-brane. The unique crossing annihilates the original $(1, 0)$ 5-branes, and we get a detached 7-brane. As seen in fig. 6.3, rotating the monodromy clockwise is equivalent to acting on the $(2, 1)$ 5-brane charges by $M_{-1,0}^{-1}$, merging with the original $(1, 1)$ 5-brane.

In fact, the geometric moduli from the deformation in eq. (6.12) is a smooth hypersurface in $\mathbb{V}_{\mathbb{C}^4}(xy - uv) \times \mathbb{C}$, the total space of deformations of the orbifold. Taking the limit of the 7-brane going to infinity, $\mu \rightarrow \infty$, the resulting web is dual to the regular 2-simplex. In the T^2 -dual picture of the 5-brane web, this implies that the D3-brane is no longer probing a singular CY 3-fold, which no longer decays into a bound state of $\mathcal{N} = 2$ fractional branes. When a D3-brane is placed at nonsingular point it sees a smooth \mathbb{C}^3 geometry locally, and this

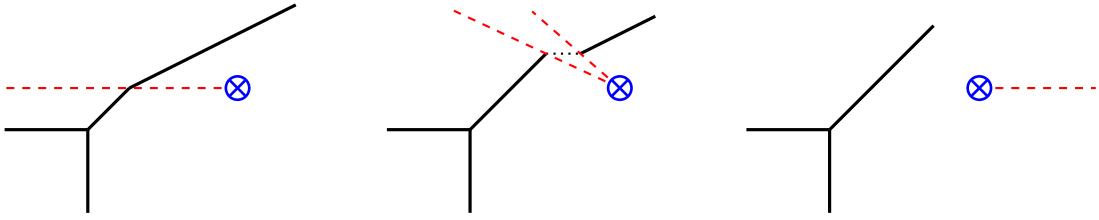


FIGURE 6.3: Hanany-Witten move of a single 7-brane ($r = 1$). As we rotate the monodromy cut (dashed red), with direction (x, y) , we observe a conical gap open due to the identification of directions $(x, y) \sim M_{-1,0}^{-1}(x, y) = (x - y, y)$ of the two semi-infinite lines. The 5-branes crossing the gap/cut are also identified (dotted line).

gives rise to $\mathcal{N} = 4$ Yang–Mills worldvolume theory in the IR. The Gorenstein toric variety from this toric diagram is simply $\mathbb{C}^3 = C_{\mathbb{R}}(S^5)$.

The 5-brane web resulting from the Hanany-Witten move of a single D7-brane attached to the parallel 5-brane does not reproduce the geometry of the conifold, but rather it describes the complex FI deformation of the $\mathcal{N} = 2$ quiver gauge theory on D3-branes probing an A_1 singularity. In order to reproduce the conifold, we need the Hanany-Witten move to generate two 5-branes during the single crossing, so that the annihilation of 5-branes still leaves one $(1, 0)$ 5-brane attached to the $[1, 0]$ 7-brane. Additionally, in order to maintain the S-rule [121] the monodromy action must act on the $(2, 1)$ brane to generate a $(0, 1)$ 5-brane. We note that acting twice with $M_{-1,0}^{-1}$ (clockwise rotation) on the external 5-brane

$$(M_{-1,0}^{-1})^2 \begin{pmatrix} 2 \\ 1 \end{pmatrix} = M_{-1,0}^{-1} \begin{pmatrix} 1 \\ 1 \end{pmatrix} = \begin{pmatrix} 0 \\ 1 \end{pmatrix} \quad (6.17)$$

recovers the expected charges. In order to generate the conifold geometry, we therefore need to attach the single 5-brane (mapped to η) to a bound state of two $[1, 0]$ 7-branes, which we then move horizontally. We contrast this Hanany-Witten move, in fig. 6.4, with the previous move for $r = 1$. For zig-zag deformations from polytopes with no internal points, we expect

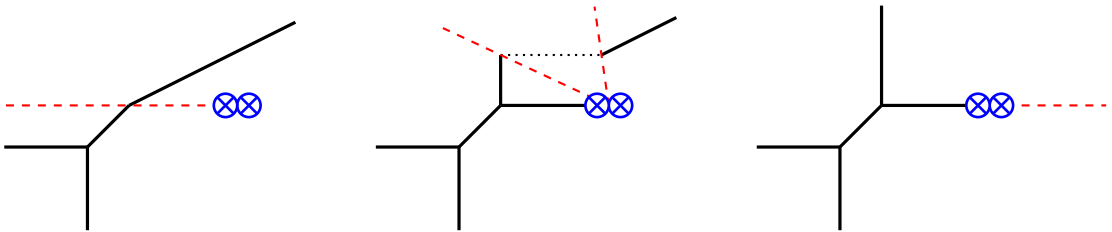


FIGURE 6.4: Hanany-Witten move of a bound state of two 7-brane ($r = 2$). The conical gap represents the identification $(x, y) \sim (M_{-1,0}^{-1})^2(x, y) = (x - 2y, y)$ associated to the monodromy cut (dashed red).

that we need to use the operator $\mathcal{O}_{\eta,r}$ for $r = 2$, since these cases are the ones where a single crossing occur.

Assuming we have s number (p, q) 5-branes suspended between r -bound state of $[p, q]$ 7-branes and a (a, b) 5-brane, the theory background still has preserves supersymmetry if the generalized S-rule holds:

$$s \leq r|aq - bp| . \quad (6.18)$$

Increasing the number r of 7-branes in the bound state, the number s of 5-branes that can be suspended compatibly with supersymmetry increases. We expect the generalized zig-zag deformation by $\mathcal{O}_{\eta, r}$ in the dimer model to be dual to a Hanany-Witten move of r $[1, 0]$ 7-branes attached to a single $(1, 0)$ 5-brane. However, the quiver description of the deformation is currently not understood if $s > 1$, since the 5-brane web describes a deformation of a (partially) frozen non-isolated singularity, which cannot be (fully) resolved. In fact, the field theory description may be non-Lagrangian.

Note that we can count the number of crossings with NS5-branes when moving (perpendicularly) a bound state of D7-brane from the toric diagram. Given a polytope, a facet normal (p, q) , associated to the zig-zag η defines a set of perpendicular lines $px + qy = h$, with integer height $h \in \mathbb{Z}$, whose intersection with the toric diagram is $\Delta_{\eta, h} = \text{Conv}(\{\mathbf{v} \in \Delta \mid \langle \eta, \mathbf{v} \rangle = h\}) \cap \mathbb{Z}^2$. Furthermore, there exists a range of heights $h_{\min} \leq h \leq h_{\max}$ such that $\Delta_{\eta, h}$ is nonempty. We denote the lattice width with respect to the normal η by $w_{\eta} = h_{\max} - h_{\min}$.

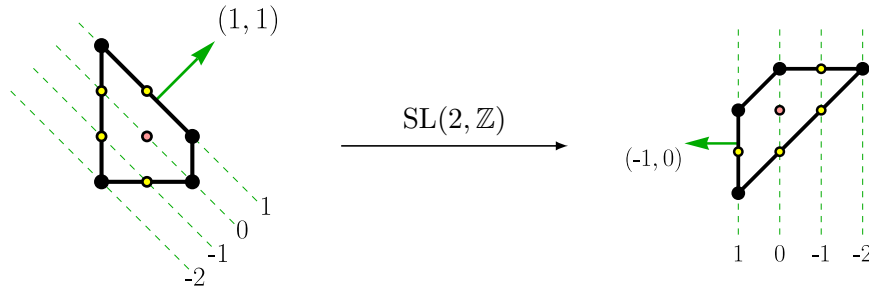


FIGURE 6.5: Lattice width w_{η} with respect to toric diagram facet normal η .

On the other hand, using the convention above, we can apply the appropriate $\text{SL}(2, \mathbb{Z})$ transformation such that η maps to a facet with normal $(-1, 0)$. The lattice width w_{η} with respect to η is simply the width of the transformed polytope in the $(1, 0)$ -direction. It is easy to check that the number of crossings of the D7-branes in the Hanany-Witten move matches w_{η} . See example in fig. 6.5.

In order to recover a toric geometry from a zig-zag deformation of an initial toric quiver gauge theory it must flow to an IR theory where the dual web contains only single 5-brane external legs attached to a single D7-branes, sent to infinity ($\mu \rightarrow \infty$). In the aforementioned context, we can pick η and r in two ways: either $w_{\eta} = 2$ and we deform the superpotential by $\delta W = \mu \mathcal{O}_{\eta, 2}$, or we have $w_{\eta} = 2$ and $\delta W = \mu \mathcal{O}_{\eta, 1}$. The first case are the mass deformations

between pairs of geometries in the subfamily $L^{k,n-k,k}$, with $n \geq 2k > 0$, fully covered in [108]. We will continue to explore the second case in the following section, continuing the work in [1].

For $r + w_\eta > 3$, we expect the zig-zag operator $\mathcal{O}_{\eta,r}$ to induce more general deformations. When moving a single ($r = 1$) 7-brane across $w_\eta \geq 3$ crossings, the endpoint is described by web with $w_\eta - 1$ parallel 5-branes ending on a single 7-brane. The later geometry is often depicted by a generalized toric polytope (GTP) [123], containing “white dots” to symbolize that some parallel 5-branes cannot be separated as they are suspended in the same 7-brane. We note that the GTPs in the literature correspond to $r = 1$, but can be generalized to higher r as outlined above.

6.2 Polytopes with 2 internal points

In this section, we continue the exploration of zig-zag deformations of toric quiver gauge theories. While we managed to study in depth all the zig-zag deformations between reflexive models, we wanted to verify the proposed arguments holds when the nice properties of the reflexivity are not present.

We will use the excellent work of Bao, J. *et al.* [124] as a guide, in which they apply the inverse algorithm [43, 47] to find the 4d $\mathcal{N} = 1$ toric superpotentials describing the worldvolume theory resulting from probing CY_3 cones described by the 45 polytopes with 2 internal points enumerated in [125] (up to $\text{SL}(2, \mathbb{Z})$ lattice equivalence). While the list of superpotentials in [124] does not extensively cover all toric phases of the models (which are relevant for the study of the zig-zag deformations), we will use the provided superpotentials to find the graph of toric dual brane tilings.³ The toric diagrams with 2 internal divisors belong to 4 classes of families of toric varieties (and orbifolds thereof):⁴

- $Y^{p,q}$ [33] are a well-studied family of Sasaki-Einstein manifold, whose toric vertices as given by

$$\{(0, 0), (1, 0), (p, p), (p - q - 1, p - q)\} . \quad (6.19)$$

- $X^{p,q}$ [126] define a set of quiver gauge theories, which extend the toric diagram of $Y^{p,q}$ to

$$\{(0, 0), (1, 0), (p, p), (p - q, p - q + 1), (p - q - 1, p - q)\} . \quad (6.20)$$

The toric diagram of $X^{p,q}$ can be blown down to $Y^{p,q}$ or $Y^{p,q-1}$.

³Strongly connected graph to duals, with edges signifying a toric-Seiberg duality.

⁴Following the families described in [124] we found two typos relating the labelling of the toric diagram: where it reads $K^{4,4,2,4}$ it should read $K^{4,4,2,3}$; where it reads $L^{1,3,2}$ it should read $L^{4,3,2}$.

- $L^{a,b,c}$ [32, 34] is a Sasaki-Einstein manifold whose real cone is an affine Gorenstein 3-fold singularity, where a, b, c are integers with $0 < a \leq b$, $0 < c < a + b$, and with $\gcd(a, b, c, a + b - c) = 1$ (mutually coprime). The toric diagram has vertices

$$\{(0, 0), (1, 0), (ak, b), (-am, c)\}, \quad (6.21)$$

where the integers $k, m \in \mathbb{Z}$ obey the condition $ck + bm = 1$. Notice the $L^{p-q, p+q, p}$ spaces reduce to $Y^{p,q}$.

- $K^{a,b,c,d}$ [124] corresponds to the affine Gorenstein 3-fold singularity whose toric diagram is the pentagon with vertices

$$\{(0, 0), (1, 0), (a(k+l), b-d), (ak, b), (-am, c)\}, \quad (6.22)$$

obeying $ck + bm = 1$, $dm = cl$. The case with $d = 0$ reduces to $L^{a,b,c}$.

Toric diagrams simultaneously define the affine 3-dimensional cone of the CY 3-fold, by taking the span of $(\Delta, 1)$, and the 2-dimensional compact base surfaces(s). Using the Star-projection(s) (2.58) along a compact divisor, we can generate a fan of a 2-dimensional compact base variety. For a single internal point, we just have a single compact 4-cycle D_ρ , isomorphic to a 2-dimensional Gorenstein Fano toric surfaces. In the present of 2 internal points, we might obtain different base toric varieties as it depends on which of the two compact divisors ρ_1, ρ_2 the projection is performed. In many cases, we obtain different 2 inequivalent complete fans $\Sigma_1(\Delta), \Sigma_2(\Delta)$, however these might match due to the symmetries of the toric diagrams. While compact surfaces $X_{\Sigma_1(\Delta)}, X_{\Sigma_2(\Delta)}$ are no longer Gorenstein, these are still \mathbb{Q} -Gorenstein of degree 2.⁵

In this section, we will present an algorithmic way to find zig-zag deformations between toric endpoints. We will exemplify with the dimer model $L^{5,6,1}$ in specific, and detail all the zig-zag flows to multiple toric phases of quiver gauge theories, whose geometric moduli are the $K^{2,4,1,3}$ and $K^{4,3,2,2}$ affine CY 3-folds. Due to the increased amount of toric phases in polytope with 2 internal points, we simply present the remaining zig-zag deformations. The data collected can be found in github.com/jose-a-sa/zig-zag-deformation-data.

6.2.1 Algorithmic approach

In lattice polytopes with two internal points, $I = 2$, having an increased number of number groups factors g in the quiver and boundary points B on the toric diagram, due to Pick's

⁵The anticanonical divisor $-K_X$ is not ample but $-2K_X$ is. This is equivalent to looking at height 2 in the lattice of generators.

theorem,

$$g - 1 = (B - 3) + 2I , \quad (6.23)$$

increases the chances of having a non-isolated singularity of A_k -type with higher rank. This implies a larger possibility in deformations and toric-Seiberg duals. While we can use the Hanany-Witten argument or apply a polytope mutation to find the toric endpoint of a deformation, these methods ignore the fact that we can obtain different toric phases by triggering a zig-zag deformations of the same type.

Instead of trying out the possible combinations of zig-zag deformations, we decided to pursue a computer-assisted route. Here, we explain how we obtain all the toric phases connected to a single toric superpotential by toric-Seiberg dualities. Using the toric phases obtained, we use the definition (6.2) to find all possible deformations. More importantly, we describe the algorithm used to find the necessary find the chiral field redefinitions and how to match the IR superpotential with the aforementioned obtained toric phases.

6.2.1.1 Generating toric phases

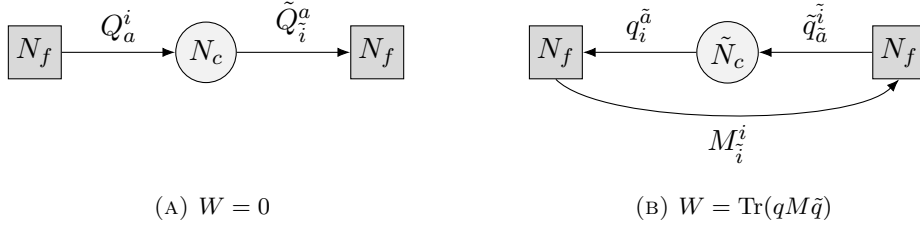
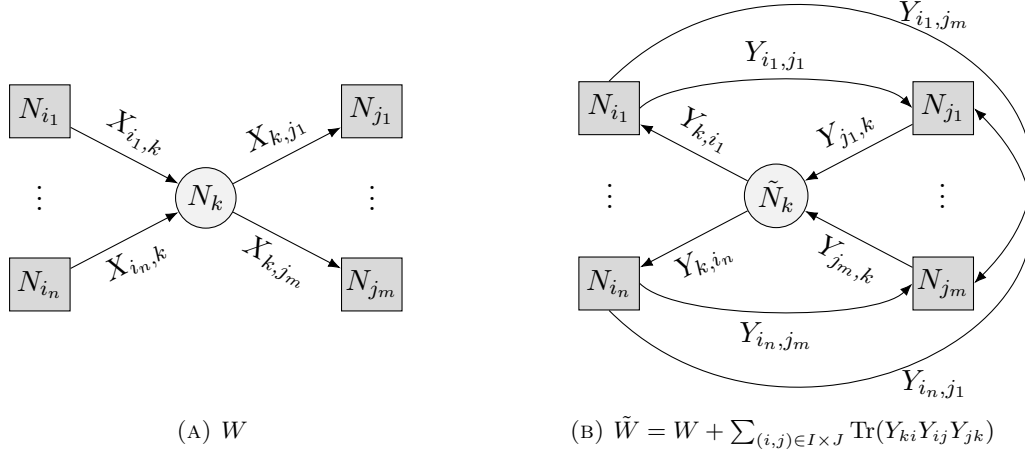
Seiberg duality represents an infrared equivalence between two different supersymmetric QCD theories at UV scales. Under a renormalization group, they flow to the same IR fixed point. Specifically, all low-energy features such as moduli space, chiral ring, global symmetries, 't Hooft anomalies, etc., are consistent across Seiberg dual theories.

The quintessential case of Seiberg duality is observed in the $\mathcal{N} = 1$ $SU(N_c)$ gauge theory [48], which features N_f fundamental/anti-fundamental multiplets Q_a^i, \tilde{Q}_i^a of flavors $SU(N_f)_L \times SU(N_f)_R$ and no superpotential $W = 0$. Note $a \in \{1, \dots, N_c\}$ represent the electric color indices, whereas $i, \tilde{i} \in \{1, \dots, N_f\}$ are the fundamental/antifundamental representation flavor indices. These are also charged by a baryonic and a $U(1)_R$ R-charge. The magnetic dual description in terms of a $SU(\tilde{N}_c)$ gauge theory with N_f flavors of dual quarks $q_{\tilde{a}}^i$ and antiquarks $\tilde{q}_{\tilde{i}}^{\tilde{a}}$, where $\tilde{a} \in \{1, \dots, \tilde{N}_c\}$ represent the magnetic (or dual) color indices. Additionally, we have a set of $SU(\tilde{N}_c)$ singlet ‘‘mesons’’ $M_{\tilde{i}}^i$ that transform as bifundamentals under the flavor symmetry, which couple to the dual quarks in superpotential $W = \text{Tr}(qM\tilde{q})$.⁶ See fig. 6.6 for a description of the duality, using quivers. The duality In the conformal window, $3N_c/2 \leq N_f \leq 3N_c$, Seiberg demonstrated that these two UV theories flow to the same interacting infrared fixed point, provided that

$$\tilde{N}_c = N_f - N_c , \quad M_{\tilde{i}}^i = Q_a^i \tilde{Q}_{\tilde{i}}^a . \quad (6.24)$$

It can be shown that the choice above for the Seiberg ‘‘mesons’’ is precisely what is needed for both chiral rings to match. This duality implies that the two seemingly different gauge

⁶Trace is taken to be over color indices, implicitly assuming contraction over flavor indices.

FIGURE 6.6: Original Seiberg duality of a $\mathcal{N} = 1$ SQCD $SU(N_c)$ gauge field theory.FIGURE 6.7: Seiberg duality of a $\mathcal{N} = 1$ quiver gauge theory, with $G = \prod_{i=1}^g SU(N_i)$. The mutated node has $\tilde{N}_k = \sum_{i \neq k} N_i a_{ik} - N_k = \sum_{j \neq k} a_{kj} N_j - N_k$.

theories describe the same physics in the infrared limit, with matching moduli spaces, chiral rings, and global symmetries and anomalies.

The Seiberg duality in the context of quiver gauge theories [26, 49, 50, 52] is generalized to the mathematical concept of quiver mutation. Given a quiver and superpotential (\mathcal{Q}, W) with gauge group $G = \prod_{i=1}^g SU(N_i)$, we can pick any “color” node $N_c = N_k$, $1 \leq k \leq g$, and perform a mutation in order to obtain a dual theory. By fixing a node $k \in \mathcal{Q}_0$, we will have a set of “incoming” superfields $\{X_{ik}\}_{i \in I}$, and “outgoing” superfields $\{X_{kj}\}_{j \in J}$, connecting the node being mutated with the “flavor” nodes $I, J \subset \mathcal{Q}_0$. In this case, we need to sum all contributions of the incoming/outgoing charges in

$$N_f = \sum_{i \in I} N_i a_{ik} = \sum_{j \in J} a_{kj} N_j, \quad (6.25)$$

where $a_{ij} = |\{i \rightarrow j \in \mathcal{Q}_1\}|$ is the adjacency matrix of the quiver \mathcal{Q} . Note that the second equality is a consequence of gauge anomaly cancellation. Under Seiberg duality, the mutated quiver \mathcal{Q}' reverses the original incoming/outgoing arrows, introducing new chiral fields $\{Y_{ki}\}_{i \in I}$, $\{Y_{jk}\}_{j \in J}$. Furthermore, for each pair of incoming and outgoing nodes we add

a Seiberg meson to the superpotential

$$W' = W(X) + \sum_{(i,j) \in I \times J} \text{Tr}(Y_{ki}Y_{ij}Y_{jk}), \quad \text{where} \quad X_{ik}X_{kj} = Y_{ij} \quad \forall (i,j) \in I \times J. \quad (6.26)$$

It is important to note that, in the mutated superpotential, composite chiral fields $X_{ik}X_{kj}$ are replaced by a new chiral Y_{ij} in the magnetic dual.

In order to guarantee that we have a brane tiling description before and after the mutation, we will require that all quiver nodes have the same rank, $N_i = N, \forall i \in \mathcal{Q}_0$. This requires that $\tilde{N}_k = N_k$, which reduces to the case where we have exactly incoming/outgoing bifundamentals, $\sum_{j \neq k} a_{kj} = \sum_{i \neq k} a_{ik} = 2$. After the mutation we obtain a node with rank

$$\tilde{N}_k = \sum_{i \neq k} N_i a_{ik} - N_k = \sum_{j \neq k} a_{kj} N_j - N_k, \quad (6.27)$$

which simplifies to $\tilde{N}_k = 2N - N = N$ in the referred case. From the perspective of brane tilings, this node is a square face and the mutation is precisely the transformation in fig. 3.2.

To describe an algorithm to find a family to toric phases for a given geometry, we can think of the toric-Seiberg duality as an involution acting on a dimer model. Note that applying the transformation shown in fig. 3.2 may unlock other “square faces” – after reducing the dimer, *i.e.*, integrating-in mass terms in the superpotential – on which we can continue to apply this operation. While this recursion might initially seem to lead to an infinite family of duals, when we consider models (\mathcal{Q}, W) up to *isomorphism*⁷ of the dimer models, we expect the tree of toric phases to close into a strongly connected graph. This procedure does not guarantee that all the toric phases of a given geometry are visited. Restricting to only toric-Seiberg duality means we are discarding mutations paths between toric phases, where at some point the ranks of the quiver nodes are no longer equal (we set $N_i = N = 1$ for simplicity).

Given these assumptions, the problem of finding all toric phases is equivalent to traversing a finite undirected graph. This type of problem is well-known and can be easily tackled by one of the classical graph traversal algorithms: depth-first search (DFS) [127] or breadth-first search (BFS) [128, 129]. As the names suggest, the first prioritizes depth by always selecting the first non-visited neighbor of the current node to be visited next, while the second traverses the graph nodes in increasing edge distance to the starting node. There are small caveats to using each approach, but in this case it is irrelevant, so we will describe in more detail the BFS version in algorithm 1. In this algorithm we assume that the reader has access to methods that can perform the toric duality or check for isomorphism of models (*e.g.*, `SeibergDual` and `DimerIsomorphic`, respectively), as these are heavily dependent on the choice of data representation of the dimer models.

⁷Dimer models $(\mathcal{Q}, W), (\mathcal{Q}', W')$ are isomorphic if we can find a graph isomorphism between $\mathcal{Q}, \mathcal{Q}'$ preserving/reversing the direction of all edges, and if W, W' match up to an overall sign under the edge this bijection. For *e.g.*, we can use `FindGraphIsomorphism` in Mathematica for the former step.

Algorithm 1 TORICSEIBERGDUALSGRAPH(\mathcal{Q}, W). Pseudocode describing the BFS algorithm to obtain a graph of toric duals for a given seed.

Input: Seed dimer model (\mathcal{Q}, W)

Output: Graph of toric dual phases \mathbf{G}

```

G ← Graph()                                ▷ Create a graph structure  $\mathbf{G} = (\mathbf{G}_0, \mathbf{G}_1)$ .
AddVertex(G, ( $\mathcal{Q}, W$ ))
bfs ← {}                                     ▷ Create a queue structure.
Enqueue(bfs, ( $\mathcal{Q}, W$ ))
while ¬Empty(bfs) do
  ( $\mathcal{Q}^{\text{cur}}, W^{\text{cur}}$ ) ← Dequeue(bfs)      ▷ Current phase being visited.
  for  $k \in \mathcal{Q}_0^{\text{cur}}$  do                       ▷ Check all nodes for square faces.
    if  $|\{k \rightarrow j \in \mathcal{Q}_1^{\text{cur}} \mid j \in \mathcal{Q}_0^{\text{cur}}\}| = |\{i \rightarrow k \in \mathcal{Q}_1^{\text{cur}} \mid i \in \mathcal{Q}_0^{\text{cur}}\}| = 2$  then
      ( $\mathcal{Q}^{\text{mut}}, W^{\text{mut}}$ ) ← SEIBERGDUAL( $(\mathcal{Q}^{\text{cur}}, W^{\text{cur}}), k, \{N_i = 1\}_{i \leq g}$ )
      visited ← False
      for  $(\mathcal{Q}', W') \in \mathbf{G}_0$  do
        if DimerIsomorphic( $(\mathcal{Q}', W'), (\mathcal{Q}^{\text{mut}}, W^{\text{mut}})$ ) then
          ( $\mathcal{Q}^{\text{mut}}, W^{\text{mut}}$ ) ←  $(\mathcal{Q}', W')$ 
          visited ← True
          break
        end if
      end for
      if ¬visited then
        Enqueue(bfs, ( $\mathcal{Q}^{\text{mut}}, W^{\text{mut}}$ ))
        AddVertex(G, ( $\mathcal{Q}^{\text{mut}}, W^{\text{mut}}$ ))
      end if
      AddEdge(G, ( $\mathcal{Q}^{\text{cur}}, W^{\text{cur}}$ ), ( $\mathcal{Q}^{\text{mut}}, W^{\text{mut}}$ ))
    end if
  end for
end while
return G

```

The rough description of the algorithm goes as follows:

- We start with a seed model (\mathcal{Q}, W) and initialize a queue data-structure (first in, first out) to store toric phases still to be visited and a some graph-like data-structure to store the found toric phases and connecting toric dualities.
- While we still have nodes to be visited (queue not empty) we will remove the next dimer model in the queue to be visited, $(\mathcal{Q}^{\text{cur}}, W^{\text{cur}})$. For each “square face” in the current dimer model being visited:
 1. Apply the toric-Seiberg duality as in figs. 3.2 and 6.7 and obtain a new toric phase $(\mathcal{Q}^{\text{mut}}, W^{\text{mut}})$.
 2. Check this new toric phase against all previously found phases in stored for other isomorphic phases. If an isomorphic phase is found, we will use that representative for $(\mathcal{Q}^{\text{mut}}, W^{\text{mut}})$ instead. Add an edge between the current toric phase being visited, and the toric phase obtained by the toric-Seiberg mutation.

$\mathbb{C}^3/\mathbb{Z}_6$ (1, 1, 4)	1	$L^{2,5,1}$	1	$K^{2,5,1,4}$	7
$\mathbb{C}^3/\mathbb{Z}_5$ (1, 2, 2)	1	$L^{5,6,1}$	1	$K^{2,5,1,3}$	12
$\mathbb{C}^3/\mathbb{Z}_8$ (1, 3, 4)	1	$L^{2,4,1}$	1	$K^{2,5,1,2}$	10
$\mathbb{C}^3/(\mathbb{Z}_2 \times \mathbb{Z}_5)$ (1, 0, 1)(0, 1, 4)	1	$L^{5,4,1}$	1	$K^{2,5,1,1}$	4
$\mathbb{C}^3/(\mathbb{Z}_2 \times \mathbb{Z}_6)$ (1, 0, 1)(1, 0, 5)	1	$L^{1,5,1}/\mathbb{Z}_2$ (1, 0, 0, 1)	2	$K^{4,4,2,3}$	25
$L^{3,3,1}$	1	SPP/\mathbb{Z}_3 (1, 0, 0, 2)	3	$K^{4,4,2,2}$	19
$L^{3,3,2}$	2	$\mathcal{C}/(\mathbb{Z}_3 \times \mathbb{Z}_2)$ (1, 0, 0, 2)(0, 1, 1, 0)	11	$K^{2,4,1,3}$	5
$Y^{3,0}$	2	$L^{4,3,2}$	2	$K^{2,4,1,2}$	7
$\text{SPP}/(\mathbb{Z}_2 \times \mathbb{Z}_2)$ (1, 0, 0, 1)(0, 1, 1, 0)	8	\mathcal{C}/\mathbb{Z}_4 (0, 1, 2, 1)	4	$K^{2,4,1,1}$	3
$L^{2,3,2}/\mathbb{Z}_2$ (1, 0, 0, 1)	6	$X^{3,2}$	3	$K^{4,3,2,2}$	9
dP_1/\mathbb{Z}_2 (1, 0, 0, 1)	3	$X^{3,1}$	5	PdP_{4e} (3)	13
$L^{1,4,1}/\mathbb{Z}_2$ (1, 0, 0, 1)	2	PdP_{4c} (2)	8	PdP_{5c} (3)	40
$\text{PdP}_2/\mathbb{Z}_2$ (1, 1, 1, 1)	3	PdP_{4d} (2)	8	PdP_{6b} (3)	23
$L^{1,3,1}/\mathbb{Z}_2$ (1, 0, 0, 1)	2	PdP_{5b} (2)	8	PdP_{4f} (2)	13
$L^{3,5,2}$	2	PdP_{6a} (2)	4	PdP_{6c} (3)	33

TABLE 6.1: Number of toric phases connected by toric-Seiberg dualities, for all the toric geometries from polytope with 2 internal points.

3. If $(Q^{\text{mut}}, W^{\text{mut}})$ dimer is yet to be visited, we added it to the queue.

- We will eventually visit all nodes and the queue will become empty. At this point we found all the graph of toric phases connected by toric dualities.

For example, in fig. 6.8 we can see how this algorithm explores the multiple phases of the $K^{4,3,2,2}$.

The procedure outlined above provides a robust method for exploring the toric phases of dimer models. However, it is unclear if all the toric phases are recovered, as we limited the Seiberg duality to nodes with 2 incoming/outgoing edges, which heavily constrains the “mutation paths” explored, keeping the graph of toric phases finite. Note that we can apply a mutation to any node in the quiver, and we might have a chain of node mutations where we eventually recover equal-ranks and a brane tiling description. In other words, we can have other connected components not reachable by toric dualities alone.

However, for the purposes of this work, the toric phases found via this method were sufficient to compare against the quiver gauge theories found via zig-zag deformations in the case of polytopes with 2 internal points. We can see that for these polytopes, the count of phases can be as high as 40, larger than the toric phases obtained in [124]. We present the toric phases in a supplementary file in github.com/jose-a-sa/zig-zag-deformation-data, fixing the labelling of the phases, as these are heavily used in the next sections.

6.2.1.2 Finding zig-zag deformations

In our examination of gauge theories derived from reflexive polytopes, after deforming the superpotential by $\delta W = \sum_{i \in I} \mathcal{O}_{\eta_i}$ the potential does not obey the cancellation property

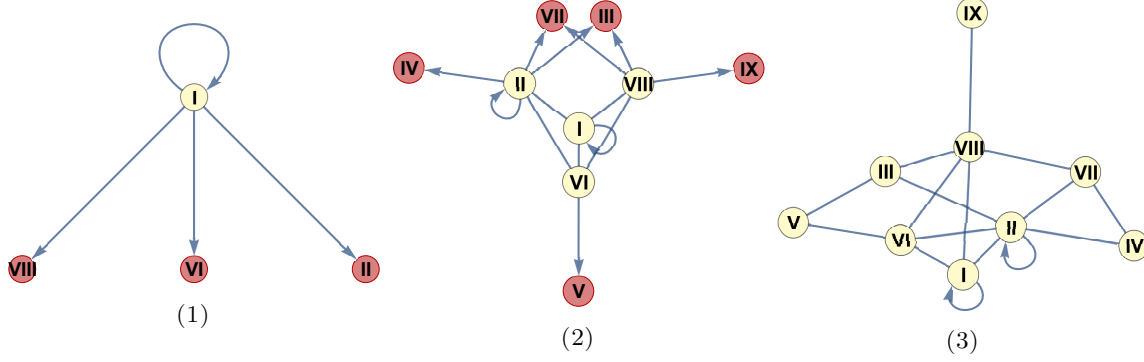


FIGURE 6.8: Steps in the BFS exploring the graph toric phases of $K^{4,3,2,2}$. Undirected edges correspond to a pair of directed edges in both directions. Highlighted nodes/phases in red have been found in a previous step but not yet *visited*.

required to be described as a dimer model. To show that such a flat family of deformations can degenerate into a toric IR fixed point (from the point of view of the 4d $\mathcal{N} = 1$ theory) we typically try to find a chiral field redefinition

$$X_{ij} = \alpha_{ij} \tilde{X}_{ij} + \sum_{l=1}^{n_{ij}} \beta_{ij}^{(l)} \tilde{X}_{il} \tilde{X}_{lj} , \quad (6.28)$$

where α_{ij} and β_{ilj} are specific constant coefficients with the obvious condition $\alpha_{ij} \neq 0$.⁸ The redefinition only allows terms that maintain gauge invariance, *i.e.* terms made of other paths such as $X_{il}X_{lj}$ in the quiver, starting and ending in the same nodes. By choosing the coefficients to scale inversely with the deformation parameter, $\alpha_{ij}, \beta_{ilj} = \pm \frac{1}{\mu}$, a valid redefinition leads to

$$W_{\text{def}}(X) = W(X) + \mu \delta W(X) = \frac{1}{\mu} W'(\tilde{X}) , \quad (6.29)$$

where W' is the IR model toric superpotential.

Given that we aim to map out the possible zig-zag deformation between theories generated from polytopes with 2 internal points with a much larger set of toric phases than in the reflexive case, we need to tackle this problem with computational aid. A few key insights are needed to do so. The main working assumption is that if the chiral multiplet X_{ij} needs to be redefined to restore toric symmetry, then the condition

$$\alpha_{ij} + \sum_{l=1}^{n_{ij}} \beta_{ij}^{(l)} = 0 \quad (6.30)$$

must be obeyed, as it is a necessary condition to obtain $\frac{\partial W'}{\partial \tilde{X}} \Big|_{\tilde{X}_{ij}=0} = 0$. However, the condition (6.30) itself is not sufficient to guarantee the toric F-term condition $\partial_{\tilde{X}} W' = F^+(\tilde{X}) - F^-(\tilde{X})$ is recovered. However, it will be relevant for the speeding up of the procedure.

⁸We omitted the case where quiver can have higher multiplicity for simplicity.

To understand how the process of finding the redefinition can be systematized, let's look at a particular example of a zig-zag deformation

$$\delta W = \mu (X_{12}X_{28}X_{81} - X_{57}X_{76}X_{65}) \quad (6.31)$$

of the dimer model $L^{3,5,2}$ in fig. 6.9 (toric phase I). Such a dimer model has quite a few

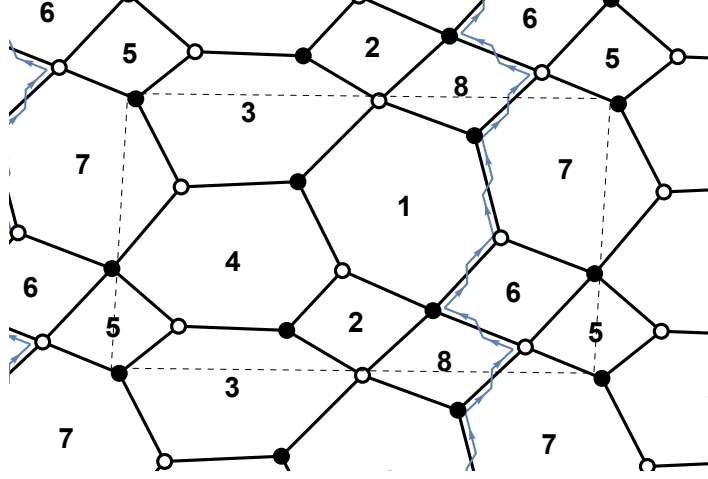


FIGURE 6.9: Brane tiling of generalized conifold $L^{3,5,2}$.

possible redefinitions of the form eq. (6.28), which can be read from the quiver/tiling:

$$\begin{aligned} X_{12} &= \alpha_{12} \tilde{X}_{12} + \beta_{12} \tilde{X}_{13} \tilde{X}_{32} & X_{47} &= \alpha_{47} \tilde{X}_{47} + \beta_{47} \tilde{X}_{41} \tilde{X}_{17} \\ X_{13} &= \alpha_{13} \tilde{X}_{13} + \beta_{13} \tilde{X}_{17} \tilde{X}_{73} & X_{57} &= \alpha_{57} \tilde{X}_{57} + \beta_{57} \tilde{X}_{54} \tilde{X}_{47} \\ X_{34} &= \alpha_{34} \tilde{X}_{34} + \beta_{34} \tilde{X}_{35} \tilde{X}_{54} + \gamma_{34} \tilde{X}_{32} \tilde{X}_{24} & X_{76} &= \alpha_{76} \tilde{X}_{76} + \beta_{76} \tilde{X}_{78} \tilde{X}_{86} \\ X_{43} &= \alpha_{43} \tilde{X}_{43} + \beta_{43} \tilde{X}_{47} \tilde{X}_{73} + \gamma_{43} \tilde{X}_{41} \tilde{X}_{13} & X_{81} &= \alpha_{81} \tilde{X}_{81} + \beta_{81} \tilde{X}_{86} \tilde{X}_{61} \end{aligned} \quad (6.32)$$

To find the parameters α_{ij} and β_{ij} , we note that each F-term of the rescaled μW_{def} must be composed of only two monomials in the chiral superfields and each monomial is free of μ . In the above example, we can look that the F-terms

$$\begin{aligned} \mu \frac{\partial W_{\text{def}}}{\partial \tilde{X}_{12}} &= (\mu^2 \alpha_{12} \beta_{81} - \mu \alpha_{12}) \tilde{X}_{28} \tilde{X}_{86} \tilde{X}_{61} + \mu^2 \alpha_{12} \alpha_{81} \tilde{X}_{28} \tilde{X}_{81} + \mu \alpha_{12} \tilde{X}_{24} \tilde{X}_{41} \\ \mu \frac{\partial W_{\text{def}}}{\partial \tilde{X}_{57}} &= (\mu \alpha_{57} - \mu^2 \alpha_{57} \beta_{76}) \tilde{X}_{78} \tilde{X}_{86} \tilde{X}_{65} - \mu^2 \alpha_{57} \alpha_{76} \tilde{X}_{76} \tilde{X}_{65} - \mu \alpha_{57} \tilde{X}_{73} \tilde{X}_{35} \\ \mu \frac{\partial W_{\text{def}}}{\partial \tilde{X}_{43}} &= \mu \alpha_{43} \tilde{X}_{35} \tilde{X}_{54} - \mu \alpha_{43} \tilde{X}_{32} \tilde{X}_{24} \end{aligned} \quad (6.33)$$

and apply a dimensional analysis argument with respect to μ . The presence of the terms $\mu^2 \alpha_{12} \alpha_{81}$, $\mu \alpha_{12}$, $\mu^2 \alpha_{57} \alpha_{76}$, $\mu \alpha_{57}$, $\mu \alpha_{43}$ tells us that the fields X_{12} , X_{81} , X_{57} , X_{76} , X_{43} must be redefined non-trivially. In other words, we must have

$$\alpha_{ij} = \zeta_{ij} \frac{1}{\mu}, \quad \zeta_{ij} = \pm 1 \quad \text{for} \quad \alpha_{ij} \in \{\alpha_{12}, \alpha_{81}, \alpha_{57}, \alpha_{76}, \alpha_{43}\}, \quad (6.34)$$

in order to cancel the μ and μ^2 terms, as α_{ij} cannot vanish. Then we can use the condition (6.30) to eliminate $\beta_{ij}^{(1)}$, for example, which greatly simplifies the F-terms. On the other hand, we can use the same argument to set $\beta_{13} = \beta_{47} = 0$ as the F-terms

$$\begin{aligned}\mu \frac{\partial W_{\text{def}}}{\partial \tilde{X}_{81}} &= (\alpha_{13}\zeta_{81} - \zeta_{12}\zeta_{81})\tilde{X}_{13}\tilde{X}_{32}\tilde{X}_{28} + \zeta_{81}\beta_{13}\tilde{X}_{17}\tilde{X}_{73}\tilde{X}_{32}\tilde{X}_{28} + \zeta_{12}\zeta_{81}\tilde{X}_{12}\tilde{X}_{28} - \zeta_{81}\tilde{X}_{17}\tilde{X}_{78} \\ \mu \frac{\partial W_{\text{def}}}{\partial \tilde{X}_{76}} &= (\zeta_{57}\zeta_{76} - \alpha_{47}\zeta_{76})\tilde{X}_{65}\tilde{X}_{54}\tilde{X}_{47} - \beta_{47}\zeta_{76}\tilde{X}_{65}\tilde{X}_{54}\tilde{X}_{41}\tilde{X}_{17} + \zeta_{76}\tilde{X}_{61}\tilde{X}_{17} - \zeta_{57}\zeta_{76}\tilde{X}_{65}\tilde{X}_{57}\end{aligned}\quad (6.35)$$

do not depend on μ and, consequently, implies the chiral fields X_{13} , X_{13} transform trivially ($\alpha_{13} = \alpha_{47} = 1$). In this example, we are still missing if X_{43} transforms trivially or non-trivially, but after the above results, the F-term

$$\mu \frac{\partial W_{\text{def}}}{\partial \tilde{X}_{34}} = \mu\alpha_{34}\tilde{X}_{47}\tilde{X}_{73} - \mu\alpha_{34}\tilde{X}_{41}\tilde{X}_{13} \quad (6.36)$$

implies that X_{43} redefinition is the same as in (6.34). It seems we applied a rescaling of the coefficients α_{ij} , $\beta_{ij}^{(l)}$ and that we are nowhere near finding the field redefinition. However, at this point, we already completed the task of finding which fields X_{ij} are non-trivially shifted. We still have F-terms not in bi-monomial form, *e.g.*,

$$\begin{aligned}\mu \frac{\partial W_{\text{def}}}{\partial \tilde{X}_{12}} &= \zeta_{12}\tilde{X}_{24}\tilde{X}_{41} + \zeta_{81}\zeta_{12}\tilde{X}_{28}\tilde{X}_{81} - \zeta_{12}(\zeta_{81} + 1)\tilde{X}_{28}\tilde{X}_{61}\tilde{X}_{86} \\ \mu \frac{\partial W_{\text{def}}}{\partial \tilde{X}_{17}} &= \zeta_{76}\tilde{X}_{61}\tilde{X}_{76} - \zeta_{81}\tilde{X}_{78}\tilde{X}_{81} + (\zeta_{81} - \zeta_{76})\tilde{X}_{61}\tilde{X}_{78}\tilde{X}_{86} \\ \mu \frac{\partial W_{\text{def}}}{\partial \tilde{X}_{76}} &= \zeta_{76}\tilde{X}_{17}\tilde{X}_{61} - \zeta_{57}\zeta_{76}\tilde{X}_{57}\tilde{X}_{65} + \zeta_{76}(\zeta_{57} - 1)\tilde{X}_{47}\tilde{X}_{54}\tilde{X}_{65} \\ \mu \frac{\partial W_{\text{def}}}{\partial \tilde{X}_{35}} &= \zeta_{43}\tilde{X}_{54}\tilde{X}_{43} - \zeta_{57}\tilde{X}_{57}\tilde{X}_{73} + [\mu(\beta_{34} + \beta_{43}) + \zeta_{57}]\tilde{X}_{54}\tilde{X}_{47}\tilde{X}_{73} \\ &\quad - [\mu(\beta_{34} + \beta_{43}) + \zeta_{43}]\tilde{X}_{54}\tilde{X}_{41}\tilde{X}_{13}\end{aligned}\quad (6.37)$$

for which we need to solve the combinatorial problem of finding the signs ζ_{ij} and possible linear relations between the $\beta_{ij}^{(l)}$ if a parametrized family of redefinitions is allowed. By looking at the coefficients of the chiral field products, we note that some terms must vanish, since the first 2 terms do not vanish under the assumption that $\zeta_{ij} = \pm 1$. For this reason, we are required to have $\zeta_{81} = \zeta_{76} = -1$, $\zeta_{43} = \zeta_{57} = 1$, and $\beta_{43} = -\frac{1}{\mu} - \beta_{34}$. Thus, we can gather these results to write the field redefinition that recovers the cancellation property of the deformed superpotential,

$$\begin{aligned}X_{12} &= \frac{1}{\mu}\tilde{X}_{12} - \frac{1}{\mu}\tilde{X}_{13}\tilde{X}_{32} & X_{57} &= \frac{1}{\mu}\tilde{X}_{57} - \frac{1}{\mu}\tilde{X}_{54}\tilde{X}_{47} \\ X_{34} &= \frac{1}{\mu}\tilde{X}_{34} - \left(\frac{1}{\mu} + \beta_{34}\right)\tilde{X}_{24}\tilde{X}_{32} + \beta_{34}\tilde{X}_{35}\tilde{X}_{54} & X_{76} &= -\frac{1}{\mu}\tilde{X}_{76} + \frac{1}{\mu}\tilde{X}_{78}\tilde{X}_{86} \\ X_{43} &= \frac{1}{\mu}\tilde{X}_{43} - \left(\frac{1}{\mu} + \beta_{34}\right)\tilde{X}_{47}\tilde{X}_{73} + \beta_{34}\tilde{X}_{13}\tilde{X}_{41} & X_{81} &= -\frac{1}{\mu}\tilde{X}_{81} + \frac{1}{\mu}\tilde{X}_{86}\tilde{X}_{61}\end{aligned}\quad (6.38)$$

where the parameter $\beta_{34} \in \mathbb{C}$ is free. For this deformation, the tiling describing the toric IR endpoint is given in fig. 6.10, where we observe the expected reversal of the zig-zag path, as described in section 4.3.

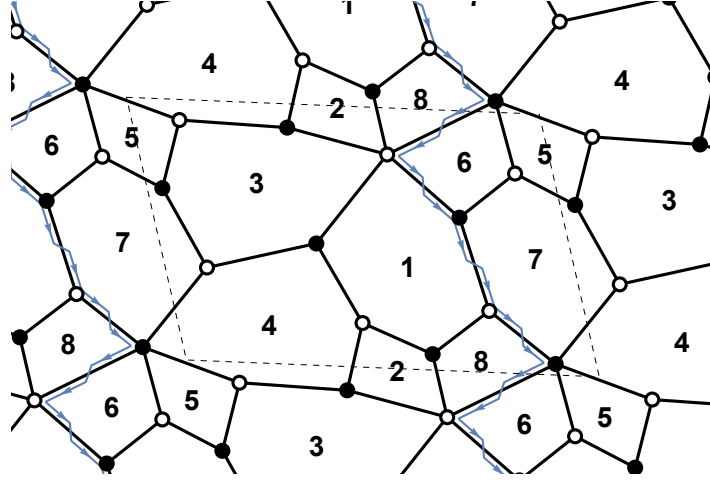


FIGURE 6.10: Brane tiling of model $K^{2,4,1,2}$.

We need to repeat this process multiple times for multiple toric phases, which may have more than one possible zig-zag deformation leading to another toric phase. As seen above, the process is fairly algorithmic and can be implemented in a couple of steps:

1. Apply the redefinition of the form (6.28) from the model quiver \mathcal{Q} . For any field X_{ij} , this involves finding all length 2 paths in \mathcal{Q} between nodes i and j . It turns out that higher length terms are not needed.
2. Compute the F-terms of W_{def} , collected in terms of unique monomials

$$\mu \frac{\partial W_{\text{def}}}{\partial X_{ij}} = \sum_{\substack{p=E_1 \cdots E_n \\ t(E_1)=j \\ h(E_n)=i}} f_{ji}^p X_{E_1} \cdots X_{E_n}. \quad (6.39)$$

In this step we apply the dimensional argument with respect to μ . While there is dependence on the coefficients α_{ij} , we repeatedly separate non-trivially/trivially redefined fields as:

- For every F-term monomial coefficient of the form $|f_{ab}^p| = |\mu|^n \prod_{k=1}^n |\alpha_{i_k, j_k}|$, we add the fields $\{X_{i_k, j_k}\}_k$ to the group of non-trivially redefined and set

$$\alpha_{i_k, j_k} = \zeta_{i_k, j_k} \frac{1}{\mu}, \quad \beta_{i_k, j_k}^{(1)} = -\zeta_{i_k, j_k} \frac{1}{\mu} - \sum_{l=2}^{n_{i_k, j_k}} \beta_{i_k, j_k}^{(l)} \quad (6.40)$$

- For every monomial coefficient $|f_{ab}^p| = \prod_{k=1}^n |x_{i_k, j_k}|$, where $x \in \{\alpha, \beta^{(l)}\}$, i.e., if f_{ab}^p is a product free of μ , we add the $\{X_{i_k, j_k}\}_k$ to the group of trivially redefined bifundamentals. We set $\alpha_{i_k, j_k} = 1$ and $\beta_{i_k, j_k}^{(l)} = 0$ in this case.

- Simplify the F-terms and repeat the process.
3. At this point, we have determined the redefined chirals, as well as some simplifying many coefficients to $|f_{ab}^p| = 1$. We use the fact that terms $|f_{ab}^p| \propto |\zeta_{i_k, j_k} \pm 1|$ must vanish (they are never = 1) to fix signs ζ_{i_k, j_k} .
 4. If a family of field redefinitions is allowed (f_{ab}^p still depends on redefinition coefficients), we can reduce the linear dependent of $\beta_{i_k, j_k}^{(l)}$ by solving

$$\sum_{\substack{p=E_1 \cdots E_n \\ t(E_1)=j \\ h(E_n)=i}} |f_{ji}^p| = 2 \quad , \quad \sum_{\substack{p=E_1 \cdots E_n \\ t(E_1)=j \\ h(E_n)=i}} f_{ji}^p = 0 . \quad (6.41)$$

These will be much simpler equations due to the previous steps.

6.2.2 Non-orbifold example: zig-zag deformations of $L^{5,4,1}$

In this section, we will study use the model $L^{5,4,1}$ as a starting point to a rich amount of zig-zag deformations. The 4d $\mathcal{N} = 1$ quiver gauge theory has a superpotential

$$\begin{aligned} W_{L^{5,4,1}} = & X_{12}X_{23}X_{31} + X_{14}X_{42}X_{21} + X_{1,10}X_{10,11}X_{11,1} + X_{2,11}X_{11,10}X_{10,2} \\ & + X_{35}X_{57}X_{73} + X_{67}X_{79}X_{96} + X_{68}X_{87}X_{76} + X_{89}X_{9,10}X_{10,8} \\ & + X_{8,11}X_{11,9}X_{98} + X_{36}X_{65}X_{54}X_{43} - X_{12}X_{2,11}X_{11,1} - X_{14}X_{43}X_{31} \\ & - X_{1,10}X_{10,2}X_{21} - X_{36}X_{67}X_{73} - X_{57}X_{76}X_{65} - X_{68}X_{89}X_{96} \\ & - X_{79}X_{98}X_{87} - X_{8,11}X_{11,10}X_{10,8} - X_{9,10}X_{10,11}X_{11,9} - X_{23}X_{35}X_{54}X_{42} \end{aligned} \quad (6.42)$$

which can more simply be encoded in the brane tiling in fig. 6.11.

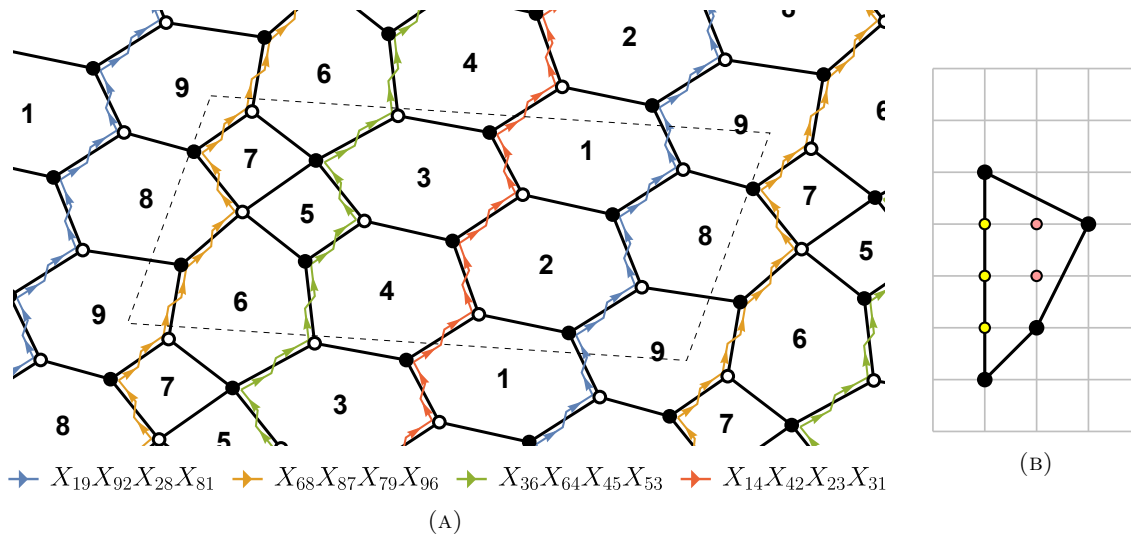


FIGURE 6.11: Brane tiling (a) and toric diagram (b) of the single toric phase of $L^{5,4,1}$

This geometry has an A_3 non-isolated singularity and a single toric phase, which allows us to showcase the multiple zig-zag deformations. From the toric diagram, we can obtain the lattice of generators, from which we can find all the relations in the mesonic ideal. In the reflexive case, the toric diagram and polar dual both sit at height 1 in a 3-dimensional lattice. In the case of 2 internal points, we need to look at the generators of the polytope

$$P_{-2K_X} = \{m \in \mathbb{R}^2 \mid \langle m, u_\rho \rangle + 2 \geq 0, \rho \in \Sigma(\Delta)\} \quad (6.43)$$

to obtain the Hilbert basis of the dual cone $(\sigma_\Delta)^\vee = \text{Cone}((v, 1) \mid v \in \Delta)^\vee$. For the model $L^{5,4,1}$, the Hilbert basis is presented in fig. 6.12.

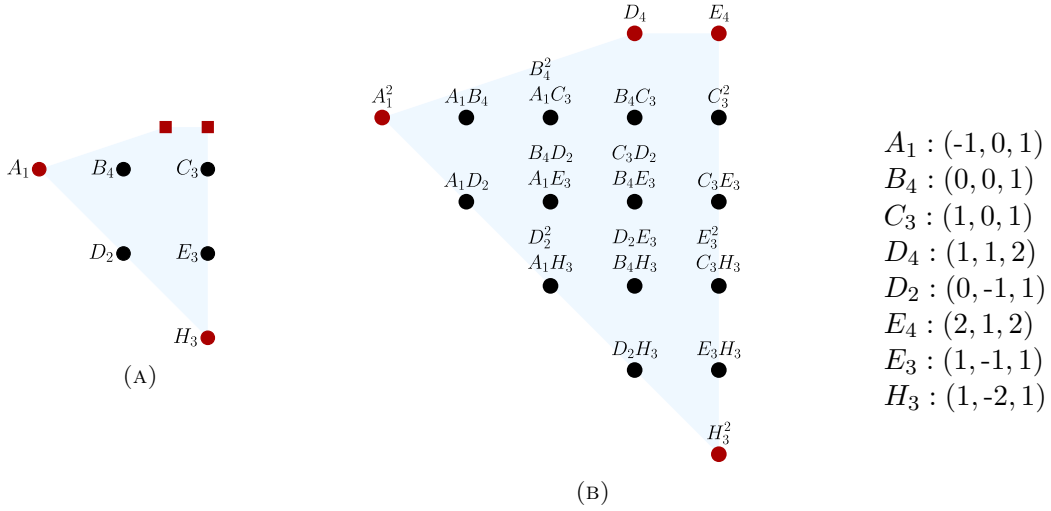


FIGURE 6.12: Lattice of generators of $L^{5,4,1}$, at height 1 in (a) and height 2 in (b). Some points in (b) represent relations in the mesonic ideal. The labelled triplets represent the points in the 3d lattice, as well as the $U(1)^3$ consistent charges of the mesonic global symmetry.

Linear relations between the lattice generators translate to multiplicative relations between the mesonic ideal generators. Some relations can be found at height 2, if the lattice point is a positive linear combination of more than a pair of generators from height 1. At height 3, we can find all necessary relations that generate the chiral ring

$$\begin{aligned} I_{\text{mes}} = \langle & E_3^2 - C_3 H_3, E_3 D_4 - E_4 D_2, E_3 D_2 - B_4 H_3, C_3 D_4 - E_4 B_4, B_4 D_4 - E_4 B_1, \\ & D_2^2 - B_1 H_3, C_3 D_2 - E_3 B_4, B_4 D_2 - E_3 B_1, B_4^2 - B_1 C_3, E_3 C_3^2 - E_4 H_3, \\ & E_3 B_4 C_3 - D_4 H_3, C_3^3 - E_3 E_4, B_4 C_3^2 - E_4 D_2, B_1 C_3^2 - D_2 D_4 \rangle \end{aligned} \quad (6.44)$$

The full mesonic moduli of for the brane tiling model associated to $L^{5,4,1}$ contains an extra component describing moduli of $\mathcal{N} = 2$ fractional branes probing the locus of the non-isolated A_3 singularity. This branch is parametrized by the generators,

$$A_1 = X_{89} X_{98}, \quad A_2 = X_{34} X_{43}, \quad A_3 = X_{12} X_{21}, \quad B_1 = X_{56} X_{67} X_{75}, \quad (6.45)$$

which intersects the geometric ideal (6.44) at the non-isolated singularity, defined by $B_1 = A_3 = A_2 = A_1$. Associated to this A_3 singularity are the four zig-zag paths

$$\begin{aligned} \eta_4 &= X_{19}X_{92}X_{28}X_{81}, & \eta_5 &= X_{68}X_{87}X_{79}X_{96}, \\ \eta_6 &= X_{36}X_{64}X_{45}X_{53}, & \eta_7 &= X_{14}X_{42}X_{23}X_{31}, \end{aligned} \quad (6.46)$$

defining relevant zig-zag operators 6.2 with conformal R-charge $R_{\text{sc}}[\mathcal{O}_{\eta_{4,5,6,7}}] = 1.3759\dots$, obtained via a-maximization. As we have seen before, we can trigger a RG flow either by including a single zig-zag operator \mathcal{O}_{η_i} or a combination of two zig-zag operator $\mathcal{O}_{\eta_i} + \mathcal{O}_{\eta_j}$. For a one-parameter deformation of $L^{5,4,1}$ we do not need to include more combinations of \mathcal{O}_{η_i} . Furthermore, we can use the fact that the sum

$$\mathcal{O}_{\eta_4} + \mathcal{O}_{\eta_5} + \mathcal{O}_{\eta_6} + \mathcal{O}_{\eta_7} \simeq 0 \quad (= 0) \quad (6.47)$$

is by default trivial in the chiral ring, allowing us to halve the combinations of operators \mathcal{O}_{η_i} .

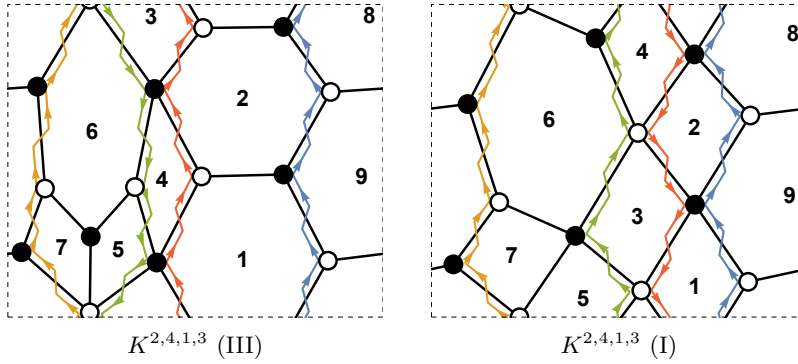


FIGURE 6.13: Toric phases of $K^{2,4,1,3}$ obtained from deforming $L^{5,4,1}$ by a single operator \mathcal{O}_{η_i} , as summarized in fig. 6.19. Dimer (III) is isomorphic to dimer (I) by mutating node 7.

Starting by analyzing the deformations of the form, $\delta W = \mu \mathcal{O}_{\eta_i}$ we can integrate out mass terms in the deformed potential and proceed with the algorithm procedure defined in section 6.2.1.2. In the dual (p, q) -web picture, this corresponds to reversing any one of the 4 external legs associated to the A_3 facet in the toric diagram. After the polytope mutation, we obtain the toric diagram of the affine cone $K^{2,4,1,3}$. This geometry contains 5 toric phases connected via a non-trivial graph to toric-Seiberg dualities. The deformations above can be further divided into two subgroups, depending on which toric phase the UV model flows to:

- $\delta W = \mu \mathcal{O}_{\eta_4}$ or $\mu \mathcal{O}_{\eta_7}$ flows to $K^{2,4,1,3}$ phase I,
- $\delta W = \mu \mathcal{O}_{\eta_5}$ or $\mu \mathcal{O}_{\eta_6}$ flows to $K^{2,4,1,3}$ phase III.

The remaining toric phases are not accessible by such deformation, but by toric duality. On the other hand, by reversing the 2 zig-zag paths the

- $\delta W = \mu (\mathcal{O}_{\eta_5} + \mathcal{O}_{\eta_6})$ flows to $K^{4,3,2,2}$ phase III,

- $\delta W = \mu (\mathcal{O}_{\eta_5} + \mathcal{O}_{\eta_7})$ flows to $K^{4,3,2,2}$ phase I,
- $\delta W = \mu (\mathcal{O}_{\eta_6} + \mathcal{O}_{\eta_7})$ flows to $K^{4,3,2,2}$ phase V.

The results of regarding this model can be summarized by the graph in fig. 6.15.

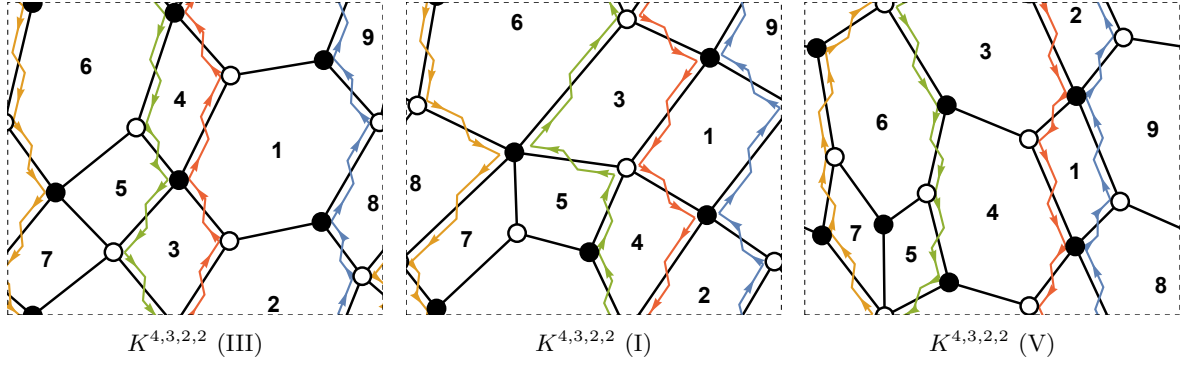


FIGURE 6.14: Toric phases of $K^{4,3,2,2}$ obtained from deforming $L^{5,4,1}$ by an operator $\mathcal{O}_{\eta_i} + \mathcal{O}_{\eta_j}$, as summarized in B.3.2. Dimers (III) and (V) are isomorphic by mutating node 5 or 7.

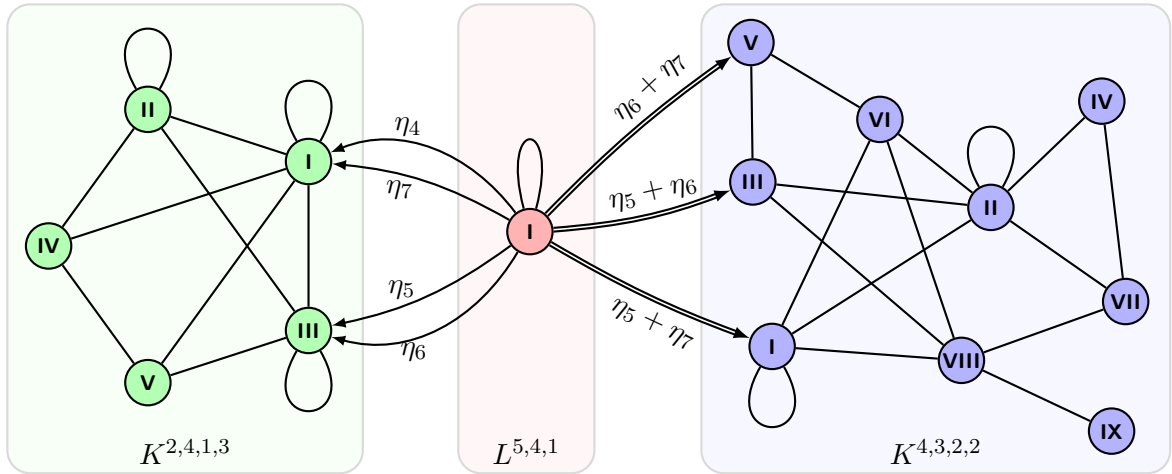


FIGURE 6.15: Graph of zig-zag deformations starting from $L^{5,4,1}$, as well as the graph of toric-Seiberg dualities of the involved models, showcasing flows between different toric phases depending on zig-zag paths triggering the deformation.

6.2.3 Summary of zig-zag deformations for 2 internal points

In this section we summarize all RG flows from toric gauge theories living in the world-volume of D3-branes probing a toric CY cone with a polytope with 2 internal points. Most of the cases were computed manually, with insights from the reflexive case, matching against the algorithmic approach described above. For sake of completeness, we include the all the case where $g = 6$, for completeness, while skipping the single orbifold with $g = 5$. These are all one parameter deformations where 1,2 and 3 combinations of zig-zag operators are presented in a single, double and triple arrows, respectively.

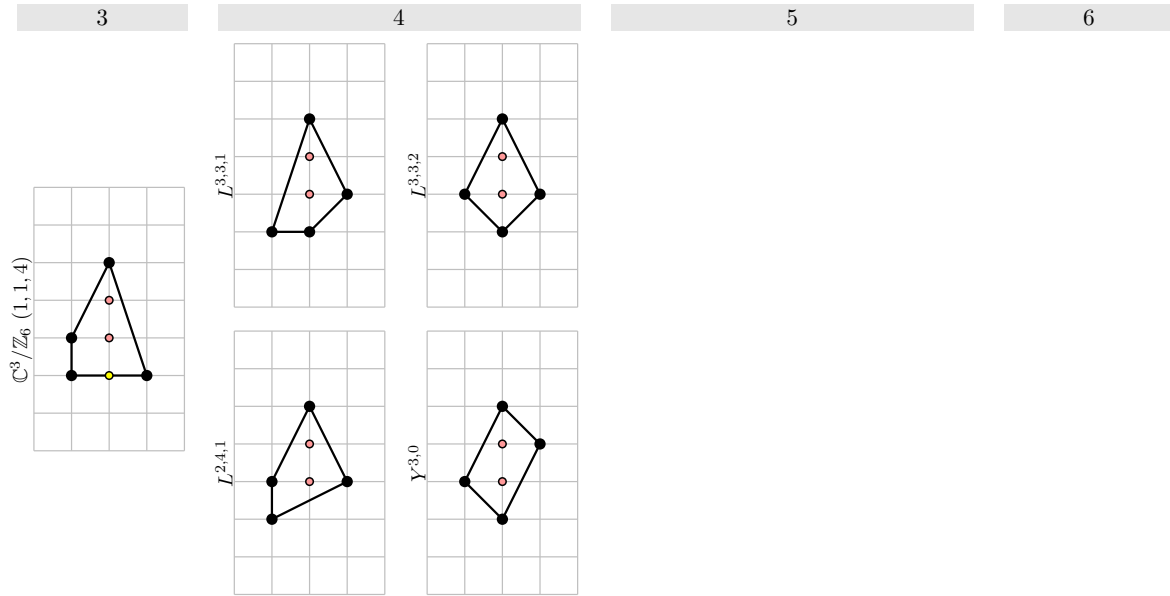


FIGURE 6.16: Zig-zag deformation between polytopes with $g = 6$.

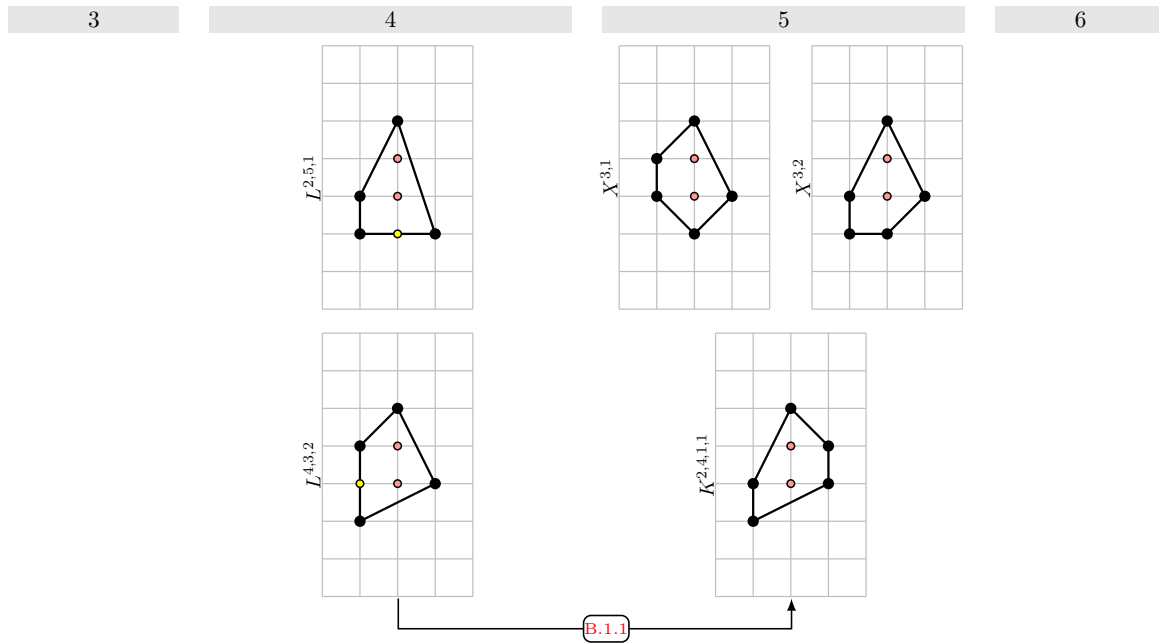


FIGURE 6.17: Zig-zag deformation between polytopes with $g = 7$.

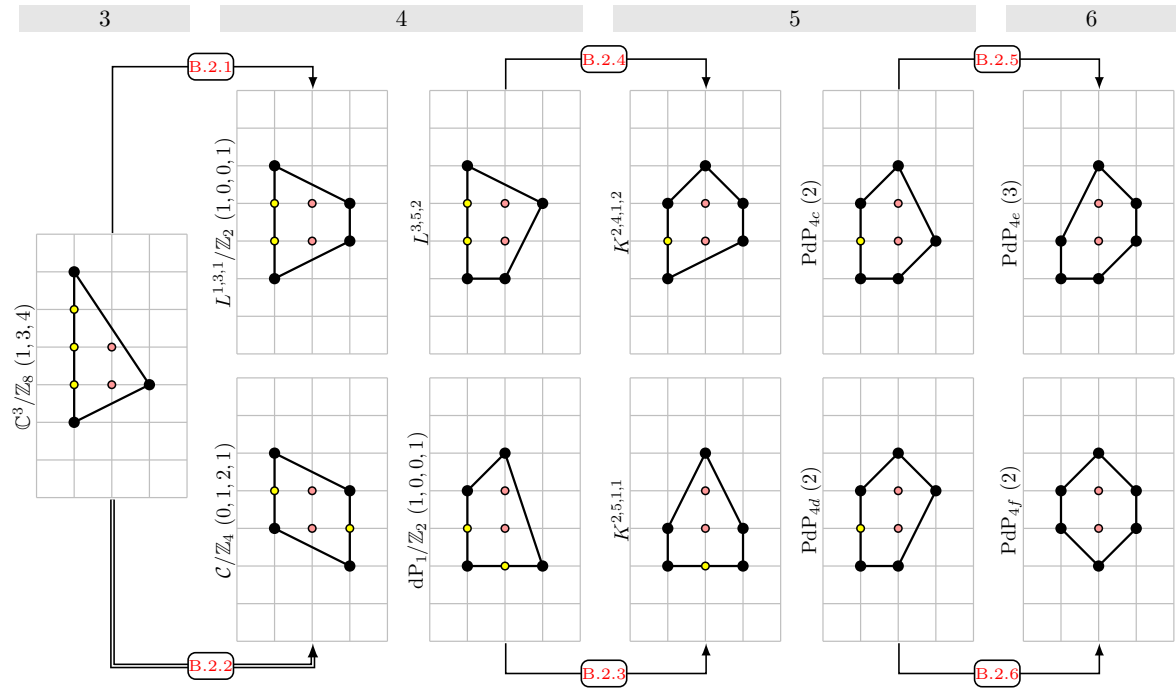


FIGURE 6.18: Zig-zag deformation between polytopes with $g = 8$.

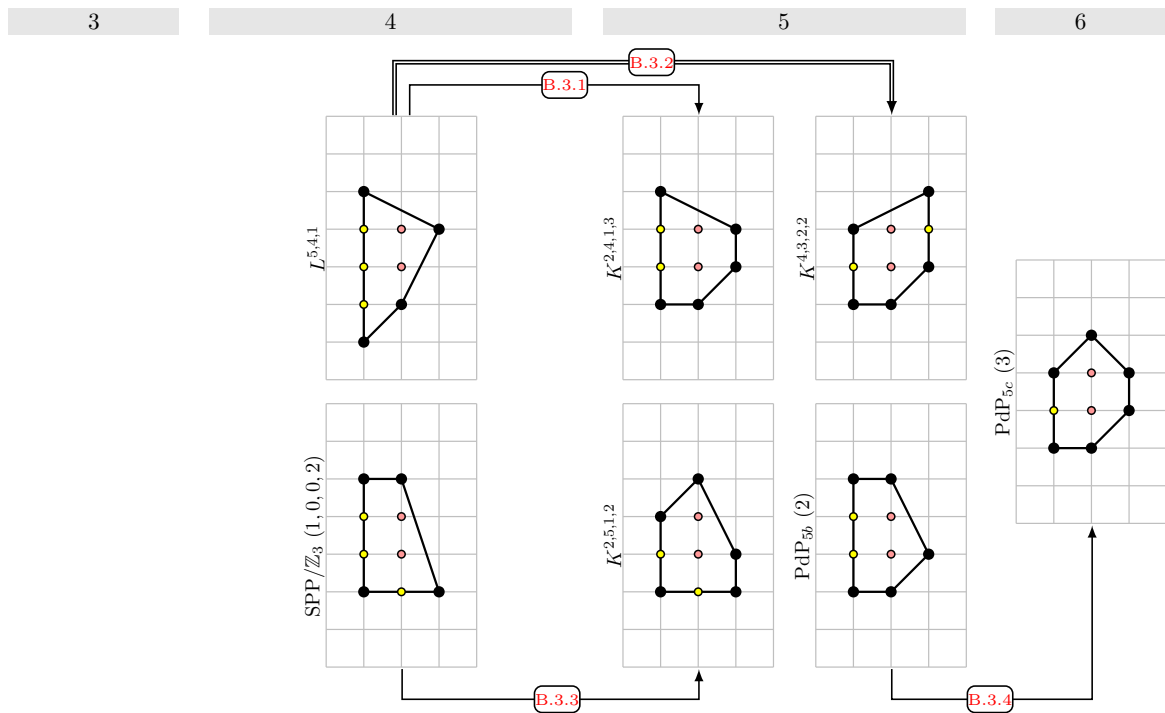


FIGURE 6.19: Zig-zag deformation between polytopes with $g = 9$.

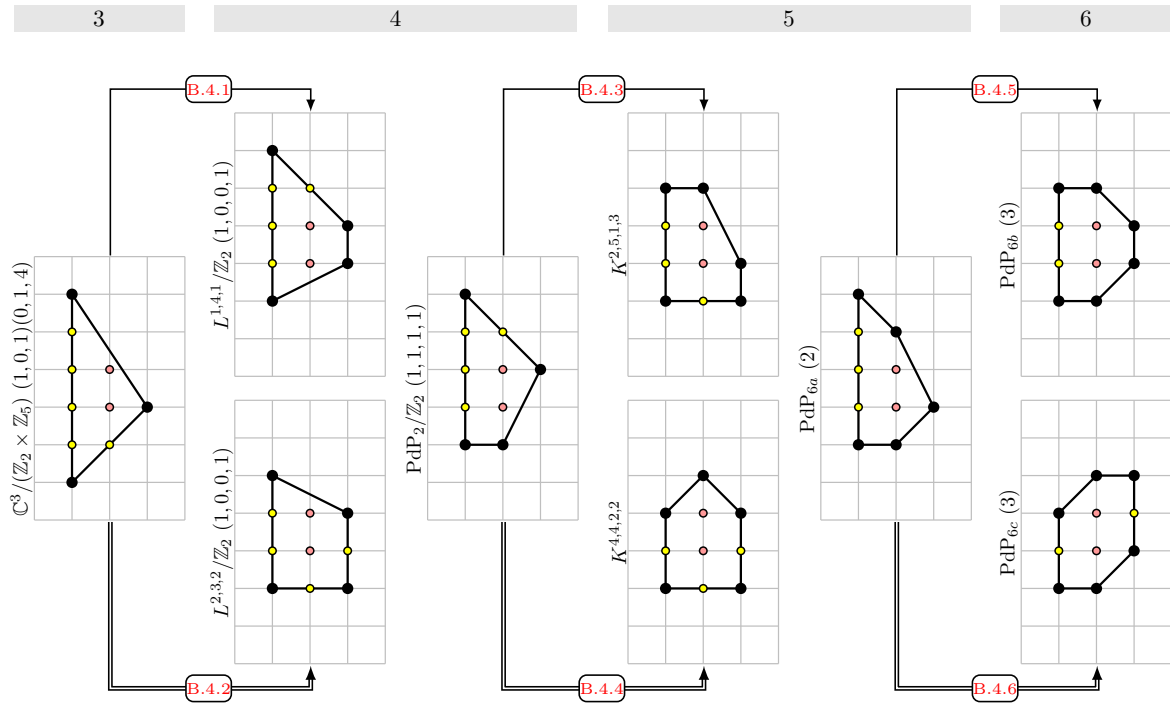


FIGURE 6.20: Zig-zag deformation between polytopes with $g = 10$.

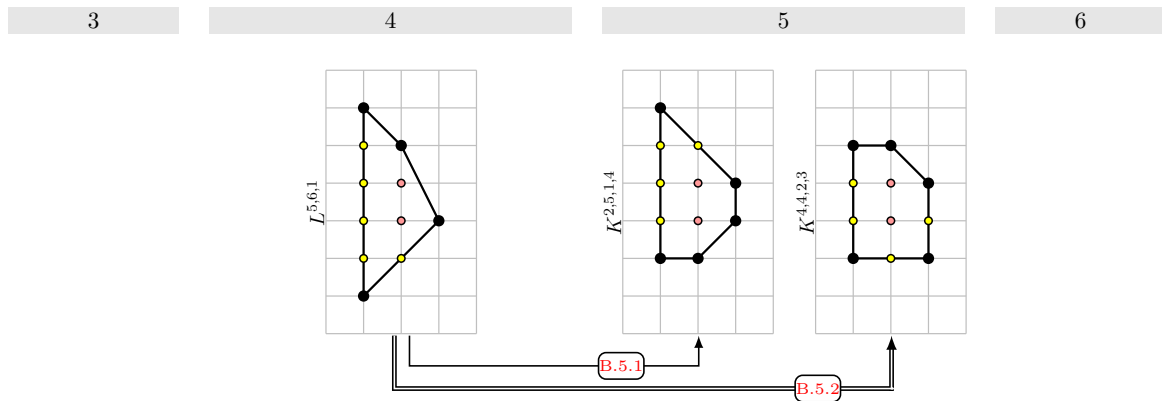


FIGURE 6.21: Zig-zag deformation between polytopes with $g = 11$.

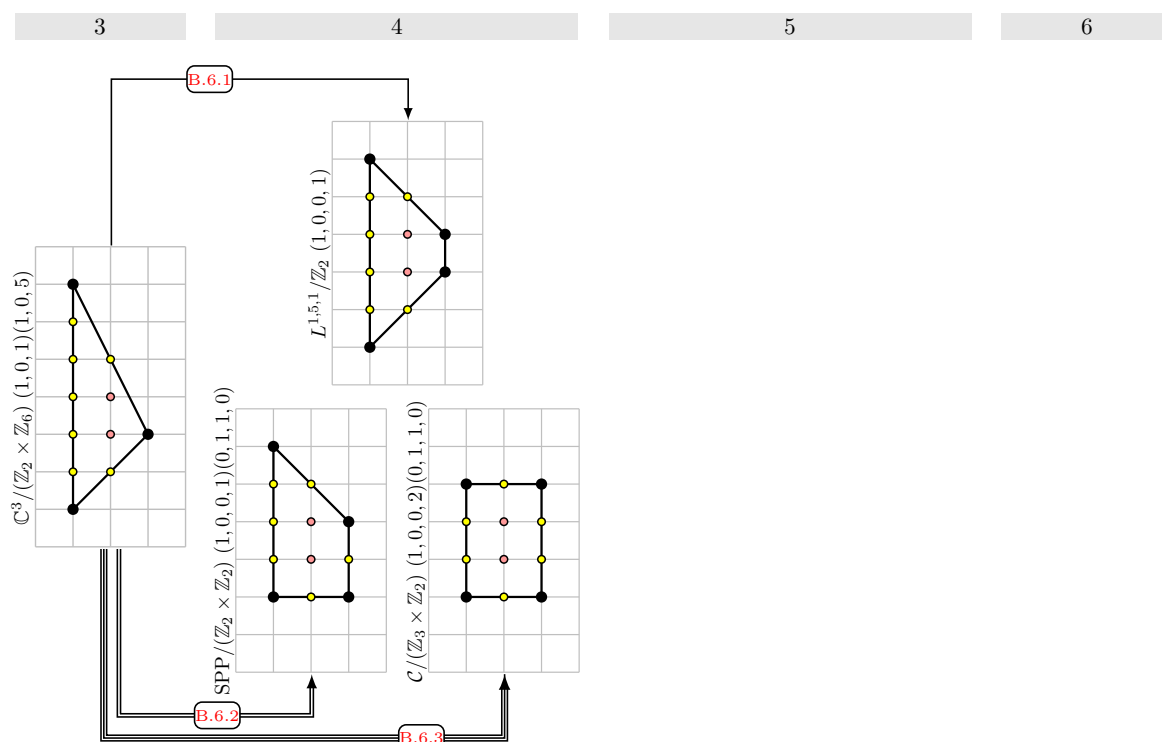


FIGURE 6.22: Zig-zag deformation between polytopes with $g = 12$.

Chapter 7

Discussion

In this work, we have investigated nontoric deformations of a specific type, focusing on the construction of one-parameter families of deformations of toric quiver gauge theories. These gauge theories arise in the worldvolume of D3-branes probing a toric Calabi-Yau 3-fold singularity. The deformations in question preserve a $U(1)^2$ symmetry within the $U(1)^3$ mesonic symmetry for generic values of the deformation parameter $\mu \in \mathbb{C} \cup \infty \cong \mathbb{P}^1$, and they interpolate between two distinct toric models at $\mu = 0$ and $\mu = \infty$, respectively.

To induce the deformation, we define a zig-zag operator completely specified by zig-zag path η in the brane tiling description. This path adheres to the edges of the tiling, making maximal turns left at white nodes and right at black nodes. The zig-zag path is associated with an outward-pointing normal vector to an edge of the toric diagram and corresponds to an external leg in the dual (p, q) -web. The operator represents the difference between two mesonic chiral operators, each associated with loops winding oppositely around the zig-zag path in the tiling.

This deformation is non-trivial in the chiral ring if, and only if, the chosen zig-zag path is parallel to other zig-zag paths in the tiling, indicating a type A_k non-isolated singularity in the geometry. In such cases, the mesonic operators involved in $\mathcal{O}_\eta = \mathcal{O}_\eta^L - \mathcal{O}_\eta^R$ parametrize $\mathcal{N} = 2$ Coulomb moduli of the undeformed toric quiver gauge theory, which are subsequently lifted by the deformation. Concurrently, the geometric branch of the abelian theory on the regular D-brane's worldvolume undergoes deformation, which partially or fully lifts the non-isolated singularity.

Our study further demonstrates that the deformed geometry leads to the emergence of another toric model as $\mu \rightarrow \infty$, characterized by a toric diagram that is a mutation of the original diagram at $\mu = 0$. Specifically, when the selected zig-zag operator has a length 4, the $\mu = \infty$ model can be described by a new brane tiling derived from the $\mu = 0$ model via an operation that reverses the direction of the chosen zig-zag. Furthermore, when examining all possible deformations of this type in gauge theories spanned from toric del Pezzo theories, we find this deformation induces a RG flow between 4d $\mathcal{N} = 1$ toric SCFTs, leading to an IR model with

fewer $\mathcal{N} = 2$ Coulomb moduli than the UV model and a geometry with reduced non-isolated singularity. This observation generalizes the findings of previous work on mass deformations.

Alternatively, the $\mu = \infty$ brane tiling can be obtained from the $\mu = 0$ tiling through a sequence of operations: applying specular duality, performing a toric-Seiberg duality on the face corresponding to the chosen zig-zag, and then applying specular duality once more. For large but finite μ , the resulting model is also deformed by a (potentially trivial) zig-zag deformation proportional to $\frac{1}{\mu}\mathcal{O}'_{\eta'}$, where η' represents the reversed zig-zag path. This process aligns with recent studies that relate mutations of generalized toric polytopes (GTPs) [123] to mutations of twin quivers [115, 130]. The results are consistent with our field theory analysis, where we introduce the zig-zag deformation, integrate out massive fields, and redefine the fields to recover the quiver and toric superpotential of a new toric model as $\mu \rightarrow \infty$.

For arbitrary resolution parameters, we confirm that the triangulated toric diagrams of the $\mu = 0$ and $\mu = \infty$ geometries are connected through a mutation of a triangulated polytope. This mutation is dual to reversing a fivebrane in the (p, q) -web by terminating it on a 7-brane, sliding the 7-brane along the fivebrane while accounting for Hanany-Witten transitions, and rotating the $\text{SL}(2, \mathbb{Z})$ monodromy cut until it vanishes in the limit. We have thoroughly tested this observation against field-theoretical predictions, including the superpotential, by matching the Kähler chambers of stable representations of the $\mu = 0$ and $\mu = \infty$ theories.

Finally, we introduce a generalized approach for obtaining the IR dimer model a set of zig-zag deformations and an algorithm that finds all toric(-Seiberg dual) phases given a seed brane tiling. We argue that as long as the zig-zag η is of length 4 and the toric diagram lattice size in the parallel direction w_η is 2, the zig-zag deformation still parametrizes a flat family of deformations to connect two toric endpoints. If these conditions hold, moving the associated $[p, q]$ D7-brane will precisely lead to one annihilation and one creation of the suspended 5-brane external leg via Hanany-Witten effect, as it crosses the single 4-cycle. The final (p, q) -web configuration is guaranteed to be dual to a toric diagram.

This observation allows us to go beyond the reflexive case. In particular, polytopes with 2 internal points contain relevant zig-zag operators of the satisfying the above conditions. We describe and apply a methodology that finds all $\mathcal{N} = 1$ field redefinition needed to be applied in the field theory context in order to obtain show the RG flow to an IR toric model. Furthermore, turning zig-zag deformations associated to the same A -type singularity often lead to different toric phases of the same $\mu = \infty$ geometry. As such, in order to more easily identify the IR model/phase, we successfully applied the BFS algorithm to explore toric phases strongly connected to a seed model via toric-Seiberg dualities.

Appendices

Appendix A

Details of deformations for reflexive polytopes

In this appendix we collect details of the zig-zag deformations of UV toric models and the field redefinitions needed to obtain new toric models in the IR. We describe the deformations δW of toric superpotentials by a (or multiple) relevant zig-zag operator \mathcal{O}_η , which flow into a toric model or a marginal deformation of one. We divide these into appendix [A.1](#) and appendix [A.2](#). Each subsection is titled “ \mathcal{X} to \mathcal{Y} ”. Furthermore, when different toric phases are involved these are also pointed out.

A.1 Deformations to toric models

The deformations listed here include only the relevant steps, which are fully described in section [4.3](#). In each subsection, describing the deformation between 2 specific geometries, we include the original starting superpotential W . Additionally, each deformation is in a unique equation block with:

1. The deformation $\delta W = \mu \sum_{i \in I} \mathcal{O}_{\eta_i}$, associated to one or more zig-zag paths η_i .
2. The non-trivial field redefinitions of the type in eq. [\(4.15\)](#), if any. Some redefinitions include free parameters $\beta_i \in \mathbb{C}$, which do not affect the final result.
3. The toric superpotential W' representing the IR theory.

The redefinition in item 2 is for the superpotential $W + \delta W$, after integrating out massive fields using the F-terms [\(4.13\)](#).

A.1.1 PdP₁, $\mathbb{C}^3/\mathbb{Z}_4(1, 1, 2)$ to $\mathbb{F}_0, \mathcal{C}/\mathbb{Z}_2(1, 1, 1, 1)$

$$\begin{aligned}
W &= X_{13}X_{34}^1X_{41}^2 + X_{24}X_{41}^1X_{12}^2 + X_{31}X_{12}^1X_{23}^2 + X_{42}X_{23}^1X_{34}^2 \\
&\quad - X_{13}X_{34}^2X_{41}^1 - X_{24}X_{41}^2X_{12}^1 - X_{31}X_{12}^2X_{23}^1 - X_{42}X_{23}^2X_{34}^1
\end{aligned} \tag{A.1}$$

$$\delta W = \mu(X_{13}X_{31} - X_{24}X_{42})$$

$$\begin{aligned}
W' &= X_{12}^1X_{23}^2X_{34}^2X_{41}^1 + X_{12}^2X_{23}^1X_{34}^1X_{41}^2 - X_{12}^1X_{23}^1X_{34}^2X_{41}^2 - X_{12}^2X_{23}^2X_{34}^1X_{41}^1 \\
&= -\epsilon_{ab}\epsilon_{cd}X_{12}^aX_{23}^bX_{34}^cX_{41}^d
\end{aligned} \tag{A.2}$$

A.1.2 PdP₂ to dP₂

$$\begin{aligned}
W &= X_{12}X_{25}^1X_{51}^2 + X_{14}X_{42}X_{21} + X_{53}X_{32}X_{25}^2 + X_{13}X_{34}X_{45}X_{51}^1 \\
&\quad - X_{12}X_{25}^2X_{51}^1 - X_{13}X_{32}X_{21} - X_{14}X_{45}X_{51}^2 - X_{34}X_{42}X_{25}^1X_{53}
\end{aligned} \tag{A.3}$$

$$\delta W = \mu(X_{12}X_{21} - X_{34}X_{45}X_{53})$$

$$X_{45} \mapsto +\frac{1}{\mu}X_{45} - \frac{1}{\mu}X_{42}X_{25}^1 \quad X_{53} \mapsto -\frac{1}{\mu}X_{53} + \frac{1}{\mu}X_{51}^1X_{13} \tag{A.4}$$

$$\begin{aligned}
W' &= X_{34}X_{45}X_{53} + X_{13}X_{32}X_{25}^1X_{51}^2 + X_{14}X_{42}X_{25}^2X_{51}^1 \\
&\quad - X_{14}X_{45}X_{51}^2 - X_{32}X_{25}^2X_{53} - X_{13}X_{34}X_{42}X_{25}^1X_{51}^1
\end{aligned}$$

A.1.3 PdP_{3a}, $\mathbb{C}^3/\mathbb{Z}_6(1, 2, 3)$ to PdP_{3c}, SPP/ $\mathbb{Z}_2(0, 1, 1, 1)$ **Phase A to Phase A**

$$\begin{aligned}
W &= X_{12}X_{26}X_{61} + X_{13}X_{35}X_{51} + X_{15}X_{54}X_{41} + X_{24}X_{43}X_{32} \\
&\quad + X_{25}X_{56}X_{62} + X_{34}X_{46}X_{63} - X_{12}X_{25}X_{51} - X_{13}X_{34}X_{41} \\
&\quad - X_{15}X_{56}X_{61} - X_{24}X_{46}X_{62} - X_{26}X_{63}X_{32} - X_{35}X_{54}X_{43}
\end{aligned} \tag{A.5}$$

$$\begin{aligned}
\delta W &= \mu (X_{15}X_{51} - X_{34}X_{43}) \\
X_{26} &\mapsto -\frac{1}{\mu}X_{26} + \left(\frac{1}{\mu} - \beta_1\right) X_{24}X_{46} + \beta_1 X_{25}X_{56} \\
X_{62} &\mapsto -\frac{1}{\mu}X_{62} + \left(\frac{1}{\mu} - \beta_1\right) X_{61}X_{12} + \beta_1 X_{63}X_{32}
\end{aligned} \tag{A.6}$$

$$\begin{aligned}
W' &= X_{24}X_{46}X_{62} + X_{26}X_{63}X_{32} + X_{12}X_{25}X_{54}X_{41} + X_{13}X_{35}X_{56}X_{61} \\
&\quad - X_{12}X_{26}X_{61} - X_{25}X_{56}X_{62} - X_{13}X_{32}X_{24}X_{41} - X_{35}X_{54}X_{46}X_{63}
\end{aligned}$$

$$\begin{aligned}
\delta W &= \mu (X_{26}X_{62} - X_{15}X_{51}) \\
X_{34} &\mapsto -\frac{1}{\mu}X_{34} + \left(\frac{1}{\mu} - \beta_1\right) X_{32}X_{24} + \beta_1 X_{35}X_{54} \\
X_{43} &\mapsto -\frac{1}{\mu}X_{43} + \left(\frac{1}{\mu} - \beta_1\right) X_{41}X_{14} + \beta_1 X_{46}X_{63}
\end{aligned} \tag{A.7}$$

$$\begin{aligned}
W' &= X_{13}X_{34}X_{41} + X_{35}X_{54}X_{43} + X_{12}X_{24}X_{46}X_{61} + X_{25}X_{56}X_{63}X_{32} \\
&\quad - X_{24}X_{43}X_{32} - X_{34}X_{46}X_{63} - X_{12}X_{25}X_{54}X_{41} - X_{13}X_{35}X_{56}X_{61}
\end{aligned}$$

A.1.4 PdP_{3c}, SPP/ \mathbb{Z}_2 (0, 1, 1, 1) to PdP_{3b}

Phase A to Phase A

$$\begin{aligned}
W &= X_{25}X_{56}X_{62} + X_{36}X_{65}X_{53} + X_{13}X_{34}X_{45}X_{51} + X_{16}X_{64}X_{42}X_{21} \\
&\quad - X_{16}X_{65}X_{51} - X_{45}X_{56}X_{64} - X_{13}X_{36}X_{62}X_{21} - X_{25}X_{53}X_{34}X_{42}
\end{aligned} \tag{A.8}$$

$$\begin{aligned}
\delta W &= \mu (X_{16}X_{62}X_{21} - X_{34}X_{45}X_{53}) \\
X_{16} &\mapsto -\frac{1}{\mu}X_{16} + \frac{1}{\mu}X_{13}X_{36} & X_{62} &\mapsto \frac{1}{\mu}X_{62} - \frac{1}{\mu}X_{64}X_{42} \\
X_{53} &\mapsto -\frac{1}{\mu}X_{53} + \frac{1}{\mu}X_{51}X_{13} & X_{45} &\mapsto \frac{1}{\mu}X_{45} - \frac{1}{\mu}X_{42}X_{25}
\end{aligned} \tag{A.9}$$

$$\begin{aligned}
W' &= X_{16}X_{65}X_{51} + X_{25}X_{56}X_{62} + X_{34}X_{45}X_{53} + X_{13}X_{36}X_{64}X_{42}X_{21} \\
&\quad - X_{16}X_{62}X_{21} - X_{36}X_{65}X_{53} - X_{45}X_{56}X_{64} - X_{13}X_{34}X_{42}X_{25}X_{51}
\end{aligned}$$

Phase B to Phase B

$$\begin{aligned}
W &= X_{12}X_{23}X_{31} + X_{25}X_{56}X_{62} + X_{26}X_{64}X_{42} + X_{34}X_{45}X_{53}^2 \\
&\quad + X_{15}X_{53}^1X_{36}X_{61} - X_{12}X_{26}X_{61} - X_{15}X_{53}^2X_{31} - X_{23}X_{36}X_{62} \\
&\quad - X_{45}X_{56}X_{64} - X_{25}X_{53}^1X_{34}X_{42}
\end{aligned} \tag{A.10}$$

$$\begin{aligned}
\delta W &= \mu (X_{26}X_{62} - X_{15}X_{53}^1X_{31}) \\
X_{31} &\mapsto -\frac{1}{\mu}X_{31} + \frac{1}{\mu}X_{36}X_{61} & X_{53}^1 &\mapsto \frac{1}{\mu}X_{53}^1 - \frac{1}{\mu}X_{53}^2 \\
X_{45} &\mapsto \frac{1}{\mu}X_{45} - \frac{1}{\mu}X_{42}X_{25}
\end{aligned} \tag{A.11}$$

$$\begin{aligned}
W' &= X_{15}X_{53}^1X_{31} + X_{34}X_{45}X_{53}^2 + X_{12}X_{25}X_{56}X_{61} + X_{23}X_{36}X_{64}X_{42} \\
&\quad - X_{12}X_{23}X_{31} - X_{45}X_{56}X_{64} - X_{15}X_{53}^2X_{36}X_{61} - X_{25}X_{53}^1X_{34}X_{42}
\end{aligned}$$

A.1.5 PdP_{3b} to dP₃**Phase A to Phase A**

$$\begin{aligned}
W &= X_{12}X_{26}X_{61} + X_{14}X_{42}X_{21} + X_{25}X_{53}X_{32} + X_{13}X_{34}X_{46}X_{65}X_{51} \\
&\quad - X_{12}X_{25}X_{51} - X_{13}X_{32}X_{21} - X_{14}X_{46}X_{61} - X_{26}X_{65}X_{53}X_{34}X_{42}
\end{aligned} \tag{A.12}$$

$$\begin{aligned}
\delta W &= \mu (X_{12}X_{21} - X_{34}X_{46}X_{65}X_{53}) \\
X_{53} &\mapsto -\frac{1}{\mu}X_{53} + \frac{1}{\mu}X_{51}X_{13} & X_{46} &\mapsto \frac{1}{\mu}X_{46} - \frac{1}{\mu}X_{42}X_{26}
\end{aligned} \tag{A.13}$$

$$\begin{aligned}
W' &= X_{13}X_{32}X_{26}X_{61} + X_{14}X_{42}X_{25}X_{51} + X_{34}X_{46}X_{65}X_{53} \\
&\quad - X_{14}X_{46}X_{61} - X_{25}X_{53}X_{32} - X_{13}X_{34}X_{42}X_{26}X_{65}X_{51}
\end{aligned}$$

Phase B to Phase B

$$\begin{aligned}
W &= X_{53}X_{32}X_{25}^2 + X_{56}X_{62}X_{25}^1 + X_{13}X_{34}X_{45}X_{51} + X_{16}X_{64}X_{42}X_{21} \\
&\quad - X_{13}X_{32}X_{21} - X_{45}X_{56}X_{64} - X_{16}X_{62}X_{25}^2X_{51} - X_{34}X_{42}X_{25}^1X_{53}
\end{aligned} \tag{A.14}$$

$$\begin{aligned}
\delta W &= \mu (X_{12}X_{21} - X_{34}X_{46}X_{65}X_{53}) \\
X_{53} &\mapsto -\frac{1}{\mu}X_{53} + \frac{1}{\mu}X_{51}X_{13} & X_{45} &\mapsto \frac{1}{\mu}X_{45} - \frac{1}{\mu}X_{42}X_{25}^1 \\
X_{21} &\mapsto -\frac{1}{\mu}X_{21} + \frac{1}{\mu}X_{25}^2X_{51} & X_{62} &\mapsto \frac{1}{\mu}X_{62} - \frac{1}{\mu}X_{64}X_{42}
\end{aligned} \tag{A.15}$$

$$\begin{aligned}
W' &= X_{13}X_{32}X_{21} + X_{34}X_{45}X_{53} + X_{56}X_{62}X_{25}^1 + X_{16}X_{64}X_{42}X_{25}^2X_{51} \\
&\quad - X_{16}X_{62}X_{21} - X_{45}X_{56}X_{64} - X_{53}X_{32}X_{25}^2 - X_{13}X_{34}X_{42}X_{25}^1X_{51}
\end{aligned}$$

Phase C to Phase C

$$\begin{aligned}
W &= X_{13}X_{35}X_{51} + X_{16}X_{62}^2X_{21} + X_{24}X_{43}X_{32}^2 + X_{53}X_{32}^1X_{25}^2 \\
&\quad + X_{46}X_{62}^1X_{25}^1X_{54} - X_{13}X_{32}^1X_{21} - X_{24}X_{46}X_{62}^2 - X_{35}X_{54}X_{43} \\
&\quad - X_{53}X_{32}^2X_{25}^1 - X_{16}X_{62}^1X_{25}^2X_{51}
\end{aligned} \tag{A.16}$$

$$\begin{aligned}
\delta W &= \mu (X_{12}X_{21} - X_{34}X_{46}X_{65}X_{53}) \\
X_{21} &\mapsto \frac{1}{\mu}X_{21} - \frac{1}{\mu}X_{25}^2X_{51} & X_{62}^1 &\mapsto -\frac{1}{\mu}X_{62}^1 + \frac{1}{\mu}X_{62}^2 \\
X_{24} &\mapsto -\frac{1}{\mu}X_{24} + \frac{1}{\mu}X_{25}^1X_{54}
\end{aligned} \tag{A.17}$$

$$\begin{aligned}
W' &= X_{16}X_{62}^1X_{21} + X_{24}X_{46}X_{62}^2 + X_{13}X_{32}^2X_{25}^1X_{51} + X_{43}X_{32}^1X_{25}^2X_{54} \\
&\quad - X_{13}X_{32}^1X_{21} - X_{24}X_{43}X_{32}^2 - X_{16}X_{62}^2X_{25}^2X_{51} - X_{46}X_{62}^1X_{25}^1X_{54}
\end{aligned}$$

A.1.6 PdP_{4b} to PdP_{4a}

$$\begin{aligned}
W &= X_{16}X_{67}X_{71} + X_{17}X_{72}X_{21} + X_{25}X_{56}X_{62} + X_{26}X_{64}X_{42} \\
&\quad + X_{37}X_{75}X_{53} + X_{13}X_{34}X_{45}X_{51} - X_{13}X_{37}X_{71} - X_{16}X_{62}X_{21} \\
&\quad - X_{17}X_{75}X_{51} - X_{26}X_{67}X_{72} - X_{45}X_{56}X_{64} - X_{25}X_{53}X_{34}X_{42}
\end{aligned} \tag{A.18}$$

Phase A to Phase A

$$\begin{aligned}
\delta W &= \mu (X_{17}X_{71} - X_{26}X_{62}) \\
X_{45} &\mapsto -\frac{1}{\mu}X_{45} + \frac{1}{\mu}X_{42}X_{25} & X_{53} &\mapsto -\frac{1}{\mu}X_{53} + \frac{1}{\mu}X_{51}X_{13}
\end{aligned} \tag{A.19}$$

$$\begin{aligned}
W' &= X_{45}X_{56}X_{64} + X_{13}X_{37}X_{72}X_{21} + X_{16}X_{67}X_{75}X_{51} + X_{25}X_{53}X_{34}X_{42} \\
&\quad - X_{37}X_{75}X_{53} - X_{13}X_{34}X_{45}X_{51} - X_{16}X_{64}X_{42}X_{21} - X_{25}X_{56}X_{67}X_{72}
\end{aligned}$$

Phase A to Phase B

$$\begin{aligned}
\delta W &= \mu (X_{26}X_{62} - X_{34}X_{45}X_{53}) \\
X_{45} &\mapsto \frac{1}{\mu}X_{45} - \frac{1}{\mu}X_{42}X_{25} & X_{53} &\mapsto -\frac{1}{\mu}X_{53} + \frac{1}{\mu}X_{51}X_{13} \\
X_{17} &\mapsto -\frac{1}{\mu}X_{17} + \left(\frac{1}{\mu} - \beta_1\right)X_{13}X_{37} + \beta_1 X_{16}X_{67} \\
X_{71} &\mapsto -\frac{1}{\mu}X_{71} + \left(\frac{1}{\mu} - \beta_1\right)X_{72}X_{21} + \beta_1 X_{75}X_{51}
\end{aligned} \tag{A.20}$$

$$\begin{aligned}
W' &= X_{13}X_{37}X_{71} + X_{17}X_{75}X_{51} + X_{34}X_{45}X_{53} + X_{16}X_{64}X_{42}X_{21} \\
&\quad + X_{25}X_{56}X_{67}X_{72} - X_{16}X_{67}X_{71} - X_{17}X_{72}X_{21} - X_{37}X_{75}X_{53} \\
&\quad - X_{45}X_{56}X_{64} - X_{13}X_{34}X_{42}X_{25}X_{51}
\end{aligned}$$

$$\begin{aligned}
\delta W &= \mu (X_{17}X_{71} - X_{34}X_{45}X_{53}) \\
X_{45} &\mapsto \frac{1}{\mu}X_{45} - \frac{1}{\mu}X_{42}X_{25} & X_{53} &\mapsto -\frac{1}{\mu}X_{53} + \frac{1}{\mu}X_{51}X_{13} \\
X_{26} &\mapsto \frac{1}{\mu}X_{26} + \left(-\frac{1}{\mu} - \beta_1\right)X_{21}X_{16} + \beta_1 X_{25}X_{56} \\
X_{62} &\mapsto \frac{1}{\mu}X_{62} + \left(-\frac{1}{\mu} - \beta_1\right)X_{64}X_{42} + \beta_1 X_{67}X_{72}
\end{aligned} \tag{A.21}$$

$$\begin{aligned}
W' &= X_{25}X_{56}X_{62} + X_{26}X_{64}X_{42} + X_{34}X_{45}X_{53} + X_{13}X_{37}X_{72}X_{21} \\
&\quad + X_{16}X_{67}X_{75}X_{51} - X_{16}X_{62}X_{21} - X_{26}X_{67}X_{72} - X_{37}X_{75}X_{53} \\
&\quad - X_{45}X_{56}X_{64} - X_{13}X_{34}X_{42}X_{25}X_{51}
\end{aligned}$$

A.1.7 $\mathbb{C}^3 / (\mathbb{Z}_4 \times \mathbb{Z}_2) (1, 0, 3)(0, 1, 1)$ to $L^{1,3,1} / \mathbb{Z}_2 (0, 1, 1, 1)$ **Phase A to Phase A**

$$\begin{aligned}
W &= X_{12}X_{28}X_{81} + X_{14}X_{43}X_{31} + X_{17}X_{72}X_{21} + X_{23}X_{34}X_{42} \\
&\quad + X_{36}X_{65}X_{53} + X_{45}X_{56}X_{64} + X_{58}X_{87}X_{75} + X_{67}X_{78}X_{86} \\
&\quad - X_{12}X_{23}X_{31} - X_{14}X_{42}X_{21} - X_{17}X_{78}X_{81} - X_{28}X_{87}X_{72} \\
&\quad - X_{34}X_{45}X_{53} - X_{36}X_{64}X_{43} - X_{56}X_{67}X_{75} - X_{58}X_{86}X_{65}
\end{aligned} \tag{A.22}$$

$$\begin{aligned}
\delta W &= \mu (X_{12}X_{21} - X_{34}X_{43}) \\
X_{56} &\mapsto \frac{1}{\mu}X_{56} + \left(-\frac{1}{\mu} - \beta_1\right) X_{58}X_{86} + \beta_1 X_{53}X_{36} \\
X_{65} &\mapsto \frac{1}{\mu}X_{65} + \left(-\frac{1}{\mu} - \beta_1\right) X_{64}X_{45} + \beta_1 X_{67}X_{75} \\
X_{78} &\mapsto \frac{1}{\mu}X_{78} + \left(-\frac{1}{\mu} - \beta_2\right) X_{72}X_{28} + \beta_2 X_{75}X_{58} \\
X_{87} &\mapsto \frac{1}{\mu}X_{87} + \left(-\frac{1}{\mu} - \beta_2\right) X_{86}X_{67} + \beta_2 X_{81}X_{17}
\end{aligned} \tag{A.23}$$

$$\begin{aligned}
W' &= X_{36}X_{65}X_{53} + X_{45}X_{56}X_{64} + X_{58}X_{87}X_{75} + X_{67}X_{78}X_{86} \\
&\quad + X_{14}X_{42}X_{28}X_{81} + X_{17}X_{72}X_{23}X_{31} - X_{17}X_{78}X_{81} - X_{28}X_{87}X_{72} \\
&\quad - X_{56}X_{67}X_{75} - X_{58}X_{86}X_{65} - X_{14}X_{45}X_{53}X_{31} - X_{23}X_{36}X_{64}X_{42}
\end{aligned}$$

$$\begin{aligned}
\delta W &= \mu (X_{34}X_{43} - X_{54}X_{43}) \\
X_{12} &\mapsto \frac{1}{\mu}X_{12} + \left(-\frac{1}{\mu} - \beta_1\right) X_{17}X_{72} + \beta_1 X_{14}X_{42} \\
X_{21} &\mapsto \frac{1}{\mu}X_{21} + \left(-\frac{1}{\mu} - \beta_1\right) X_{23}X_{31} + \beta_1 X_{28}X_{81} \\
X_{78} &\mapsto \frac{1}{\mu}X_{78} + \left(-\frac{1}{\mu} - \beta_2\right) X_{75}X_{58} + \beta_2 X_{72}X_{28} \\
X_{87} &\mapsto \frac{1}{\mu}X_{87} + \left(-\frac{1}{\mu} - \beta_2\right) X_{81}X_{17} + \beta_2 X_{86}X_{67}
\end{aligned} \tag{A.24}$$

$$\begin{aligned}
W' &= X_{12}X_{28}X_{81} + X_{17}X_{72}X_{21} + X_{58}X_{87}X_{75} + X_{67}X_{78}X_{86} \\
&\quad + X_{14}X_{45}X_{53}X_{31} + X_{23}X_{36}X_{64}X_{42} - X_{12}X_{23}X_{31} - X_{14}X_{42}X_{21} \\
&\quad - X_{17}X_{78}X_{81} - X_{28}X_{87}X_{72} - X_{36}X_{67}X_{75}X_{53} - X_{45}X_{58}X_{86}X_{64}
\end{aligned}$$

$$\begin{aligned}
\delta W &= \mu (X_{56}X_{65} - X_{78}X_{87}) \\
X_{12} &\mapsto \frac{1}{\mu}X_{12} + \left(-\frac{1}{\mu} - \beta_1\right) X_{14}X_{42} + \beta_1 X_{17}X_{72} \\
X_{21} &\mapsto \frac{1}{\mu}X_{21} + \left(-\frac{1}{\mu} - \beta_1\right) X_{28}X_{81} + \beta_1 X_{23}X_{31} \\
X_{34} &\mapsto \frac{1}{\mu}X_{34} + \left(-\frac{1}{\mu} - \beta_2\right) X_{31}X_{14} + \beta_2 X_{36}X_{64} \\
X_{43} &\mapsto \frac{1}{\mu}X_{43} + \left(-\frac{1}{\mu} - \beta_2\right) X_{45}X_{53} + \beta_2 X_{42}X_{23}
\end{aligned} \tag{A.25}$$

$$\begin{aligned}
W' &= X_{12}X_{28}X_{81} + X_{14}X_{43}X_{31} + X_{17}X_{72}X_{21} + X_{23}X_{34}X_{42} \\
&\quad + X_{36}X_{67}X_{75}X_{53} + X_{45}X_{58}X_{86}X_{64} - X_{12}X_{23}X_{31} - X_{14}X_{42}X_{21} \\
&\quad - X_{34}X_{45}X_{53} - X_{36}X_{64}X_{43} - X_{17}X_{75}X_{58}X_{81} - X_{28}X_{86}X_{67}X_{72}
\end{aligned}$$

$$\begin{aligned}
\delta W &= \mu (X_{78}X_{87} - X_{12}X_{21}) \\
X_{34} &\mapsto \frac{1}{\mu}X_{34} + \left(-\frac{1}{\mu} - \beta_1\right) X_{36}X_{64} + \beta_1 X_{31}X_{14} \\
X_{43} &\mapsto \frac{1}{\mu}X_{43} + \left(-\frac{1}{\mu} - \beta_1\right) X_{42}X_{23} + \beta_1 X_{45}X_{53} \\
X_{56} &\mapsto \frac{1}{\mu}X_{56} + \left(-\frac{1}{\mu} - \beta_2\right) X_{53}X_{36} + \beta_2 X_{58}X_{86} \\
X_{65} &\mapsto \frac{1}{\mu}X_{65} + \left(-\frac{1}{\mu} - \beta_2\right) X_{67}X_{75} + \beta_2 X_{64}X_{45}
\end{aligned} \tag{A.26}$$

$$\begin{aligned}
W' &= X_{14}X_{43}X_{31} + X_{23}X_{34}X_{42} + X_{36}X_{65}X_{53} + X_{45}X_{56}X_{64} \\
&\quad + X_{17}X_{75}X_{58}X_{81} + X_{28}X_{86}X_{67}X_{72} - X_{34}X_{45}X_{53} - X_{36}X_{64}X_{43} \\
&\quad - X_{56}X_{67}X_{75} - X_{58}X_{86}X_{65} - X_{14}X_{42}X_{28}X_{81} - X_{17}X_{72}X_{23}X_{31}
\end{aligned}$$

A.1.8 $\mathbb{C}^3 / (\mathbb{Z}_4 \times \mathbb{Z}_2) (1, 0, 3)(0, 1, 1)$ to $\text{PdP}_5, \mathcal{C} / \mathbb{Z}_2 \times \mathbb{Z}_2 (1, 0, 0, 1)(0, 1, 1, 0)$

$$\begin{aligned}
W &= X_{12}X_{28}X_{81} + X_{14}X_{43}X_{31} + X_{17}X_{72}X_{21} + X_{23}X_{34}X_{42} \\
&\quad + X_{36}X_{65}X_{53} + X_{45}X_{56}X_{64} + X_{58}X_{87}X_{75} + X_{67}X_{78}X_{86} \\
&\quad - X_{12}X_{23}X_{31} - X_{14}X_{42}X_{21} - X_{17}X_{78}X_{81} - X_{28}X_{87}X_{72} \\
&\quad - X_{34}X_{45}X_{53} - X_{36}X_{64}X_{43} - X_{56}X_{67}X_{75} - X_{58}X_{86}X_{65}
\end{aligned} \tag{A.27}$$

Phase A to Phase A

$$\begin{aligned}
\delta W &= \mu (X_{12}X_{21} - X_{34}X_{43} + X_{56}X_{65} - X_{78}X_{87}) \\
W' &= X_{14}X_{42}X_{28}X_{81} + X_{17}X_{72}X_{23}X_{31} + X_{36}X_{67}X_{75}X_{53} \\
&\quad + X_{45}X_{58}X_{86}X_{64} - X_{14}X_{45}X_{53}X_{31} - X_{17}X_{75}X_{58}X_{81} \\
&\quad - X_{23}X_{36}X_{64}X_{42} - X_{28}X_{86}X_{67}X_{72}
\end{aligned} \tag{A.28}$$

Phase A to Phase B

$$\begin{aligned}
\delta W &= \mu (X_{12}X_{21} - X_{56}X_{65}) \\
X_{34} &\mapsto -\frac{1}{\mu}X_{34} + \left(\frac{1}{\mu} - \beta_1\right) X_{31}X_{14} + \beta_1 X_{36}X_{64} \\
X_{43} &\mapsto -\frac{1}{\mu}X_{43} + \left(\frac{1}{\mu} - \beta_1\right) X_{45}X_{53} + \beta_1 X_{42}X_{23} \\
X_{78} &\mapsto \frac{1}{\mu}X_{78} + \left(-\frac{1}{\mu} - \beta_2\right) X_{72}X_{28} + \beta_2 X_{75}X_{58} \\
X_{87} &\mapsto \frac{1}{\mu}X_{87} + \left(-\frac{1}{\mu} - \beta_2\right) X_{86}X_{67} + \beta_2 X_{81}X_{17}
\end{aligned} \tag{A.29}$$

$$\begin{aligned}
W' &= X_{34}X_{45}X_{53} + X_{36}X_{64}X_{43} + X_{58}X_{87}X_{75} + X_{67}X_{78}X_{86} \\
&\quad + X_{14}X_{42}X_{28}X_{81} + X_{17}X_{72}X_{23}X_{31} - X_{14}X_{43}X_{31} - X_{17}X_{78}X_{81} \\
&\quad - X_{23}X_{34}X_{42} - X_{28}X_{87}X_{72} - X_{36}X_{67}X_{75}X_{53} - X_{45}X_{58}X_{86}X_{64}
\end{aligned}$$

$$\begin{aligned}
\delta W &= \mu (X_{34}X_{43} - X_{78}X_{87}) \\
X_{12} &\mapsto \frac{1}{\mu}X_{12} + \left(-\frac{1}{\mu} - \beta_1\right) X_{14}X_{42} + \beta_1 X_{17}X_{72} \\
X_{21} &\mapsto \frac{1}{\mu}X_{21} + \left(-\frac{1}{\mu} - \beta_1\right) X_{28}X_{81} + \beta_1 X_{23}X_{31} \\
X_{56} &\mapsto -\frac{1}{\mu}X_{56} + \left(\frac{1}{\mu} - \beta_2\right) X_{53}X_{36} + \beta_2 X_{58}X_{86} \\
X_{65} &\mapsto -\frac{1}{\mu}X_{65} + \left(\frac{1}{\mu} - \beta_2\right) X_{67}X_{75} + \beta_2 X_{64}X_{45}
\end{aligned} \tag{A.30}$$

$$\begin{aligned}
W' &= X_{12}X_{28}X_{81} + X_{17}X_{72}X_{21} + X_{56}X_{67}X_{75} + X_{58}X_{86}X_{65} \\
&\quad + X_{14}X_{45}X_{53}X_{31} + X_{23}X_{36}X_{64}X_{42} - X_{12}X_{23}X_{31} - X_{14}X_{42}X_{21} \\
&\quad - X_{36}X_{65}X_{53} - X_{45}X_{56}X_{64} - X_{17}X_{75}X_{58}X_{81} - X_{28}X_{86}X_{67}X_{72}
\end{aligned}$$

A.2 Deformations to marginal deformations of toric models

Listed here are relevant zig-zag deformations of toric models for which the endpoint of the RG flow is not toric. Instead, the IR models in this section are described by a toric superpotential plus an exactly marginal zig-zag deformation. In each subsection, we present the original toric superpotential W . Each deformation is in a unique equation block with:

1. The deformation $\delta W = \mu \mathcal{O}_\eta$, associated to a zig-zag path η .
2. The field redefinitions of the type in eq. (4.15), if any.
3. The superpotential W' representing the IR theory, which is of the form $W'_{\text{toric}} + \frac{1}{\mu} \mathcal{O}'_{\eta'}$, where $R_{sc}[\mathcal{O}'_{\eta'}] = 2$. The superpotential W'_{toric} defines a brane tiling model, and $\mathcal{O}'_{\eta'}$ corresponds to the zig-zag operator of W'_{toric} for the reversed zig-zag path η' .

A.2.1 $L^{1,3,1}/\mathbb{Z}_2(0, 1, 1, 1)$ to PdP₅, $\mathcal{C}/\mathbb{Z}_2 \times \mathbb{Z}_2(1, 0, 0, 1)(0, 1, 1, 0)$

Phase A to Phase A

$$\begin{aligned}
W = & X_{17}X_{78}X_{81} + X_{18}X_{83}X_{31} + X_{27}X_{73}X_{32} + X_{37}X_{75}X_{53} \\
& + X_{14}X_{45}X_{56}X_{61} + X_{24}X_{48}X_{86}X_{62} - X_{14}X_{48}X_{81} - X_{17}X_{73}X_{31} \\
& - X_{18}X_{86}X_{61} - X_{37}X_{78}X_{83} - X_{24}X_{45}X_{53}X_{32} - X_{27}X_{75}X_{56}X_{62}
\end{aligned} \tag{A.31}$$

$$\delta W = \mu (X_{37}X_{73} - X_{18}X_{81})$$

$$X_{17} \mapsto \mu X_{17}$$

$$X_{83} \mapsto \mu X_{83}$$

(A.32)

$$\begin{aligned}
W' = & X_{14}X_{45}X_{56}X_{61} + X_{17}X_{75}X_{53}X_{31} + X_{24}X_{48}X_{86}X_{62} + X_{27}X_{78}X_{83}X_{32} \\
& - X_{14}X_{48}X_{83}X_{31} - X_{17}X_{78}X_{86}X_{61} - X_{24}X_{45}X_{53}X_{32} - X_{27}X_{75}X_{56}X_{62} \\
& + \frac{1}{\mu} (X_{14}X_{48}X_{86}X_{61} - X_{27}X_{75}X_{53}X_{32})
\end{aligned}$$

Phase A to Phase B

$$\begin{aligned}
W = & X_{17}X_{78}X_{81} + X_{18}X_{83}X_{31} + X_{27}X_{73}X_{32} + X_{37}X_{75}X_{53} \\
& + X_{14}X_{45}X_{56}X_{61} + X_{24}X_{48}X_{86}X_{62} - X_{14}X_{48}X_{81} - X_{17}X_{73}X_{31} \\
& - X_{18}X_{86}X_{61} - X_{37}X_{78}X_{83} - X_{24}X_{45}X_{53}X_{32} - X_{27}X_{75}X_{56}X_{62}
\end{aligned} \tag{A.33}$$

$$\begin{aligned}
\delta W &= \mu (X_{18}X_{81} - X_{24}X_{45}X_{56}X_{62}) \\
X_{61} &\mapsto \mu X_{61} \\
X_{48} &\mapsto \mu X_{48} \\
W' &= X_{24}X_{46}X_{62} + X_{27}X_{73}X_{32} + X_{37}X_{75}X_{53} + X_{45}X_{56}X_{64} \\
&\quad + X_{14}X_{48}X_{83}X_{31} + X_{17}X_{78}X_{86}X_{61} - X_{14}X_{46}X_{61} - X_{17}X_{73}X_{31} \\
&\quad - X_{37}X_{78}X_{83} - X_{48}X_{86}X_{64} - X_{24}X_{45}X_{53}X_{32} - X_{27}X_{75}X_{56}X_{62} \\
&\quad + \frac{1}{\mu} (X_{46}X_{64} - X_{17}X_{78}X_{83}X_{31})
\end{aligned} \tag{A.34}$$

Phase B to Phase C

$$\begin{aligned}
W &= X_{17}X_{78}X_{81} + X_{18}X_{83}X_{31} + X_{23}X_{34}X_{42} + X_{26}X_{67}X_{72} + X_{37}X_{75}X_{53} \\
&\quad + X_{48}X_{86}X_{64} + X_{14}X_{45}X_{56}X_{61} - X_{14}X_{48}X_{81} - X_{18}X_{86}X_{61} - X_{26}X_{64}X_{42} \\
&\quad - X_{34}X_{45}X_{53} - X_{37}X_{78}X_{83} - X_{56}X_{67}X_{75} - X_{17}X_{72}X_{23}X_{31}
\end{aligned} \tag{A.35}$$

$$\begin{aligned}
\delta W &= \mu (X_{18}X_{81} - X_{45}X_{56}X_{64}) \\
X_{14} &\mapsto \mu X_{14} \\
X_{86} &\mapsto \mu X_{86} \\
X_{64} &\mapsto \frac{1}{\mu} X_{64} + X_{61}X_{14} \\
W' &= X_{23}X_{34}X_{42} + X_{26}X_{67}X_{72} + X_{37}X_{75}X_{53} + X_{45}X_{56}X_{64} \\
&\quad + X_{14}X_{48}X_{83}X_{31} + X_{17}X_{78}X_{86}X_{61} - X_{34}X_{45}X_{53} - X_{37}X_{78}X_{83} \\
&\quad - X_{48}X_{86}X_{64} - X_{56}X_{67}X_{75} - X_{14}X_{42}X_{26}X_{61} - X_{17}X_{72}X_{23}X_{31} \\
&\quad + \frac{1}{\mu} (X_{26}X_{64}X_{42} - X_{17}X_{78}X_{83}X_{31})
\end{aligned} \tag{A.36}$$

Appendix B

Details of deformations for polytopes with 2 internal points

In this appendix, we present the details about the zig-zag deformations between dimer models with polytopes with 2 internal points. Due to the amount of possible flows, we present the details in a shorter form than appendix A. Each subsection is titled “ \mathcal{X} to \mathcal{Y} ”, pointing out the geometries where the flow occurs. Then, each flow is presented as a triplet of

$$(\text{UV toric phase} , \quad \text{zig-zag paths set } \eta \in S , \quad \text{IR toric phase}) ,$$

which triggered by a single-parameter $\sum_{\eta \in S} \mathcal{O}_\eta$. Field redefinitions to the recover explicit toric form of the final superpotential can be done via the algorithm in section 6.2.1.2. Similarly, toric phases form are tabled at <https://github.com/jose-a-sa/zig-zag-deformation-datagithub.com/jose-a-sa/zig-zag-deformation-data>, obtain by the algorithm in section 6.2.1.1.

B.1 Deformations between toric phases with $g = 7$

B.1.1 $L^{4,3,2}$ to $K^{2,4,1,1}$

W_i	Deformation zig-zags η	W_f
$L^{4,3,2}$ (I)	$X_{15}X_{54}X_{43}X_{31}$	$K^{2,4,1,1}$ (I)
$L^{4,3,2}$ (II)	$X_{15}X_{54}X_{43}X_{31}$	$K^{2,4,1,1}$ (II)

B.2 Deformations between toric phases with $g = 8$

B.2.1 $\mathbb{C}^3/\mathbb{Z}_8(1, 3, 4)$ to $L^{1,3,1}/\mathbb{Z}_2(1, 0, 0, 1)$

W_i	Deformation zig-zags η	W_f
$\mathbb{C}^3/\mathbb{Z}_8$ (I)	$X_{13}X_{38}X_{82}X_{21}$	$L^{1,3,1}/\mathbb{Z}_2$ (I)
$\mathbb{C}^3/\mathbb{Z}_8$ (I)	$X_{16}X_{68}X_{87}X_{71}$	$L^{1,3,1}/\mathbb{Z}_2$ (I)
$\mathbb{C}^3/\mathbb{Z}_8$ (I)	$X_{25}X_{53}X_{34}X_{42}$	$L^{1,3,1}/\mathbb{Z}_2$ (I)
$\mathbb{C}^3/\mathbb{Z}_8$ (I)	$X_{46}X_{65}X_{57}X_{74}$	$L^{1,3,1}/\mathbb{Z}_2$ (I)

B.2.2 $\mathbb{C}^3/\mathbb{Z}_8(1, 3, 4)$ to $\mathcal{C}/\mathbb{Z}_4(0, 1, 2, 1)$

W_i	Deformation zig-zags η	W_f
$\mathbb{C}^3/\mathbb{Z}_8$ (I)	$X_{46}X_{65}X_{57}X_{74}, X_{13}X_{38}X_{82}X_{21}$	\mathcal{C}/\mathbb{Z}_4 (I)
$\mathbb{C}^3/\mathbb{Z}_8$ (I)	$X_{25}X_{53}X_{34}X_{42}, X_{13}X_{38}X_{82}X_{21}$	\mathcal{C}/\mathbb{Z}_4 (II)
$\mathbb{C}^3/\mathbb{Z}_8$ (I)	$X_{46}X_{65}X_{57}X_{74}, X_{25}X_{53}X_{34}X_{42}$	\mathcal{C}/\mathbb{Z}_4 (II)

B.2.3 $d\mathbb{P}_1/\mathbb{Z}_2(1, 0, 0, 1)$ to $K^{2,5,1,1}$

W_i	Deformation zig-zags η	W_f
$d\mathbb{P}_1/\mathbb{Z}_2$ (I)	$X_{12}X_{28}X_{83}X_{31}$	$K^{2,5,1,1}$ (I)
$d\mathbb{P}_1/\mathbb{Z}_2$ (II)	$X_{14}X_{42}X_{23}X_{31}$	$K^{2,5,1,1}$ (II)
$d\mathbb{P}_1/\mathbb{Z}_2$ (III)	$X_{58}X_{86}X_{67}X_{75}$	$K^{2,5,1,1}$ (III)

B.2.4 $L^{3,5,2}$ to $K^{2,4,1,2}$

W_i	Deformation zig-zags η	W_f
$L^{3,5,2}$ (I)	$X_{13}X_{32}X_{24}X_{41}$	$K^{2,4,1,2}$ (II)
$L^{3,5,2}$ (I)	$X_{35}X_{54}X_{47}X_{73}$	$K^{2,4,1,2}$ (II)
$L^{3,5,2}$ (I)	$X_{17}X_{78}X_{86}X_{61}$	$K^{2,4,1,2}$ (III)
$L^{3,5,2}$ (II)	$X_{13}X_{32}X_{24}X_{41}$	$K^{2,4,1,2}$ (I)
$L^{3,5,2}$ (II)	$X_{18}X_{82}X_{26}X_{61}$	$K^{2,4,1,2}$ (VI)
$L^{3,5,2}$ (II)	$X_{35}X_{54}X_{47}X_{73}$	$K^{2,4,1,2}$ (VI)

B.2.5 PdP_{4c}(2) to PdP_{4e}(3)

W_i	Deformation zig-zags η	W_f
PdP _{4c} (I)	$X_{13}X_{32}X_{25}X_{51}$	PdP _{4e} (I)
PdP _{4c} (II)	$X_{13}X_{38}X_{82}X_{21}$	PdP _{4e} (II)
PdP _{4c} (III)	$X_{36}X_{65}X_{54}X_{43}$	PdP _{4e} (III)
PdP _{4c} (IV)	$X_{13}X_{32}X_{25}X_{51}$	PdP _{4e} (VI)
PdP _{4c} (V)	$X_{14}X_{43}X_{35}X_{51}$	PdP _{4e} (IV)
PdP _{4c} (VI)	$X_{36}X_{65}X_{54}X_{43}$	PdP _{4e} (VIII)
PdP _{4c} (VII)	$X_{14}X_{43}X_{35}X_{51}$	PdP _{4e} (X)
PdP _{4c} (VIII)	$X_{14}X_{43}X_{35}X_{51}$	PdP _{4e} (IX)

B.2.6 PdP_{4d}(2) to PdP_{4f}(2)

W_i	Deformation zig-zags η	W_f
PdP _{4d} (I)	$X_{17}X_{72}X_{28}X_{81}$	PdP _{4f} (I)
PdP _{4d} (II)	$X_{17}X_{72}X_{28}X_{81}$	PdP _{4f} (II)
PdP _{4d} (III)	$X_{25}X_{53}X_{36}X_{62}$	PdP _{4f} (III)
PdP _{4d} (IV)	$X_{23}X_{34}X_{46}X_{62}$	PdP _{4f} (VI)
PdP _{4d} (V)	$X_{25}X_{53}X_{36}X_{62}$	PdP _{4f} (VII)
PdP _{4d} (VI)	$X_{35}X_{54}X_{46}X_{63}$	PdP _{4f} (IX)
PdP _{4d} (VII)	$X_{14}X_{47}X_{72}X_{21}$	PdP _{4f} (VIII)
PdP _{4d} (VIII)	$X_{17}X_{72}X_{28}X_{81}$	PdP _{4f} (X)

B.3 Deformations between toric phases with $g = 9$

B.3.1 $L^{5,4,1}$ to $K^{2,4,1,3}$

W_i	Deformation zig-zags η	W_f
$L^{5,4,1}$ (I)	$X_{14}X_{42}X_{23}X_{31}$	$K^{2,4,1,3}$ (I)
$L^{5,4,1}$ (I)	$X_{19}X_{92}X_{28}X_{81}$	$K^{2,4,1,3}$ (I)
$L^{5,4,1}$ (I)	$X_{36}X_{64}X_{45}X_{53}$	$K^{2,4,1,3}$ (III)
$L^{5,4,1}$ (I)	$X_{68}X_{87}X_{79}X_{96}$	$K^{2,4,1,3}$ (III)

B.3.2 $L^{5,4,1}$ to $K^{4,3,2,2}$

W_i	Deformation zig-zags η	W_f
$L^{5,4,1}$ (I)	$X_{68}X_{87}X_{79}X_{96}, X_{14}X_{42}X_{23}X_{31}$	$K^{4,3,2,2}$ (I)
$L^{5,4,1}$ (I)	$X_{68}X_{87}X_{79}X_{96}, X_{36}X_{64}X_{45}X_{53}$	$K^{4,3,2,2}$ (III)
$L^{5,4,1}$ (I)	$X_{36}X_{64}X_{45}X_{53}, X_{14}X_{42}X_{23}X_{31}$	$K^{4,3,2,2}$ (V)

B.3.3 SPP/ \mathbb{Z}_3 (1, 0, 0, 2) to $K^{2,5,1,2}$

W_i	Deformation zig-zags η	W_f
SPP/ \mathbb{Z}_3 (I)	$X_{14}X_{43}X_{35}X_{51}$	$K^{2,5,1,2}$ (I)
SPP/ \mathbb{Z}_3 (I)	$X_{19}X_{92}X_{28}X_{81}$	$K^{2,5,1,2}$ (I)
SPP/ \mathbb{Z}_3 (I)	$X_{48}X_{86}X_{67}X_{74}$	$K^{2,5,1,2}$ (I)
SPP/ \mathbb{Z}_3 (II)	$X_{19}X_{93}X_{32}X_{21}$	$K^{2,5,1,2}$ (II)
SPP/ \mathbb{Z}_3 (II)	$X_{14}X_{43}X_{35}X_{51}$	$K^{2,5,1,2}$ (III)
SPP/ \mathbb{Z}_3 (II)	$X_{48}X_{86}X_{67}X_{74}$	$K^{2,5,1,2}$ (V)
SPP/ \mathbb{Z}_3 (III)	$X_{14}X_{43}X_{35}X_{51}$	$K^{2,5,1,2}$ (IV)
SPP/ \mathbb{Z}_3 (III)	$X_{19}X_{93}X_{32}X_{21}$	$K^{2,5,1,2}$ (VI)
SPP/ \mathbb{Z}_3 (III)	$X_{46}X_{65}X_{57}X_{74}$	$K^{2,5,1,2}$ (VI)

B.3.4 PdP_{5b} (2) to PdP_{5c} (3)

W_i	Deformation zig-zags η	W_f
PdP _{5b} (I)	$X_{19}X_{92}X_{28}X_{81}$	PdP _{5c} (I)
PdP _{5b} (I)	$X_{13}X_{32}X_{24}X_{41}$	PdP _{5c} (II)
PdP _{5b} (I)	$X_{58}X_{86}X_{67}X_{75}$	PdP _{5c} (IV)
PdP _{5b} (II)	$X_{13}X_{32}X_{24}X_{41}$	PdP _{5c} (VIII) ¹
PdP _{5b} (II)	$X_{28}X_{89}X_{97}X_{72}$	PdP _{5c} (VIII) ¹
PdP _{5b} (II)	$X_{37}X_{75}X_{56}X_{63}$	PdP _{5c} (VIII) ¹
PdP _{5b} (III)	$X_{16}X_{63}X_{34}X_{41}$	PdP _{5c} (III)
PdP _{5b} (III)	$X_{45}X_{56}X_{67}X_{74}$	PdP _{5c} (IX)
PdP _{5b} (III)	$X_{19}X_{93}X_{32}X_{21}$	PdP _{5c} (X)
PdP _{5b} (IV)	$X_{19}X_{93}X_{32}X_{21}$	PdP _{5c} (XII)
PdP _{5b} (IV)	$X_{16}X_{63}X_{34}X_{41}$	PdP _{5c} (XIII)
PdP _{5b} (IV)	$X_{58}X_{86}X_{67}X_{75}$	PdP _{5c} (XXIII)
PdP _{5b} (V)	$X_{13}X_{32}X_{24}X_{41}$	PdP _{5c} (XV)
PdP _{5b} (V)	$X_{19}X_{92}X_{28}X_{81}$	PdP _{5c} (XVI)
PdP _{5b} (V)	$X_{57}X_{76}X_{69}X_{95}$	PdP _{5c} (XXVI)
PdP _{5b} (VI)	$X_{69}X_{97}X_{78}X_{86}$	PdP _{5c} (XVIII)
PdP _{5b} (VI)	$X_{19}X_{92}X_{28}X_{81}$	PdP _{5c} (XIX)
PdP _{5b} (VI)	$X_{16}X_{63}X_{34}X_{41}$	PdP _{5c} (XXIX)
PdP _{5b} (VII)	$X_{16}X_{64}X_{45}X_{51}$	PdP _{5c} (XXI)
PdP _{5b} (VII)	$X_{58}X_{86}X_{67}X_{75}$	PdP _{5c} (XXII)
PdP _{5b} (VII)	$X_{19}X_{92}X_{28}X_{81}$	PdP _{5c} (XXXI)
PdP _{5b} (VIII)	$X_{19}X_{92}X_{28}X_{81}$	PdP _{5c} (XVII)
PdP _{5b} (VIII)	$X_{13}X_{32}X_{24}X_{41}$	PdP _{5c} (XXVII)
PdP _{5b} (VIII)	$X_{69}X_{97}X_{78}X_{86}$	PdP _{5c} (XXVIII)

B.4 Deformations between toric phases with $g = 10$

B.4.1 $\mathbb{C}^3/(\mathbb{Z}_2 \times \mathbb{Z}_5) (1, 0, 1)(0, 1, 4)$ to $L^{1,4,1}/\mathbb{Z}_2 (1, 0, 0, 1)$

W_i	Deformation zig-zags η	W_f
$\mathbb{C}^3/(\mathbb{Z}_2 \times \mathbb{Z}_5)$ (I)	$X_{16}X_{62}X_{25}X_{51}$	$L^{1,4,1}/\mathbb{Z}_2$ (I)
$\mathbb{C}^3/(\mathbb{Z}_2 \times \mathbb{Z}_5)$ (I)	$X_{18}X_{82}X_{27}X_{71}$	$L^{1,4,1}/\mathbb{Z}_2$ (I)
$\mathbb{C}^3/(\mathbb{Z}_2 \times \mathbb{Z}_5)$ (I)	$X_{37}X_{74}X_{48}X_{83}$	$L^{1,4,1}/\mathbb{Z}_2$ (I)
$\mathbb{C}^3/(\mathbb{Z}_2 \times \mathbb{Z}_5)$ (I)	$X_{39}X_{94}X_{4,10}X_{10,3}$	$L^{1,4,1}/\mathbb{Z}_2$ (I)
$\mathbb{C}^3/(\mathbb{Z}_2 \times \mathbb{Z}_5)$ (I)	$X_{59}X_{96}X_{6,10}X_{10,5}$	$L^{1,4,1}/\mathbb{Z}_2$ (I)

¹Missing to match the potential, but matched the quiver.

B.4.2 $\mathbb{C}^3/(\mathbb{Z}_2 \times \mathbb{Z}_5) (1, 0, 1)(0, 1, 4)$ to $L^{2,3,2}/\mathbb{Z}_2 (1, 0, 0, 1)$

W_i	Deformation zig-zags η	W_f
$\mathbb{C}^3/(\mathbb{Z}_2 \times \mathbb{Z}_5) (I)$	$X_{18}X_{82}X_{27}X_{71}, X_{39}X_{94}X_{4,10}X_{10,3}$	$L^{2,3,2}/\mathbb{Z}_2 (I)$
$\mathbb{C}^3/(\mathbb{Z}_2 \times \mathbb{Z}_5) (I)$	$X_{18}X_{82}X_{27}X_{71}, X_{59}X_{96}X_{6,10}X_{10,5}$	$L^{2,3,2}/\mathbb{Z}_2 (I)$
$\mathbb{C}^3/(\mathbb{Z}_2 \times \mathbb{Z}_5) (I)$	$X_{37}X_{74}X_{48}X_{83}, X_{16}X_{62}X_{25}X_{51}$	$L^{2,3,2}/\mathbb{Z}_2 (I)$
$\mathbb{C}^3/(\mathbb{Z}_2 \times \mathbb{Z}_5) (I)$	$X_{39}X_{94}X_{4,10}X_{10,3}, X_{16}X_{62}X_{25}X_{51}$	$L^{2,3,2}/\mathbb{Z}_2 (I)$
$\mathbb{C}^3/(\mathbb{Z}_2 \times \mathbb{Z}_5) (I)$	$X_{59}X_{96}X_{6,10}X_{10,5}, X_{37}X_{74}X_{48}X_{83}$	$L^{2,3,2}/\mathbb{Z}_2 (I)$
$\mathbb{C}^3/(\mathbb{Z}_2 \times \mathbb{Z}_5) (I)$	$X_{18}X_{82}X_{27}X_{71}, X_{16}X_{62}X_{25}X_{51}$	$L^{2,3,2}/\mathbb{Z}_2 (III)$
$\mathbb{C}^3/(\mathbb{Z}_2 \times \mathbb{Z}_5) (I)$	$X_{18}X_{82}X_{27}X_{71}, X_{37}X_{74}X_{48}X_{83}$	$L^{2,3,2}/\mathbb{Z}_2 (III)$
$\mathbb{C}^3/(\mathbb{Z}_2 \times \mathbb{Z}_5) (I)$	$X_{39}X_{94}X_{4,10}X_{10,3}, X_{37}X_{74}X_{48}X_{83}$	$L^{2,3,2}/\mathbb{Z}_2 (III)$
$\mathbb{C}^3/(\mathbb{Z}_2 \times \mathbb{Z}_5) (I)$	$X_{39}X_{94}X_{4,10}X_{10,3}, X_{59}X_{96}X_{6,10}X_{10,5}$	$L^{2,3,2}/\mathbb{Z}_2 (III)$
$\mathbb{C}^3/(\mathbb{Z}_2 \times \mathbb{Z}_5) (I)$	$X_{59}X_{96}X_{6,10}X_{10,5}, X_{16}X_{62}X_{25}X_{51}$	$L^{2,3,2}/\mathbb{Z}_2 (III)$

B.4.3 $\text{PdP}_2/\mathbb{Z}_2 (1, 1, 1, 1)$ to $K^{2,5,1,3}$

W_i	Deformation zig-zags η	W_f
$\text{PdP}_2/\mathbb{Z}_2 (I)$	$X_{14}X_{42}X_{23}X_{31}$	$K^{2,5,1,3} (IV)$
$\text{PdP}_2/\mathbb{Z}_2 (I)$	$X_{18}X_{82}X_{2,10}X_{10,1}$	$K^{2,5,1,3} (IV)$
$\text{PdP}_2/\mathbb{Z}_2 (I)$	$X_{46}X_{65}X_{57}X_{74}$	$K^{2,5,1,3} (IV)$
$\text{PdP}_2/\mathbb{Z}_2 (I)$	$X_{69}X_{97}X_{78}X_{86}$	$K^{2,5,1,3} (IV)$
$\text{PdP}_2/\mathbb{Z}_2 (II)$	$X_{46}X_{65}X_{57}X_{74}$	$K^{2,5,1,3} (I)$
$\text{PdP}_2/\mathbb{Z}_2 (II)$	$X_{14}X_{43}X_{35}X_{51}$	$K^{2,5,1,3} (II)$
$\text{PdP}_2/\mathbb{Z}_2 (II)$	$X_{69}X_{97}X_{78}X_{86}$	$K^{2,5,1,3} (II)$
$\text{PdP}_2/\mathbb{Z}_2 (II)$	$X_{18}X_{82}X_{2,10}X_{10,1}$	$K^{2,5,1,3} (VI)$
$\text{PdP}_2/\mathbb{Z}_2 (III)$	$X_{14}X_{43}X_{35}X_{51}$	$K^{2,5,1,3} (V)$
$\text{PdP}_2/\mathbb{Z}_2 (III)$	$X_{46}X_{65}X_{57}X_{74}$	$K^{2,5,1,3} (V)$
$\text{PdP}_2/\mathbb{Z}_2 (III)$	$X_{12}X_{23}X_{3,10}X_{10,1}$	$K^{2,5,1,3} (VII)$
$\text{PdP}_2/\mathbb{Z}_2 (III)$	$X_{69}X_{97}X_{78}X_{86}$	$K^{2,5,1,3} (VII)$

B.4.4 $\text{PdP}_2/\mathbb{Z}_2(1, 1, 1, 1)$ to $K^{4,4,2,2}$

W_i	Deformation zig-zags η	W_f
$\text{PdP}_2/\mathbb{Z}_2$ (I)	$X_{46}X_{65}X_{57}X_{74}, X_{14}X_{42}X_{23}X_{31}$	$K^{4,4,2,2}$ (II)
$\text{PdP}_2/\mathbb{Z}_2$ (I)	$X_{69}X_{97}X_{78}X_{86}, X_{14}X_{42}X_{23}X_{31}$	$K^{4,4,2,2}$ (III)
$\text{PdP}_2/\mathbb{Z}_2$ (I)	$X_{69}X_{97}X_{78}X_{86}, X_{46}X_{65}X_{57}X_{74}$	$K^{4,4,2,2}$ (X)
$\text{PdP}_2/\mathbb{Z}_2$ (II)	$X_{69}X_{97}X_{78}X_{86}, X_{14}X_{43}X_{35}X_{51}$	$K^{4,4,2,2}$ (I)
$\text{PdP}_2/\mathbb{Z}_2$ (II)	$X_{46}X_{65}X_{57}X_{74}, X_{14}X_{43}X_{35}X_{51}$	$K^{4,4,2,2}$ (V)
$\text{PdP}_2/\mathbb{Z}_2$ (II)	$X_{69}X_{97}X_{78}X_{86}, X_{46}X_{65}X_{57}X_{74}$	$K^{4,4,2,2}$ (V)
$\text{PdP}_2/\mathbb{Z}_2$ (III)	$X_{69}X_{97}X_{78}X_{86}, X_{14}X_{43}X_{35}X_{51}$	$K^{4,4,2,2}$ (IV)
$\text{PdP}_2/\mathbb{Z}_2$ (III)	$X_{46}X_{65}X_{57}X_{74}, X_{14}X_{43}X_{35}X_{51}$	$K^{4,4,2,2}$ (VII)
$\text{PdP}_2/\mathbb{Z}_2$ (III)	$X_{69}X_{97}X_{78}X_{86}, X_{46}X_{65}X_{57}X_{74}$	$K^{4,4,2,2}$ (XI)

B.4.5 $\text{PdP}_{6a}(2)$ to $\text{PdP}_{6b}(3)$

W_i	Deformation zig-zags η	W_f
PdP_{6a} (I)	$X_{36}X_{65}X_{57}X_{73}$	PdP_{6b} (I)
PdP_{6a} (I)	$X_{68}X_{87}X_{7,10}X_{10,6}$	PdP_{6b} (I)
PdP_{6a} (I)	$X_{13}X_{34}X_{45}X_{51}$	PdP_{6b} (V)
PdP_{6a} (I)	$X_{2,10}X_{10,9}X_{98}X_{82}$	PdP_{6b} (V)
PdP_{6a} (II)	$X_{68}X_{87}X_{7,10}X_{10,6}$	PdP_{6b} (II)
PdP_{6a} (II)	$X_{2,10}X_{10,9}X_{98}X_{82}$	PdP_{6b} (VII)
PdP_{6a} (II)	$X_{36}X_{65}X_{57}X_{73}$	PdP_{6b} (IX)
PdP_{6a} (II)	$X_{13}X_{32}X_{24}X_{41}$	PdP_{6b} (XV)
PdP_{6a} (III)	$X_{13}X_{32}X_{24}X_{41}$	PdP_{6b} (X)
PdP_{6a} (III)	$X_{19}X_{92}X_{2,10}X_{10,1}$	PdP_{6b} (X)
PdP_{6a} (III)	$X_{36}X_{65}X_{57}X_{73}$	PdP_{6b} (XII)
PdP_{6a} (III)	$X_{68}X_{87}X_{7,10}X_{10,6}$	PdP_{6b} (XII)
PdP_{6a} (IV)	$X_{2,10}X_{10,9}X_{98}X_{82}$	PdP_{6b} (XIII)
PdP_{6a} (IV)	$X_{68}X_{87}X_{7,10}X_{10,6}$	PdP_{6b} (XIII)
PdP_{6a} (IV)	$X_{19}X_{93}X_{32}X_{21}$	PdP_{6b} (XVI)
PdP_{6a} (IV)	$X_{36}X_{65}X_{57}X_{73}$	PdP_{6b} (XVI)

B.4.6 PdP_{6a} (2) to PdP_{6c} (3)

W_i	Deformation zig-zags η	W_f
PdP _{6a} (I)	$X_{68}X_{87}X_{7,10}X_{10,6}, X_{13}X_{34}X_{45}X_{51}$	PdP _{6c} (I)
PdP _{6a} (I)	$X_{68}X_{87}X_{7,10}X_{10,6}, X_{36}X_{65}X_{57}X_{73}$	PdP _{6c} (IV)
PdP _{6a} (I)	$X_{36}X_{65}X_{57}X_{73}, X_{13}X_{34}X_{45}X_{51}$	PdP _{6c} (X)
PdP _{6a} (II)	$X_{68}X_{87}X_{7,10}X_{10,6}, X_{13}X_{32}X_{24}X_{41}$	PdP _{6c} (VII)
PdP _{6a} (II)	$X_{36}X_{65}X_{57}X_{73}, X_{13}X_{32}X_{24}X_{41}$	PdP _{6c} (XV)
PdP _{6a} (II)	$X_{68}X_{87}X_{7,10}X_{10,6}, X_{36}X_{65}X_{57}X_{73}$	PdP _{6c} (XVI)
PdP _{6a} (III)	$X_{68}X_{87}X_{7,10}X_{10,6}, X_{19}X_{92}X_{2,10}X_{10,1}$	PdP _{6c} (V)
PdP _{6a} (III)	$X_{36}X_{65}X_{57}X_{73}, X_{19}X_{92}X_{2,10}X_{10,1}$	PdP _{6c} (VI)
PdP _{6a} (III)	$X_{36}X_{65}X_{57}X_{73}, X_{68}X_{87}X_{7,10}X_{10,6}$	PdP _{6c} (XXIII)
PdP _{6a} (IV)	$X_{68}X_{87}X_{7,10}X_{10,6}, X_{19}X_{93}X_{32}X_{21}$	PdP _{6c} (VIII)
PdP _{6a} (IV)	$X_{68}X_{87}X_{7,10}X_{10,6}, X_{2,10}X_{10,9}X_{98}X_{82}$	PdP _{6c} (XIX)
PdP _{6a} (IV)	$X_{2,10}X_{10,9}X_{98}X_{82}, X_{19}X_{93}X_{32}X_{21}$	PdP _{6c} (XXIV)

B.5 Deformations between toric phases with $g = 11$ **B.5.1** $L^{5,6,1}$ to $K^{2,5,1,4}$

W_i	Deformation zig-zags η	W_f
$L^{5,6,1}$ (I)	$X_{8,11}X_{11,9}X_{9,10}X_{10,8}$	$K^{2,5,1,4}$ (I)
$L^{5,6,1}$ (I)	$X_{1,10}X_{10,2}X_{2,11}X_{11,1}$	$K^{2,5,1,4}$ (II)
$L^{5,6,1}$ (I)	$X_{68}X_{87}X_{79}X_{96}$	$K^{2,5,1,4}$ (II)
$L^{5,6,1}$ (I)	$X_{14}X_{42}X_{23}X_{31}$	$K^{2,5,1,4}$ (IV)
$L^{5,6,1}$ (I)	$X_{36}X_{65}X_{57}X_{73}$	$K^{2,5,1,4}$ (IV)

B.5.2 $L^{5,6,1}$ to $K^{4,4,2,3}$

W_i	Deformation zig-zags η	W_f
$L^{5,6,1}$ (I)	$X_{68}X_{87}X_{79}X_{96}, X_{1,10}X_{10,2}X_{2,11}X_{11,1}$	$K^{4,4,2,3}$ (I)
$L^{5,6,1}$ (I)	$X_{14}X_{42}X_{23}X_{31}, X_{8,11}X_{11,9}X_{9,10}X_{10,8}$	$K^{4,4,2,3}$ (II)
$L^{5,6,1}$ (I)	$X_{36}X_{65}X_{57}X_{73}, X_{8,11}X_{11,9}X_{9,10}X_{10,8}$	$K^{4,4,2,3}$ (II)
$L^{5,6,1}$ (I)	$X_{14}X_{42}X_{23}X_{31}, X_{68}X_{87}X_{79}X_{96}$	$K^{4,4,2,3}$ (III)
$L^{5,6,1}$ (I)	$X_{36}X_{65}X_{57}X_{73}, X_{1,10}X_{10,2}X_{2,11}X_{11,1}$	$K^{4,4,2,3}$ (III)
$L^{5,6,1}$ (I)	$X_{14}X_{42}X_{23}X_{31}, X_{36}X_{65}X_{57}X_{73}$	$K^{4,4,2,3}$ (VI)
$L^{5,6,1}$ (I)	$X_{68}X_{87}X_{79}X_{96}, X_{8,11}X_{11,9}X_{9,10}X_{10,8}$	$K^{4,4,2,3}$ (VII)
$L^{5,6,1}$ (I)	$X_{8,11}X_{11,9}X_{9,10}X_{10,8}, X_{1,10}X_{10,2}X_{2,11}X_{11,1}$	$K^{4,4,2,3}$ (VII)
$L^{5,6,1}$ (I)	$X_{14}X_{42}X_{23}X_{31}, X_{1,10}X_{10,2}X_{2,11}X_{11,1}$	$K^{4,4,2,3}$ (XVI)
$L^{5,6,1}$ (I)	$X_{36}X_{65}X_{57}X_{73}, X_{68}X_{87}X_{79}X_{96}$	$K^{4,4,2,3}$ (XVI)

B.6 Deformations between toric phases with $g = 12$

B.6.1 $\mathbb{C}^3/(\mathbb{Z}_2 \times \mathbb{Z}_6) (1, 0, 1)(1, 0, 5)$ to $L^{1,5,1}/\mathbb{Z}_2 (1, 0, 0, 1)$

W_i	Deformation zig-zags η	W_f
$\mathbb{C}^3/(\mathbb{Z}_2 \times \mathbb{Z}_6) (I)$	$X_{16}X_{62}X_{25}X_{51}$	$L^{1,5,1}/\mathbb{Z}_2 (I)$
$\mathbb{C}^3/(\mathbb{Z}_2 \times \mathbb{Z}_6) (I)$	$X_{19}X_{92}X_{2,10}X_{10,1}$	$L^{1,5,1}/\mathbb{Z}_2 (I)$
$\mathbb{C}^3/(\mathbb{Z}_2 \times \mathbb{Z}_6) (I)$	$X_{37}X_{74}X_{48}X_{83}$	$L^{1,5,1}/\mathbb{Z}_2 (I)$
$\mathbb{C}^3/(\mathbb{Z}_2 \times \mathbb{Z}_6) (I)$	$X_{39}X_{94}X_{4,10}X_{10,3}$	$L^{1,5,1}/\mathbb{Z}_2 (I)$
$\mathbb{C}^3/(\mathbb{Z}_2 \times \mathbb{Z}_6) (I)$	$X_{5,12}X_{12,6}X_{6,11}X_{11,5}$	$L^{1,5,1}/\mathbb{Z}_2 (I)$
$\mathbb{C}^3/(\mathbb{Z}_2 \times \mathbb{Z}_6) (I)$	$X_{7,12}X_{12,8}X_{8,11}X_{11,7}$	$L^{1,5,1}/\mathbb{Z}_2 (I)$

B.6.2 $\mathbb{C}^3/(\mathbb{Z}_2 \times \mathbb{Z}_6) (1, 0, 1)(1, 0, 5)$ to $SPP/(\mathbb{Z}_2 \times \mathbb{Z}_2) (1, 0, 0, 1)(0, 1, 1, 0)$

W_i	Deformation zig-zags η	W_f
$\mathbb{C}^3/(\mathbb{Z}_2 \times \mathbb{Z}_6) (I)$	$X_{16}X_{62}X_{25}X_{51}, X_{39}X_{94}X_{4,10}X_{10,3}$	$SPP/(\mathbb{Z}_2 \times \mathbb{Z}_2) (I)$
$\mathbb{C}^3/(\mathbb{Z}_2 \times \mathbb{Z}_6) (I)$	$X_{16}X_{62}X_{25}X_{51}, X_{7,12}X_{12,8}X_{8,11}X_{11,7}$	$SPP/(\mathbb{Z}_2 \times \mathbb{Z}_2) (I)$
$\mathbb{C}^3/(\mathbb{Z}_2 \times \mathbb{Z}_6) (I)$	$X_{37}X_{74}X_{48}X_{83}, X_{19}X_{92}X_{2,10}X_{10,1}$	$SPP/(\mathbb{Z}_2 \times \mathbb{Z}_2) (I)$
$\mathbb{C}^3/(\mathbb{Z}_2 \times \mathbb{Z}_6) (I)$	$X_{39}X_{94}X_{4,10}X_{10,3}, X_{7,12}X_{12,8}X_{8,11}X_{11,7}$	$SPP/(\mathbb{Z}_2 \times \mathbb{Z}_2) (I)$
$\mathbb{C}^3/(\mathbb{Z}_2 \times \mathbb{Z}_6) (I)$	$X_{5,12}X_{12,6}X_{6,11}X_{11,5}, X_{19}X_{92}X_{2,10}X_{10,1}$	$SPP/(\mathbb{Z}_2 \times \mathbb{Z}_2) (I)$
$\mathbb{C}^3/(\mathbb{Z}_2 \times \mathbb{Z}_6) (I)$	$X_{5,12}X_{12,6}X_{6,11}X_{11,5}, X_{37}X_{74}X_{48}X_{83}$	$SPP/(\mathbb{Z}_2 \times \mathbb{Z}_2) (I)$
$\mathbb{C}^3/(\mathbb{Z}_2 \times \mathbb{Z}_6) (I)$	$X_{16}X_{62}X_{25}X_{51}, X_{37}X_{74}X_{48}X_{83}$	$SPP/(\mathbb{Z}_2 \times \mathbb{Z}_2) (II)$
$\mathbb{C}^3/(\mathbb{Z}_2 \times \mathbb{Z}_6) (I)$	$X_{39}X_{94}X_{4,10}X_{10,3}, X_{5,12}X_{12,6}X_{6,11}X_{11,5}$	$SPP/(\mathbb{Z}_2 \times \mathbb{Z}_2) (II)$
$\mathbb{C}^3/(\mathbb{Z}_2 \times \mathbb{Z}_6) (I)$	$X_{7,12}X_{12,8}X_{8,11}X_{11,7}, X_{19}X_{92}X_{2,10}X_{10,1}$	$SPP/(\mathbb{Z}_2 \times \mathbb{Z}_2) (II)$
$\mathbb{C}^3/(\mathbb{Z}_2 \times \mathbb{Z}_6) (I)$	$X_{16}X_{62}X_{25}X_{51}, X_{19}X_{92}X_{2,10}X_{10,1}$	$SPP/(\mathbb{Z}_2 \times \mathbb{Z}_2) (IV)$
$\mathbb{C}^3/(\mathbb{Z}_2 \times \mathbb{Z}_6) (I)$	$X_{16}X_{62}X_{25}X_{51}, X_{5,12}X_{12,6}X_{6,11}X_{11,5}$	$SPP/(\mathbb{Z}_2 \times \mathbb{Z}_2) (IV)$
$\mathbb{C}^3/(\mathbb{Z}_2 \times \mathbb{Z}_6) (I)$	$X_{39}X_{94}X_{4,10}X_{10,3}, X_{19}X_{92}X_{2,10}X_{10,1}$	$SPP/(\mathbb{Z}_2 \times \mathbb{Z}_2) (IV)$
$\mathbb{C}^3/(\mathbb{Z}_2 \times \mathbb{Z}_6) (I)$	$X_{39}X_{94}X_{4,10}X_{10,3}, X_{37}X_{74}X_{48}X_{83}$	$SPP/(\mathbb{Z}_2 \times \mathbb{Z}_2) (IV)$
$\mathbb{C}^3/(\mathbb{Z}_2 \times \mathbb{Z}_6) (I)$	$X_{5,12}X_{12,6}X_{6,11}X_{11,5}, X_{7,12}X_{12,8}X_{8,11}X_{11,7}$	$SPP/(\mathbb{Z}_2 \times \mathbb{Z}_2) (IV)$
$\mathbb{C}^3/(\mathbb{Z}_2 \times \mathbb{Z}_6) (I)$	$X_{7,12}X_{12,8}X_{8,11}X_{11,7}, X_{37}X_{74}X_{48}X_{83}$	$SPP/(\mathbb{Z}_2 \times \mathbb{Z}_2) (IV)$

B.6.3 $\mathbb{C}^3/(\mathbb{Z}_2 \times \mathbb{Z}_6) (1, 0, 1)(1, 0, 5)$ to $\mathcal{C}/(\mathbb{Z}_3 \times \mathbb{Z}_2) (1, 0, 0, 2)(0, 1, 1, 0)$

W_i	Deformation zig-zags η	W_f
$\mathbb{C}^3/(\mathbb{Z}_2 \times \mathbb{Z}_6)$ (I)	$X_{5,12}X_{12,6}X_{6,11}X_{11,5}, X_{37}X_{74}X_{48}X_{83}, X_{19}X_{92}X_{2,10}X_{10,1}$	$\mathcal{C}/(\mathbb{Z}_3 \times \mathbb{Z}_2)$ (I)
$\mathbb{C}^3/(\mathbb{Z}_2 \times \mathbb{Z}_6)$ (I)	$X_{39}X_{94}X_{4,10}X_{10,3}, X_{5,12}X_{12,6}X_{6,11}X_{11,5}, X_{19}X_{92}X_{2,10}X_{10,1}$	$\mathcal{C}/(\mathbb{Z}_3 \times \mathbb{Z}_2)$ (II)
$\mathbb{C}^3/(\mathbb{Z}_2 \times \mathbb{Z}_6)$ (I)	$X_{39}X_{94}X_{4,10}X_{10,3}, X_{5,12}X_{12,6}X_{6,11}X_{11,5}, X_{37}X_{74}X_{48}X_{83}$	$\mathcal{C}/(\mathbb{Z}_3 \times \mathbb{Z}_2)$ (II)
$\mathbb{C}^3/(\mathbb{Z}_2 \times \mathbb{Z}_6)$ (I)	$X_{39}X_{94}X_{4,10}X_{10,3}, X_{5,12}X_{12,6}X_{6,11}X_{11,5}, X_{7,12}X_{12,8}X_{8,11}X_{11,7}$	$\mathcal{C}/(\mathbb{Z}_3 \times \mathbb{Z}_2)$ (II)
$\mathbb{C}^3/(\mathbb{Z}_2 \times \mathbb{Z}_6)$ (I)	$X_{39}X_{94}X_{4,10}X_{10,3}, X_{7,12}X_{12,8}X_{8,11}X_{11,7}, X_{19}X_{92}X_{2,10}X_{10,1}$	$\mathcal{C}/(\mathbb{Z}_3 \times \mathbb{Z}_2)$ (II)
$\mathbb{C}^3/(\mathbb{Z}_2 \times \mathbb{Z}_6)$ (I)	$X_{5,12}X_{12,6}X_{6,11}X_{11,5}, X_{7,12}X_{12,8}X_{8,11}X_{11,7}, X_{19}X_{92}X_{2,10}X_{10,1}$	$\mathcal{C}/(\mathbb{Z}_3 \times \mathbb{Z}_2)$ (II)
$\mathbb{C}^3/(\mathbb{Z}_2 \times \mathbb{Z}_6)$ (I)	$X_{7,12}X_{12,8}X_{8,11}X_{11,7}, X_{37}X_{74}X_{48}X_{83}, X_{19}X_{92}X_{2,10}X_{10,1}$	$\mathcal{C}/(\mathbb{Z}_3 \times \mathbb{Z}_2)$ (II)
$\mathbb{C}^3/(\mathbb{Z}_2 \times \mathbb{Z}_6)$ (I)	$X_{39}X_{94}X_{4,10}X_{10,3}, X_{37}X_{74}X_{48}X_{83}, X_{19}X_{92}X_{2,10}X_{10,1}$	$\mathcal{C}/(\mathbb{Z}_3 \times \mathbb{Z}_2)$ (VII)
$\mathbb{C}^3/(\mathbb{Z}_2 \times \mathbb{Z}_6)$ (I)	$X_{39}X_{94}X_{4,10}X_{10,3}, X_{7,12}X_{12,8}X_{8,11}X_{11,7}, X_{37}X_{74}X_{48}X_{83}$	$\mathcal{C}/(\mathbb{Z}_3 \times \mathbb{Z}_2)$ (VII)
$\mathbb{C}^3/(\mathbb{Z}_2 \times \mathbb{Z}_6)$ (I)	$X_{5,12}X_{12,6}X_{6,11}X_{11,5}, X_{7,12}X_{12,8}X_{8,11}X_{11,7}, X_{37}X_{74}X_{48}X_{83}$	$\mathcal{C}/(\mathbb{Z}_3 \times \mathbb{Z}_2)$ (VII)

Appendix C

Kähler chamber mapping of PdP_{3a} to PdP_{3c} phase A

In this appendix we present the mapping of the multiple Kähler chambers associated to the main publication, for the zig-zag deformation between the dimer models PdP_{3a} ($\mu = 0$) and PdP_{3c} phase A ($\mu = \infty$).

For the sake of self-containedness, we include the toric superpotential W , quiver \mathcal{Q} , toric diagram Δ , perfect matching matrix P , zig-zag path η , and zig-zag operator \mathcal{O}_η . Additionally, we make reference to the Kähler chambers $\{K_i\}_i$ and fine triangulations $\{T_\Delta^{(i)}\}_i$ of a particular toric diagram. We distinguish the data of the models by a prime in the variables: *e.g.* (W, \mathcal{Q}) and (W', \mathcal{Q}') denote the dimer models at $\mu = 0$ and $\mu = \infty$, respectively. We also include the deformation $\delta W = \mu \mathcal{O}_\eta$ that triggers the flow from PdP_{3a} to PdP_{3c} phase A, which approaches the latter from the direction $\delta W' = \frac{1}{\mu} \mathcal{O}'_{\eta'}$.

PdP_{3a} quiver, superpotential and perfect matching data

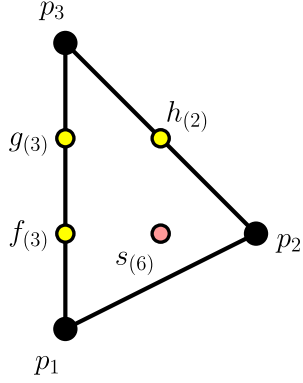
- *Superpotential:*

$$\begin{aligned} W = & X_{12}X_{26}X_{61} + X_{13}X_{35}X_{51} + X_{15}X_{54}X_{41} + X_{24}X_{43}X_{32} \\ & + X_{25}X_{56}X_{62} + X_{34}X_{46}X_{63} - X_{12}X_{25}X_{51} - X_{13}X_{34}X_{41} \\ & - X_{15}X_{56}X_{61} - X_{24}X_{46}X_{62} - X_{26}X_{63}X_{32} - X_{35}X_{54}X_{43} \end{aligned}$$

- *Zig-zag deformation (zig-zag η and corresponding operator):*

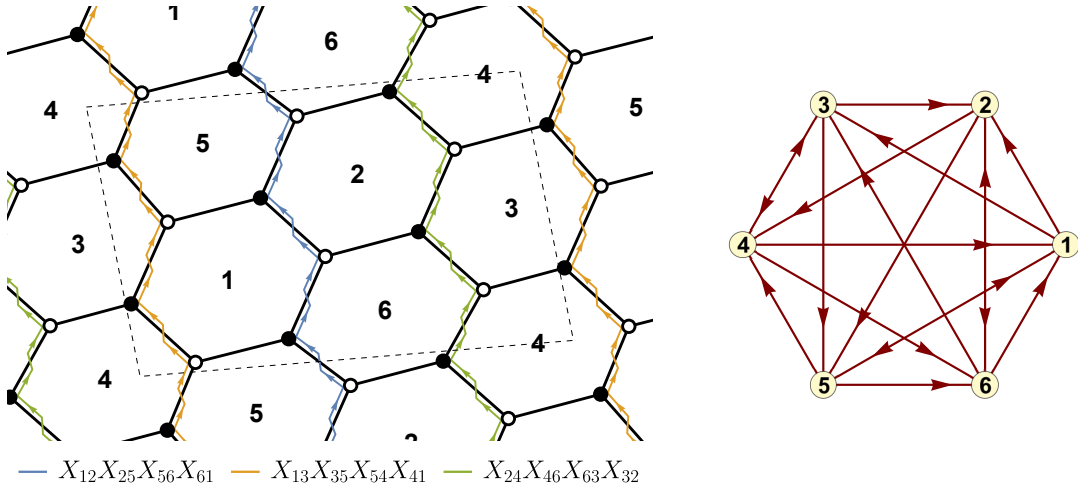
$$\eta = X_{12}X_{25}X_{56}X_{61} \quad \delta W = \mu \mathcal{O}_\eta = \mu (X_{15}X_{51} - X_{26}X_{62})$$

- *Perfect matching matrix (variable labelling):*



$$P = \begin{pmatrix} & f_1 & f_2 & f_3 & g_1 & g_2 & g_3 & h_1 & h_2 & p_1 & p_2 & p_3 & s_1 & s_2 & s_3 & s_4 & s_5 & s_6 \\ X_{12} & 1 & 1 & 0 & 1 & 0 & 0 & 0 & 0 & 1 & 0 & 0 & 1 & 1 & 0 & 0 & 0 & 0 \\ X_{13} & 1 & 0 & 0 & 1 & 1 & 0 & 1 & 0 & 0 & 0 & 1 & 1 & 0 & 0 & 0 & 0 & 0 \\ X_{15} & 0 & 0 & 0 & 0 & 0 & 0 & 1 & 0 & 0 & 1 & 0 & 1 & 1 & 1 & 0 & 0 & 0 \\ X_{24} & 1 & 0 & 1 & 0 & 1 & 0 & 0 & 0 & 1 & 0 & 0 & 0 & 0 & 1 & 1 & 0 & 0 \\ X_{25} & 0 & 0 & 1 & 0 & 1 & 1 & 1 & 0 & 0 & 0 & 1 & 0 & 0 & 1 & 0 & 0 & 0 \\ X_{26} & 0 & 0 & 0 & 0 & 0 & 0 & 1 & 0 & 0 & 1 & 0 & 0 & 0 & 1 & 1 & 1 & 0 \\ X_{32} & 0 & 1 & 0 & 1 & 0 & 1 & 0 & 1 & 0 & 0 & 1 & 0 & 1 & 0 & 0 & 0 & 0 \\ X_{34} & 0 & 0 & 0 & 0 & 0 & 0 & 0 & 1 & 0 & 1 & 0 & 0 & 1 & 1 & 1 & 0 & 0 \\ X_{35} & 0 & 1 & 1 & 0 & 0 & 1 & 0 & 0 & 1 & 0 & 0 & 0 & 1 & 1 & 0 & 0 & 0 \\ X_{41} & 0 & 1 & 1 & 0 & 0 & 1 & 0 & 0 & 1 & 0 & 0 & 0 & 0 & 0 & 0 & 1 & 1 \\ X_{43} & 0 & 0 & 0 & 0 & 0 & 0 & 1 & 0 & 0 & 1 & 0 & 1 & 0 & 0 & 0 & 1 & 1 \\ X_{46} & 0 & 1 & 0 & 1 & 0 & 1 & 1 & 0 & 0 & 0 & 1 & 0 & 0 & 0 & 0 & 1 & 0 \\ X_{51} & 0 & 0 & 0 & 0 & 0 & 0 & 0 & 1 & 0 & 1 & 0 & 0 & 0 & 0 & 1 & 1 & 1 \\ X_{54} & 1 & 0 & 0 & 1 & 1 & 0 & 0 & 1 & 0 & 0 & 1 & 0 & 0 & 0 & 1 & 0 & 0 \\ X_{56} & 1 & 1 & 0 & 1 & 0 & 0 & 0 & 0 & 1 & 0 & 0 & 0 & 0 & 0 & 1 & 1 & 0 \\ X_{61} & 0 & 0 & 1 & 0 & 1 & 1 & 0 & 1 & 0 & 0 & 1 & 0 & 0 & 0 & 0 & 0 & 1 \\ X_{62} & 0 & 0 & 0 & 0 & 0 & 0 & 0 & 1 & 0 & 1 & 0 & 1 & 1 & 0 & 0 & 0 & 1 \\ X_{63} & 1 & 0 & 1 & 0 & 1 & 0 & 0 & 0 & 1 & 0 & 0 & 1 & 0 & 0 & 0 & 0 & 1 \end{pmatrix}$$

- *Brane tiling, quiver and toric diagram:*



PdP_{3c} phase A quiver, superpotential and perfect matching data

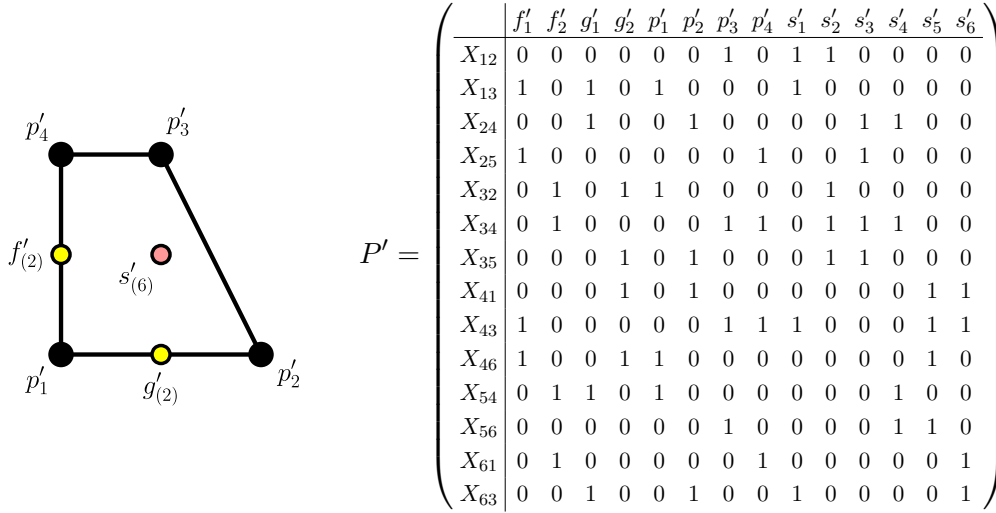
- *Superpotential:*

$$W' = X_{24}X_{43}X_{32} + X_{34}X_{46}X_{63} + X_{12}X_{25}X_{54}X_{41} + X_{13}X_{35}X_{56}X_{61} \\ - X_{13}X_{34}X_{41} - X_{35}X_{54}X_{43} - X_{12}X_{24}X_{46}X_{61} - X_{25}X_{56}X_{63}X_{32}$$

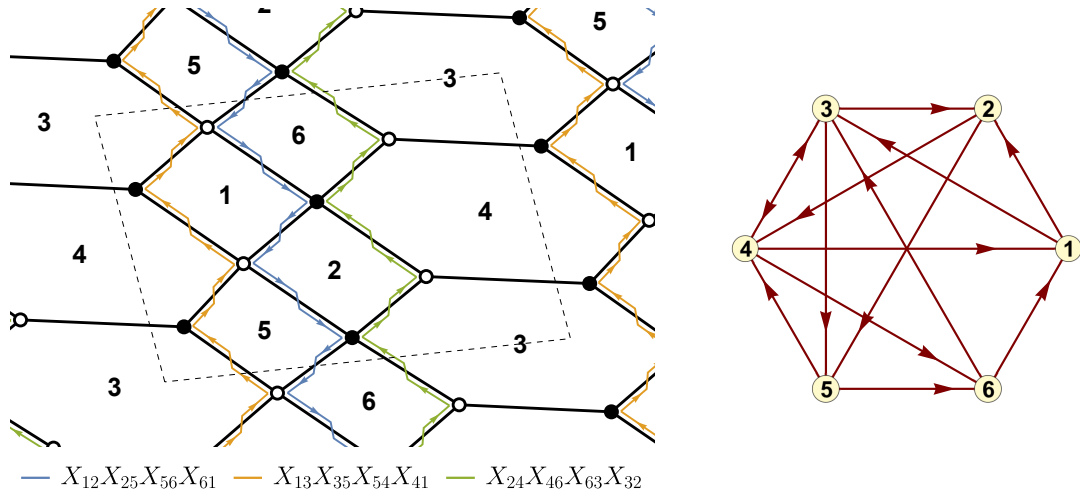
- *Zig-zag deformation (zig-zag η and corresponding operator):*

$$\eta' = X_{12}X_{25}X_{56}X_{61} \quad \delta W' = \frac{1}{\mu} \mathcal{O}'_{\eta'} = \frac{1}{\mu} (X_{24}X_{46}X_{63}X_{32} - X_{13}X_{35}X_{54}X_{51})$$

- *Toric diagram and perfect matching matrix (variable labelling):*



- *Brane tiling and quiver:*



Merging of Kähler chambers

Recall that a Kähler chamber compatible with the choice K of a unique perfect matching in the toric diagram and a full resolution described by T_Δ is

$$\mathcal{R}(K, T_\Delta) = \bigcap_{(x,y) \in T_\Delta} \mathcal{R}(\mathcal{Q}_{K_x}) \cap \mathcal{R}(\mathcal{Q}_{K_y}) \cap \mathcal{R}(\mathcal{Q}_{K_x, K_y}),$$

where K_x represents the choice of perfect matching associated to the lattice point $x \in \Delta$. We define the subquiver \mathcal{Q}_{K_x} as the quiver \mathcal{Q} with edges not in the perfect matching K_x .

The intersection of the θ -semistability conditions for a general module in all the sub- quiver representation spaces $\text{Rep}(\mathcal{Q}_p, \mathbb{1})$, $p \in K$, defines the region of compatibility in the resolutions space $\xi \in \mathbb{R}^G$, written as

$$\mathcal{R}(\mathcal{Q}) = \left\{ \xi \in \mathbb{R}^G \left| \xi \cdot \dim V \leq 0, \sum_i \xi_i = 0, \forall V \in \text{Rep}(\mathcal{Q}, \mathbb{1}) \right. \right\}.$$

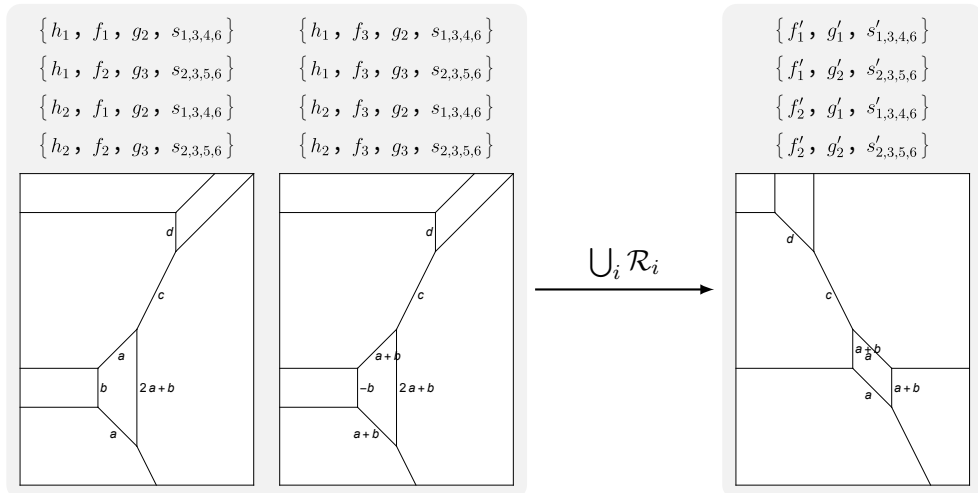
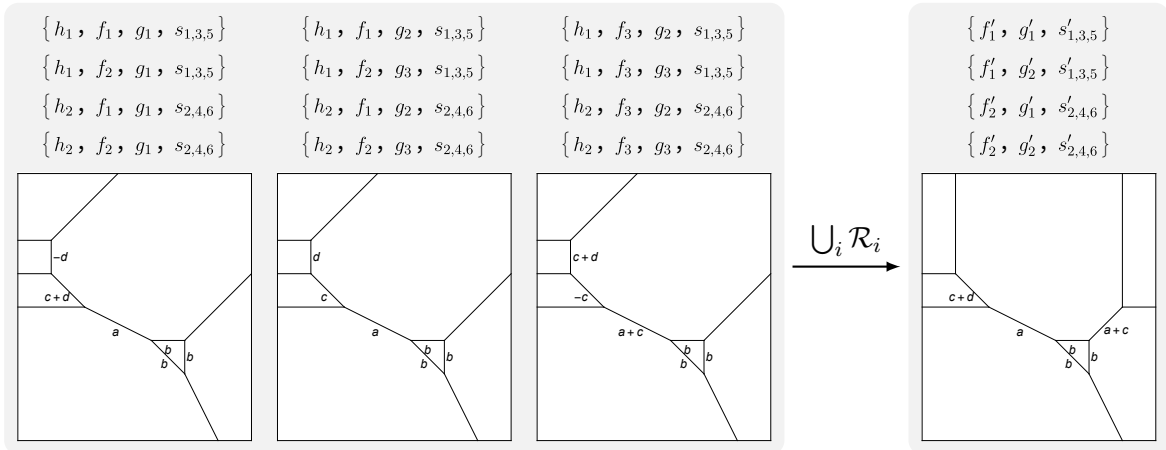
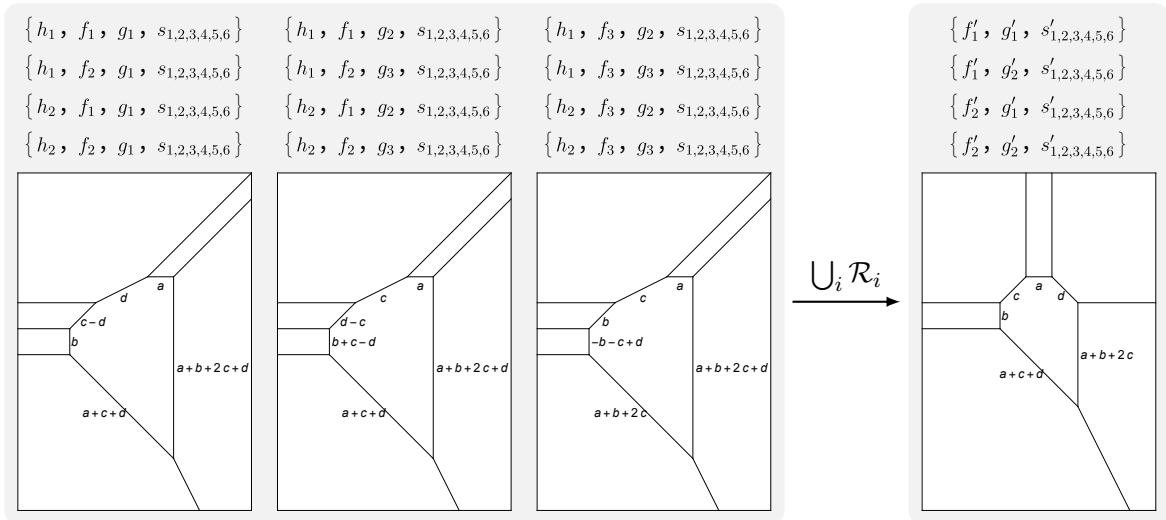
Below, we will represent how the Kähler chamber merge when flowing from PdP_{3a} ($\mu = 0$) to PdP_{3c} phase A ($\mu = \infty$). Each row of diagrams follows the following pattern:

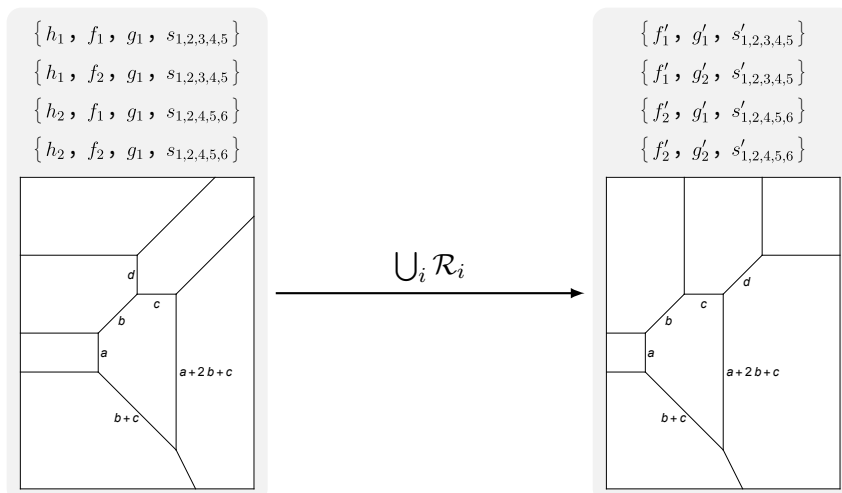
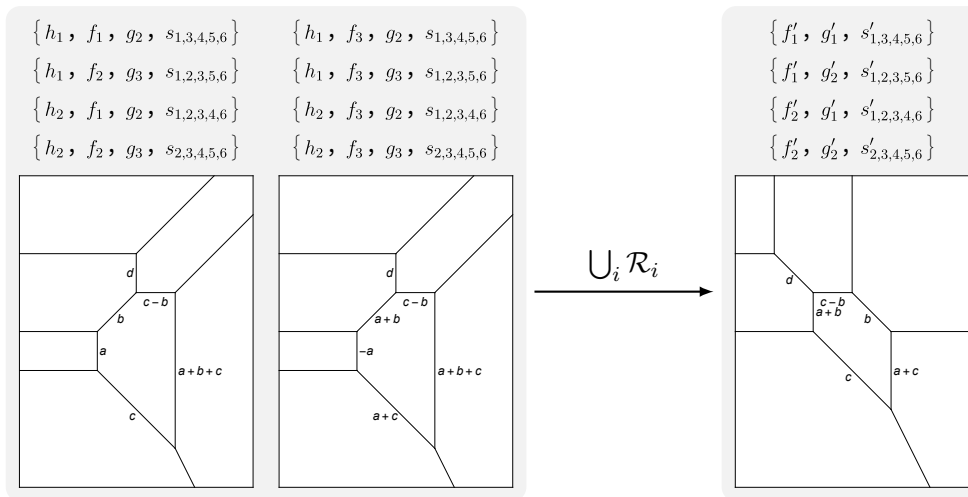
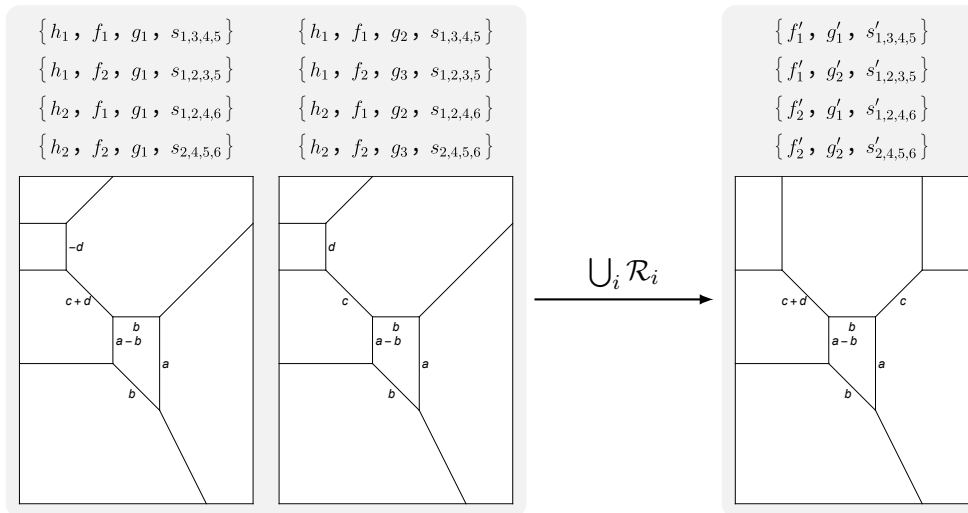
- The *left* rectangle represents the multiple chambers $\{\mathcal{R}(-, T_\Delta)\}$ of PdP_{3a} , which merge to $\mathcal{R}(-, T'_\Delta)$ of PdP_{3c} phase A, in the *right* rectangle, between pairs of (p, q) -webs dual to triangulations (T_Δ, T'_Δ) .
- The left (p, q) -web figures are labelled (above) by the *multiple* triplets $\{K_1, K_2, K_3\}$, pairs $\{K_1, K_2\}$, or chamber K_1 , compatible with the T_Δ , which merge with the chambers K' labelling the (p, q) -web figure on the right, following the same line-by-line ordering, as presented.

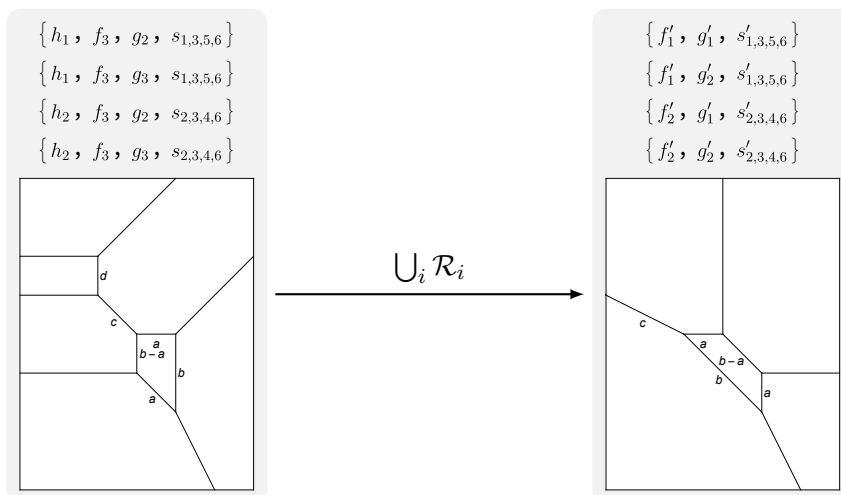
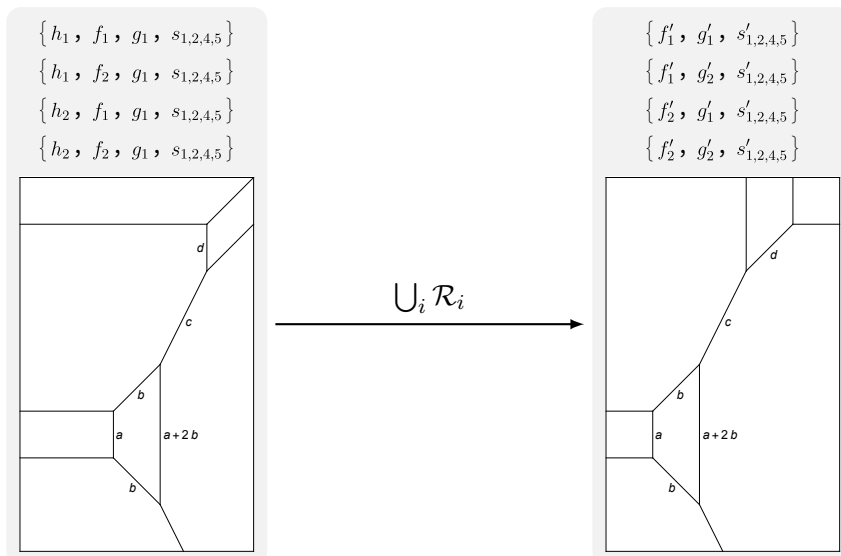
$$\bigcup_{i=1}^{3,2,1} \mathcal{R}(T_\Delta, K_i) = \mathcal{R}(T'_\Delta, K')$$

Due to the large amount of combinations K, K' we decided to group the internal point perfect matchings s_i, s'_i . For example, $\{h_1, f_1, g_1, s_{1,2,3,4,5,6}\}$ means K can be any of $\{h_1, f_1, g_1, s_i\}$ for $i \leq 6$.

- Each finite segment of the (p, q) -web is “dressed” with the volume of the corresponding \mathbb{P}^1 , which obeys positivity conditions for each choice region $\mathcal{R}(K_i, T_\Delta)$. When merging the regions on the left, they are consistent with the positivity constraint of the volumes in the right region $\mathcal{R}(K', T'_\Delta)$. Fundamental volumes are given by variables $\{a, b, c, d\}$, which can be thought of as piecewise linear functions of the FI parameters $\{\xi_i\}_{i \leq 6}$ (depending on the choice of K).







Bibliography

- [1] S. Cremonesi and J. Sá, *Zig-zag deformations of toric quiver gauge theories. Part I. Reflexive polytopes*, *JHEP* **05** (2024) 114 [2312.13909].
- [2] J. Sá, “QuiverGaugeTheory: a Mathematica package for 4d $\mathcal{N} = 1$ quiver gauge theories.” Available at github.com/jose-a-sa/QuiverGaugeTheory, 2023.
- [3] J. Sá, “InterfaceM2: a Macaulay2 interface for Mathematica.” Available at github.com/jose-a-sa/InterfaceM2, 2023.
- [4] J. Sá, “LieACh: a LieART extension for 1-dim Lie algebra representations.” Available at github.com/jose-a-sa/LieACh, 2023.
- [5] J. Polchinski, *String theory. Vol. 1: An introduction to the bosonic string*, Cambridge Monographs on Mathematical Physics. Cambridge University Press, 12, 2007, 10.1017/CBO9780511816079.
- [6] J. Polchinski, *String theory. Vol. 2: Superstring theory and beyond*, Cambridge Monographs on Mathematical Physics. Cambridge University Press, 12, 2007, 10.1017/CBO9780511618123.
- [7] A. Uranga, “Graduate Course in String Theory.” Published in <https://members.ift.uam-csic.es/auranga/firstpage.html>, 2005.
- [8] C. V. Johnson, *D-Branes*, Cambridge Monographs on Mathematical Physics. Cambridge University Press, 2002.
- [9] D. Tong, *String Theory*, 0908.0333.
- [10] K. Becker, M. Becker and J. H. Schwarz, *String Theory and M-Theory: A Modern Introduction*. Cambridge University Press, 2006.
- [11] M. Born and L. Infeld, *Foundations of the new field theory*, *Proc. Roy. Soc. Lond. A* **144** (1934) 425.
- [12] S. S. Gubser, I. R. Klebanov and A. M. Polyakov, *Gauge theory correlators from noncritical string theory*, *Phys. Lett. B* **428** (1998) 105 [hep-th/9802109].

- [13] A. Hanany and E. Witten, *Type IIB superstrings, BPS monopoles, and three-dimensional gauge dynamics*, *Nucl. Phys. B* **492** (1997) 152 [[hep-th/9611230](#)].
- [14] E. Witten, *Branes and the dynamics of QCD*, *Nucl. Phys. B* **507** (1997) 658 [[hep-th/9706109](#)].
- [15] O. Aharony, S. S. Gubser, J. M. Maldacena, H. Ooguri and Y. Oz, *Large N field theories, string theory and gravity*, *Phys. Rept.* **323** (2000) 183 [[hep-th/9905111](#)].
- [16] M. R. Douglas and G. W. Moore, *D-branes, quivers, and ALE instantons*, [hep-th/9603167](#).
- [17] A. E. Lawrence, N. Nekrasov and C. Vafa, *On conformal field theories in four-dimensions*, *Nucl. Phys. B* **533** (1998) 199 [[hep-th/9803015](#)].
- [18] M. Bertolini, *Four lectures on the gauge/gravity correspondence*, *Int. J. Mod. Phys. A* **18** (2003) 5647 [[hep-th/0303160](#)].
- [19] M. R. Douglas, B. R. Greene and D. R. Morrison, *Orbifold resolution by D-branes*, *Nucl. Phys. B* **506** (1997) 84 [[hep-th/9704151](#)].
- [20] D.-E. Diaconescu, M. R. Douglas and J. Gomis, *Fractional branes and wrapped branes*, *JHEP* **02** (1998) 013 [[hep-th/9712230](#)].
- [21] J. McKay, *Graphs, Singularities, and Finite Groups*, in *The Santa Cruz Conference on Finite Groups*, vol. 37 of *Proceedings of Symposia in Pure Mathematics*, pp. 183–186, American Mathematical Society, 1981, [DOI](#).
- [22] I. R. Klebanov and E. Witten, *Superconformal field theory on three-branes at a Calabi-Yau singularity*, *Nucl. Phys. B* **536** (1998) 199 [[hep-th/9807080](#)].
- [23] B. S. Acharya, J. M. Figueroa-O’Farrill, C. M. Hull and B. J. Spence, *Branes at conical singularities and holography*, *Adv. Theor. Math. Phys.* **2** (1999) 1249 [[hep-th/9808014](#)].
- [24] D. R. Morrison and M. R. Plesser, *Nonspherical horizons. 1.*, *Adv. Theor. Math. Phys.* **3** (1999) 1 [[hep-th/9810201](#)].
- [25] C. Beasley, B. R. Greene, C. I. Lazaroiu and M. R. Plesser, *D3-branes on partial resolutions of Abelian quotient singularities of Calabi-Yau threefolds*, *Nucl. Phys. B* **566** (2000) 599 [[hep-th/9907186](#)].
- [26] B. Feng, A. Hanany and Y.-H. He, *D-brane gauge theories from toric singularities and toric duality*, *Nucl. Phys. B* **595** (2001) 165 [[hep-th/0003085](#)].
- [27] A. Hanany and A. Iqbal, *Quiver theories from D6 branes via mirror symmetry*, *JHEP* **04** (2002) 009 [[hep-th/0108137](#)].

- [28] J. M. Maldacena, *The Large N limit of superconformal field theories and supergravity*, *Adv. Theor. Math. Phys.* **2** (1998) 231 [[hep-th/9711200](#)].
- [29] E. Witten, *Anti-de Sitter space and holography*, *Adv. Theor. Math. Phys.* **2** (1998) 253 [[hep-th/9802150](#)].
- [30] H. Verlinde and M. Wijnholt, *Building the standard model on a $D3$ -brane*, *JHEP* **01** (2007) 106 [[hep-th/0508089](#)].
- [31] M. Wijnholt, *Geometry of Particle Physics*, *Adv. Theor. Math. Phys.* **13** (2009) 947 [[hep-th/0703047](#)].
- [32] M. Cvetič, H. Lu, D. N. Page and C. N. Pope, *New Einstein-Sasaki spaces in five and higher dimensions*, *Phys. Rev. Lett.* **95** (2005) 071101 [[hep-th/0504225](#)].
- [33] J. P. Gauntlett, D. Martelli, J. Sparks and D. Waldram, *Sasaki-Einstein metrics on $S^2 \times S^3$* , *Adv. Theor. Math. Phys.* **8** (2004) 711 [[hep-th/0403002](#)].
- [34] D. Martelli and J. Sparks, *Toric Sasaki-Einstein metrics on $S^2 \times S^3$* , *Phys. Lett. B* **621** (2005) 208 [[hep-th/0505027](#)].
- [35] A. Butti, D. Forcella and A. Zaffaroni, *Counting BPS baryonic operators in CFTs with Sasaki-Einstein duals*, *JHEP* **06** (2007) 069 [[hep-th/0611229](#)].
- [36] A. Butti, D. Forcella, A. Hanany, D. Vegh and A. Zaffaroni, *Counting Chiral Operators in Quiver Gauge Theories*, *JHEP* **11** (2007) 092 [[0705.2771](#)].
- [37] M. Wijnholt, *Large volume perspective on branes at singularities*, *Adv. Theor. Math. Phys.* **7** (2003) 1117 [[hep-th/0212021](#)].
- [38] C. P. Herzog, *Exceptional collections and del Pezzo gauge theories*, *JHEP* **04** (2004) 069 [[hep-th/0310262](#)].
- [39] F. Cachazo, B. Fiol, K. A. Intriligator, S. Katz and C. Vafa, *A Geometric unification of dualities*, *Nucl. Phys. B* **628** (2002) 3 [[hep-th/0110028](#)].
- [40] A. Hanany and K. D. Kennaway, *Dimer models and toric diagrams*, [hep-th/0503149](#).
- [41] S. Franco, A. Hanany, K. D. Kennaway, D. Vegh and B. Wecht, *Brane dimers and quiver gauge theories*, *JHEP* **01** (2006) 096 [[hep-th/0504110](#)].
- [42] S. Franco, A. Hanany, D. Martelli, J. Sparks, D. Vegh and B. Wecht, *Gauge theories from toric geometry and brane tilings*, *JHEP* **01** (2006) 128 [[hep-th/0505211](#)].
- [43] B. Feng, Y.-H. He, K. D. Kennaway and C. Vafa, *Dimer models from mirror symmetry and quivering amoebae*, *Adv. Theor. Math. Phys.* **12** (2008) 489 [[hep-th/0511287](#)].

- [44] K. D. Kennaway, *Brane Tilings*, *Int. J. Mod. Phys. A* **22** (2007) 2977 [0706.1660].
- [45] R. Kenyon, *An introduction to the dimer model*, 2003.
- [46] R. Kenyon, *Lectures on dimers*, 2009.
- [47] A. Hanany and D. Vegh, *Quivers, tilings, branes and rhombi*, *JHEP* **10** (2007) 029 [hep-th/0511063].
- [48] N. Seiberg, *Electric - magnetic duality in supersymmetric nonAbelian gauge theories*, *Nucl. Phys. B* **435** (1995) 129 [hep-th/9411149].
- [49] D. Berenstein and M. R. Douglas, *Seiberg duality for quiver gauge theories*, hep-th/0207027.
- [50] C. E. Beasley and M. R. Plesser, *Toric duality is Seiberg duality*, *JHEP* **12** (2001) 001 [hep-th/0109053].
- [51] B. Feng, A. Hanany and Y.-H. He, *Phase structure of D-brane gauge theories and toric duality*, *JHEP* **08** (2001) 040 [hep-th/0104259].
- [52] B. Feng, A. Hanany, Y.-H. He and A. M. Uranga, *Toric duality as Seiberg duality and brane diamonds*, *JHEP* **12** (2001) 035 [hep-th/0109063].
- [53] O. Aharony, A. Hanany and B. Kol, *Webs of (p,q) five-branes, five-dimensional field theories and grid diagrams*, *JHEP* **01** (1998) 002 [hep-th/9710116].
- [54] N. C. Leung and C. Vafa, *Branes and toric geometry*, *Adv. Theor. Math. Phys.* **2** (1998) 91 [hep-th/9711013].
- [55] A. Hanany and R.-K. Seong, *Brane Tilings and Reflexive Polygons*, *Fortsch. Phys.* **60** (2012) 695 [1201.2614].
- [56] Wolfram Research, Inc., “Mathematica, Version 13.2.” <https://www.wolfram.com/mathematica>.
- [57] D. R. Grayson and M. E. Stillman, “Macaulay2, a software system for research in algebraic geometry.” Available at <http://www.math.uiuc.edu/Macaulay2/>.
- [58] R. Feger, T. W. Kephart and R. J. Saskowski, *LieART 2.0 – A Mathematica application for Lie Algebras and Representation Theory*, *Comput. Phys. Commun.* **257** (2020) 107490 [1912.10969].
- [59] J. Fuchs and C. Schweigert, *Symmetries, Lie Algebras and Representations: A Graduate Course for Physicists*, Cambridge Monographs on Mathematical Physics. Cambridge University Press, 2003.

- [60] C. Romelsberger, *Counting chiral primaries in $N = 1$, $d=4$ superconformal field theories*, *Nucl. Phys. B* **747** (2006) 329 [[hep-th/0510060](#)].
- [61] J. Kinney, J. M. Maldacena, S. Minwalla and S. Raju, *An Index for 4 dimensional super conformal theories*, *Commun. Math. Phys.* **275** (2007) 209 [[hep-th/0510251](#)].
- [62] F. A. Dolan and H. Osborn, *Applications of the Superconformal Index for Protected Operators and q -Hypergeometric Identities to $N=1$ Dual Theories*, *Nucl. Phys. B* **818** (2009) 137 [[0801.4947](#)].
- [63] A. Gadde, L. Rastelli, S. S. Razamat and W. Yan, *The Superconformal Index of the E_6 SCFT*, *JHEP* **08** (2010) 107 [[1003.4244](#)].
- [64] A. Gadde, L. Rastelli, S. S. Razamat and W. Yan, *On the Superconformal Index of $N=1$ IR Fixed Points: A Holographic Check*, *JHEP* **03** (2011) 041 [[1011.5278](#)].
- [65] S. Franco, A. Hanany and P. Kazakopoulos, *Hidden exceptional global symmetries in 4-D CFTs*, *JHEP* **07** (2004) 060 [[hep-th/0404065](#)].
- [66] D. Cox, J. Little and D. O’Shea, *Ideals, Varieties, and Algorithms: An Introduction to Computational Algebraic Geometry and Commutative Algebra*, Undergraduate Texts in Mathematics. Springer New York, 2008.
- [67] D. Patil and U. Storch, *Introduction to Algebraic Geometry and Commutative Algebra*, IISc lecture note series. World Scientific, 2010.
- [68] D. Cox, J. Little and H. Schenck, *Toric Varieties*, Graduate studies in mathematics. American Mathematical Soc., 2011.
- [69] K. Hori, S. Katz, A. Klemm, R. Pandharipande, R. Thomas, C. Vafa et al., *Mirror symmetry*, vol. 1 of *Clay mathematics monographs*. AMS, Providence, USA, 2003.
- [70] Y.-H. He, R.-K. Seong and S.-T. Yau, *Calabi–Yau Volumes and Reflexive Polytopes*, *Commun. Math. Phys.* **361** (2018) 155 [[1704.03462](#)].
- [71] B. Nill, *Gorenstein toric Fano varieties*, *manuscripta mathematica* **116** (2005) 183 [[math/0405448](#)].
- [72] B. Nill, *Volume and lattice points of reflexive simplices*, *Discrete & Computational Geometry* **37** (2007) 301 [[math/0412480v3](#)].
- [73] A. Soibelman, *Lecture notes on quiver representations and moduli problems in algebraic geometry*, [1909.03509v2](#).
- [74] H. Derksen, J. Weyman and A. Zelevinsky, *Quivers with potentials and their representations I: Mutations*, *Selecta Mathematica* **14** (2008) 59 [[0704.0649](#)].

- [75] H. Derksen, J. Weyman and A. Zelevinsky, *Quivers with potentials and their representations II: Applications to cluster algebras*, *Journal of the American Mathematical Society* **23** (2009) 749 [[0904.0676](#)].
- [76] R. Bocklandt, T. Schedler and M. Wemyss, *Superpotentials and higher order derivations*, *Journal of Pure and Applied Algebra* **214** (2010) 1501.
- [77] A. D. King, *Moduli of representations of finite dimensional algebras*, *The Quarterly Journal of Mathematics* **45** (1994) 515.
- [78] R. Bocklandt, *Consistency conditions for dimer models*, *Glasgow Mathematical Journal* **54** (2012) 429.
- [79] D. Mumford, J. Fogarty and F. Kirwan, *Geometric Invariant Theory*, vol. 34 of *Ergebnisse der Mathematik und ihrer Grenzgebiete (2)*. Springer-Verlag, 3 ed., 1994.
- [80] J. Marsden and A. Weinstein, *Reduction of symplectic manifolds with symmetry*, *Rept. Math. Phys.* **5** (1974) 121.
- [81] B. Kostant and S. Sternberg, *Symplectic reduction, BRS cohomology, and infinite-dimensional clifford algebras*, *Annals of Physics* **176** (1987) 49.
- [82] G. Kempf and L. Ness, *The length of vectors in representation spaces*, in *Algebraic Geometry*, K. Lønsted, ed., Springer Berlin Heidelberg, 1979.
- [83] R. Hartshorne, *Algebraic Geometry*, Graduate Texts in Mathematics. Springer, 1977.
- [84] P. Newstead, *Introduction to Moduli Problems and Orbit Spaces*, Lectures on Mathematics and Physics. Tata Institute of Fundamental Research, 2012.
- [85] A. C. da Silva, *Lectures on Symplectic Geometry*, Lecture Notes in Mathematics. Springer, 2001.
- [86] Y. Tachikawa, *Lectures on 4d $N=1$ dynamics and related topics*, [1812.08946](#).
- [87] M. A. Luty and W. Taylor, *Varieties of vacua in classical supersymmetric gauge theories*, *Phys. Rev. D* **53** (1996) 3399 [[hep-th/9506098](#)].
- [88] N. Seiberg, *Naturalness versus supersymmetric nonrenormalization theorems*, *Phys. Lett. B* **318** (1993) 469 [[hep-ph/9309335](#)].
- [89] D. Martelli and J. Sparks, *Symmetry-breaking vacua and baryon condensates in AdS/CFT*, *Phys. Rev. D* **79** (2009) 065009 [[0804.3999](#)].
- [90] M. Buican, D. Malyshev, D. R. Morrison, H. Verlinde and M. Wijnholt, *D-branes at Singularities, Compactification, and Hypercharge*, *JHEP* **01** (2007) 107 [[hep-th/0610007](#)].

- [91] S. Benvenuti and A. Hanany, *New results on superconformal quivers*, *JHEP* **04** (2006) 032 [[hep-th/0411262](#)].
- [92] A. Hanany and A. Zaffaroni, *The master space of supersymmetric gauge theories*, *Adv. High Energy Phys.* **2010** (2010) 427891.
- [93] D. Forcella, A. Hanany, Y.-H. He and A. Zaffaroni, *The Master Space of $N=1$ Gauge Theories*, *JHEP* **08** (2008) 012 [[0801.1585](#)].
- [94] D. Forcella, A. Hanany, Y.-H. He and A. Zaffaroni, *Mastering the Master Space*, *Lett. Math. Phys.* **85** (2008) 163 [[0801.3477](#)].
- [95] D. Forcella, A. Hanany and A. Zaffaroni, *Master Space, Hilbert Series and Seiberg Duality*, *JHEP* **07** (2009) 018 [[0810.4519](#)].
- [96] D. Berenstein, *Reverse geometric engineering of singularities*, *JHEP* **04** (2002) 052 [[hep-th/0201093](#)].
- [97] D. Forcella, A. Hanany and A. Zaffaroni, *Baryonic Generating Functions*, *JHEP* **12** (2007) 022 [[hep-th/0701236](#)].
- [98] S. Franco, A. Hanany, F. Saad and A. M. Uranga, *Fractional branes and dynamical supersymmetry breaking*, *JHEP* **01** (2006) 011 [[hep-th/0505040](#)].
- [99] K. A. Intriligator and B. Wecht, *The Exact superconformal R symmetry maximizes a* , *Nucl. Phys. B* **667** (2003) 183 [[hep-th/0304128](#)].
- [100] A. Butti and A. Zaffaroni, *R -charges from toric diagrams and the equivalence of a -maximization and Z -minimization*, *JHEP* **11** (2005) 019 [[hep-th/0506232](#)].
- [101] A. Butti and A. Zaffaroni, *From toric geometry to quiver gauge theory: The Equivalence of a -maximization and Z -minimization*, *Fortsch. Phys.* **54** (2006) 309 [[hep-th/0512240](#)].
- [102] V. A. Novikov, M. A. Shifman, A. I. Vainshtein and V. I. Zakharov, *Exact Gell-Mann-Low Function of Supersymmetric Yang-Mills Theories from Instanton Calculus*, *Nucl. Phys. B* **229** (1983) 381.
- [103] A. Hanany, *Brane tilings: The NSVZ beta function*, *Int. J. Mod. Phys. A* **25** (2010) 381.
- [104] S. Lee and S.-J. Rey, *Comments on anomalies and charges of toric-quiver duals*, *JHEP* **03** (2006) 068 [[hep-th/0601223](#)].
- [105] E. Witten, *Phases of $N=2$ theories in two-dimensions*, *Nucl. Phys. B* **403** (1993) 159 [[hep-th/9301042](#)].

- [106] A. Hanany and R.-K. Seong, *Brane Tilings and Specular Duality*, *JHEP* **08** (2012) 107 [[1206.2386](#)].
- [107] B. Feng, S. Franco, A. Hanany and Y.-H. He, *UnHiggsing the del Pezzo*, *JHEP* **08** (2003) 058 [[hep-th/0209228](#)].
- [108] M. Bianchi, S. Cremonesi, A. Hanany, J. F. Morales, D. Ricci Pacifici and R.-K. Seong, *Mass-deformed Brane Tilings*, *JHEP* **10** (2014) 027 [[1408.1957](#)].
- [109] A. Hanany, C. P. Herzog and D. Vegh, *Brane tilings and exceptional collections*, *JHEP* **07** (2006) 001 [[hep-th/0602041](#)].
- [110] Z. Komargodski, S. S. Razamat, O. Sela and A. Sharon, *A Nilpotency Index of Conformal Manifolds*, *JHEP* **10** (2020) 183 [[2003.04579](#)].
- [111] S. Benvenuti, B. Feng, A. Hanany and Y.-H. He, *Counting BPS Operators in Gauge Theories: Quivers, Syzygies and Plethystics*, *JHEP* **11** (2007) 050 [[hep-th/0608050](#)].
- [112] C. Closset and S. Cremonesi, *Toric Fano varieties and Chern-Simons quivers*, *JHEP* **05** (2012) 060 [[1201.2431](#)].
- [113] K. A. Intriligator, *'Integrating in' and exact superpotentials in 4-d*, *Phys. Lett. B* **336** (1994) 409 [[hep-th/9407106](#)].
- [114] R. Eager, J. Schmude and Y. Tachikawa, *Superconformal Indices, Sasaki-Einstein Manifolds, and Cyclic Homologies*, *Adv. Theor. Math. Phys.* **18** (2014) 129 [[1207.0573](#)].
- [115] S. Franco and R.-K. Seong, *Twin theories, polytope mutations and quivers for GTPs*, *JHEP* **07** (2023) 034 [[2302.10951](#)].
- [116] J. Sá, *to appear*, .
- [117] F. Carta, S. Cremonesi and J. Sá, *to appear*, .
- [118] A. Butti, A. Zaffaroni and D. Forcella, *Deformations of conformal theories and non-toric quiver gauge theories*, *JHEP* **02** (2007) 081 [[hep-th/0607147](#)].
- [119] D. R. Gulotta, *Properly ordered dimers, R-charges, and an efficient inverse algorithm*, *JHEP* **10** (2008) 014 [[0807.3012](#)].
- [120] O. DeWolfe, A. Hanany, A. Iqbal and E. Katz, *Five-branes, seven-branes and five-dimensional $E(n)$ field theories*, *JHEP* **03** (1999) 006 [[hep-th/9902179](#)].
- [121] F. Benini, S. Benvenuti and Y. Tachikawa, *Webs of five-branes and $N=2$ superconformal field theories*, *JHEP* **09** (2009) 052 [[0906.0359](#)].

-
- [122] M. van Beest, A. Bourget, J. Eckhard and S. Schafer-Nameki, *(Symplectic) Leaves and (5d Higgs) Branches in the Poly(go)nesian Tropical Rain Forest*, *JHEP* **11** (2020) 124 [[2008.05577](#)].
- [123] A. Bourget, A. Collinucci and S. Schafer-Nameki, *Generalized Toric Polygons, T-branes, and 5d SCFTs*, [2301.05239](#).
- [124] J. Bao, G. B. Colverd and Y.-H. He, *Quiver Gauge Theories: Beyond Reflexivity*, *JHEP* **20** (2020) 161 [[2004.05295](#)].
- [125] X. Wei and R. Ding, *Lattice polygons with two interior lattice points*, *Mathematical Notes* **91** (2012) 868.
- [126] A. Hanany, P. Kazakopoulos and B. Wecht, *A New infinite class of quiver gauge theories*, *JHEP* **08** (2005) 054 [[hep-th/0503177](#)].
- [127] R. E. Tarjan, *Depth-first search and linear graph algorithms*, *SIAM Journal on Computing* **1** (1972) 146.
- [128] E. F. Moore, *The shortest path through a maze*, in *Proceedings of the International Symposium on the Theory of Switching*, pp. 285–292, Harvard University Press, 1959.
- [129] C. Y. Lee, *An algorithm for path connections and its applications*, *IRE Transactions on Electronic Computers* **EC-10** (1961) 346.
- [130] S. Franco and D. Rodriguez-Gomez, *Quiver Tails and Brane Webs*, [2310.10724](#).